Feasibility study using remote sensing technologies to improve zonal vineyard management

Leeko Hyun Suk Lee, H.B.Sc.

Department of Biological Sciences

Submitted in partial fulfillment

of the requirements for the degree of

Doctor of Philosophy

Faculty of Mathematics and Science, Brock University

St. Catharines, Ontario

Abstract

The primary purpose of this research was to examine the feasibility of using remote sensing data to improve efficiency of zonal vineyard management. To achieve this goal, correlation analysis between the significant vineyard management variables and different remote sensing data analysis tools were undertaken. The variables included leaf water potential, soil moisture, canopy size, vine health, vineyard yield, and fruit composition, which further impacts wine quality. The remote sensing data analysis tools included normalized difference vegetation index (NDVI), and other indices extracted from electromagnetic reflectance data of grapevine leaves and canopies. In each site, sentinel vines (i.e., 72-81) were identified in a grid form. GPS-based geolocation was carried out for six Cabernet Franc vineyards in Ontario's Niagara wine country.

Even though remote sensing data analysis tools were not associated with several other important variables for quality grape production, this research still confirmed that remote sensing data analysis has significant potential to differentiate specific zones of canopy size, water stress, yield, some superior fruit compositions, and the resulting wine sensory attributes within a single vineyard site. This study also confirmed that the mechanism of plant defense systems against biotic stress could have impacts on the spectral behaviour of grapevine leaves and hyperspectral remote sensing technologies could be applied as a tool to identify the spectral behaviour changes due to stress.

Overall, this study verified the feasibility of remote sensing technologies to enhance the efficiency of vineyard management in the correlation of data from various remote sensing data-analysis techniques and viticulturally important variables for plant health and growth, and fruit and wine quality. As a first step to develop a site-specific crop management (SSCM) model for

vineyard management, it also proposes future research opportunities to test and develop an efficient vineyard management decision making model.

Key words: zonal vineyard management, precision viticulture, remote sensing, selective harvesting, NDVI, grapevine virus detection, remotely piloted aircraft system (RPAS), GreenSeeker, multispectral sensor, hyperspectral sensor, GLRaV3.

Acknowledgements

Many people have supported, guided, educated, and offered friendship to me over the past five years, and I am immensely grateful for all of them. First of all, I wish to thank my supervisors, Dr. Debbie Inglis and Dr. Jim Willwerth, for their support and encouragement during this challenging period. The guidance they provided, along with their expertise, was vital to finish this thesis. Also, I am deeply grateful for CCOVI members and students, especially Briann Dorin, Lisa Dowling, Shufen Xu, Dr. Jennifer Kelly, and Dr. Sudarsana Poojari, for their enthusiasm and willingness to help this research. My committee members, Dr. Ralph Brown and Dr. Marilyne Carrey, also deserve special thanks for their encouragement and insightful input in this research. Dr. Andrew Reynolds has also contributed greatly to the interest I have developed in the fascinating field of viticulture research and has been a great source of encouragement during my pursuit of a graduate degree. Finally, this entire process would not have been possible without the support and encouragement of my friends and family. I especially thank my loving wife, Hae Yean, and my loving son, Ceeo. Your laugh is the most beautiful sound in the world and brings me to life!

Contents

CHAPTER 2: MATERIALS AND METHODS

TABLES

Table 4.3. Pearson's correlation results between NDVI/thermal from the RPAS flight vs yield and berry composition data in six Niagara vineyards from 2015, 2016 and 2017. Those variables with significant (95% confidence) were listed in bold, with blank cells representing no correlation: blue boxes= positive correlation with NDVI, red boxes= negative correlation with NDVI, black boxes= no data collected. Abbreviations: Clusters= Number of clusters, Berry Wt= Berry weight, TA= Titratable acidity.

Table 4.4. Other vegetation indices (VIs) to characterize the plant yield and quality production.

Table 4.5. Pearson's correlation results sorted **by indices** between indices from RPAS flight vs yield and berry composition data in six Niagara vineyards from 2016. The indices from RPAS flight included green, red, red edge, NIR, CI green, CI red edge, NDRE, GNDVI and RVI. Those variables with significant (95% confidence) were listed in bold, with blank cells representing no correlation: blue boxes= positive correlation with indices, red boxes= negative correlation with indices, black boxes= no data collected. Abbreviations: Berry WT= Berry weight, TA= Titratable acidity, CI green= Green chlorophyll index, CI red edge= Red edge chlorophyll index, NDRE= Red edge normalized difference vegetation index, GNDVI= NDVI green, RVI= Ratio vegetation index.

Table 4.6. Pearson's correlation results sorted **by sites** between indices from the RPAS flight vs yield and berry composition data in six Niagara vineyards from 2016. The indices from the RPAS flight included green, red, red edge, NIR, CI green, CI red edge, NDRE, GNDVI and RVI. Those variables with significant (95% confidence) were listed in bold, with blank cells representing no correlation: blue boxes= positive correlation with indices, red boxes= negative correlation with indices, black boxes= no data collected. Abbreviations: Berry WT= Berry weight, TA= Titratable acidity, CI green= Green chlorophyll index, CI red edge= Red edge chlorophyll index, NDRE= Red edge normalized difference vegetation index, GNDVI= NDVI green, RVI= Ratio vegetation index.

Table 4.7A. Moran's I analysis results (z-score) for data from the RPAS flight, proximal sensing, yield, and berry composition in six Niagara vineyards from 2015, 2016 and 2017 (95% confidence): blue boxes= clustered, red boxes= random, yellow boxes= dispersed, black boxes= no data collected. Abbreviations: NDVI= Normalized difference vegetation index, P-NDVI= Proximal sensing NDVI, Clusters = Number of clusters, Berry WT= Berry weight, TA= Titratable acidity.

Table 4.7B. Moran's I analysis results (Moran's Index and p-value) for data from the RPAS flight, proximal sensing, yield, and berry composition in six Niagara vineyards from 2015, 2016 and 2017 (95% confidence): blue boxes= clustered, red boxes= random, yellow boxes= dispersed, black boxes= no data collected. Abbreviations: NDVI= Normalized difference vegetation index, P-NDVI= Proximal sensing NDVI, Clusters = Number of clusters, Berry WT= Berry weight, TA= Titratable acidity.

Table 6.1. Real-Time qPCR results in the presence of GLRaV-2 and -3 for grapevine leaf samples collected from two study sites. "-" indicated negative result, "+" indicated cycle threshold (CT) value in the range of 36 to 38, "++" indicated CT value below 35.

Table 6.2. Remote sensing indices characterize vine health and virus infections.

Table 6.3. Pearson's correlation results between GLRaV-3 presence and remote sensing indices in the two virus infected vineyards. Those variables with significant (95% confidence) were listed in bold, with blank cells representing no correlation: blue boxes= positive relationship, red boxes= negative relationship. Abbreviations: NIR= Near infrared, NDVI= Normalized difference vegetation Index, NDRE= Red edge normalized vegetation index, GNDVI= NDVI green, GRVI= Green-red vegetation index, MTCI= MERIS terrestrial chlorophyll index, RTVI core= Core red edge triangular vegetation index.

FIGURES

Figure 2.1. Photos of Cabernet franc leaves: a) GLRaV-3 positive symptomatic leaves, b) GLRaV-3 positive asymptomatic leaves, and c) GLRaV-3 negative leaves.

Figure 2.2. Maps of different NDVI zones (low and high) from RPAS flights used for Cabernet franc winemaking. Maps were created in ArcMap 10.6. Legend: A: site 1 in the Niagara Lakeshore; B: site 2 in the Beamsville Bench; C: site 3 in the St. David's Bench; D: site 4 in the Lincoln Lakeshore; E: site 5 in the Lincoln Lakeshore; F: site 6 in the Four Mile Creek.

Figure 3.1. PCA results between remote sensing data and viticulturally important variables in site 1, 2, and 3 vineyards from 2015, 2016 and 2017. Abbreviations: NDVI= Normalized difference vegetation index, Leaf Ψ= Leaf water potential, Gs= Stomatal conductance, LT50= Temperature that kills 50% of the primary buds.

Figure 3.2. PCA results between remote sensing data and viticulturally important variables in site 4, 5, and 6 vineyards from 2015, 2016 and 2017. Abbreviations: NDVI= Normalized difference vegetation index, Leaf Ψ= Leaf water potential, Gs= Stomatal conductance, LT50= Temperature that kills 50% of the primary buds.

Figure 3.3. Mean growing season (May to September) temperature (°C), total growing season rainfall (mm), and average minimum dormant season (December to March) temperature (°C) from two Niagara resign locations. Port Weller AUT represented Niagara-on-the-lake vineyards and Vineland Research Station represented vineland vineyards. Historical climate normal data from St. Catharines A station 1981-2010.

Figure 3.4. Spatial maps of vineyard variables extracted from RS data and viticulturally important variables in site 1and 2 vineyards from 2015, 2016 and 2017. Abbreviations: NDVI= Normalized difference vegetation index, Leaf Ψ= Leaf water potential, Gs= Stomatal conductance, LT50= Temperature that kills 50% of the primary buds.

Figure 3.5. Spatial maps of vineyard variables extracted from RS data and viticulturally important variables in site 3 and 4 vineyards from 2015, 2016 and 2017. Abbreviations: NDVI= Normalized difference vegetation index, Leaf Ψ= Leaf water potential, Gs= Stomatal conductance, LT50= Temperature that kills 50% of the primary buds.

Figure 3.6. Spatial maps of vineyard variables extracted from RS data and viticulturally important variables in site 5 and 6 vineyards from 2015, 2016 and 2017. Abbreviations: NDVI= Normalized difference vegetation index, Leaf Ψ= Leaf water potential, Gs= Stomatal conductance, LT50= Temperature that kills 50% of the primary buds.

Figure 4.1. PCA results among data from proximal sensing, RPAS flight, vineyard yield and berry composition in site 1, 2, and 3 vineyards from 2015, 2016 and 2017. No harvest data collected at site 3 vineyard in 2015. Abbreviations: NDVI= Normalized difference vegetation index, Clusters= Number of clusters, Berry WT= Berry weight, TA= Titratable acidity, P-NDVI 1= Proximal sensing NDVI at berry set, P-NDVI 2= Proximal sensing NDVI at lag phase, P-NDVI 3= Proximal sensing NDVI at veraison, NDVI= NDVI from RPAS flight at veraison, Thermal= Thermal imaging from RPAS flight at veraison.

Figure 4.2. PCA results among data from proximal sensing, RPAS flight, vineyard yield and berry composition in site 4, 5, and 6 vineyards from 2015, 2016 and 2017. No harvest data was collected at site 3 vineyard in 2015. Abbreviations: NDVI= Normalized difference vegetation index, Clusters= Number of clusters, Berry WT= Berry weight, TA= Titratable acidity, P-NDVI 1= Proximal sensing NDVI at berry set, P-NDVI 2= Proximal sensing NDVI at lag phase, P-NDVI 3= Proximal sensing NDVI at veraison, NDVI= NDVI from RPAS flight at veraison, Thermal= Thermal imaging from RPAS flight at veraison.

Figure 4.3. Mean growing season (May to September) temperature (°C) and total growing season rainfall (mm) from two Niagara resign locations. Port Weller AUT represented Niagara-on-the-lake vineyards and Vineland Research Station represented vineland vineyards. Historical climate normal data from St. Catharines A station 1981-2010.

Figure 4.4. PCA results among indices from the RPAS flight, vineyard yield and berry composition in six Niagara vineyards from 2016. Variables include data in six Ontario vineyards in 2016. Abbreviations: Berry WT= Berry weight, TA= Titratable acidity, CI green= Green chlorophyll index, CI red edge= Red edge chlorophyll index, NDRE= Red edge normalized difference vegetation index, GNDVI= NDVI green, RVI= Ratio vegetation index.

Figure 4.5. Spatial maps of data from the proximal sensing, RPAS flight, vineyard yield and berry composition at site 4 vineyard from 2015, 2016, and 2017. Abbreviations: NDVI= Normalized difference vegetation index, P-NDVI1= Proximal sensing NDVI measured at fruit set, P-NDVI2= Proximal sensing NDVI measured at lag phase, P-NDVI3= Proximal sensing NDVI measured at veraison, TA= Titratable acidity.

Figure 5.1. Comparison of grape must analysis results from 2016 and 2017 Low vs High NDVI in the six vineyard sites. * p-values of significantly different between the treatments ($p<0.05$).

Figure 5.2. Comparison of wine analysis results from 2016 and 2017 Low vs High NDVI in in the six vineyard sites. * p-values of significantly different between the treatments ($p<0.05$).

Figure 5.3. MDS Kruskal stress test results in Cabernet Franc wines from site 1, 2, and 3 vineyards. A co-occurrence matrix was generated from the results of the wine sorting test.

Figure 5.4. MDS Kruskal stress test results in Cabernet Franc wines from site 4, 5, and 6 vineyards. A co-occurrence matrix was generated from the results of the wine sorting test.

Figure 5.5. AHC results in Cabernet Franc wines from site 1, 2, and 3 vineyards. The dendrograms illustrated the hierarchical division of categories according to the level of difference.

Figure 5.6. AHC results in Cabernet Franc wines from site 4, 5, and 6 vineyards. The dendrograms illustrated the hierarchical division of categories according to the level of difference.

Figure 5.7. Significance of difference in the concentrations(μg/L) of key odor active aroma compounds in the 2016 Cabernet franc wines from two different NDVI zones (low and high NDVI) using a t-test with two samples: * significant p-values (95% confidence).

Figure 5.8. Significance of difference in the concentrations(μg/L) of key odor active aroma compounds in the 2017 Cabernet franc wines from two different NDVI zones (low and high NDVI using a t-test with two samples: * significant p-values (95% confidence).

Figure 5.9. Comparison of mean concentrations(μg/L) of key odor active aroma compounds between 2016 and 2017 vintage Cabernet franc wines from the six Niagara vineyards using a t-test with two samples: * significant p-values (95% confidence).

Figure 5.10. PCA results of sensory descriptive analysis (DA) for Cabernet Franc wines from site 1, 2, and 3 vineyards. Left: PCA results of orthonasal- and retronasal-sensory descriptors for low NDVI vs high NDVI, middle: PCA results of colour and mouthfeel sensory descriptors for low NDVI vs high NDVI, and right: Sensory sorting results in the agglomerative hierarchical clustering dendrogram.

Figure 5.11. PCA results of sensory descriptive analysis (DA) for Cabernet Franc wines from site 4, 5, and 6 vineyards. Left: PCA results of orthonasal- and retronasal-sensory descriptors for low NDVI vs high NDVI, middle: PCA results of colour and mouthfeel sensory descriptors for low NDVI vs high NDVI, and right: Sensory sorting results in the agglomerative hierarchical clustering dendrogram.

Figure 5.12. Significance of difference in the concentrations (μg/L) of key odor active aroma compounds from sorted NDVI replicates in the 2016 Cabernet franc wines using a t-test with two samples: * significant p-values (95% confidence).

Figure 5.13. PLSR analysis results of Cabernet Franc wines from low and high NDVI zone at the six vineyard sites in 2016 based on sensory attributes from DA and key odor active aroma compounds concentration from GC-MS. The p-values represent a significant difference in value of variables for low and high NDVI ($P \leq 0.05$ in bold).

Figure 6.1. The series of electromagnetic spectra from healthy and GLRaV-3 infected Cabernet franc leaves measured by hand-held spectrometer at site 1.

Figure 6.2. The series of electromagnetic spectra from healthy and GLRaV-3 infected Cabernet franc leaves measured by hand-held spectrometer at site 2.

Figure 6.3. Comparison of mean reflectance (%) of EM spectrums of green, red, red edge, and NIR peaks from healthy (n=25) and GLRaV-3 infected (n=50) Cabernet Franc leaves measured by hand-held spectrometer in both site 1 and site 2 using a t-test with two samples: * significant p-values (95% confidence).

Figure 6.4. The series of electromagnetic spectra from healthy and GLRaV-3 symptomatic and asymptomatic Cabernet franc leaves measured by hand-held spectrometer at site 1.

Figure 6.5. The series of electromagnetic spectra from healthy and GLRaV-3 symptomatic and asymptomatic Cabernet franc leaves measured by hand-held spectrometer at site 2.

Figure 6.6. Comparison of mean reflectance (%) of EM spectrums of green, red, red edge, and NIR peaks from healthy (n=25), asymptomatic (n=25) and symptomatic (n=25) GLRaV-3 infected Cabernet franc leaves measured by hand-held spectrometer at site 1 using a t-test with two samples: * significant p-values (95% confidence).

Figure 6.7. Comparison of mean reflectance (%) of EM spectrums of green, red, red edge, and NIR peaks from healthy (n=25), asymptomatic (n=25) and symptomatic (n=25) GLRaV-3 infected Cabernet franc leaves measured by hand-held spectrometer at site 2 using a t-test with two samples: * significant p-values (95% confidence).

Figure 6.8. The series of the first derivative values of electromagnetic spectrums in red and red edge regions from healthy and GLRaV-3 symptomatic and asymptomatic Cabernet franc leaves measured by hand-held spectrometer at site 1.

Figure 6.9. The series of the first derivative values of electromagnetic spectrums in red and red edge regions from healthy and GLRaV-3 symptomatic and asymptomatic Cabernet franc leaves measured by hand-held spectrometer at site 2.

Figure 6.10. The series of relative reflectance change (ΔRn) of EMS in red and red edge regions from healthy and GLRaV-3 symptomatic and asymptomatic Cabernet franc leaves measured by hand-held spectrometer at site 1.

Figure 6.11. The series of relative reflectance change (ΔRn) of EMS in red and red edge regions from healthy and GLRaV-3 symptomatic and asymptomatic Cabernet franc leaves measured by hand-held spectrometer at site 2.

Figure 6.12. PCA results for GLRaV-3 presence vs. remote sensing indices including green, red, red edge, NIR, NDVI, NDRE, GNDVI, GRVI, MTCI, and RTVI core. Abbreviations: NIR= Near infrared, NDVI= Normalized difference vegetation Index, NDRE= Red edge normalized vegetation index, GNDVI= NDVI green, GRVI= Green-red vegetation index, MTCI= MERIS terrestrial chlorophyll index, RTVI core= Core red edge triangular vegetation index.

APPENDIX TABLES AND FIGURES

Table A1. Quality report of RPAS remote sensing data processing by Air-Tech Solutions, Inverary, ON (please double click the image).

Table A2. End-point PCR results in GRBV presence for three virus infected sites: – and +: negative and positive respectively in the PCR.

Table A3. Pearson's correlation results between GRBV presence and remote sensing indices in the two virus infected vineyards. Those variables with significant (95% confidence) were listed in bold, with blank cells representing no correlation: blue boxes= positive relationship, red boxes= negative relationship. Abbreviations: NIR= Near infrared, NDVI= Normalized difference vegetation Index, NDRE= Red edge normalized vegetation index, GNDVI= NDVI green, GRVI= Green-red vegetation index, MTCI= MERIS terrestrial chlorophyll index, RTVI core= Core red edge triangular vegetation index.

Figure A1. PCA results for GRBV presence vs. remote sensing indices including green, red, red edge, NIR, NDVI, NDRE, GNDVI, GRVI, MTCI, and RTVI core. Abbreviations: NIR= Near infrared, NDVI= Normalized difference vegetation Index, NDRE= Red edge normalized vegetation index, GNDVI= NDVI green, GRVI= Green-red vegetation index, MTCI= MERIS terrestrial chlorophyll index, RTVI core= Core red edge triangular vegetation index.

CHAPTER 1: INTRODUCTION AND LITERATURE REVIEW

1.1 Introduction and objectives

1.1.1 Introduction

The primary objective of this research was to examine the feasibility of using remote sensing data to improve efficiency of zonal vineyard management. To accomplish this objective, remote sensing data analysis tools, such as normalized difference vegetation index (NDVI), along with classic viticultural data (vine performance, yield, and fruit chemistry) were applied in detecting vineyard spatial/temporal variability and relationships elucidated. Precision viticulture (PV) endeavours to manage the variability within a vineyard, resulting in greater consistency with respect to yield and quality.[1]

PV depends on the factors responsible for determination of the spatial variation, possibility of zoning the variation, and possibilities of managing the zonal parameters.[1] The detection of spatial variations in vineyards needs to comprise a combination of different supporting technologies for acquiring and analyzing data. Geospatial technology can be described as a tool used to acquire and analyze data that has a reference to the earth, including remote sensing, geographic information systems (GIS), global positioning systems (GPS), and information technology.[2] PV has evolved with the development of spectral sensor technologies and geospatial technologies. Research has been conducted to investigate various types of remote sensing for use in vineyard variation detection, and advanced remote sensing technologies are constantly being introduced. In particular, this includes progress in the application of spectral sensor technologies to carrier platforms like remotely piloted aircraft systems (RPAS)[3], satellite and Trimble® GreenSeeker®[4,5], and in the improvement of spatial resolution of sensors[4,6,7]. Further

application of variable rate technology (VRT) based on remote sensing data also brings opportunities for site-specific fertilizing and spraying management.[8]

This study was conducted to examine the performance of remote sensing technologies recently introduced and determine if their application can enhance the health and sustainability of Niagara vineyards by providing scientific and evidence-based support. In addition, the ability to separate vineyard zones based on measurable quality attributes will provide a more efficient and intelligent way of managing vineyard variability to produce high quality vines and grapes.

1.1.2 Precision viticulture in zonal management

A significant increase in research for application of PV to vineyard management has occurred for decades. Spatial maps of soil and airborne images have been applied to demonstrate a usefulness of remote sensing technologies[9,10], and zonal management at the field level[11]. Zonal harvesting of grapes also proved to bring significant profits to the growers.[12,13] Furthermore, PV also brought many environmental benefits from the better use of farm resources such as minimizing the use of fertilizer and pesticides.[14,15]

Even though PV research has addressed zonal management in vineyards, which is demonstrated as subfield regions of different vine physiology, yield, and fruit quality,[16-18] many grape growers tend to perform uniform management in a single vineyard block but various environmental and biological aspects can have effects on quality and productivity of grapevines in a single block.[19,20] Researchers have demonstrated an existence of significant variabilities in quality and productivity of grape in accordance to the different vine physiologies (canopy size, sun exposure, water status) within individual vineyard blocks.[9,21-33] Sensory attributes of wines produced from different water stressed grapevines in a single vineyard block were also

differentiated from one another through sensory analysis.[25,34-38] To adopt PV, it must be possible to have distinct spatial variability coupled with long term stability. Many researchers have also investigated the temporal stability of viticulturally important variables such as canopy area, vine size, soil moisture, leaf water status, yield, and fruit quality.[9,39-44]

Additionally, an environment at individual vineyard block level can influence quality and productivity of grapevines. For example, vineyard soils can vary within a block in accordance with soil composition and nutrients level.[45-47] Researchers have also demonstrated the effects of variabilities in soil and nutrient on grape quality and quantity in single vineyard blocks of Riesling[38] and Cabernet franc[48].

Even though the grapevines are biologically identical, yield and grape quality are influenced by various physiological and environmental factors in the viticulture system such as canopy size, disease pressure, soil type, microclimate, sun exposure, nutrition availability, and water status.[9,21-33] Many researchers in PV have mainly focused on refining methods to identify the spatial variations of these factors in a single vineyard block, such that if the spatial variations can be identified, grapes can be managed differently in these subfield regions to maximize fruit quality and/or vine health or possibly harvest fruit into different lots based on this spatial variation to maximize wine quality.[40,49]

1.1.3 Detecting vineyard variability with remote sensing technology

Conventional methods of detecting vineyard variability involve direct ground surveys by well-trained personnel or specialized equipment. Limitations associated with these methods range from being time-consuming and labour-intensive, to requiring elaborate field and laboratory procedures and expertise, and measurement accuracies, depending on the plant variable under investigation.[50,51] For these reasons, conventional detection methods of vineyard variabilities

are not viable options for processing large numbers of plant samples due to the time and labour involved in their proper execution.[50] Despite the utility of traditional ground surveys, there remains a high demand for an efficient method for rapid detection of plant stress.[52] A solution to this demand could be in the use of remote sensing technologies.

1.1.4 Thesis goal and objectives

The main goal of this research is to examine the feasibility of using remote sensing data to improve efficiency of zonal vineyard management. The goal has been achieved through these short-term objectives. The first short-term objective was to examine the feasibility of using remote sensing NDVI to detect important vineyard variations that affect the viability of vineyards such as leaf water potential, soil moisture, canopy size, and LT50. We hypothesize that remote sensing NDVI will correspond to local variations in several vineyard variables that affect the viability of vineyards, and the correlations would be temporally stable. The second short-term objective was to examine the feasibility of using remote sensing technologies to monitor yield and fruit quality. We hypothesize that remote sensing data-analysis (NDVI, thermal, other indices) would correlate with yield and berry composition and vegetative growth in different stages of growing season could have different impact on yield and fruit quality. The third short-term objective was to investigate the zonal effect of remote sensing NDVI on wine sensory and chemical attributes. It was hypothesized that if vineyard blocks were harvested based on zones corresponding to low and high NDVI, resulting wines would differ in their chemical and sensory attributes. The last short-term objective was to examine the effects of grapevine leafroll-associated virus 3 (GLRaV3) infection and its symptoms on electromagnetic reflectance of grapevine leaf. We hypothesized that

the presence of grapevine virus and its infected leaves have unique electromagnetic signatures which could be detected by a narrow-band, hyperspectral spectrometer.

1.2 Literature review

1.2.1 Precision viticulture (PV) and site-specific crop management

The identification of variability and its subsequent responding within an individual vineyard block is one of the important concepts of PV. Site specific crop management (SSCM) is an integrated information-based farming management system that is designated to incorporate spatial variability into a farming decision-making system at the field or farm level. Spatial variability within a farming block can be better managed in farming operations using a SSCM system. For example, adapting crop inputs, such as fertilizers and chemicals, to a field's varying conditions would improve production efficiency and minimize environmental damages. Additionally, information about factors that affect crop growth and yield at a specific site would also improve the efficacy and profitability of production.[53] SSCM needs to comprise systems that combine remote sensing, GPS/GIS, variable rate technologies and data analysis to maximize production by accounting for variability and uncertainties in a field. GPS has become more accurate, portable, and rapidly developed, making georeferenced measurements now more relevant to apply for SSCM. A range of commercial sensors linked to GPS systems could be suitable for measuring the spatial and temporal evolution of crop parameters within a field.[54]

For an SSCM system to be proven useful for vineyard management, a model would first need to be established using input data collected from the vineyard that captures all the vineyard variability, and then that model would need to be tested in a subsequent year for making decisions in vineyard management. As a first step to developing that model, variations in the field such as

a spatial and temporal variation of crop quality and quantity are required.[12] Similarly, precision viticulture (PV) focuses on this concept within the context of vineyard variability. Grapevine physiological changes, productivity and quality are variables that can be affected by the crop and the conditions in the field.[55] However, in the absence of accurate methods for analyzing varietal differences, vineyards are more likely to be managed homogeneously.[49] PV faces several challenges with regards to gaining a proper knowledge of the spatial variation and distribution in a single vineyard site. Multiple sources can contribute to variability, so identifying this variance and determining its significance for agriculture is essential. Monitoring vineyard performance and associated attributes are the first step of PV implementation, and interpretation and evaluation take place once these data have been collected.[56,57]

1.2.2 Vineyard zoning

As part of the PV application, fields are grouped into homogeneous subregions, typically referred to as management zones. However, a complex system of interconnections and spatial variability in the agricultural environment makes determining the management zones complicated.[58] A vineyard block is subdivided into homogeneous zones based on the extent of spatial variation seen in the block, the spatial distribution, as well as their persistence through time.[59] To differentiate vineyard zones, three different segmentation algorithms have been widely used.[60] First, in the statistical approach, the region shape and the region's content are analyzed jointly.[61] Second, methods of splitting and merging zones are also widely used; however, they have a tendency to favour rectangular regions despite their simplicity. A further concern is that there is high sensitivity to boundaries applied to calculate uniformity and similarity of the areas.[62] The last approach is the region growing method. The use of this method is well

suited for delineating a unique region on a map.[63] Mixture of the methods by using Gabor filters to characterize vine rows and a region-growing algorithm and by using a categorization strategy according to the visual interpretation of vine rows can be implemented.[60]

Variability in vineyard yields and fruit composition can be managed to create wines with distinct qualities or wine products with a variety of price points to target different consumer segments. Wine products can be significantly different when harvested from different crop areas, which can be economically beneficial and result in unique final products.[13] Analyses of sensory content in two Pinot noir wine samples from Oregon involving vines of differing vigour zones revealed both anthocyanin levels and different pigmented polymer compositions.[64] Also, descriptions demonstrated different levels of intensity for various characteristics, for instance, wines from low NDVI areas exhibited high levels of heat, astringency, and earthiness than wines from high NDVI areas.[65] Existing research studies indicate that vineyard variance is related to various factors, including water level, soil structure, and vine size, all influencing the chemistry and taste of fruit and wine.[4,13,40,45,49,66,67]

Precision viticulture management is believed to enhance resource efficiency and quality control by identifying distinct and uniform management zones in a field.[68] Direct *in-situ* sampling for yield and quality is a common method of delineating management zones despite several challenges and limitations with the method[69], which is why the use of remote sensing technology has become increasingly common to establish zonal vineyard management. GIS, GPS, and other technologies also provide many new possibilities for mapping vineyard spatial variability. Through remote sensing software, unique zones can be identified and then linked to variables, including leaf water potential, soil moisture, canopy size, vine nutrition status, vineyard yield, and fruit composition.[70-75]

There has been evidence that remote sensing can detect different attributes of wine in vineyard zones and researchers examined the effectiveness of multispectral aerial imaging for vineyard management and winemaking using remotely sensed vigour zonation.[16,76-80] The Plant Cell Density Index (NIR/red) was utilized for measuring canopy vigour using multispectral remote sensing imagery[11] and the zonation of two Sangiovese vineyards was also determined by using multispectral data combined with soil conductance data [81]. Commercial scale vinification utilized multiple vigour zones, and untrained panelists could distinguish wine from certain vineyard areas by tasting it, but only to a limited degree from certain vineyard areas.[45] In nine vineyard plots in France, multispectral remote sensors were also used to identify different vineyard zones of abiotic stress, vegetative and reproductive growth, but differing berry compositions were not found in the zones.[9] Despite substantial research undertaken to investigate the use of remote sensing vine vigour data to detect vineyard variations across a range of grapevine and crop variables, the effectiveness of these technologies in optimizing vineyard management and selective harvesting needs further study.

1.2.3 Vineyard variation and temporal stability

1.2.3.1 Viticulturally important vineyard variability

In the environment, natural systems display periodic or structured variation in time and space (i.e., temporal or spatial dependence). The viticulture system is yet another example where patterns develop due to variations in microclimate, soil, water status, and vine physiology.[82] The quality and production of grapes can be significantly affected by the spatial variation of vineyard blocks.[45-47] A significant glacial activity in the Niagara Region has created soils with a high degree of variability.[83,84] Water status in grapevines can be directly impacted by differences in soil hydrology in vineyard soils.[85] A drought can negatively affect the growth of individual vines

and their photosynthesis[86,87] while an excessive amount of water can lead to a greater risk of disease [88], poor root growth[89], and leaching nutrients from the soil[90]. Vineyard soil moisture (SM) can differ significantly within a vineyard block[91] and differences in vine water status can be seen throughout the growing season[92]. Different soil types and vine vegetative growth are responsible for the variations in vine and vineyard water stress levels.[9,93]

Vineyards can also vary in vegetative growth. Plant stress levels can be influenced by the vegetation status of plants depending on their environment. In addition to water stress, plant chlorophyll level can be affected by plant life cycle, air contamination, nutrient status, and pathogens.[94] Stress in vegetation can be attributed to many factors.[51] Geospatial data associated with canopy features or data about an area designated as a water resource [4], disease detection[95] and canopy characterization[96-98] can be tracked efficiently and effectively. Vineyard canopy characterization by remote sensing is an improvement over manual characterization of the canopy, ensuring high levels of accuracy, efficiency and reliability.[56]

Another important vineyard variation, especially in northern viticulture areas like Ontario, is winter hardiness. Grapevine winter hardiness is attributed to cold acclimation, triggered by a reduced photoperiod and lower temperatures.[99,100] When the temperatures drop below the hardiness level of the vine, winter injury may occur. Depending on the severity of damage, the vine may be impaired in vegetative and reproductive growth, suffer increased disease pressure, as well as reduced yield.[101-103] Understanding the spatial variability of winter hardiness can lead to targeting management strategies to less winter-hardy areas, maximizing the effectiveness and response of the vineyard. Researchers have rarely attempted to determine the variability in cold hardiness in a vineyard block; nevertheless, researchers have demonstrated that the level of

hardiness varies significantly with other vineyard factors such as leaf water potential[103,104], vine vigour[105] and yield[101,105].

1.2.3.2 Vineyard variation in yield and fruit composition

Previous research demonstrated that significant within vineyard variation has been detected in berry compositions.[32,106-108] Spatial variability has also been linked to temporal variability, where the ripening and maturation of grape berries (Concord and Cabernet franc) showed the highest variability early in fruit development and decreased considerably by harvest.[109] Another study also demonstrated the spatial pattern of variability in berry compositions for Cabernet Sauvignon and Ruby Cabernet were distinct and mostly consistent from year to year.[13] Vineyard variation, especially canopy size, can significantly affect fruit quantity and quality. The vine canopy largely affects the microclimate within a single vineyard block, resulting in differences in light exposure, leaf temperature, air circulation, and moisture.[28,110,111] Sun exposure can lead to high sugar content, increases in colour development and aroma compounds, and lowering of acid compounds.[31,33,112,113]

Additionally, grapes are inversely affected by drought stress. As a consequence of water stress, yield is decreased mainly due to reduced photosynthesis resulting in decreased carbohydrate content, which is detrimental for the development of cluster primordium.[26,114,115] A lack of water results in fewer primordia per bud, lower primordia weight, resulting in smaller berries and clusters.[26] Increased water stress intensity and prolonged exposure to water stress lead to greater yield losses.[27] However, vines that have been stressed by water produce berries with higher sugar content, higher colour and aroma compounds, and lower acid compounds.[24-26] Taking the time of water stress into account is also very crucial, as water stress at an early stage of the fruit cycle, from flowering to pre-veraison, has the largest negative impact on berry weight.[116] Up to pre-

veraison, increased water stress shows a negative, linear impact on berry quality whereas light-to-mild levels of water stress increased berry quality post-veraison.[22] There is a wide range of variations within vineyard blocks when it comes to many important variables that impact grape productivity and quality which has led to increased interest in precision viticulture and developing enhanced methods to accurately detect vineyard variability.

1.2.3.3 Vineyard variation in wine quality

In winemaking, harvesting blocks of grapes of differing quality and producing wines from those different blocks can result in significantly different final wines, with some wines of exceptional quality which may result economic benefits.[13,117] The identification of high-quality vineyard blocks/zones based upon vine performance and fruit characteristics identified using remote sensing data analyses would help winemakers take advantage of these quality differences and support the management decision making process.

Wines from different areas of a uniformly managed vineyard can have different characteristics and it reinforces the notion that 'terroir' differs between vineyards according to its spatial characteristics.[11,45] Terroir can be defined as the interaction between environment and cultural practices that produce wine characteristics typical of a region.[118] Cultural practices are highly influential on the characteristics of wine, but these are themselves ultimately dependent upon the local environment. A wine's terroir is the result of a range of climatic, soil, and physical factors, which include microclimate, canopy size, biotic and abiotic stresses, and cultural practices, making the study of it multidisciplinary and occurring across geographical scales.[11,119] A difference in grape quality and quantity may allow varietal wines to be made at different price points and market segments. This is often accomplished by harvesting selective zones within a

vineyard, in which berries with varying physiological conditions are harvested according to their composition and yield.[13]

As geospatial tools have developed, zonal management has become increasingly studied as a way of finding out how vines are spatially distributed and patterned within vineyard blocks.[120] Wines from different vineyard zones based on water status were found to be distinguishable in aroma, taste, and mouthfeel profiles.[25,35-37,121] Wines from different canopy zones were reportedly different in anthocyanin, colour, and sensory attributes as well.[38,64,65] Even though identification of high-quality vineyard blocks could help winemakers separate that fruit to produce premium-grade wine, the process of identifying and determining zonal variation in a vineyard can be complicated. There is, therefore, a requirement for a contiguous set of high-quality spatial data for selective harvesting and winemaking. A primary tool for collecting such data is remote sensing, which has proven to be robust in detecting zones with varying vineyard vigour.[122] Many researchers interested in precision viticulture have examined the effects of variations in vegetative growth on wine production and developed the remotely sensed vine vigour (NDVI) map for that purpose to assess the different zonal distribution of wine sensory attributes.[11,45,81,117,122]

1.2.3.4 Vineyard variation in grapevine health related to virus infections

Many vineyards around the world suffer economic losses due to virus infections. Grapevine leafroll virus (GLRaV-3) is one such virus that commonly affects grape production quality in nearly every major grape-growing region.[123,124] According to a study conducted in Ontario, grapevine rupestris stem pitting-associated virus (GRSPaV) was a predominant type in vineyard blocks, followed by GLRaV-3, with close to 50% overall infection.[125] Previous research indicated that GRSPAV did not affect plant development or yield substantially and might even

mitigate some environmental stresses.[126-128] However, there is clear evidence that GLRaV-3 negatively impacts the productivity and grape quality of the infected vines.[129-132] An American study found that GLRaV can negatively impact the profitability of grape businesses by up to $40,000 per hectare over 25 years in New York.[133] Downward-rolling leaves with red colour and greenish veins are the visible phenotypic features of GLRaV-3 in red grapevine varieties.[129] Research has reported that vine damage from GLRaV-3 include significant declining photosynthetic ability[131,134], and reduced colour intensity and soluble solid levels in berries[131,135]. A significant increase in expression of a sugar transporter gene was also observed in leaves of vines infected with GLRaV-3.[136]

Grapevine red blotch-associated virus (GRBaV) discovered in 2008 in northern California has emerged as a major economic concern for North American wineries.[137] Red varieties of grapevines are damaged by this virus, which turns their leaves completely red including their veins but it is almost asymptomatic in some white cultivars.[137] Phytochemistry of grapevine leaves and development of berries appear to be affected by GRBaV based on the symptoms in red cultivars. A recent study also reveals its detrimental impact on vine growth and grape quality resulting in reduced vine size and yield, and reduced sugar, pigment, tannin and yeast assimilable nitrogen in the berries while increasing berry pH and titratable acidity.[138]

In most cases, grapevine virus is detected in infected leaf tissue of a vine by amplifying the viral genome sequence with the polymerase chain reaction (PCR).[139] However, the main diagnostic challenges with the PCR method are that infected vines have uneven symptom distribution so not all leaves may contain the virus at the same level, new infections are low in virus titer, and multiple viruses can infect grapevines at high rates requiring multiple tests to detect all viruses present.[123,125] Sampling grapevines and testing is also time consuming and expensive.

Since effective control and treatments for the grapevine virus has not been developed yet, recommendations are to remove infected vines before they act as a source of transmission in the vineyard. There is an urgent demand to develop an efficient method for the rapid and early detection of viruses.

1.2.3.5 Conventional methods of vineyard variability detection

Conventional means of vineyard variability detection involve direct ground surveys by well trained personnel or specialized equipment. For example, time-domain reflectometry (TDR) for measuring soil moisture, pressure bomb for directly measuring leaf water potential, and porometers for measuring leaf stomatal conductance are a few such techniques.[140] Manual ground scouting of vine size (pruning cane weight), yield (kg), measuring winter hardiness (LT50), and visual observation of phenotypical changes can also provide information about viticulturally important variations within a vineyard block.[45]

Often, direct *in-situ* sampling for yield and quality is used for delineating management zones although there remain many problems and limitations with this method as it is time-consuming, labour-intensive, requires elaborate field and laboratory procedures, and inaccuracy of the measurement that are tailored to detect each specific plant variable.[50,51] For these reasons, the conventional methods of detecting vineyard variability are not viable options for processing large numbers of plant samples.[50] Despite the utility of the traditional ground surveys, rapid, sensitive, and affordable methods for detecting plant stress still remain in high demand.[52] A solution to this demand could be in the use of remote sensing technologies.

1.2.4 Remote sensing

Remote sensing technologies are used to measure electromagnetic energy reflected by a surface, such as plants and soil, to obtain information about the object.[141] A remote sensing application for agriculture uses electromagnetic waves to sense soil or plant matter. The majority of remote sensing applications involve measuring the reflected radiation instead of the transmitted or absorbed radiation.[142] Plant leaves can also emit energy via fluorescence or expulsion of heat.[143]

Photosynthesizing plants, such as *Vitis vinifera*, require external energy in the form of sunlight to execute their photosynthetic activity. Biological pigments absorb energy from photons of sunlight, which carry energy proportional to their radiation frequency. These pigment molecules are responsible for the colour that we visually perceive from plants, as they interact with specific wavelengths in the visible range of the electromagnetic reflectance; absorbing particular wavelengths for energy harvesting and reflecting all others.[144-146] Due to the role of pigment molecules in plant photosynthesis and productivity, pigment content in leaves is a good indicator of plant health and photosynthetic activity.[144] The reductions in a plants' capacity for photosynthetic activity due to a stress could be demonstrated through changes in pigment quantities and ratios, which can significantly alter the plant’s interaction with electromagnetic energy. Stresses such as water, nutrients, and viral infection have demonstrated physical symptoms associated with changes in leaf colour and patterns, indicative of changes in their pigment content. These changes would further impact the specific wavelengths of light being absorbed and utilized by the plant, and those being reflected.[147-151]

It has been demonstrated that the photosynthetic capacity of a plant depends on abiotic stresses, for example water stress and nutrient availability[86,144,152], and that the quantities and

ratios of pigments in a leaf can be altered in response to changes in photosynthetic capacity[145]. There are a variety of biological pigments found in plants, the most common being chlorophylls, which are responsible for a significant portion of energy harvesting from light.[153] Another important group of accessory pigment molecules are carotenoids, which are critical in light energy absorption and efficiency for several higher order plants.[154] A major function of carotenoids is light-harvesting in the spectral region of 450–550 nm. Carotenoids are also important in protecting the cell from excess light.[154,155] Another group of pigment molecules that act as secondary metabolites and may help in dissipating excess energy are flavonoids.[156] Specifically, anthocyanins have been shown to protect leaves from excess light[157] and it was shown that flavonoid leaf content in several plants is also higher when grown under various abiotic stresses such as water, nutrient, and temperature[158].

Several remote sensing technologies are employed in PV research, allowing the mapping of a variety of variables, including the detection of vineyard water stress[4,159-161], leaf area index (LAI)[41], yield[162], and berry composition[79,108,161]. Despite the multitude of studies demonstrating remote sensing's capability to detect vineyard variations, there is a lack of literature regarding its ability to detect certain variables such as winter hardiness, selective harvest, and virus infection. The correlation of remote sensing data to berry quality and quantity has been shown to be incompatible across vineyards and vintages, and the need for more study of varieties and site-specific methodologies should be investigated.[34,79,108,161]

1.2.4.1 Advanced technologies and opportunities for site specific vineyard management

To distinguish and map high-quality grapes in a vineyard, comprehensive spatial models of microclimate, soil structure, and plant physiological characteristics need to be developed, as well as how these properties change over time.[163] Various studies are underway comparing

different remote sensing methods for detecting vineyard variability as advanced remote sensing technologies are developed and advanced. This involves a comparison of remote sensing tools[3], sensor capabilities[4,6,7], and vegetation indices used[4,5].

Originally remote sensing relied on aerial photography, which were costly and offered lower spatial resolution.[3] However, today's technical developments have made it possible to collect data closer to the area being studied with greater spatial resolutions. These advancements have also resulted in easier access to data and are more cost effective.[3,69] As an alternative to traditional methods, using local remote sensing tools, such as those available in tractors, off-road vehicles, or remotely piloted aircraft systems (RPASs), rapid sampling of large areas is possible.[1] Remote sensing devices are mounted on various platforms, with each platform influencing quality and processing of the collected data. Because of their close observation, proximity sensors collect data about the vine canopy from the sides.[69] A ground-based (proximal) sensor, attached to a tractor or other vehicles, avoids many of the complications associated with aerial remote sensing and satellite imagery. Due to their close proximity to objects, these sensors can provide higher spatial resolutions, do not have to account for soil and ground cover reflection between rows, do not require intensive post-acquisition image processing, and provide usable data in real-time.[162,164] In addition, these sensors can often be equipped with their own light source, which makes them less dependent on climate conditions.[162] Data acquisition by proximal sensing, however, may take longer depending on the size of the area being examined.[164] NDVI data from vine canopies were initially compiled using proximal sensing.[165] Study in Greece showed that there was a positive correlation between proximal sensing data and canopy size as well as berry colour intensity.[166] A previous study also indicated that proximal sensing NDVI could detect a

plant stress due to limited water uptake and nitrogen input.[167] In addition, the instrument showed ability to detect downy mildew in northern Italy.[168]

RPAS technology also for flights at much lower altitude, enabling the collection of imagery at much higher spatial resolutions, in the range of one centimeter/pixel.[169] This type of remote sensing platform is gaining scientific interest, and several reports have already been published in the literature on its use in precision viticulture. Several promising approaches to mapping leaf water potential[4,159] and vegetative growth[77] have been suggested. New generations of inexpensive autopilots have been enabled by the compact size of spectral sensors, GPS/GIS tools, and built-in computer systems.[170] Portable spectrometers typically carry hundreds of bands and proved to have a potential application of hyperspectral remote sensing with many wavebands of spectral information.[171] Various crop health parameters are measured, including vegetation indexes and diseases detection, by using portable sensors that can be hand-held or mobile for continuous and real-time observation.[8]

The EM reflectance of vegetation in agriculture is measured in multiple wavelength bands, mostly the green, red, red edge and near-infrared bands (NIR) and the reflectance is computationally transformed to the vegetative indices (Vis).[1] Plants receive radiation on the wavelengths of 400-700 nm, which are absorbed by their pigment molecules and utilized for their individual energy potentials.[154] Radiation reflected is therefore inversely proportional to its absorption of radiation; vascular plants, for example, contain two chlorophyll molecules, a and b.[144] Chlorophyll a has a blue-green colour (absorption maxima at 430-433 nm and 660-663 nm) and chlorophyll b a yellow-green colour (absorption maxima at 450-455 nm and 643-645 nm).[144] There are approximately three times as many chlorophyll a molecules to chlorophyll b molecules.[144] There are many other types of key pigment molecules in plants for remote sensing,

such as carotenoids[153], flavonoids, and anthocyanins[156]. Moreover, plants reflecting NIR wavelengths primarily because of their foliar structure enabled the development of VIs using the reflectance from red and NIR components of EM reflectance.[69]

1.2.4.2 NDVI and other indices to detect vineyard variability

The vegetative growth of plants can be used to estimate stress levels experienced in their surroundings.[94] Chlorophyll is the primary molecule that absorbs light energy and converts the energy for photosynthesis and is also a fundamental determinant of a plant vegetation.[172] The concept of stressed vegetation involves any event or situation that inversely affects photosynthesis and growth of plants.[51] One of the main causes of this stress is a lack of water and subsequent decrease in evaporation rates on the surface of leaves.[51] The concentration of chlorophyll could also be altered by external conditions such as sunlight, air contamination, insufficient nutrients, toxic chemicals, pathogens, and other environmental stresses.[94] Chlorophyll content is negatively correlated to the red reflectance peak because chlorophyll strongly absorbs red radiation for the electron transitions for photosynthesis at the magnesium component of the photoactive site.[172] Previous research has proven that chlorophyll concentration is negatively correlated to the red edge and NIR peaks.[173-175] Because of the reduction in chlorophyll concentration in stressed leaves, vegetation stress would have negative impacts on red edge and NIR peaks.

There have been several techniques developed to identify changes in vegetation condition using spectra composed of EM spectrum data at each pixel level.[176] As an example, the normalized difference vegetation index (NDVI) was based on calculations by transferring individual wavelength data into the ratio between near infrared and red reflectance in each band[177]: NDVI= [(near infrared)-(red)] / [(near infrared)+(red)]. NDVI provides the benefit of not affecting its calculation by the light intensity of the target.[177] As an indicator of vegetative

growth, NDVI is correlated to fractional cover, biomass, shaded area, leaf area index (LAI)[41,70], and grape quality[178]. Various researchers have also examined how NDVI affects grape yield and quality, including LAI, fruit composition, yield, water stress, and vegetative expression.[5,38,40,75,79,179-182] Other remote sensing indices in viticulture are also well summarized to detect vegetation status in plants.[5]

Remote sensors have been compared for their capabilities.[55] The range of wavebands captured by multispectral imaging and hyperspectral imaging is different.[55] A multispectral sensor measures more than one band of wavelengths while a hyperspectral sensor provides a narrow spectral resolution down to 1 nm.[7] In hyperspectral imaging, it is possible to analyze spectra of highly specific species under certain conditions, corresponding more precisely to their spectral signatures.[183] Hyperspectral sensors offer a lot of potential for remote sensing of plant stresses and especially for detecting virus infection [184], phylloxera infestation[185], and differences in nutrient status and uptake[74]. VIs from hyperspectral imagery were more effective at detecting species-specific spectral patterns under various stress conditions than those from multispectral sensors.[6] NDVI and other VIs created by multispectral imaging are less effective in detecting vineyard variation in fruit quality.[6]

1.2.5 Concluding remarks and impacts

Grapevines are subjected to many physiological and environmental stresses that influence their vegetative and reproductive growth. Water stress, cold damage, and pathogen attacks are highly relevant stresses in this research in many grape growing regions including Canada's cool climate production areas. In single cultivar blocks, there is a considerable amount of vine variability due to the stresses on their vegetative and reproductive growth, and site-specific crop

management enables precision viticulture, stratified according to vegetation stress, poor yield, or different quality of fruit.

In addition, the variability in fruit quality from sub-block zones can be incorporated into selective harvesting, which can improve economic value of products and winemaking. As PV has advantages both economically and environmentally, developing a low-cost, effective, and precise way to identify vineyard variation is necessary for it to become widely accepted. There has been good progress in using remote sensing technology to detect the spatial allocations and patterns of viticulturally meaningful variations in vineyards, yet further research is required to fully evaluate their effectiveness in crop- and site-specific ways.

This study mainly aimed to improve current knowledge about remote sensing applications in viticulture and their feasibility in cool climate vineyards as a precision management tool to help increase yields, quality or used for selective harvesting based on wine making potential. Through an exploration of a wide range of vineyard variables and their relationship with remote sensing data, this research will contribute in-depth knowledge about how remote sensing technologies can improve vineyard management practices in Ontario's viticultural areas and other cool climate regions. Many cool climate regions that have cold winters, a wide range of soil types, variable growing seasons and presence of viruses may have more inherent vineyard variability with respect to vegetative growth, yield and fruit composition which may impact the feasibility of remote sensing capabilities. This may lead to a lack of temporal stability in the vineyard in addition to confounding variables that impact remote sensing analyses and their reliability to use as a vineyard management tool. Therefore, research to examine remote sensing feasibility as a potential site-specific management tool is essential.

It is expected that the results of this research will have the following impacts for grape and wine industries: 1) validation of remote sensing as a feasible tool for more precise vineyard management in Canada; 2) a greater number of distinct vineyard lots will provide the winemaker with increased latitude in blending options if separate wines are made from those lots; 3) grapes from these individual wine lots might lead to increased quality of wine; 4) getting vineyards zoned by spatial data from remote sensing will assist winemakers to wisely manage the variations in wine quality; 5) lastly, it will be also anticipated that these findings will help to improve grape growers' access to and adoption of precision viticulture.

1.3 References

1. Arnó Satorra, J.; Martínez Casasnovas, J.A.; Ribes Dasi, M.; Rosell Polo, J.R. Precision viticulture. Research topics, challenges and opportunities in site-specific vineyard management. *Spanish Journal of Agricultural Research* **2009**, *7*, 779-790.

2. Panda, S.S.; Hoogenboom, G.; Paz, J.O. Remote sensing and geospatial technological applications for site-specific management of fruit and nut crops: A review. *Remote Sensing* **2010**, *2*, 1973-1997.

3. Matese, A.; Toscano, P.; Di Gennaro, S.; Genesio, L.; Vaccari, F.; Primicerio, J.; Belli, C.; Zaldei, A.; Bianconi, R.; Gioli, B. Intercomparison of UAV, Aircraft and Satellite Remote Sensing Platforms for Precision Viticulture. *Remote Sensing* **2015**, *7*, 2971-2990, doi:10.3390/rs70302971.

4. Baluja, J.; Diago, M.P.; Balda, P.; Zorer, R.; Meggio, F.; Morales, F.; Tardaguila, J. Assessment of vineyard water status variability by thermal and multispectral imagery using an unmanned aerial vehicle (UAV). *Irrigation Science* **2012**, *30*, 511-522.

5. Rey-Caramés, C.; Diago, M.; Martín, M.; Lobo, A.; Tardaguila, J. Using RPAS multi-spectral imagery to characterise vigour, leaf development, yield components and berry composition variability within a vineyard. *Remote Sensing* **2015**, *7*, 14458-14481.

6. Meggio, F.; Zarco-Tejada, P.J.; Núñez, L.C.; Sepulcre-Cantó, G.; González, M.; Martín, P. Grape quality assessment in vineyards affected by iron deficiency chlorosis using narrow-band physiological remote sensing indices. *Remote Sensing of Environment* **2010**, *114*, 1968-1986.

7. Roberts, D.A.; Roth, K.L.; Perroy, R.L. hyperspectral vegetation indices. *Hyperspectral remote sensing of vegetation.* **2016**, 309.

8. Li, Z.; Taylor, J.; Frewer, L.; Zhao, C.; Yang, G.; Liu, Z.; Gaulton, R.; Wicks, D.; Mortimer, H.; Cheng, X. A comparative review of the state and advancement of Site-Specific Crop Management in the UK and China. *Frontiers of Agricultural Science and Engineering* **2019**, *6*, doi:10.15302/j-fase-2018240.

9. Acevedo-Opazo, C.; Tisseyre, B.; Guillaume, S.; Ojeda, H. The potential of high spatial resolution information to define within-vineyard zones related to vine water status. *Precision Agriculture* **2008**, *9*, 285-302.

10. Roux, S.; Gaudin, R.; Tisseyre, B. Why does spatial extrapolation of the vine water status make sense? Insights from a modelling approach. *Agricultural Water Management* **2019**, *217*, 255-264, doi:10.1016/j.agwat.2019.03.013.

11. Bramley, R.G.; Hamilton, R. Terroir and precision viticulture: are they compatible? *Journal International des Sciences de la Vigne et du Vin* **2007**, *41*, 1.

12. Bramley, R.; Lamb, D. Making sense of vineyard variability in Australia. In Proceedings of the Proc. Internat. Symp. on Precision Viticulture, Ninth Latin American Congr. on Viticulture and Oenology, **2003**; pp. 35-54.

13. Bramley, R. Understanding variability in winegrape production systems 2. Within vineyard variation in quality over several vintages. *Australian Journal of Grape and Wine Research* **2005**, *11*, 33-42.

14. Schumann, A.W. Precise placement and variable rate fertilizer application technologies for horticultural crops. *HortTechnology* **2010**, *20*, 34-40.

15. Lescot, J.-M.; Rousset, S.; Souville, G. *Assessing investment in precision farming for reducing pesticide use in French viticulture*; **2011**.

16. Anastasiou, E.; Castrignano, A.; Arvanitis, K.; Fountas, S. A multi-source data fusion approach to assess spatial-temporal variability and delineate homogeneous zones: A use case in a table grape vineyard in Greece. *Sci Total Environ* **2019**, *684*, 155-163, doi:10.1016/j.scitotenv.2019.05.324.

17. Hubbard, S.S.; Schmutz, M.; Balde, A.; Falco, N.; Peruzzo, L.; Dafflon, B.; Léger, E.; Wu, Y.J.P.A. Estimation of soil classes and their relationship to grapevine vigour in a Bordeaux vineyard: advancing the practical joint use of electromagnetic induction (EMI) and NDVI datasets for precision viticulture. **2021**, 1-24.

18. Urretavizcaya, I.; Royo, J.; Miranda, C.; Tisseyre, B.; Guillaume, S.; Santesteban, L.J.P.A. Relevance of sink-size estimation for within-field zone delineation in vineyards. **2017**, *18*, 133-144.

19. Sarri, D.; Priori, S.; Lisci, R.; Lombardo, S.; D'Avino, L.; L'Abate, G.; Vieri, M.; Mattii, G.; Salvi, L.; Antoni, M. A comparison of canopy and soil proximal sensing to implement selective harvesting in viticulture. In Proceedings of the International Symposium on Precision Management of Orchards and Vineyards 1314, **2019**; pp. 157-164.

20. Matese, A.; Di Gennaro, S.F.; Santesteban, L.G. Methods to compare the spatial variability of UAV-based spectral and geometric information with ground autocorrelated data. A case of study for precision viticulture. *Computers and Electronics in Agriculture* **2019**, *162*, 931-940, doi:10.1016/j.compag.2019.05.038.

21. Chaves, M.M.; Santos, T.P.; Souza, C.d.; Ortuño, M.; Rodrigues, M.; Lopes, C.; Maroco, J.; Pereira, J.S. Deficit irrigation in grapevine improves water-use efficiency while controlling vigour and production quality. *Annals of Applied Biology* **2007**, *150*, 237-252.

22. Girona, J.; Marsal, J.; Mata, M.; Del Campo, J.; Basile, B. Phenological sensitivity of berry growth and composition of Tempranillo grapevines (Vitis vinifera L.) to water stress. *Australian Journal of Grape and Wine Research* **2009**, *15*, 268-277.

23. Reynolds, A.G.; Parchomchuk, P.; Berard, R.; Naylor, A.P.; Hogue, E. Gewurztraminer grapevines respond to length of water stress duration. *International journal of fruit science* **2005**, *5*, 75-94.

24. Roby, G.; Harbertson, J.F.; Adams, D.A.; Matthews, M.A. Berry size and vine water deficits as factors in winegrape composition: anthocyanins and tannins. *Australian Journal of Grape and Wine Research* **2004**, *10*, 100-107.

25. Koundouras, S.; Marinos, V.; Gkoulioti, A.; Kotseridis, Y.; van Leeuwen, C. Influence of vineyard location and vine water status on fruit maturation of nonirrigated cv. Agiorgitiko (Vitis vinifera L.). Effects on wine phenolic and aroma components. *Journal of Agricultural and Food Chemistry* **2006**, *54*, 5077-5086.

26. Shellie, K.C. Vine and berry response of Merlot (Vitis vinifera L.) to differential water stress. *American Journal of Enology and Viticulture* **2006**, *57*, 514-518.

27. Salón, J.L.; Chirivella, C.; Castel, J.R. Response of cv. Bobal to timing of deficit irrigation in Requena, Spain: water relations, yield, and wine quality. *American Journal of Enology and Viticulture* **2005**, *56*, 1-8.

28. Smart, R.E. Principles of grapevine canopy microclimate manipulation with implications for yield and quality. A review. *American Journal of Enology and Viticulture* **1985**, *36*, 230-239.

29. Reynolds, A.G.; Heuvel, J.E.V. Influence of grapevine training systems on vine growth and fruit composition: a review. *American Journal of Enology and Viticulture* **2009**, *60*, 251-268.

30. Terry, D.B.; Kurtural, S.K. Achieving vine balance of Syrah with mechanical canopy management and regulated deficit irrigation. *American journal of enology and viticulture* **2011**, *62*, 426-437.

31. Dokoozlian, N.; Kliewer, W. Influence of light on grape berry growth and composition varies during fruit development. *Journal of the American Society for Horticultural Science* **1996**, *121*, 869-874.

32. Cortell, J.M.; Halbleib, M.; Gallagher, A.V.; Righetti, T.L.; Kennedy, J.A. Influence of vine vigour on grape (Vitis vinifera L. cv. Pinot Noir) anthocyanins. 1. Anthocyanin concentration and composition in fruit. *Journal of Agricultural and Food Chemistry* **2007**, *55*, 6575-6584.

33. Reynolds, A.G.; Wardle, D.A. Influence of fruit microclimate on monoterpene levels of Gewürztraminer. *American Journal of Enology and Viticulture* **1989**, *40*, 149-154.

34. Marciniak, M.; Brown, R.; Reynolds, A.G.; Jollineau, M. Use of remote sensing to understand the terroir of the Niagara Peninsula. Applications in a Riesling vineyard. *OENO One* **2015**, *49*, 1-26.

35. Willwerth, J.; Reynolds, A.; Lesschaeve, I. Sensory analysis of Ontario Riesling wines from various water status zones. *OENO One* **2018**, *52*, 145-171.

36. Ledderhof, D.; Reynolds, A.G.; Manin, L.; Brown, R. Influence of water status on sensory profiles of Ontario Pinot noir wines. *LWT-Food Science and Technology* **2014**, *57*, 65-82.

37. CHAPMAN, D.M.; ROBY, G.; EBELER, S.E.; GUINARD, J.X.; MATTHEWS, M.A. Sensory attributes of Cabernet Sauvignon wines made from vines with different water status. *Australian Journal of Grape and Wine Research* **2005**, *11*, 339-347.

38. Reynolds, A.G.; Senchuk, I.V.; van der Reest, C.; De Savigny, C. Use of GPS and GIS for elucidation of the basis for terroir: Spatial variation in an Ontario Riesling vineyard. *American Journal of Enology and Viticulture* **2007**, *58*, 145-162.

39. Tisseyre, B.; Mazzoni, C.; Fonta, H. Whithin-field temporal stability of some parameters in viticulture: Potential toward a site specific management. *OENO One* **2008**, *42*, 27-39.

40. Hall, A.; Lamb, D.W.; Holzapfel, B.P.; Louis, J.P. Within-season temporal variation in correlations between vineyard canopy and winegrape composition and yield. *Precision Agriculture* **2011**, *12*, 103-117.

41. Johnson, L.F. Temporal stability of an NDVI-LAI relationship in a Napa Valley vineyard. *Australian Journal of Grape and Wine Research* **2003**, *9*, 96-101.

42. Arnó, J.; Rosell, J.; Blanco, R.; Ramos, M.; Martínez-Casasnovas, J. Spatial variability in grape yield and quality influenced by soil and crop nutrition characteristics. *Precision Agriculture* **2012**, *13*, 393-410.

43. Urretavizcaya, I.; Santesteban, L.G.; Tisseyre, B.; Guillaume, S.; Miranda, C.; Royo, J.B. Oenological significance of vineyard management zones delineated using early grape sampling. *Precision Agriculture* **2013**, *15*, 111-129, doi:10.1007/s11119-013-9328-3.

44. Hall, A.; Louis, J.; Lamb, D.W. Low-resolution remotely sensed images of winegrape vineyards map spatial variability in planimetric canopy area instead of leaf area index. *Australian journal of grape and wine research* **2008**, *14*, 9-17.

45. Bramley, R.; Ouzman, J.; Boss, P.K. Variation in vine vigour, grape yield and vineyard soils and topography as indicators of variation in the chemical composition of grapes, wine and wine sensory attributes. *Australian Journal of Grape and Wine Research* **2011**, *17*, 217-229.

46. Rodríguez-Pérez, J.R.; Plant, R.E.; Lambert, J.-J.; Smart, D.R. Using apparent soil electrical conductivity (EC a) to characterize vineyard soils of high clay content. *Precision Agriculture* **2011**, *12*, 775-794.

47. Trought, M.C.; Dixon, R.; Mills, T.; Greven, M.; Agnew, R.; Mauk, J.L.; Praat, J.-P. The impact of differences in soil texture within a vineyard on vine vigour, vine earliness and juice composition. *OENO One* **2008**, *42*, 67-72.

48. Reynolds, A.G.; Rezaei, J.H. Spatial variability in Ontario Cabernet franc vineyards: III. Relationships among berry composition variables and soil and vine water status. *Journal of Applied Horticulture* **2014**, *16*, 167-192.

49. Bramley, R.; Hamilton, R. Understanding variability in winegrape production systems: 1. Within vineyard variation in yield over several vintages. *Australian Journal of Grape and Wine Research* **2004**, *10*, 32-45.

50. Govender, M.; Govender, P.; Weiersbye, I.; Witkowski, E.; Ahmed, F.J.W.S. Review of commonly used remote sensing and ground-based technologies to measure plant water stress. **2009**, *35*.

51. Jackson, R.D. Remote sensing of biotic and abiotic plant stress. *Annual review of Phytopathology* **1986**, *24*, 265-287.

52. Sankaran, S.; Mishra, A.; Ehsani, R.; Davis, C.J.C.; Agriculture, E.i. A review of advanced techniques for detecting plant diseases. **2010**, *72*, 1-13.

53. Hummel, J.; Gaultney, L.; Sudduth, K. Soil property sensing for site-specific crop management. *Computers Electronics in Agriculture* **1996**, *14*, 121-136.

54. Gebbers, R.; Adamchuk, V.I. Precision agriculture and food security. *Science* **2010**, *327*, 828-831.

55. Hall, A.; Lamb, D.; Holzapfel, B.; Louis, J. Optical remote sensing applications in viticulture-a review. *Australian journal of grape and wine research* **2002**, *8*, 36-47.

56. de Castro, A.; Jiménez-Brenes, F.; Torres-Sánchez, J.; Peña, J.; Borra-Serrano, I.; López-Granados, F. 3-D characterization of vineyards using a novel UAV imagery-based OBIA procedure for precision viticulture applications. *Remote Sensing* **2018**, *10*, 584.

57. Jimenez-Brenes, F.M.; Lopez-Granados, F.; Torres-Sanchez, J.; Pena, J.M.; Ramirez, P.; Castillejo-Gonzalez, I.L.; de Castro, A.I. Automatic UAV-based detection of Cynodon dactylon for site-specific vineyard management. *PLoS One* **2019**, *14*, e0218132, doi:10.1371/journal.pone.0218132.

58. Milne, A.; Webster, R.; Ginsburg, D.; Kindred, D. Spatial multivariate classification of an arable field into compact management zones based on past crop yields. *Computers and electronics in agriculture* **2012**, *80*, 17-30.

59. McClymont, L.; Goodwin, I.; Mazza, M.; Baker, N.; Lanyon, D.; Zerihun, A.; Chandra, S.; Downey, M. Effect of site-specific irrigation management on grapevine yield and fruit quality attributes. *Irrigation science* **2012**, *30*, 461-470.

60. Da Costa, J.P.; Michelet, F.; Germain, C.; Lavialle, O.; Grenier, G. Delineation of vine parcels by segmentation of high resolution remote sensed images. *Precision Agriculture* **2007**, *8*, 95-110.

61. Geman, S.; Geman, D. Stochastic relaxation, Gibbs distributions, and the Bayesian restoration of images. *IEEE Transactions on pattern analysis and machine intelligence* **1984**, 721-741.

62. Spann, M.; Wilson, R. A quad-tree approach to image segmentation which combines statistical and spatial information. *Pattern Recognition* **1985**, *18*, 257-269.

63. Chang, Y.-L.; Li, X. Adaptive image region-growing. *IEEE transactions on image processing* **1994**, *3*, 868-872.

64. Cortell, J.M.; Halbleib, M.; Gallagher, A.V.; Righetti, T.L.; Kennedy, J.A. Influence of vine vigour on grape (Vitis vinifera L. cv. Pinot noir) anthocyanins. 2. Anthocyanins and pigmented polymers in wine. *Journal of agricultural and food chemistry* **2007**, *55*, 6585-6595.

65. Cortell, J.M.; Sivertsen, H.K.; Kennedy, J.A.; Heymann, H. Influence of vine vigour on Pinot noir fruit composition, wine chemical analysis, and wine sensory attributes. *American journal of enology and viticulture* **2008**, *59*, 1-10.

66. Diago, M.P.; Bellincontro, A.; Scheidweiler, M.; Tardaguila, J.; Tittmann, S.; Stoll, M. Future opportunities of proximal near infrared spectroscopy approaches to determine the variability of vineyard water status. *Australian Journal of Grape and Wine Research* **2017**, *23*, 409-414, doi:10.1111/ajgw.12283.

67. Romero, M.; Luo, Y.; Su, B.; Fuentes, S. Vineyard water status estimation using multispectral imagery from an UAV platform and machine learning algorithms for irrigation scheduling management. *Computers and Electronics in Agriculture* **2018**, *147*, 109-117, doi:10.1016/j.compag.2018.02.013.

68. Khosla, R.; Inman, D.; Westfall, D.; Reich, R.; Frasier, M.; Mzuku, M.; Koch, B.; Hornung, A. A synthesis of multi-disciplinary research in precision agriculture: Site-specific management zones in the semi-arid western Great Plains of the USA. *Precision Agriculture* **2008**, *9*, 85-100.

69. Mulla, D.J. Twenty five years of remote sensing in precision agriculture: Key advances and remaining knowledge gaps. *Biosystems engineering* **2013**, *114*, 358-371.

70. Hall, A.; Louis, J.; Lamb, D. Characterising and mapping vineyard canopy using high-spatial-resolution aerial multispectral images. *Computers & Geosciences* **2003**, *29*, 813-822.

71. Lamb, D.W.; Weedon, M.; Bramley, R. Using remote sensing to predict grape phenolics and colour at harvest in a Cabernet Sauvignon vineyard: Timing observations against vine phenology and optimising image resolution. *Australian Journal of Grape and Wine Research* **2004**, *10*, 46-54.

72. Zarco-Tejada, P.J.; Berjón, A.; López-Lozano, R.; Miller, J.R.; Martín, P.; Cachorro, V.; González, M.; De Frutos, A. Assessing vineyard condition with hyperspectral indices: Leaf and canopy reflectance simulation in a row-structured discontinuous canopy. *Remote Sensing of Environment* **2005**, *99*, 271-287.

73. Martín, P.; Zarco-Tejada, P.; González, M.; Berjón, A. Using hyperspectral remote sensing to map grape quality inTempranillo'vineyards affected by iron deficiency chlorosis. *VITIS-GEILWEILERHOF-* **2007**, *46*, 7.

74. Gil-Pérez, B.; Zarco-Tejada, P.; Correa-Guimaraes, A.; Relea-Gangas, E.; Navas-Gracia, L.; Hernández-Navarro, S.; Sanz-Requena, J.; Berjon, A.; Martín-Gil, J. Remote sensing detection of nutrient uptake in vineyards using narrow-band hyperspectral imagery. *Vitis* **2010**, *49*, 167-173.

75. Hall, A.; Wilson, M.A. Object-based analysis of grapevine canopy relationships with winegrape composition and yield in two contrasting vineyards using multitemporal high spatial resolution optical remote sensing. *International journal of remote sensing* **2013**, *34*, 1772-1797.

76. Sun, L.; Gao, F.; Anderson, M.; Kustas, W.; Alsina, M.; Sanchez, L.; Sams, B.; McKee, L.; Dulaney, W.; White, W.; et al. Daily Mapping of 30 m LAI and NDVI for Grape Yield Prediction in California Vineyards. *Remote Sensing* **2017**, *9*, 317, doi:10.3390/rs9040317.

77. Mathews, A.J.; Jensen, J.L. An airborne LiDAR-based methodology for vineyard parcel detection and delineation. *International journal of remote sensing* **2012**, *33*, 5251-5267.

78. Martinez-Casasnovas, J.A.; Agelet-Fernandez, J.; Arnó, J.; Ramos, M. Analysis of vineyard differential management zones and relation to vine development, grape maturity and quality. *Spanish Journal of Agricultural Research* **2012**, *10*, 326-337.

79. González-Flor, C.; Serrano, L.; Gorchs, G.; Pons, J.M. Assessment of grape yield and composition using reflectance-based indices in rainfed vineyards. *Agronomy Journal* **2014**, *106*, 1309-1316.

80. Crestey, T.; Pichon, L.; Tisseyre, B. Potential of freely available remote sensing visible images to support growers in delineating within field zones. *Advances in Animal Biosciences* **2017**, *8*, 372-376, doi:10.1017/s2040470017000437.

81. Priori, S.; Martini, E.; Biagi, M.; Andrenelli, M.; Magini, S.; Agnelli, A.; Natarelli, L.; Bucelli, P.; Comina, C.; Pellegrini, S. Improving wine quality through a harvest zoning based upon the combined use of proximal and remote sensing. In Proceedings of the Second Global Workshop on Proximal Soil Sensing, **2011**; pp. 152-155.

82. Shaddad, S.; Madrau, S.; Castrignanò, A.; Mouazen, A. Data fusion techniques for delineation of site-specific management zones in a field in UK. *Precision agriculture* **2016**, *17*, 200-217.

83. Reynolds, A.G.; Rezaei, J.H. Spatial variability in Ontario Cabernet Franc vineyards: I. Interrelationships among soil composition, soil texture, soil and vine water status. *Journal of Applied Horticulture* **2014**, *16*.

84. Haynes, S.J. Geology and wine 2. A geological foundation for terroirs and potential sub-appellations of Niagara Peninsula wines, Ontario, Canada. *Geoscience Canada* **2000**.

85. Saxton, K.E.; Rawls, W.J. Soil water characteristic estimates by texture and organic matter for hydrologic solutions. *Soil science society of America Journal* **2006**, *70*, 1569-1578.

86. Escalona, J.M.; Flexas, J.; Medrano, H. Stomatal and non-stomatal limitations of photosynthesis under water stress in field-grown grapevines. *Functional Plant Biology* **2000**, *27*, 87-87.

87. PELLEGRINO, A.; LEBON, E.; SIMONNEAU, T.; WERY, J. Towards a simple indicator of water stress in grapevine (Vitis vinifera L.) based on the differential sensitivities of vegetative growth components. *Australian Journal of Grape and Wine Research* **2005**, *11*, 306-315.

88. Halleen, F.; Fourie, P.H.; Crous, P.W. A review of black foot disease of grapevine. *Phytopathologia Mediterranea* **2006**, *45*, S55-S67.

89. Myburgh, P.; Moolman, J. Ridging—a soil preparation practice to improve aeration of vineyard soils. *South African Journal of Plant and Soil* **1991**, *8*, 189-193.

90. Lambert, J.; Anderson, M.; Wolpert, J. Vineyard nutrient needs vary with rootstocks and soils. *California agriculture* **2008**, *62*, 202-207.

91. Hubbard, S.; Grote, K.; Rubin, Y. Mapping the volumetric soil water content of a California vineyard using high-frequency GPR ground wave data. *The Leading Edge* **2002**, *21*, 552-559.

92. Tisseyre, B.; Ojeda, H.; Carillo, N.; Deis, L.; Heywang, M. Precision viticulture and water status, mapping the pre-dawn water potential to define within vineyard zones. In Proceedings of the Proceedings of 14th GESCO Congress, **2005**; pp. 23-27.

93. Taylor, J.A.; Acevedo-Opazo, C.; Ojeda, H.; Tisseyre, B. Identification and significance of sources of spatial variation in grapevine water status. *Australian Journal of Grape and Wine Research* **2010**, *16*, 218-226.

94. Larcher, W. *Physiological plant ecology: ecophysiology and stress physiology of functional groups*; Springer Science & Business Media: **2003**.

95. Albetis, J.; Duthoit, S.; Guttler, F.; Jacquin, A.; Goulard, M.; Poilvé, H.; Féret, J.-B.; Dedieu, G. Detection of Flavescence dorée grapevine disease using Unmanned Aerial Vehicle (UAV) multispectral imagery. *Remote Sensing* **2017**, *9*, 308.

96. Weiss, M.; Baret, F. Using 3D point clouds derived from UAV RGB imagery to describe vineyard 3D macro-structure. *Remote Sensing* **2017**, *9*, 111.

97. Mathews, A.J.; Jensen, J.L. Visualizing and quantifying vineyard canopy LAI using an unmanned aerial vehicle (UAV) collected high density structure from motion point cloud. *Remote sensing* **2013**, *5*, 2164-2183.

98. Poblete-Echeverría, C.; Olmedo, G.; Ingram, B.; Bardeen, M. Detection and Segmentation of Vine Canopy in Ultra-High Spatial Resolution RGB Imagery Obtained

from Unmanned Aerial Vehicle (UAV): A Case Study in a Commercial Vineyard. *Remote Sensing* **2017**, *9*, 268, doi:10.3390/rs9030268.

99. Fennell, A. Freezing tolerance and injury in grapevines. *Journal of Crop Improvement* **2004**, *10*, 201-235.

100. Janská, A.; Maršík, P.; Zelenková, S.; Ovesná, J. Cold stress and acclimation–what is important for metabolic adjustment? *Plant Biology* **2010**, *12*, 395-405.

101. Dami, I.; Ferree, D.; Kurtural, S.; Taylor, B. Influence of crop load on 'Chambourcin'yield, fruit quality, and winter hardiness under midwestern United States environmental conditions. *Acta Hort* **2005**, *689*, 203-208.

102. Jasinski, M. The terroir of winter hardiness: investigation of winter hardiness, water metrics, and yield of Riesling and Cabernet Franc in the Niagara region using geomatic technologies. **2013**.

103. Reynolds, A.G.; Jasinski, M.; Di Profio, F.; Pasquier, A.; Touffet, M.; Fellman, R. The terroir of winter hardiness: a three year investigation of spatial variation in winter hardiness, water status, yield, and berry composition of Cabernet Franc in the Niagara Region using geomatic technologies. In Proceedings of the Proc. 10th International Terroir Congress, Tokaji, Hungary, **2014**; pp. 36-42.

104. Basinger, A.R.; Hellman, E.W. Evaluation of regulated deficit irrigation on grape in Texas and implications for acclimation and cold hardiness. *International journal of fruit science* **2007**, *6*, 3-22.

105. Howell, G.S.; Stergios, B.G.; Stackhouse, S. Interrelation of productivity and cold hardiness of Concord grapevines. *American Journal of Enology and Viticulture* **1978**, *29*, 187-191.

106. Tardáguila, J.; Baluja, J.; Arpon, L.; Balda, P.; Oliveira, M. Variations of soil properties affect the vegetative growth and yield components of "Tempranillo" grapevines. *Precision Agriculture* **2011**, *12*, 762-773.

107. Baluja, J.; Tardaguila, J.; Ayestaran, B.; Diago, M.P. Spatial variability of grape composition in a Tempranillo (Vitis vinifera L.) vineyard over a 3-year survey. *Precision Agriculture* **2013**, *14*, 40-58.

108. Urretavizcaya, I.; Santesteban, L.; Tisseyre, B.; Guillaume, S.; Miranda, C.; Royo, J. Oenological significance of vineyard management zones delineated using early grape sampling. *Precision Agriculture* **2014**, *15*, 111-129.

109. Pagay, V.; Cheng, L. Variability in berry maturation of Concord and Cabernet franc in a cool climate. *American Journal of Enology and Viticulture* **2010**, *61*, 61-67.

110. Dry, P.R. Canopy management for fruitfulness. *Australian Journal of Grape and Wine Research* **2000**, *6*, 109-115.

111. Vasconcelos, M.C.; Greven, M.; Winefield, C.S.; Trought, M.C.; Raw, V. The flowering process of Vitis vinifera: a review. *American Journal of Enology and Viticulture* **2009**, *60*, 411-434.

112. Cortell, J.M.; Kennedy, J.A. Effect of shading on accumulation of flavonoid compounds in (Vitis vinifera L.) pinot noir fruit and extraction in a model system. *Journal of Agricultural and Food Chemistry* **2006**, *54*, 8510-8520.

113. Belancic, A.; Agosin, E.; Ibacache, A.; Bordeu, E.; Baumes, R.; Razungles, A.; Bayonove, C. Influence of sun exposure on the aromatic composition of Chilean Muscat grape cultivars Moscatel de Alejandria and Moscatel rosada. *American Journal of Enology and Viticulture* **1997**, *48*, 181-186.

114. Kliewer, W.M.; Freeman, B.M.; Hosssom, C. Effect of irrigation, crop level and potassium fertilization on Carignane vines. I. Degree of water stress and effect on growth and yield. *American Journal of Enology and Viticulture* **1983**, *34*, 186-196.

115. Medrano, H.; Escalona, J.M.; Cifre, J.; Bota, J.; Flexas, J. A ten-year study on the physiology of two Spanish grapevine cultivars under field conditions: effects of water availability from leaf photosynthesis to grape yield and quality. *Functional Plant Biology* **2003**, *30*, 607-619.

116. Reynolds, A.G.; Naylor, A.P. Pinot noir'andRiesling'Grapevines Respond to Water Stress Duration and Soil Water-holding Capacity. *HortScience* **1994**, *29*, 1505-1510.

117. Bramley, R.; Ouzman, J.; Thornton, C. Selective harvesting is a feasible and profitable strategy even when grape and wine production is geared towards large fermentation volumes. *Australian Journal of Grape and Wine Research* **2011**, *17*, 298-305.

118. Van Leeuwen, C.; Seguin, G. The concept of terroir in viticulture. *Journal of wine research* **2006**, *17*, 1-10.

119. Spielmann, N.; Gélinas-Chebat, C. Terroir? That's not how I would describe it. *International Journal of Wine Business Research* **2012**.

120. Cox, S. Information technology: the global key to precision agriculture and sustainability. *Computers and electronics in agriculture* **2002**, *36*, 93-111.

121. Marciniak, M.; Reynolds, A.G.; Brown, R. Influence of water status on sensory profiles of Ontario Riesling wines. *Food research international* **2013**, *54*, 881-891.

122. Johnson, L.; Bosch, D.; Williams, D.; Lobitz, B. Remote sensing of vineyard management zones: Implications for wine quality. *Applied Engineering in Agriculture* **2001**, *17*, 557.

123. Maree, H.J.; Almeida, R.P.; Bester, R.; Chooi, K.M.; Cohen, D.; Dolja, V.V.; Fuchs, M.F.; Golino, D.A.; Jooste, A.E.; Martelli, G.P. Grapevine leafroll-associated virus 3. *Frontiers in microbiology* **2013**, *4*, 82.

124. BaSSO, M.F.; FAJARDO, T.V.; SalDaRellI, P. Grapevine virus diseases: economic impact and current advances in viral prospection and management. *Revista Brasileira de Fruticultura* **2017**, *39*.

125. Xiao, H.; Shabanian, M.; Moore, C.; Li, C.; Meng, B. Survey for major viruses in commercial Vitis vinifera wine grapes in Ontario. *Virology journal* **2018**, *15*, 127.

126. Reynolds, A.G.; Lanterman, W.; Wardle, D.A.J.A.J.o.E.; Viticulture. Yield and berry composition of five Vitis cultivars as affected by Rupestris stem pitting virus. **1997**, *48*, 449-458.

127. Gambino, G.; Cuozzo, D.; Fasoli, M.; Pagliarani, C.; Vitali, M.; Boccacci, P.; Pezzotti, M.; Mannini, F.J.J.o.E.B. Co-evolution between Grapevine rupestris stem pitting-associated virus and Vitis vinifera L. leads to decreased defence responses and increased transcription of genes related to photosynthesis. **2012**, *63*, 5919-5933.

128. Pantaleo, V.; Vitali, M.; Boccacci, P.; Miozzi, L.; Cuozzo, D.; Chitarra, W.; Mannini, F.; Lovisolo, C.; Gambino, G.J.S.r. Novel functional microRNAs from virus-free and infected Vitis vinifera plants under water stress. **2016**, *6*, 1-14.

129. Naidu, R.A.; Maree, H.J.; Burger, J.T. Grapevine leafroll disease and associated viruses: a unique pathosystem. *Annual Review of Phytopathology* **2015**, *53*, 613-634.

130. Alabi, O.J.; Casassa, L.F.; Gutha, L.R.; Larsen, R.C.; Henick-Kling, T.; Harbertson, J.F.; Naidu, R.A. Impacts of grapevine leafroll disease on fruit yield and grape and wine chemistry in a wine grape (Vitis vinifera L.) cultivar. *PLoS One* **2016**, *11*.

131. Gutha, L.R.; Casassa, L.F.; Harbertson, J.F.; Naidu, R.A. Modulation of flavonoid biosynthetic pathway genes and anthocyanins due to virus infection in grapevine (Vitis viniferaL.) leaves. *BMC Plant Biology* **2010**, *10*, 187.

132. Basso, M.F.; Fajardo, T.V.; Santos, H.P.; Guerra, C.C.; Ayub, R.A.; Nickel, O. Leaf physiology and enologic grape quality of virus-infected plants. *Tropical Plant Pathology* **2010**, *35*, 351-359.

133. Atallah, S.S.; Gómez, M.I.; Fuchs, M.F.; Martinson, T.E. Economic impact of grapevine leafroll disease on Vitis vinifera cv. Cabernet franc in Finger Lakes vineyards of New York. *American Journal of Enology and Viticulture* **2012**, *63*, 73-79.

134. Mannini, F.; Mollo, A.; Credi, R. Field performance and wine quality modification in a clone of Vitis vinifera cv. Dolcetto after GLRaV-3 elimination. *American journal of enology and viticulture* **2012**, *63*, 144-147.

135. Vega, A.; Gutiérrez, R.A.; Pena-Neira, A.; Cramer, G.R.; Arce-Johnson, P. Compatible GLRaV-3 viral infections affect berry ripening decreasing sugar accumulation and anthocyanin biosynthesis in Vitis vinifera. *Plant Molecular Biology* **2011**, *77*, 261.

136. Espinoza, C.; Medina, C.; Somerville, S.; Arce-Johnson, P. Senescence-associated genes induced during compatible viral interactions with grapevine and Arabidopsis. *Journal of Experimental Botany* **2007**, *58*, 3197-3212.

137. Sudarshana, M.R.; Perry, K.L.; Fuchs, M.F. Grapevine red blotch-associated virus, an emerging threat to the grapevine industry. *Phytopathology* **2015**, *105*, 1026-1032.

138. Bowen, P.; Bogdanoff, C.; Poojari, S.; Usher, K.; Lowery, T.; Úrbez-Torres, J.R.J.A.J.o.E.; Viticulture. Effects of Grapevine Red Blotch Disease on Cabernet franc Vine Physiology, Bud Hardiness, and Fruit and Wine Quality. **2020**, *71*, 308-318.

139. Osman, F.; Leutenegger, C.; Golino, D.; Rowhani, A. Comparison of low-density arrays, RT-PCR and real-time TaqMan® RT-PCR in detection of grapevine viruses. *Journal of virological methods* **2008**, *149*, 292-299.

140. Fandiño, M.; Martínez, M.; Rey, J.; Cancela, J. Plant water status in vineyards combining sensors in soil and plant. **2011**.

141. Der Meer, V. Validated surface mineralogy from high-spectral resolution remote sensing: a review and a novel approach applied to gold exploration using AVIRIS data. *Terra Nova* **1998**, *10*, 112-119.

142. Jordan, C.F. Derivation of leaf-area index from quality of light on the forest floor. *Ecology* **1969**, *50*, 663-666.

143. Apostol, S.; Viau, A.A.; Tremblay, N.; Briantais, J.-M.; Prasher, S.; Parent, L.-E.; Moya, I. Laser-induced fluorescence signatures as a tool for remote monitoring of water and nitrogen stresses in plants. *Canadian journal of remote sensing* **2003**, *29*, 57-65.

144. Palta, J.P. Leaf chlorophyll content. *Remote sensing reviews* **1990**, *5*, 207-213.

145. Merzlyak, M.N.; Gitelson, A.A.; Chivkunova, O.B.; Rakitin, V.Y. Non-destructive optical detection of pigment changes during leaf senescence and fruit ripening. *Physiologia plantarum* **1999**, *106*, 135-141.

146. Pimputkar, S.; Speck, J.S.; DenBaars, S.P.; Nakamura, S. Prospects for LED lighting. *Nature photonics* **2009**, *3*, 180-182.

147. Grant, L.; Daughtry, C.; Vanderbilt, V.J.R.s.o.e. Variations in the polarized leaf reflectance of Sorghum bicolor. **1987**, *21*, 333-339.

148. Grant, L.; Daughtry, C.; Vanderbilt, V.J.P.P. Polarized and specular reflectance variation with leaf surface features. **1993**, *88*, 1-9.

149. Vanderbilt, V.C.; Grant, L.J.I.T.o.G.; Sensing, R. Plant canopy specular reflectance model. **1985**, 722-730.

150. Gitelson, A.A.; Merzlyak, M.N.J.J.o.p.p. Signature analysis of leaf reflectance spectra: algorithm development for remote sensing of chlorophyll. **1996**, *148*, 494-500.

151. Sivanpillai, R.; Whitman, R.D. Relating leaf spectral reflectance to its color: an inquiry-based activity to enhance understanding of electromagnetic radiation. *Science Activities* **2019**, *56*, 19-26.

152. Yu, D.; Kim, S.; Lee, H. Stomatal and non-stomatal limitations to photosynthesis in field-grown grapevine cultivars. *Biologia Plantarum* **2009**, *53*, 133-137.

153. Frank, H.A.; Cogdell, R.J. Carotenoids in photosynthesis. *Photochemistry and photobiology* **1996**, *63*, 257-264.

154. Römer, S.; Fraser, P.D. Recent advances in carotenoid biosynthesis, regulation and manipulation. *Planta* **2005**, *221*, 305-308.

155. Bilger, W.; Björkman, O. Role of the xanthophyll cycle in photoprotection elucidated by measurements of light-induced absorbance changes, fluorescence and photosynthesis in leaves of Hedera canariensis. *Photosynthesis research* **1990**, *25*, 173-185.

156. Chalker-Scott, L. Environmental significance of anthocyanins in plant stress responses. *Photochemistry and photobiology* **1999**, *70*, 1-9.

157. Matus, J.T.; Loyola, R.; Vega, A.; Peña-Neira, A.; Bordeu, E.; Arce-Johnson, P.; Alcalde, J.A. Post-veraison sunlight exposure induces MYB-mediated transcriptional regulation of anthocyanin and flavonol synthesis in berry skins of Vitis vinifera. *Journal of experimental botany* **2009**, *60*, 853-867.

158. Winkel-Shirley, B. Biosynthesis of flavonoids and effects of stress. *Current opinion in plant biology* **2002**, *5*, 218-223.

159. Bellvert, J.; Zarco-Tejada, P.J.; Girona, J.; Fereres, E. Mapping crop water stress index in a 'Pinot-noir'vineyard: comparing ground measurements with thermal remote sensing imagery from an unmanned aerial vehicle. *Precision agriculture* **2014**, *15*, 361-376.

160. Soliman, A.; Heck, R.J.; Brenning, A.; Brown, R.; Miller, S. Remote sensing of soil moisture in vineyards using airborne and ground-based thermal inertia data. *Remote Sensing* **2013**, *5*, 3729-3748.

161. Ledderhof, D.; Brown, R.; Reynolds, A.; Jollineau, M. Using remote sensing to understand Pinot noir vineyard variability in Ontario. *Canadian journal of plant science* **2016**, *96*, 89-108.

162. Debuisson, S.; Germain, C.; Garcia, O.; Panigai, L.; Moncomble, D.; Le Moigne, M.; Fadaili, E.; Evain, S.; Cerovic, Z. Using Multiplex® and Greenseeker™ to manage spatial variation of vine vigour in Champagne. In Proceedings of the 10th International Conference on Precision Agriculture. Denver, Colorado, **2010**.

163. Vaudour, E. The quality of grapes and wine in relation to geography: Notions of terroir at various scales. *Journal of Wine Research* **2002**, *13*, 117-141.

164. Wójtowicz, M.; Wójtowicz, A.; Piekarczyk, J. Application of remote sensing methods in agriculture. *Communications in Biometry and Crop Science* **2016**, *11*, 31-50.

165. Drissi, R.; Goutouly, J.-P.; Forget, D.; Gaudillere, J.-P. Nondestructive measurement of grapevine leaf area by ground normalized difference vegetation index. *Agronomy Journal* **2009**, *101*, 226-231.

166. Stamatiadis, S.; Taskos, D.; Tsadilas, C.; Christofides, C.; Tsadila, E.; Schepers, J.S. Relation of ground-sensor canopy reflectance to biomass production and grape color in two Merlot vineyards. *American Journal of Enology and viticulture* **2006**, *57*, 415-422.

167. Stamatiadis, S.; Taskos, D.; Tsadila, E.; Christofides, C.; Tsadilas, C.; Schepers, J.S. Comparison of passive and active canopy sensors for the estimation of vine biomass production. *Precision Agriculture* **2010**, *11*, 306-315.

168. Mazzetto, F.; Calcante, A.; Mena, A. Comparing commercial optical sensors for crop monitoring tasks in precision viticulture. *Journal of Agricultural Engineering* **2009**, *40*, 11-18.

169. Hunt, E.R.; Hively, W.D.; Fujikawa, S.J.; Linden, D.S.; Daughtry, C.S.; McCarty, G.W. Acquisition of NIR-green-blue digital photographs from unmanned aircraft for crop monitoring. *Remote Sensing* **2010**, *2*, 290-305.

170. Zhong, Y.; Wang, X.; Xu, Y.; Wang, S.; Jia, T.; Hu, X.; Zhao, J.; Wei, L.; Zhang, L. Mini-UAV-borne hyperspectral remote sensing: From observation and processing to applications. *IEEE Geoscience and Remote Sensing Magazine* **2018**, *6*, 46-62.

171. Ryan, S.; Lewis, M. Mapping soils using high resolution airborne imagery, Barossa Valley, SA. In Proceedings of the Proceedings of the Inaugural Australian Geospatial

Information and Agriculture Conference Incorporating Precision Agriculture in Australasia 5th Annual Symposium, **2001**; pp. 17-19.

172. Danks, S.M.; Evans, E.H.; Whittaker, P.A. *Photosynthetic systems: structure, function, and assembly*; John Wiley & Sons: **1983**.

173. Ustin, S.; Martens, S.; Curtiss, B.; Vanderbilt, V. Use of high spectral resolution sensors to detect air pollution injury in conifer forests. In *Remote Sensing Applications of Acid Deposition*; EPA: **1988**; pp. 72-85.

174. Horler, D.; DOCKRAY, M.; Barber, J.J.I.j.o.r.s. The red edge of plant leaf reflectance. **1983**, *4*, 273-288.

175. Gitelson, A.A.; Merzlyak, M.N.; Lichtenthaler, H.K.J.J.o.p.p. Detection of red edge position and chlorophyll content by reflectance measurements near 700 nm. **1996**, *148*, 501-508.

176. Price, J.C.; Bausch, W.C. Leaf area index estimation from visible and near-infrared reflectance data. *Remote Sensing of Environment* **1995**, *52*, 55-65.

177. Rouse, J.; Haas, R.; Schell, J.; Deering, D. Monitoring vegetation systems in the Great Plains with ERTS. *NASA special publication* **1974**, *351*, 309.

178. Fiorillo, E.; Crisci, A.; De Filippis, T.; Di Gennaro, S.; Di Blasi, S.; Matese, A.; Primicerio, J.; Vaccari, F.; Genesio, L. Airborne high-resolution images for grape classification: changes in correlation between technological and late maturity in a Sangiovese vineyard in Central Italy. *Australian Journal of Grape and Wine Research* **2012**, *18*, 80-90.

179. Urretavizcaya, I.; Royo, J.B.; Miranda, C.; Tisseyre, B.; Guillaume, S.; Santesteban, L.G. Relevance of sink-size estimation for within-field zone delineation in vineyards. *Precision Agriculture* **2016**, *18*, 133-144, doi:10.1007/s11119-016-9450-0.

180. Bonilla, I.; de Toda Fernández, F.M.; Casasnovas, J.A.M. Vine vigour, yield and grape quality assessment by airborne remote sensing over three years: Analysis of unexpected relationships in cv. Tempranillo. *Spanish journal of agricultural research* **2015**, 15.

181. Serrano, L.; González-Flor, C.; Gorchs, G. Assessment of grape yield and composition using the reflectance based Water Index in Mediterranean rainfed vineyards. *Remote sensing of environment* **2012**, *118*, 249-258.

182. Ferrer, M.; Echeverría, G.; Pereyra, G.; Gonzalez-Neves, G.; Pan, D.; Mirás-Avalos, J.M. Mapping vineyard vigour using airborne remote sensing: relations with yield, berry composition and sanitary status under humid climate conditions. *Precision Agriculture* **2019**, 1-20.

183. Naidu, R.A.; Perry, E.M.; Pierce, F.J.; Mekuria, T. The potential of spectral reflectance technique for the detection of Grapevine leafroll-associated virus-3 in two red-berried wine grape cultivars. *Computers and Electronics in Agriculture* **2009**, *66*, 38-45.

184. MacDonald, S.L.; Staid, M.; Staid, M.; Cooper, M.L. Remote hyperspectral imaging of grapevine leafroll-associated virus 3 in cabernet sauvignon vineyards. *Computers and electronics in agriculture* **2016**, *130*, 109-117.

185. Vanegas, F.; Bratanov, D.; Powell, K.; Weiss, J.; Gonzalez, F. A Novel Methodology for Improving Plant Pest Surveillance in Vineyards and Crops Using UAV-Based Hyperspectral and Spatial Data. *Sensors (Basel)* **2018**, *18*, doi:10.3390/s18010260.

CHAPTER 2: MATERIALS AND METHODS

2.1 Vineyard selection and vineyard GPS-delineation

2.1.1 Overview

This project involved six Cabernet franc vineyard blocks located within the Niagara Peninsula of Ontario, Canada. Several Niagara sub-appellations were represented in this study, in transects from Lake Ontario to the Niagara Escarpment where soils in the region have high variation because of large-scale glacial movement. As a result, many vineyards are planted on different soil types from moderately-well drained Chinguacousy to poorly-drained Beverly/Toledo soils that can differ considerably in soil properties.[1] A variety of cultural practices such as training systems, water, floor, canopy management were also observed in the vineyards studied, as well as the overall layout of the blocks. Within each vineyard, a grid of geolocated sentinel vines (72-81 vines) was plotted in an 8m x 8m grid then its location was pinpointed via a handheld GPS receiver (Raven Industries, Sioux Falls, SD).

Since the manual collection of some variables from the research vines was labour intensive and costly, not all sentinel grapevines per site could be sampled, representative vines (15-20 vines) were selected per vineyard block for measurements of leaf water potential (Ψ), bud cold hardiness (LT50 (°C)), stomatal conductance (Gs), and virus presence. All six vineyard sites were used in chapters 3 feasibility study of remote sensing NDVI analysis to manage vineyard variation, chapter 4 feasibility study of remote sensing technologies to monitor yield and fruit qualities, and chapter 5 feasibility study of remote sensing NDVI analysis to detect oenologically relevant vineyard zones. Only vineyards (site 1 and 2) to contain GLRaV positive vines by Real Time RT-qPCR

were used in chapters 6 feasibility study of remote sensing technologies to detect grapevine virus presence.

2.1.2 Vineyard description

2.1.2.1 Site 1 vineyard in the Niagara Lakeshore

The vineyard is situated in the Niagara Lakeshore sub-appellation, several km south of Lake Ontario. Soil series is predominantly Jeddo 8, which is are moderate drained glacial till clay loam with moderate sand content.[1] This block planted in 1987 with 3309 rootstock is 0.78ha in area with 76 sentinel vines. It has Double Guyot training system with spacing 1.45m between vines and 2.8m between rows and drainage-tiled under every second rows with permanent grass for between row management.

2.1.2.2 Site 2 vineyard in the Beamsville Bench

The vineyard is situated in the Beamsville Bench sub appellation within the glacially formed slopes of the Niagara Escarpment. The soils at this site a poorly drained and primarily composed of Chinguacousy clay loam till, with some nearby Oneida clay loam deposits.[1] The surrounding ridges are scattered with naturally formed limestone caves and underground mineral rich spring water. The vineyard has a moderate north facing slope towards the foot of the Escarpment that offers excellent air movement and exposure to lake effect breezes. This block was planted in 1999 with 101-14 rootstock is 1.54ha in an area with 75 sentinel vines. It has Double Guyot training system with spacing 1.45m between vines and 2.7m between rows and drainage-tiled under every other row with permanent grass for interrow cover-crop.

2.1.2.3 Site 3 vineyard in the St. David's Bench

The vineyard is situated on the St. David's Bench sub appellation in Niagara-on-the-Lake. The soils at this site are imperfectly drained and primarily composed of Toledo and Beverley clay loam till with some Cashel and Peel clay loam.[1] The vineyard has a moderate north facing slope from the Niagara Escarpment towards Lake Ontario and benefits from cool lake effect breezes. This block planted in 1992 with 3309 rootstock is 2.29ha in area with 80 sentinel vines. It has Double Guyot training system with spacing 0.9m between vines and 2.5m between rows. The only vineyard block in this study with spur pruning system and with soil cultivated interrow, is every row equipped with drainage tiles.

2.1.2.4 Site 4 vineyard in the Lincoln Lakeshore

The main vineyard site is situated on the south shore of Lake Ontario west of Vineland, ON, and is located in the Lincoln Lakeshore sub appellation. Soil series is primarily Chinguacousy 14, which is an moderately drained glacial till soil with high sand and stone content.[1] This block planted in 1995 with SO4 rootstock is 0.9 ha in area with 72 sentinel vines. It has Double Guyot training system with spacing 1.45m between vines and 2.7m between rows and drainage-tiled under every other row with permanent grass for interrow cover-crop.

2.1.2.5 Site 5 vineyard in the Lincoln Lakeshore

The vineyard site is situated in Beamsville, Ontario on the east side of Tufford Rd, the southern portion of the Lincoln Lakeshore sub appellation. Varieties grown are primarily Cabernet franc and Cabernet Sauvignon. Soil series is predominantly poorly drained Trafalgar 7, a high clay lacustrine clay loam soil.[1] This block planted in 2006 with SO4 rootstock is 1.15ha in area with 81 sentinel vines. It has Double Guyot training system with spacing 1.72m between vines and

2.75m between rows and drainage-tiled under every other row with permanent grass for interrow cover-crop.

2.1.2.6 Site 6 vineyard in the Four Mile Creek

The vineyard site is situated on Line 2 in Niagara-on-the-lake. Soil series are mainly Chinguacousy 14 and 15, which are glacial till soils with high percentages of sand and stones. They are considered moderately drained.[1] This block planted in 2000 with 3309 rootstock is 1.81ha in area with 80 sentinel vines. It has Double Guyot training system with spacing 1.2m between vines and 2.5m between rows and drainage-tiled under every other row with permanent grass for interrow cover-crop.

2.1.3 Vineyards GPS-delineation

As sentinel vines, the research vines were selected to be typical vine in the site, were healthy, and were situated to the north and the south orientation. Vine flags and Invicta 115 GPS receiver (Raven Industries, Sioux Falls, SD) technology were applied to geolocate the sentinel vines. The Invicta 115 receiver provides a 1 to 1.4m accuracy, which was improved further with a subsequent adjustment with the Port Weller, Ontario base location, resulting in a closing precision of 30 to 50 cm.

2.2 Remote sensing data collection

In this study, three different methods were used to measure electromagnetic reflectance and emission from grapevine leaves: first, proximal remote sensing interpreted as ground-based remote sensing from a sensor mounted on a mobile platform in the vineyard; second, airborne

remote sensing as multispectral digital image collection from a remotely piloted aircraft system; and, last, field spectrometry using a hand-held non-imaging spectrometer on individual leaves.

2.2.1 Remotely piloted aircraft system (RPAS)

RPAS of the eBee Classic from Parrot group, in Switzerland was flown during veraison in 2015 and 2016 with an altitude of 90 m and a maximum speed of 60 km/h. A set of Sequoia multispectral sensors and a set of Sequoia thermomap sensors (Parrot Group, Switzerland) were selected for gaining spectral data, the former equipped with an incident light sensor operating at a resolution of 1.2 megapixels (1280 x 960 pixels), pixel size of 3.75 μm, representing a resolution of 8.47 cm in 90 m altitude in the visible and near-infrared (NIR) region of reflectance with four wide bands (green: 530-570 nm, red: 640-680 nm, red edge: 730-740 nm, and the near infrared: 770-810 nm) and the latter analyzing thermal-infrared spectrum (TIR) range emission covering 7000 to 16000 nm at a resolution of 0.3 megapixels (640 X 512 pixels), pixel size of 17 μm, representing a resolution of 17 cm in 90 m altitude. Additionally, the aircraft featured a GPS receiver, radiation monitor estimating inbound radiation, and inertial system for maintaining the alignment and positioning of imaging. The RPAS also had an autopilot system that provided a visual range of 1000 m and a radio range of 5 km. The vehicle was powered by an electric motor with a battery life of 50 minutes.

Air-Tech Solutions, Inverary, ON, provided a RPAS and its ground control station for real-time tracking and collection of images over each vineyard patch. The RPAS was equipped with a GPS receiver, sunshine sensor measuring incoming radiation, and an inertial station ensured verticality and orientation of images by correcting anomalies in flight attitude (i.e., yaw, pitch, and roll). Based on the data from the inertial station and radiation sensor, geometric and imaging

adjustments were performed for geometry, reflectivity, image distortions, sun exposures, and vignetting effects in radiometric. A geometric correction using ground control points (GCPs) was performed to adjust the geometry of the image and adjust the bidirectional reflectance for ensuring the accuracy and consistency of data. Geometric distortions caused by changes in RPAS attitude and altitude were corrected using the information provided by the inertial station. Radiometric correction was performed to correct effects of vignetting. Data were also adjusted for the input of the sunshine sensor before VI generation. A sample of detailed radiometric and geometric calibration information is shown in appendix Table 1.

NDVI and other indices were calculated from the mosaics assembled from the images acquired on each phase of each flight by choosing overlapping pixels near nadir to minimize the problems of angle distortion and directional effects during the images acquisition. The RPAS was used to collect data presented in chapters 3 feasibility study of remote sensing NDVI analysis to manage vineyard variation, chapter 4 feasibility study of remote sensing technologies to monitor yield and fruit qualities, chapter 5 feasibility study of remote sensing NDVI analysis to detect oenologically relevant vineyard zones, and chapters 6 feasibility study of remote sensing technologies to detect grapevine virus presence.

2.2.2 GreenSeeker® (proximal sensing)

GreenSeeker® RT100 (Trimble, Englewood, CO) were attached to the chassis of a GatorTM Utility Vehicle (John Deere) with adjusted height to the canopy and with its red and NIR range active optical sensors, GreenSeeker® measures NDVI using the formula (NIR-red)/(NIR+red). The optical sensors were equipped with electroluminescent diodes (LED) that pulse high intensity electromagnetic (EM) radiation at 100 Hz for both 660 ± 10 nm (Red) and 770

± 15 nm (NIR) spectrums. The sensors collect 100 scans per second with 60 cm scope (± 0.112 cm). It also differentiated between natural and pulsed illumination, thereby eliminating any interference from outdoor light situations. For adding exact spatial coordinates to each reading, they were also enhanced by an AgGPS® 162 dual channel transmitter from Trimble (Englewood, CO), with live positioning adjustments. NDVI data was recorded as the GatorTM traveled up and down each row (9 ft spacing) and measurements are unaffected by driving speed and direction.[2]

To filter out any off-boundary readings, the georeferenced data was transferred to Trimble Farmworks and ArcMap 10.6 as well as setting a minimum NDVI of 0.40 to eliminate data without plant vegetation.[2] The GreenSeeker proximal sensing was used in chapter 4 feasibility study of remote sensing technologies to monitor yield and fruit qualities.

2.2.3 Hand-held spectrometer

With a portable spectrometer model EPP2000C-100 and SpectraWiz software (StellarNet Inc., Tampa, FL), the reflectance spectra of the leaves were obtained and analyzed with a 400-850 nm range and a resolution of 10 nm per pixel. In this experiment, a 5-watt halogen bulb illuminated the entire surface of a leaf placed on a dark plate, and a fiber optic cord designed to capture the reflected spectra at 45°angle to the leaf surface. An optical spectrum of the white and dark surface was referenced frequently at every 10th measurement using a white Teflon® square and black surface pad. This equipment was used in chapters 6 feasibility study of remote sensing technologies to detect grapevine virus presence.

The spectral measurement was performed in September 2017 after the virus presence data for three strains of GLRaV-1, 2, and 3 had been obtained from Real-Time RT-qPCR test by Molecular biology lab at University of Guelph (Guelph, ON). A total of 150 leaf samples

comprising 75 leaf samples from each site (25 from healthy vines, 25 from asymptomatic vines, and 25 from symptomatic vines) were measured from the two different GLRaV3 infected sites and were pictured in the photos shown in Figure 2.1.

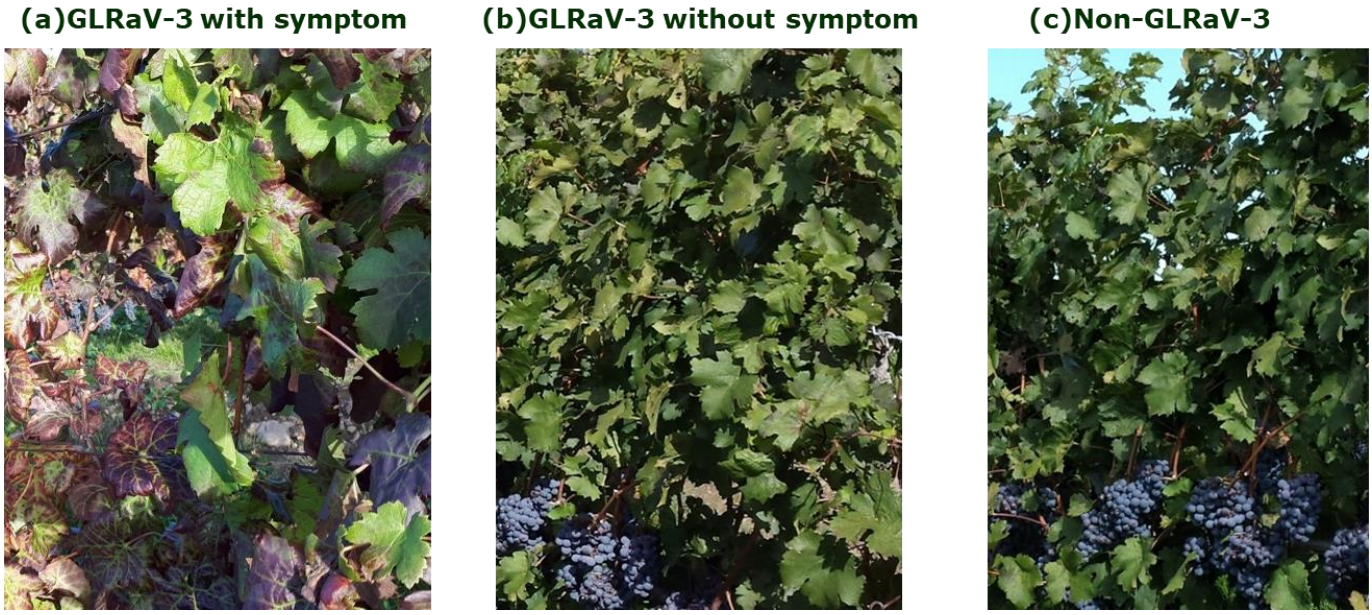

Figure 2.1. Photos of Cabernet franc leaves: a) GLRaV-3 positive symptomatic leaves, b) GLRaV-3 positive asymptomatic leaves, and c) GLRaV-3 negative leaves.

The virus-positive Cabernet franc leaves demonstrated common signs of GLRaV-3 during scouting spectral measurements by the hand-held spectrometer in September 2017 [Figure 2.1 (a)]. Previous study indicated that a visual symptom of GLRaV infection was distinct at later season.[3,4] Therefore, the late growing season measurements were used to distinguish asymptomatic leaves from symptomatic leaves. On the leaf blades of infected grapevines, the interveinal spaces contained purple pigmentation and veins appeared to have a slight band of greenish tissue on both sides. However, some GLRaV-3 positive vines remained asymptomatic [Figure 2.1 (b)]. All grapevines that tested negative for GLRaV-3 had healthy leaves without any virus symptoms

[Figure 2.1 (c)]. The spectral data were exported to a spreadsheet and further statistical analyses were applied to these data (see section 2.9.7).

2.3 Manual data acquisition from traditional methods of monitoring vineyard variation

The measurements outlined below in section 2.3.1 and 2.3.2 were used in chapter 3, feasibility study of remote sensing NDVI analysis to manage vineyard variation, over the three years (2015, 2016, and 2017) with exception of LT50 (2015 and 2016) and stomatal conductance (2016 and 2017). The measurements in section 2.3.3.1 were tested on leaf samples in 2016 and in 2.3.3.2 were tested on cane samples in 2018 and both measurements were used in chapter 6, feasibility study of remote sensing technologies to detect grapevine virus presence.

2.3.1 Measures of water status

2.3.1.1 Soil moisture (SM)

A TDR 300 model from Spectrum Tech. (East Plainfield, IL) in VWC mode, with electrodes of 20 cm length, was used to collect SM at the ground near each sentinel vine. A common method for measuring SM is time-domain reflectometry (TDR) as it is fast, damage-free, and precise in a wide range of soils.[5] With the oscillatory dielectric and electric nature of soil, TDR sends pulses of energy to the soil and measures the return speed as negatively correlated with the moisture content in soil. The result is a measure of SM in soil as a proportion of moisture to the overall soil volume. Within a 10 cm radius of each vine, soil samples were taken from both sides and the average values were calculated from three measurements in 2015 and 2016 and two measurements in 2017 of berry set, lag phase, and veraison.

2.3.1.2 Leaf water potential (LWP, ψ)

In this study, mid-day LWP was measured with the pressure bomb method. As transpiration occurs and water evaporates from the stomata, there is a build-up of water stress in the xylem because of drought conditions and an indication of leaf water potential can be obtained by applying pressure to a leaf until droplets of water have resurfaced at the petiole tip.[6,7] The study vines were chosen within each subset of sentinel vines to establish a rectangular grid layout over the sites. LWP was measured from only the selected ~15-20 water status vines per block. To ensure consistency, the readings were undertaken at solar noon hours from 10 AM to 2PM each day when the sun exposure was full capacity.[8]

To establish precision and stability of measurements, an average of at least three leaves per vine was taken, and leaves were selected from an undamaged primary shoot, mature leaves, mid canopies, and fully exposed leaves. The sampled leaf was inserted instantly in the chamber of Model 3015G4 pressure bomb (Santa Barbara, CA) with edge of petiole uncovered and a steady increase in pressure (bar) was observed as nitrogen was slowly released into the chamber.

2.3.1.3 Stomatal conductance (Gs)

Gs was also recorded on selected vines using a porometer; the parameter is highly dependent on the plant's photosynthetic capacity and plant water status, and relates to sun exposure, turgor and vapor pressure difference, temperature, and atmospheric CO_2 concentrations.[9] Model SC-1 leaf porometer from Decagon Devices Inc (Pullman, WA) assessed Gs in mmol/m ^{2} s and it was calibrated with a tool supplied by the producer. To establish accuracy and reliability, three leaves of each vine were selected from an undamaged primary shoot, mature leaves, mid canopies, and fully exposed leaves.

2.3.2 Measure of grapevine performance

2.3.2.1 Vine size

During the winter months in each location, weights of pruned canes were recorded per vine to determine vine size.[10] A digital hanging scale was used to systematically weigh each vine's pruned canes in the field immediately after pruning, providing a weight in kilograms.

2.3.2.2 Winter hardiness (LT50)

This study assessed LT50 for the 15 to 20 sentinel vines per site in 2015 and 2016. Two selected canes were taken from each vine for later differential thermal analysis, a technique commonly used to determine how hard a plant's tissues are to freeze.[11] With an artificially frozen bud LT50 method, which identifies the temperature point at which 50% of its primary bud is killed, the measurements were conducted at three different stages from January to March. Five healthy buds close to the bottom of each collected cane were taken by cutting boundary of cane bark and the bud.[11] Each bud was placed on a sample plate and soaked in moist sheets.[11] The plates contained a thermometer to measure the average temperature[12] and each unit included a silicon thermocouple sensor to measure the exothermic spikes, which occur when it freezes[11]. Afterward, the plates filled with buds were placed in computer-controlled freezers which started at 4 °C and dropped by 4 °C every hour to -40 °C, and the LT50 was determined for each plate.

2.3.3 Measure of grapevine virus presence

2.3.3.1 Virus presence for grapevine leafroll-associated virus (GLRaV)

Three variants of GLRaV-1, 2 and 3 were tested for virus presence. In September 2016, three leaves were sampled from three different sections of vine canopy for virus PCR tests at the Molecular Biology lab at University of Guelph (Guelph, Ontario). The leaves were powdered and

placed in liquid nitrogen and frozen at -80 °C. GLRaV-3 presence was calculated from Real-Time RT-qPCR results, where a higher score reflects less virus presence. In this study, actin was applied as a reference gene, a reliable marker for grapevines' response to a stress.[13]

2.3.3.2 Virus presence for grapevine red blotch virus (GRBV)

The virus presence was measured for a strain of GRBV. Two mature canes from each side of the cordon per vine were sampled in December 2018. Virus presence/absence was measured at virus testing services, Cool Climate Oenology and Viticulture Institute, Brock University, St. Catharines, ON using Endpoint PCR. DNA was extracted from composite cane samples using the DNeasy® kit by Qiagen Inc. (Valencia, CA); The samples were PCR screened using two pairs of GRBV-specific primers: GVGF1 and GVGR1 to amplify a DNA fragment containing the V1 and V2 genes[14], and GRLaV-4 For and GRLaV-4 Rev to amplify portions of the replicase gene and other genomic segments[15].

2.4 Yield and fruit composition data acquisition

2.4.1 Yield data

The yield data was collected in three consecutive years (2015, 2016, and 2017) in chapter 4, feasibility study of remote sensing technologies to monitor yield and fruit qualities. To capture yield data, sentinel grape vines were harvested as close as possible to commercial harvesting dates, and all vines were handpicked into plastic containers, and it was recorded how many clusters were harvested per vine. The weight of containers from each vine was measured via the mobile scale to calculate the amount (kg) of yield per vine. To determine mean berry weight, The sampled clusters included 100 frozen berries, which were weighed to determine their weight(g) and stored at -25 °C to proceed with analysis of the berries.

2.4.2 Basic fruit chemistry

Basic fruit chemistry was tested on all fruit collected in 2015, 2016, and 2017 in the thesis in chapter 4, feasibility study of remote sensing technologies to monitor yield and fruit qualities.

2.4.2.1 Brix, pH, and titratable acidity

In this study, frozen grape samples were heated in the Isotemp 228 heated-water incubator from Fisher Scientific (Mississauga, ON) for 30 minutes at 85 °C before a juicer was used to squeeze them after filtering the juice to eliminate any particles, the acidity and Brix were determined with Model 25 pH meter from Denver Instrument Inc. (Denver, CO) and Abbé refractometer model 10450 from American Optical (Buffalo, NY). The centrifuged juice acquired from the IEC Centra CL2 from International Equipment Company (Needham Heights, MA) was titrated to pH 8.2 with 0.1 NaOH via PC automatic titrator from Man-Tech (Guelph, ON) to determine titratable acidity (TA).

2.4.2.2 Total phenols

A micro method of Folin-Ciocalteu reagent was applied to calculate the total phenol contents in the grape juice samples.[16,17] After diluting the juice 10 fold, 20µL of this mixture were transferred to the solution of 1.58 mL of water with 100µL of Folin-Ciocalteu reagent from Sigma Aldrich (St. Louis, MO) and heated for 8 minutes. In the next steps, 300µL of sodium carbonate solution (NaCO3) were poured, blended again, and left in the dark at 20 °C for 2 hours. The absorbance at 765 nm was then obtained from the solution, and from the standard curve, the phenol concentration was calculated.

2.4.2.3 Total anthocyanins

In this study, a pH shift technique was applied to quantify anthocyanins in grape.[18] Juice samples were diluted with nine mL of each buffer solution (pH1.0 and pH4.5) and left to equilibrate for an hour in the dark prior to measurement with an 2100 pro UV/Vis spectrophotometer from Biochrom Ltd. (Cambridge, UK). According to the given formula [18], anthocyanin concentration (mg/L) was determined as: A520 (pH 1.0 - pH 4.5) X 255.75.

2.5 Delineate vineyard zone by high and low NDVI data from multispectral sensor on RPAS

The spatial distribution of NDVI in each site was displayed using ESRI (Redlands, CA)'s ArcMap 10.6, and the maps were created via the inverse-distance-weighted (IDW) technique discussed in the next section. This study assigned low and high NDVI zones for each site based on a different threshold value, with approximately the same numbers of vines in each zone, which was randomly selected around the midpoint of the NDVI distribution.

Each vineyard site was divided into two NDVI zones with three field replicates based on the 2016 RPAS NDVI (remote sensing) interpolated maps: high NDVI zone: green colour and low NDVI zone: red colour (Figure 2.2). To maintain consistency between the years (2016 and 2017), the NDVI zonal maps were the same in both years. This technique was applied to data collected in chapters 5, feasibility study of remote sensing NDVI analysis to detect oenologically relevant vineyard zones.

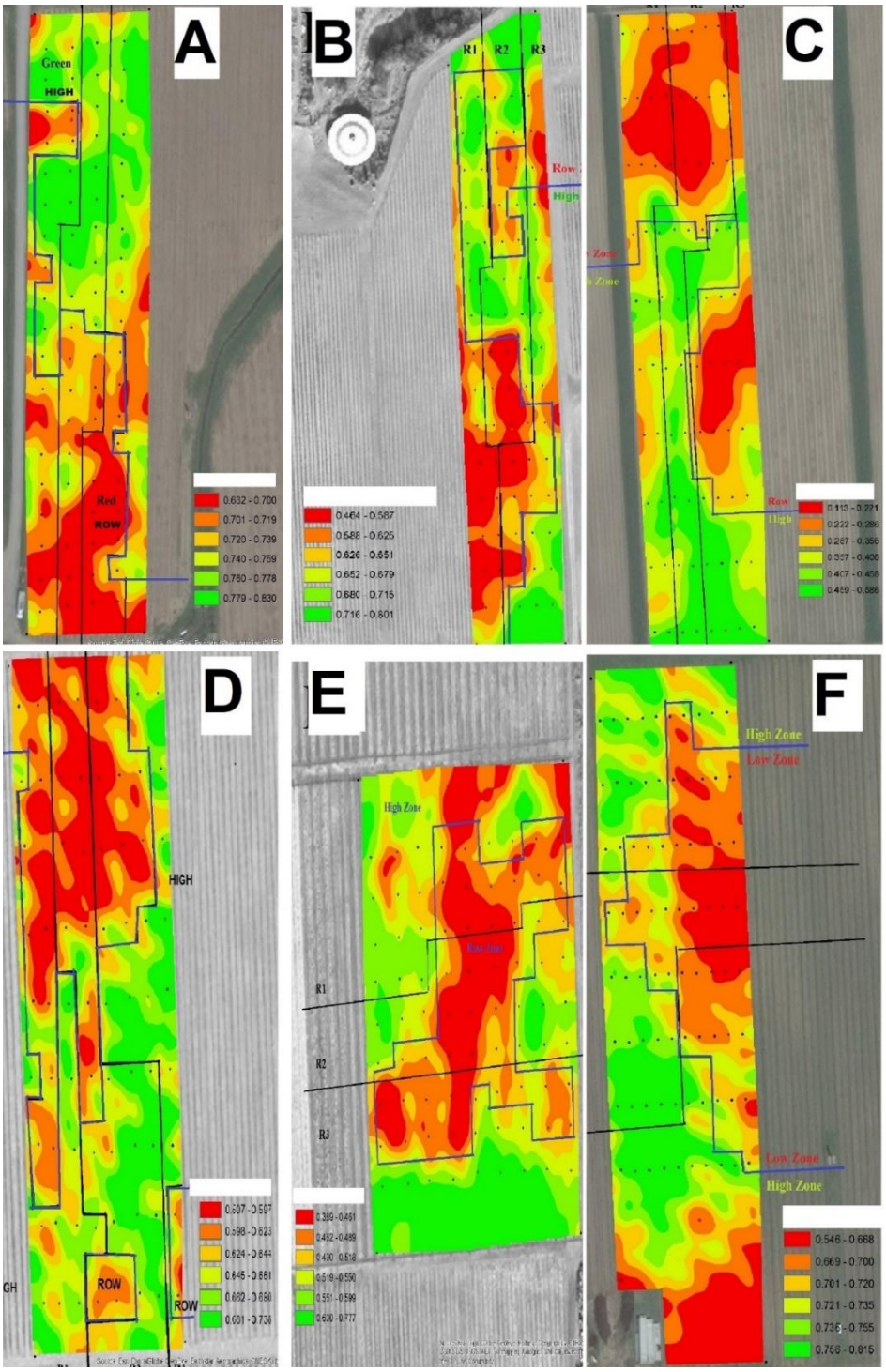

Figure 2.2. Maps of different NDVI zones (low and high) from RPAS flights used for Cabernet franc winemaking. Maps were created in ArcMap 10.6. Legend: A: site 1 in the Niagara Lakeshore; B: site 2 in the Beamsville Bench; C: site 3 in the St. David's Bench; D: site 4 in the Lincoln Lakeshore; E: site 5 in the Lincoln Lakeshore; F: site 6 in the Four Mile Creek.

2.6 Harvesting and winemaking

Wine was made from harvested grapes in 2016 and 2017 as outlined in Chapter 5, feasibility study of remote sensing NDVI analysis to detect oenologically relevant vineyard zones. Harvested grapes from different NDVI zones (low and high) were brought to Brock research winery and the grape-must was extracted by destemming and crushing process. 250 mL samples per replicate and treatment were collected for wine chemical analysis. To optimize flavour and colour extraction, the musts were chilled at 1 °C for a day with treating 0.05 g/L of Lafase® HE Grand Cru enzyme from Laffort (France), along with 25 ppm of potassium metabisulfite.

To perform a rehydration of yeast, the must was mixed with 0.4 g/L of Fermol Rouge yeast and 0.45 g/L of FermoPlus Energy GLU yeast nutrition from AEB Group (USA). After fermentation in the thermally regulated cells at 25 °C was complete, the musts from each site and treatments were then pressed into labeled 20 L carboys using a wine bladder press to a high of 2 bars and allowed to sit for two days at ambient temperature before racking into clean carboys, adding 25 ppm of potassium metabisulfite, and chilling to -1 °C to allow cold precipitation for a couple of months. Finished wines with 25 ppm of final SO_2 addition were filled manually and bottled with an automatic corking machine (San Vito, Italy). After being bottled with an additional 25 ppm of potassium metabisulfite, the finished wines were kept in a climate-regulated wine cellar for one and half year for 2016 vintage and half year for 2017 vintages before the sensory sorting test.

2.7 Wine composition and sensory analysis

2.7.1 Basic wine chemistry

Basic wine chemistry was measured for wines produced in 2016 and 2017 presented in chapter 5, feasibility study of remote sensing NDVI analysis to detect oenologically relevant vineyard zones. The methods to analyze Brix, pH, titratable acidity, total phenols, and anthocyanins were given in sections 2.4.2.1 to 2.4.2.3. GC-FID analysis of ethanol was performed at CCOVI's analytical services lab using an HP 6890 series gas chromatograph and a Carbowax column from Agilent Technologies (Santa Clara, CA).

2.7.2 Sensory sorting test

Sensory sorting test of wines was performed on wines from 2016 and 2017 vintages presented in Chapter 5, feasibility study of remote sensing NDVI analysis to detect oenologically relevant vineyard zones. The Research Ethics Board at Brock University approved the study and all panelists had provided informed consent before participation and the approval number is **REB 17-013**. It is well-documented that sensory sorting tests have been conducted on a wide range of alcoholic and non-alcoholic beverages[19-21], and it yields comparable outcomes to other sensory evaluation methods without the requirement of panel training[22].

In September 2018, wine samples from low vs high NDVI vineyard zones were sorted by 19 panelists from Brock students and staff as well as Niagara wine industry members and both 2016 and 2017 vintages were tasted simultaneously. All the panelists who were actively engaged in the wine sector were regarded as knowledgeable wine drinkers despite their lack of training. Both vintages were presented by the same panelists to eliminate the impact of variations among panelists on different years, and randomly, the order of site presentations was chosen.

Using Compusense® sensory testing from Compusense Inc. (Guelph, ON), sorting sessions were conducted in Brock's wine sensory lab involving six different sites, each with two wines of High NDVI and Low NDVI, and their corresponding three wine replicates. Compusense® requested the panelists to sort the wines by the same sensory attribute, without specifying what attributes to use and additionally, the sorting task also specified to create at least two groups and no more than five groups, to prevent all wines being grouped together nor isolated. Each panelist had approximately one to two hours for each session, with mandatory 20-minute breaks between each of the first three flights.

2.7.3 Sensory descriptive analysis

Sensory descriptive analysis of wines was performed on wines from 2016 vintages presented in Chapter 5, feasibility study of remote sensing NDVI analysis to detect oenologically relevant vineyard zones. The Research Ethics Board at Brock University approved the study and all panelists had provided informed consent before participation and the approval number is **REB 17-013**.

Descriptive analysis was conducted on the 2016 Cabernet franc wines with two treatments (low and high NDVI) and triplicates from each treatment from February 2019 until April 2019. Panelists were recruited from students of the Oenology and Viticulture program, as well as staff members from Brock University. The panelists consisted of undergraduate students, graduate students, PhD candidates, and staff, with varying degrees of experience in descriptive analysis panels. The panel was formed of nine judges, involving six females and three males. All panelists underwent six weeks of training consisting of six hours total, across six sessions.

In the first session, the panelists generated a comprehensive list of descriptive attributes found within the wine samples. In the following session, the panelists underwent a group discussion to generate a representative list of attributes which best described the wines. During sessions three and four, the panelists generated and adjusted aroma standards and terminology. No reference standards were prepared for the physical, flavor, and taste attributes. The attributes selected for the analysis and the corresponding aroma standard 'recipe' can be found in Table 2.1 and 2.2, respectively. In the final two weeks of training, the panelists were introduced to line scaling and Compusense® sensory testing from Compusense Inc. (Guelph, ON).

Table 2.1. Sensory attributes of the 2016 Cabernet franc wines from different NDVI zones (high and low) generated during descriptive analysis.

Orthonasal Descriptors	**Retronasal Descriptors**	**Taste Descriptors**
Red Fruit	Red Fruit	Colour Intensity
Dried Fruit	Dried Fruit	Colour Clarity
Dark Fruit	Dark Fruit	Acidity
Floral	Vegetal	Alcohol
Vegetal	Herbaceous	Astringency
Herbaceous	Spice	Bitterness
Spice	Earthy	Sweetness
Earthy	Tropical	
Tropical		

Table 2.2. Aroma reference standards used during descriptive analysis of Cabernet franc wines from different NDVI zones (high and low).

Attribute	Aroma Standard*
Red Fruit	10 mL fresh strawberry juice and 10 mL of fresh raspberry juice
Dried Fruit	80 mL of no name prune nectar, 6 pitted dried prune, and 15 seedless Thompson raisins
Dark Fruit	20 mL of fresh blackberry juice, 10mL of fresh blueberry juice, 25 mL of Ribena Concentrated Blackcurrant beverage, 40 mL of OASIS berry pomegranate juice
Floral	100mL of phenyl ethanol and 2 mL of cis-rose oxide
Vegetal	Additional 25 0mL of base wine, 30mL of juice from No Name French cut seasoned green beans, and 1 TBS of frozen PC® small, sweet peas
Herbaceous	2.8 g of organic cat grass, 4 fresh green beans, 1/4 leaf of fresh mint
Spice	0.1 g of ground coriander, 0.2 g of ground cloves, 0.05 g of all spice, 0.05 g of anise seed, and 0.05 g of cinnamon
Earthy	25 mL of fresh earth/soil collected from the forest floor, 10 g of wet leaves collected from the forest floor, and 5mL of mushroom stock solution **
Tropical Fruit	70 g of frozen PC® mango and peach fruit blend

* The aroma standards were mixed with standard wine (Cabernet franc) and stored at 4 °C before the sensory test

**500 mL of base red wine with 10 μL of 1-octen-3-ol

Using Compusense® sensory testing, the final descriptive analysis was performed in Brock's wine sensory lab. Panelists evaluated the wines in individual booths, using clear ISO glasses. Based on a Williams design, the wines from different NDVI zones were provided to the judges with a three-digit blind code in a random order. The panelists underwent six sensory evaluation sessions in total. A maximum of six wines were presented in session and there was a

mandatory two-minute break after each sample. Filtered water, unsalted crackers and spittoons were provided at all sessions. Panelists were reminded at each session to use the aroma standards as references. All attributes were scored on a 15 cm intensity scale with anchor terms 0.5 cm from each end. The anchor terms consisted of 'low' or 'absent' on the 0, and 'high' on the 15.

2.8 Wine aromatic compound analysis (GC-MS)

Wines produced from 2016 and 2017 were evaluated for wine aromatic compounds with data presented in chapter 5, feasibility study of remote sensing NDVI analysis to detect oenologically relevant vineyard zones.

2.8.1 Sample extraction

SBSE method, marketed as Twister® from Gerstel (Baltimore, MD), was used to extract volatiles from the aqueous solution of a wine sample. Each wine sample was spiked with 100 g/L n-dodecanol in GC-grade dichloromethane as an internal control.

2.8.2 Gas chromatography−mass spectrometry (GC-MS)

In this study, a gas chromatograph-mass spectrometer model 6890N/5975B with Agilent HP-5MS column (30, 0.25 mm and 0.25 μm) from Agilent Technologies (Santa Clara, CA) was used to analyze key odor active compounds in wines from different NDVI zones. Helium of purity 5.0 was used as the carrier gas (Praxair, Mississauga, Ontario) and the matrix scanning mode of the MS detector was used for chemical identification and SIM mode of the detector to measure the ions on each chemical (Table 2.3).

Table 2.3. Key odor active compounds of Cabernet franc wine for GC-MS analysis.

NO	Compound	CAS	RT/min	Quantitative ion (m/z)	Qualitative ion (m/z)	Group	Group ion
1	2-Methyl-1-propanol	78-83-1	8.354	43	42,41,74	1	41, 43, 55, 56, 70, 71, 74, 88
2	Isobutyl acetate	110-19-0	10.155	43	56,73,41		
3	Ethyl butanoate	105-54-4	10.973	71	43,88,41		
4	3-Methyl-1-butanol	123-51-3	11.337	55	42,43,70		
5	Ethyl 2-methylbutanoate	7452-79-1	12.537	57	102,85,74	2	43, 45, 55, 57, 60, 70, 75, 85, 88, 102
6	Ethyl 3-methylbutanoate	108-64-5	12.677	88	57,85,60		
7	Isoamyl acetate	123-92-2	13.727	43	70,55,41		
8	Ethyl lactate	97-64-3	14.81	45	43,75		
9	*cis*-3-Hexenol ((*Z*)-3-hexenol)	928-96-1	15.864	67	41,55,82	3	41, 43, 55, 56, 57, 60, 67, 82
10	1-Hexanol	111-27-3	15.946	56	43,41,55		
11	Acetic acid	64-19-7	16.153	43	45,60,42		
12	*trans*-3-Hexenol ((*E*)-3-hexenol)	928-97-2	16.31	67	41,69,82		
13	*trans*-2-Hexenol ((*E*)-2-hexenol)	928-95-0	16.844	57	41,82,44		
14	*cis*-2-Hexenol ((*Z*)-2-hexenol)	928-94-9	17.098	57	41,82,67		
15	Ethyl hexanoate	123-66-0	18.668	88	43,99,60	4	43, 55, 56, 57, 60, 70, 88, 99
16	Hexyl acetate	142-92-7	19.34	43	56,55,61		
17	1-Heptanol	111-70-6	19.804	70	56,43,55		
18	1-Octen-3-ol	3391-86-4	19.932	57	43,72,55		
19	Benzaldehyde	100-52-7	20.855	77	106,105,51	5	77, 105, 106
20	3-Methylbutanoic acid	503-74-2	23.074	60	43,41,87	6	55, 56, 60, 69, 70, 71, 87, 91, 93, 120, 139
21	Ethyl 2-hydroxy-4-methylpentanoate	53530-26-0	23.258	69	87, 41		
22	*cis*-Rose oxide	3033-23-6	23.416	139	69,41,55		
23	1-Octanol	111-87-5	23.705	56	55,41,70		
24	*trans*-Rose oxide	876-18-6	24.114	139	69,41,55		
25	Linalool	78-70-6	24.364	71	93,55,43		
26	Phenylacetaldehyde	122-78-1	24.491	91	92,120,65		
27	Ethyl octanoate	106-32-1	26.771	88	101,57,127	7	59, 60, 69, 73, 93,101, 121, 139
28	Diethyl succinate	123-25-1	27.961	101	139,55,73		
29	Hexanoic acid	142-62-1	28.098	60	73,41,87		
30	α-Terpineol	98-55-5	28.639	59	93, 121, 136		
31	Citronellol	106-22-9	30.207	69	95, 123, 138	8	69, 91, 92, 93, 95, 122, 123
32	2-Phenylethanol	60-12-8	30.486	91	92,62,122		
33	Nerol	106-25-2	30.673	69	93,68,67		
34	Ethyl phenylacetate	101-97-3	31.002	91	65,164,92	9	69, 91, 93, 104, 105, 123, 164
35	Phenylethyl acetate	103-45-7	31.623	104	43,91,105		
36	Geraniol	106-24-1	31.817	69	41, 93, 123		
37	Ethyl decanoate	110-38-3	34.116	88	101,43,41	10	55, 60, 69, 73, 85, 88, 101, 121
38	Octanoic acid	124-07-2	34.23	60	73,43,55		
39	β-Damascenone	23726-93-4	35.202	69	121,41,105		
40	γ-Nonalactone	104-61-0	36.534	85	41,43,55		
41	Eugenol	97-53-0	38.125	164	103,77,149	11	55, 69, 91, 164, 103, 135, 149, 177
IS	1-Dodecanol	112-53-8	38.134	55	43,69,56		
42	β-Ionone	79-77-6	38.732	177	91, 135, 178		
43	Syringol	91-10-1	39.366	154	139, 111	12	60, 73, 85, 103, 128, 131, 139, 154, 176
44	Ethyl cinnamate	103-36-6	39.634	131	103, 176		
45	Decanoic acid	334-48-5	39.732	60	73,41,43		
46	γ-Decalactone	706-14-9	39.825	85	128		

2.8.3 Identification and quantification

Comparing retention times and mass spectra (of the Wiley library) to the reference standards provided the means for chemical identification, and the multiple calibration curves were tested in synthetic wine to verify accuracy. To quantify a compound, the peak area of the analyte was compared with that of the internal standard.

2.9 Mapping and data analysis

The mapping and correlation analysis in section 2.9.1, 2.9.2, and 2.9.3 were used in chapter 3, feasibility study of remote sensing NDVI analysis to manage vineyard variation and chapter 4, feasibility study of remote sensing technologies to monitor yield and fruit qualities. The data analysis in section 2.9.4, 2.9.5, and 2.9.6 was used in chapter 5, feasibility study of remote sensing NDVI analysis to detect oenologically relevant vineyard zones. The data analysis in section 2.9.7 was used in chapter 6, feasibility study of remote sensing technologies to detect grapevine virus presence.

2.9.1 Mapping and data extraction

The spatial distribution of NDVI and other indices in each site was displayed using ArcMap 10.6, and the maps of the point data collected from the sentinel vines (i.e., yield, berry weight, soil moisture, etc..) were created via the inverse-distance-weighted (IDW) interpolation method. In a spatially discretized way, IDW uses a linearly weighted set of data points to calculate a point's value, where the weighted average of points sampled declines with rising gap from the unsampled location.[23] Several trials were made to identify parameters for IDW that created most accurate maps but at the same time maintained readable and interpretable maps during this study. For

instance, the highest and lowest values of original data were compared to those data from IDW and it only created the projected pattern from local variation and did not interrupt any original dataset.

Two major parameters exist in determining the accuracy of the IDW interpolations: power and search radius. IDW relies mainly on the inverse of the distance between known and unknown locations, raised to a mathematical power, which controls the significance of known points on the interpolated values based on their distance from the output point. A higher power puts more emphasis on the nearest points, and for this study the default value of 2 was used. The search radius controls the input points used in the calculation of each output cell value. For this research, a fixed search radius was used as follows: Standard Sector - Four Sectors with 45° offset; minimum neighbors: 10, maximum: 15.As a data classification method, Quantile breaks were used, which classified the data with the same number of elements in each class, and thereby avoided extraordinarily large or empty classes and facilitating the interpretation of the maps. In remote sensing applications with dense spatial data, diffusion interpolation with a smaller spatial channel enables efficient interpolation and a seamless contour plot using the same class and colour rules as IDW method.

Interpolation spatial methods also enable the extraction of spectral values at the GPS coordinated research vines from surrounding sampled data. For all remote sensing indices creation, the flight data were imported and displayed in ArcMap 10.6 with World geodetic system 1984 and projected in the Universal Transverse Mercator zone 17N. Using the IDW interpolation technique and the extract values to point tool, the resultant data were interpolated and further exported to Microsoft Excel sheets in which each study vine was associated with its dGPS coordinate points as well as data from the remote sensing flight.

2.9.2 Global Moran's I: Spatial autocorrelation

When evaluating the possibility of applying remote sensing data to measure local variations for implementing precision viticulture, it is necessary to investigate a spatial allocation of important variables for vineyard management. Spatially clustered variables may be more appropriate for precision viticulture applications due to the ease of targeting management to larger vineyard clusters/zones rather than sporadically throughout the vineyard. Spatial autocorrelations were performed using the autocorrelation tool, Moran's Global Index, determines whether a pattern expressed is clustered, dispersed, or random. A z-score or a p-value can be utilized to test if the null hypothesis of randomly dispersed data is true or false, and a Moran's I scores from -1 to +1, where plus z-score indicates clustering and minus z-score indicates dispersion.

2.9.3 Correlation-based analyses

In this study, the correlation statistics were done through XLSTAT v2021. The Shapiro-Wilk test was applied to each data to verify normality and any outliers were highlighted on boxplots after careful evaluation of the data variation. Afterward, Pearson's correlations were computed on all vintage and site data at 95% confidence level to find a meaningful relationship between remote sensing data and vineyard variable data. Prior to the next step to perform a principal component analysis (PCA), data were standardized. With PCA, a complex data set can be reduced to simple data that still contains most of the original data, and data correlated with one another can be transformed into principal components, starting with the first component describing most of the variance in the data. Each value in the first two factors was evaluated using the square cosine of the value to determine the level of relationship between the value and the axis, as part of

the PCA analysis. Square cosine near zero of short vectors are indicators that the model does not adequately explain the relationship.

2.9.4 Wine chemistry data analysis (low NDVI vs high NDVI)

A two-tailed t-test was calculated with XLSTAT 2021 on the must and wine chemistry data such as Brix, pH, TA, total phenols, anthocyanins, and ethanol to determine their correlation with different NDVI levels. The difference in treatment means as well as their standard deviations was visualized using column charts. An asterix '*' was placed by a p-value that differentiated the two treatments significantly ($p<0.05$).

2.9.5 Sorting group data analysis

The sensory sorting data analysis was done using the method suggested by Chollet (2014) [24] and Alegre (2017) [25]. Cooccurrence scores from the wine sorting test were calculated for each panelist and were then summed up to determine an overall similarity score. The results were then visualized using multidimensional scaling (MDS) in XLSTAT 2021.[26] Kruskal's stress value was used to determine whether the resulting MDS was acceptable.[27] Low values represent more similarity between data, and a common standard for stress values is 0.2.[24,25]

Further analyses of MDS were conducted by using an agglomerative hierarchical clustering (AHC) based on Ward's algorithm in XLSTAT 2021. The AHC method is a repeated classifier that computes the level of difference across all variables, then groups similar variables together to reduce the agglomeration criterion, and continuing until all variables have been grouped together.[28] It produces a dendrogram, which consisted of a grouping diagram rooted in the class including all variables and the subsequent hierarchical separation of classes.

2.9.6 Key odor active aroma compounds (GC-MS) data analysis

Statistical analysis of the 2016 wine aroma compounds data was conducted through XLSTAT 2021. Differences between the high and low NDVI wines for all key odor active aroma compounds were analyzed using a two-sample t-test. An average of the NDVI treatments for the chemical components was used due to the presentation of data files from the GC. Partial least squares regression (PLSR) analyses were performed to confirm the correlations among the NDVI treatments, the key odor active volatile compounds, which showed a significantly different concentration level in the two-sample t-test and the aroma attributes from the sensory DA for each treatment.

2.9.7 Hand-held spectrometer data analysis

The line graphs of mean electromagnetic (EM) reflectance for leaves from healthy and GLRaV3 infected grapevines were used to display the visual difference between the treatments. The two tailed t-tests and column charts of mean value were also conducted to confirm that different reflectance levels occurred through visible and NIR wavebands among symptomatic, asymptomatic, and healthy leaves.

Remote sensing indices from the multi-spectral data of the RPAS flight in 2016 were also extracted and examined to characterize vine health and GLRaV3 detection (Section 2.10.1). To run correlation-based analyses, designated clean vines by Real-Time RT-qPCR were assigned a "0" and GLRaV3 infected vines were assigned a "1". PCA and Pearson's correlations analysis were performed to compare GLRaV3 presence against the extracted remote sensing indices (Section 2.10.3).

2.10 Methods overview by Chapter

Summary of chapter-specific methodology are listed in sections below.

2.10.1 Methods for Chapter 3 feasibility study of remote sensing NDVI analysis to manage vineyard variation

The representative vines of the vineyard block were selected (Section 2.1) and geolocated (Section 2.1.3) for data collection, and three years (2015, 2016, and 2017) of data collections were completed on the same vines. The measurements of leaf water potential (Section 2.3.1.2), stomatal conductance (Section 2.3.1.3), and soil moisture (Section 2.3.1.1) were taken at the three important physiological phases of grapevine growing season: berry set, lag phase, and veraison. The average values from the three different stages were applied to a correlation analysis to reduce any impacts of temporary weather events on vine water status. To assess a vine size, the weights of pruned canes (Section 2.3.2.1) were measured for the selected vines for three years (2015, 2016, and 2017). The lethal temperature for 50% of buds (LT50, Section 2.3.2.2) was performed to measure the winter hardiness of the selected vines for two years (2015 and 2016). Air-Tech Solutions, Inverary, ON performed RPAS flights during veraison in 2015 and 2016 (Section 2.2.1). The images from a multispectral sensor attached on the RPAS were further converted to the normalized difference vegetation index (NDVI).

Data were analyzed for correlation statistics using Pearson’s correlations and principal component analysis (PCA) for each site and year (Section 2.9.3). The correlations analysis was performed to compare all variables against remote sensing data analysis (NDVI). The spatial autocorrelation of each variable was determined by Global Moran's I (Section 2.9.2), which shows

clustering patterns to evaluate zonal management options. Using interpolation methods, maps were also created in ArcGIS 10.6 to visualize the geographical orientations of each vineyard variable (Section 2.10.1).

2.10.2 Methods for Chapter 4 feasibility study of remote sensing technologies to monitor yield and fruit qualities

The representative vines of the vineyard block were selected (Section 2.1) and geolocated (Section 2.1.3) for yield and berry composition data collection, and three years (2015, 2016, and 2017) data collections were done on the same vines. The grapes of each representative vine were harvested close to the commercial harvest dates and weight of the harvested grapes (kg), number of clusters, and weight of 100 berries(g) for each vine were recorded at the sites (Section 2.4.1). To analyze basic fruit chemistry, five representative clusters from each vine were brought to the laboratory and kept at -25℃.

A John Deere Gator™ utility vehicle mounted with Trimble GreenSeeker RT100 sensors was driven throughout each vineyard block, collecting real-time NDVI of spectral reflectance from the sides of the rows in 2015, 2016, and 2017 (Section 2.2.2). The measurements were taken at the three important physiological phases of grapevine growing season (berry set, lag phase, and veraison) to investigate impacts of vegetation in different physiological stages on fruit production and quality (there was no data collection during the berry set of 2017).

Further analysis (Section 2.4.2) of Brix, pH, TA, total phenols, and total anthocyanins in grapes from each vine was performed and the NDVIs from proximal sensing data in series of 2015, 2016, and 2017 were compared with the yield and berry composition data using PCA and Pearson's correlations analysis.

The spectral reflectance data from multispectral and thermal sensor on RPAS in 2015 and 2016 also applied for the correlation analysis with the yield and berry composition data in 2015 and 2016. The reflectance data were further analyzed to NDVI, Green chlorophyll index (CI green), Red edge chlorophyll index (CI red edge), Red edge normalized difference vegetation index (NDRE), NDVI green (GNDVI), and Ratio vegetation index (RVI) (Section 2.9.1). PCA and Pearson's correlations analysis were performed to evaluate the correlation between the variables (Section 2.9.3). The spatial clustering patterns and correlations of variables were also determined by Global Moran's I and spatial map analysis (Section 2.9.1 and 2.9.2).

2.10.3 Methods for Chapter 5 feasibility study of remote sensing NDVI analysis to detect oenologically relevant vineyard zones

The representative zones of different NDVI level in each vineyard block were selected by NDVI maps created from the spectral reflectance data of RPAS flight in 2016, and data collections and analysis were done on the same NDVI zones in 2017 (Section 2.5). Based on a different threshold value, each site was assigned high and low NDVI zones with approximately the same number of vines in each zone. Separate harvesting and winemaking were performed from each zone and there were three replicates for each of the treatment wines (high and low NDVI, Section 2.6).

The analysis of basic wine chemistry of Brix, pH, titratable acidity, total phenols, anthocyanins, and ethanol from each zone were performed (Section 2.7.1) and the NDVI zonal differences were evaluated by two tailed t-tests. The differences between treatments were visualized by column charts of mean and standard deviation (Section 2.9.4).

A sensory sorting test for the 2016 and 2017 vintages (Section 2.7.2), and sensory descriptive analysis for 2016 vintage (Section 2.7.3) was performed to evaluate the variations in odour and flavour intensity between the NDVI zonal wines. Statistical methods of multi-dimensional scaling (MDS) and agglomerative hierarchical clustering (AHC) for the sorting test results were conducted to cluster similarity between the treatments and its replicates (Section 2.9.5). The principal component analysis (PCA) for the descriptive analysis results was performed to investigate correlations between the different NDVI zonal wines and sensory descriptors (Section 2.9.3).

Wine aroma compounds analysis was performed using gas chromatography–mass spectrometry (GC-MS) and conducted for 2016 and 2017 vintage wines to better understand volatile compound differences between the NDVI zonal wines (Section 2.8) and relate to sensory data. The GC-MS results were further analyzed by two tailed t-tests to investigate a difference in the level of aromatic compounds between low and high NDVI zones (Section 2.9.6). The partial least squares regression (PLSR) for GC-MS and sensory descriptive analysis results was also conducted to confirm correlations between sensory descriptors and key aromatic compounds from the different NDVI zonal wines (Section 2.9.6).

2.10.4 Methods for Chapter 6 feasibility study of remote sensing technologies to detect grapevine virus presence

The representative vines of the GLRaV3 infected vineyard blocks were selected and geolocated for detecting the virus by Real-Time reverse transcription quantitative polymerase chain reaction (RT-qPCR) test and for measuring spectral reflectance by a hand-held spectrometer.

A random sample was taken of upper, middle, and lower leaves of the vines in September 2016 and analysis of GLRaV3 presence of all samples were conducted using Real-Time RT-qPCR (Section 2.3.3.1). A random sample was also taken two mature canes from each side of the cordon per vine sampled in December 2018 and analysis of GRBV presence of all samples were conducted using Endpoint PCR (Section 2.3.3.2).

Spectral measurements of healthy and GLRaV3 infected leaves by the hand-held spectrometer were conducted at veraison in 2017 (Section 2.2.3). The measurements were made for the subset of 150 leaf samples (50 of healthy leaves, 50 of GLRaV3 infected leaves with reddening symptoms, and 50 of GLRaV-3 infected leaves without the symptoms) from the GLRaV-3 infected vineyards. Statistical analysis (Section 2,9.7) of the spectral measurements was conducted through XLSTAT 2021.

2.11 References

1. Kingston, M.S.; Presant, E. *The soils of the regional municipality of Niagara*; Ministry of Agriculture and Food: **1989**.

2. Mazzetto, F.; Calcante, A.; Mena, A.; Vercesi, A. Integration of optical and analogue sensors for monitoring canopy health and vigour in precision viticulture. *Precision Agriculture* **2010**, *11*, 636-649.

3. Naidu, R.A.; Maree, H.J.; Burger, J.T. Grapevine leafroll disease and associated viruses: a unique pathosystem. *Annual Review of Phytopathology* **2015**, *53*, 613-634.

4. Maree, H.J.; Almeida, R.P.; Bester, R.; Chooi, K.M.; Cohen, D.; Dolja, V.V.; Fuchs, M.F.; Golino, D.A.; Jooste, A.E.; Martelli, G.P. Grapevine leafroll-associated virus 3. *Frontiers in microbiology* **2013**, *4*, 82.

5. Guimarães, C.M.; Costa, C.A.G.; Filho, R.R.G.; dos Santos Silva, F.C.; da Assunção, H.F.; Carneiro, L.F.; Pedrotti, A.; Doll, K.M. Moisture Temporal Stability of a Typic Hapludox under Different Uses and Depths. *Agronomy Journal* **2019**, *111*, 2582-2589.

6. Scholander, P.F.; Bradstreet, E.D.; Hemmingsen, E.; Hammel, H. Sap pressure in vascular plants: negative hydrostatic pressure can be measured in plants. *Science* **1965**, *148*, 339-346.

7. Turner, N.C. Measurement of plant water status by the pressure chamber technique. *Irrigation science* **1988**, *9*, 289-308.

8. Williams, L.; Araujo, F. Correlations among predawn leaf, midday leaf, and midday stem water potential and their correlations with other measures of soil and plant water status in Vitis vinifera. *Journal of the American Society for Horticultural Science* **2002**, *127*, 448-454.

9. Jarvis, P. The interpretation of the variations in leaf water potential and stomatal conductance found in canopies in the field. *Philosophical Transactions of the Royal Society of London. B, Biological Sciences* **1976**, *273*, 593-610.

10. Trought, M.C.; Dixon, R.; Mills, T.; Greven, M.; Agnew, R.; Mauk, J.L.; Praat, J.-P. The impact of differences in soil texture within a vineyard on vine vigour, vine earliness and juice composition. *OENO One* **2008**, *42*, 67-72.

11. Wolf, T.K.; Cook, M.K. Cold hardiness of dormant buds of grape cultivars: Comparison of thermal analysis and field survival. *HortScience* **1994**, *29*, 1453-1455.

12. Mills, L.J.; Ferguson, J.C.; Keller, M. Cold-hardiness evaluation of grapevine buds and cane tissues. *American Journal of Enology and Viticulture* **2006**, *57*, 194-200.

13. Coito, J.L.; Rocheta, M.; Carvalho, L.; Amâncio, S. Microarray-based uncovering reference genes for quantitative real time PCR in grapevine under abiotic stress. *BMC research notes* **2012**, *5*, 220.

14. Rwahnih, M.A.; Dave, A.; Anderson, M.M.; Rowhani, A.; Uyemoto, J.K.; Sudarshana, M.R. Association of a DNA virus with grapevines affected by red blotch disease in California. *Phytopathology* **2013**, *103*, 1069-1076.

15. Poojari, S.; Alabi, O.J.; Fofanov, V.Y.; Naidu, R.A. A leafhopper-transmissible DNA virus with novel evolutionary lineage in the family geminiviridae implicated in grapevine redleaf disease by next-generation sequencing. *PloS one* **2013**, *8*.

16. Singleton, V.L.; Rossi, J.A. Colorimetry of total phenolics with phosphomolybdic-phosphotungstic acid reagents. *American journal of Enology and Viticulture* **1965**, *16*, 144-158.

17. Waterhouse, A. Folin-Ciocalteau micro method for total phenol in wine. *American Journal of Enology and Viticulture* **1999**, *28*, 1-3.

18. Fuleki, T.; Francis, F. Quantitative methods for anthocyanins. 1. Extraction and determination of total anthocyanin in cranberries. *Journal of food science* **1968**, *33*, 72-77.

19. Ballester, J.; Dacremont, C.; Le Fur, Y.; Etiévant, P. The role of olfaction in the elaboration and use of the Chardonnay wine concept. *Food quality and preference* **2005**, *16*, 351-359.

20. Parr, W.V.; Green, J.A.; White, K.G.; Sherlock, R.R. The distinctive flavour of New Zealand Sauvignon blanc: Sensory characterisation by wine professionals. *Food quality and preference* **2007**, *18*, 849-861.

21. Chollet, S.; Lelièvre, M.; Abdi, H.; Valentin, D. Sort and beer: Everything you wanted to know about the sorting task but did not dare to ask. *Food quality and preference* **2011**, *22*, 507-520.

22. Cartier, R.; Rytz, A.; Lecomte, A.; Poblete, F.; Krystlik, J.; Belin, E.; Martin, N. Sorting procedure as an alternative to quantitative descriptive analysis to obtain a product sensory map. *Food quality and preference* **2006**, *17*, 562-571.

23. Li, J.; Heap, A.D. A review of comparative studies of spatial interpolation methods in environmental sciences: Performance and impact factors. *Ecological Informatics* **2011**, *6*, 228-241.

24. Chollet, S.; Valentin, D.; Abdi, H. *Free sorting task*; Valera P. & Ares, G.(Eds.). Boca Raton: Taylor and Francis: **2014**; pp. 207-227.

25. Alegre, Y.; Sáenz-Navajas, M.-P.; Ferreira, V.; García, D.; Razquin, I.; Hernández-Orte, P. Rapid strategies for the determination of sensory and chemical differences between a wealth of similar wines. *European Food Research and Technology* **2017**, *243*, 1295-1309.

26. Abdi, H. Metric multidimensional scaling (MDS): analyzing distance matrices. *Encyclopedia of measurement and statistics* **2007**, 1-13.

27. De Leeuw, J.; Stoop, I. Upper bounds for Kruskal's stress. *Psychometrika* **1984**, *49*, 391-402.

28. Murtagh, F.; Legendre, P. Ward's hierarchical agglomerative clustering method: which algorithms implement Ward's criterion? *Journal of classification* **2014**, *31*, 274-295.

CHAPTER 3: RESULTS AND DISCUSSION – FEASIBILITY STUDY OF REMOTE SENSING NDVI ANAYSIS TO MANAGE VINEYARD VARIATION

The objective of this chapter was to examine the feasibility of using remote sensing NDVI to detect important vineyard variations that affect the viability of vineyards such as leaf water potential, soil moisture, canopy size, and LT50. We hypothesize that remote sensing NDVI will correspond to local variations in several vineyard variables that affect the viability of vineyards, and the correlations would be temporally stable.

3.1 Results

NDVI values from remote sensing data from 2015, 2016, and 2017 were compared with soil moisture (SM), leaf water potential (LWP, ψ), stomatal conductance (Gs), vine size, and winter hardiness (LT50).

3.1.1 Principal component analysis (PCA)

PCA results were derived from the first two factors, which explained between 50 and 67% of the data (Figures 3.1 and 3.2). As shown by Pearson's correlation matrices, PCA models illustrated similar configuration between variables. In site 1 2015, 2016, and 2017 (Figure 3.1), the analysis described 57.48 %, 51.74%, and 67.30% of the data and demonstrated that remote sensing NDVI positively correlated to vine size and soil moisture throughout the three-year period. NDVI somewhat negatively correlated to leaf ψ in 2015 and 2016 and to Gs in 2017. In site 2 2015, 2016, and 2017 (Figure 3.1), the analysis described 53.28 %, 54.49%, and 63.74% of the data and demonstrated that remote sensing NDVI negatively correlated to soil moisture throughout the three-year period. NDVI also negatively correlated to LT50 in 2015 and 2016 but these were

short vectors, and the first two PCAs could not adequately explain them. NDVI somewhat positively correlated to vine size and leaf ψ in the three-year period, but this does not appear to be clear in the PCA charts.

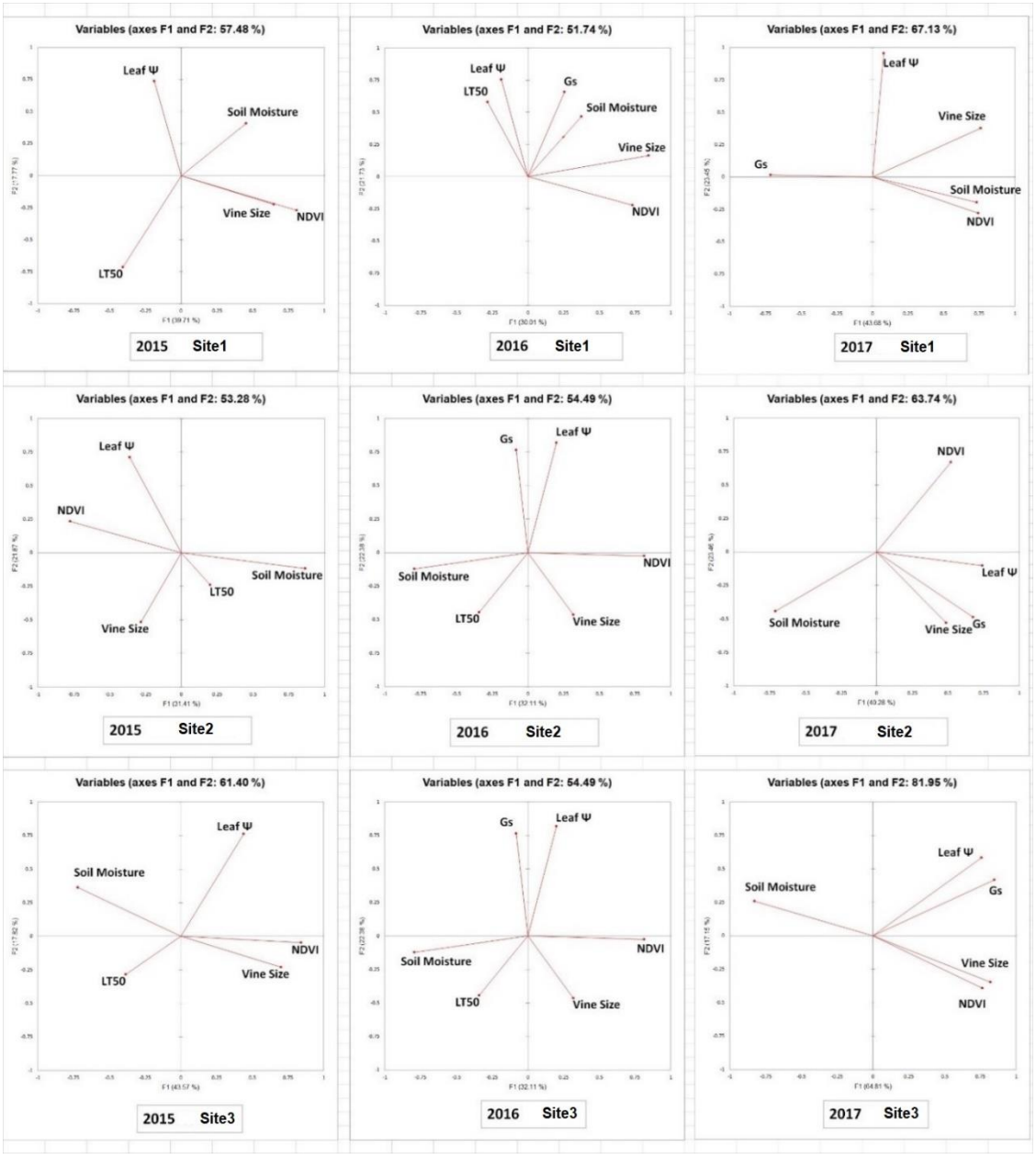

Figure 3.1. PCA results between remote sensing data and viticulturally important variables in site 1, 2, and 3 vineyards from 2015, 2016 and 2017. Abbreviations: NDVI= Normalized difference vegetation index, Leaf Ψ= Leaf water potential, Gs= Stomatal conductance, LT50= Temperature that kills 50% of the primary buds.

In site 3 2015, 2016, and 2017 (Figure 3.1), the analysis described 61.40 %, 54.49%, and 81.95% of the data and demonstrated that remote sensing NDVI showed an inverse correlation with soil moisture and LT50 and a positive correlation with vine size over a three-year period. NDVI somewhat positively correlated to Gs and leaf ψ in the three-year period but there does not appear to be clear in the PCA chart. In site 4 2015, 2016, and 2017 (Figure 3.2), the analysis described 55.66 %, 61.89%, and 63.40% of the data and demonstrated that remote sensing NDVI positively correlated to soil moisture, vine size, leaf ψ and Gs in 2015 and 2016. However, due to the relatively short vector for NDVI, it was difficult to visually interpret the relationship. All the variables were positively correlated to NDVI in 2017. In site 5 2015, 2016, and 2017 (Figure 3.2), the analysis described 58.75 %, 59.39%, and 65.82% of the data and demonstrated that remote sensing NDVI negatively correlated to soil moisture and positively correlated to vine size throughout the three-year period. NDVI somewhat positively correlated to leaf ψ in the three-year period but there does not appear to be clear in the PCA charts. In site 6 2015, 2016, and 2017 (Figure 3.2), the analysis described 49.27 %, 55.82%, and 59.57% of the data and demonstrated that remote sensing NDVI positively correlated to vine size throughout the three-year period. NDVI somewhat positively correlated to leaf ψ and inversely correlated to soil moisture but those had short vectors and thus there does not appear to be clear in the PCA charts.

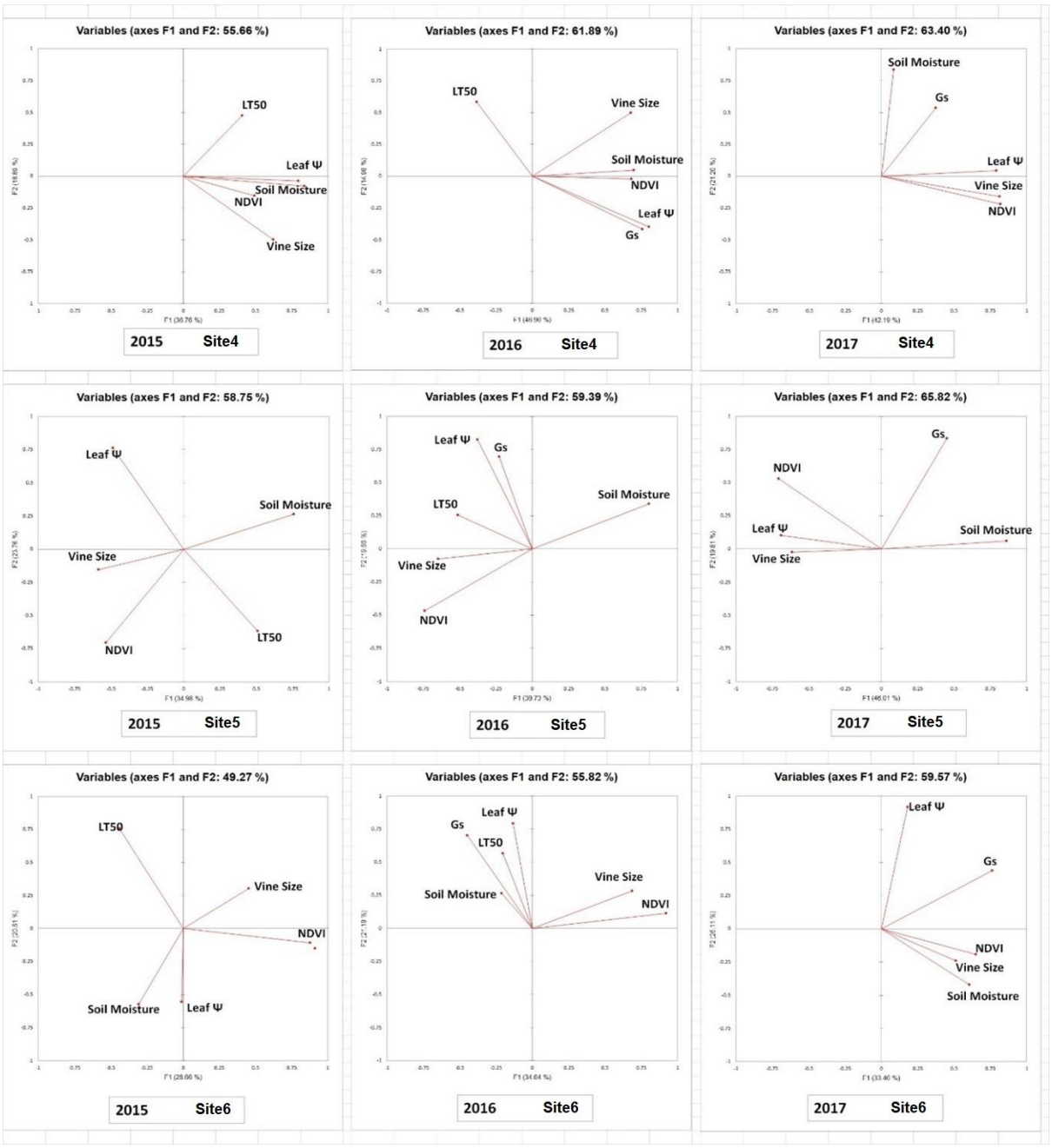

Figure 3.2. PCA results between remote sensing data and viticulturally important variables in site 4, 5, and 6 vineyards from 2015, 2016 and 2017. Abbreviations: NDVI= Normalized difference vegetation index, Leaf Ψ= Leaf water potential, Gs= Stomatal conductance, LT50= Temperature that kills 50% of the primary buds.

Overall, observing the short vectors for some variables, Pearson's correlations should be used to test whether other factors are adequately explaining some variable. It was found that the NDVI and vine size are positively correlated, while the soil moisture is inversely correlated to them.

3.1.2 Pearson's correlation analysis (p-value)

3.1.2.1 Relationships between NDVI and soil moisture (SM)

There was an inverse relationship between remote sensing NDVI and SM on three sites (site 2, 3, and 5; Table 3.1) throughout three consecutive years (2015, 2016, 2917). However, remote sensing NDVI was positively correlated to SM at site 4 in 2015 and 2016 and at site 1 in 2017. There was no statistically significant correlation between NDVI and SM at site 6.

Table 3.1. Pearson's correlation results between remote sensing data and viticulturally important variables in six Niagara vineyards from 2015, 2016 and 2017. Those variables with significant (95% confidence) were listed in bold, with blank cells representing no correlation. Abbreviations: Leaf Ψ= Leaf water potential, Gs= Stomatal conductance, LT50= Temperature that kills 50% of the primary buds.

	Correlation matrix					p-values (Pearson)				
Vineyards	**Soil Moisture**	**Leaf Ψ**	**Gs**	**LT50**	**Vine Size**	**Soil Moisture**	**Leaf Ψ**	**Gs**	**LT50**	**Vine Size**
2015 Site 1	0.187	-0.165		-0.105	**0.565**	0.106	0.155		0.368	**0.000**
2016 Site 1	-0.026	-0.158	**0.300**	**-0.343**	**0.431**	0.823	0.173	**0.009**	**0.002**	**0.000**
2017 Site 1	**0.371**	-0.142	**-0.402**		**0.441**	**0.001**	0.221	**0.000**		**0.000**
2015 Site 2	**-0.587**	**0.302**		-0.045	**0.243**	**0.000**	**0.008**		0.700	**0.035**
2016 Site 2	**-0.505**	0.053	-0.091	**-0.239**	**0.234**	**0.000**	0.710	0.891	**0.012**	**0.016**
2017 Site 2	**-0.439**	**0.238**	0.046		0.064	**0.000**	**0.043**	0.694		0.586
2015 Site 3	**-0.661**	**0.351**		**-0.249**	**0.459**	**0.000**	**0.001**		**0.026**	**0.000**
2016 Site 3	**-0.705**	**0.501**	**0.376**	**-0.336**	**0.783**	**0.000**	**0.000**	**0.001**	**0.002**	**0.000**
2017 Site 3	**-0.586**	**0.381**	**0.490**		**0.637**	**0.000**	**0.000**	**0.000**		**0.000**
2015 Site 4	**0.270**	**0.414**		-0.038	**0.289**	**0.022**	**0.000**		0.752	**0.014**
2016 Site 4	**0.411**	**0.424**	**0.521**	-0.188	**0.307**	**0.000**	**0.000**	**0.000**	0.114	**0.009**
2017 Site 4	-0.040	**0.472**	0.171		**0.583**	0.739	**0.000**	0.151		**0.000**
2015 Site 5	**-0.568**	-0.215		0.014	**0.260**	**0.000**	0.052		0.900	**0.019**
2016 Site 5	**-0.676**	-0.037	-0.031	0.058	**0.549**	**0.000**	0.745	0.780	0.606	**0.000**
2017 Site 5	**-0.522**	**0.443**	-0.015		**0.252**	**0.000**	**0.000**	0.892		**0.023**
2015 Site 6	-0.170	-0.015		**-0.347**	**0.296**	0.133	0.893		**0.002**	**0.008**
2016 Site 6	-0.146	-0.063	**-0.293**	-0.109	**0.550**	0.196	0.581	**0.008**	0.338	**0.000**
2017 Site 6	0.142	-0.057	**0.279**		**0.290**	0.208	0.617	**0.012**		**0.009**

Table 3.2. Summary of the statistical data for remote sensing and viticulturally important variables in six Niagara vineyards from 2015, 2016 and 2017. Abbreviations: NDVI= Normalized difference vegetation index, MIN= Minimum, MAX= Maximum, SD= Standard deviation, CV%= Coefficient of variation.

		Site 1 (n=76)					Site 2 (n=75)					Site 3 (n=80)				
Variable	Year	Average	MIN	MAX	SD	CV(%)	Average	MIN	MAX	SD	CV(%)	Average	MIN	MAX	SD	CV(%)
NDVI	2015	0.588	0.505	0.676	0.042	7.1	0.655	0.396	0.807	0.093	14.2	0.655	0.396	0.807	0.093	14.2
	2016	0.738	0.655	0.819	0.039	5.2	0.783	0.599	0.900	0.057	7.3	0.356	0.204	0.684	0.106	29.9
	2017	0.723	0.668	0.778	0.025	3.5	0.839	0.820	0.851	0.007	0.8	0.748	0.666	0.801	0.028	3.8
Soil Moisture (%)	2015	20.5	9.3	25.3	2.7	13.0	24.9	17.5	40.2	4.3	17.1	25.9	17.7	36.2	4.9	18.8
	2016	18.5	9.4	22.7	2.6	13.8	20.2	14.5	28.8	2.7	13.6	23.2	14.6	34.0	5.2	22.5
	2017	23.6	13.8	30.1	4.2	17.7	26.6	16.3	41.8	4.5	16.9	26.5	18.2	39.4	5.5	20.6
Leaf Ψ (MPa)	2015	-1.15	-1.22	-1.04	0.04	-3.2	-1.22	-1.32	-1.09	0.04	-2.9	-1.17	-1.43	-1.05	0.07	-5.7
	2016	-1.29	-1.42	-1.16	0.04	-3.4	-1.33	-1.45	-1.14	0.05	-3.6	-1.42	-1.63	-1.25	0.06	-4.6
	2017	-1.00	-1.21	-0.76	0.08	-8.2	-1.14	-1.35	-0.99	0.07	-5.8	-1.19	-1.45	-0.96	0.11	-9.1
Gs (mmol/m²s)	2015	—	—	—	—	—	—	—	—	—	—	—	—	—	—	—
	2016	411	298	520	40	9.7	491	245	685	55	11.1	333	133	476	56	16.7
	2017	545	350	688	71	13.0	595	509	689	24	4.1	498	350	623	65	13.1
LT50 (°C)	2015	-15.6	-18.1	-13.7	0.8	-5.3	-17.9	-21.3	-14.8	1.2	-6.5	-18.2	-20.7	-16.0	0.7	-3.9
	2016	-18.5	-21.2	-15.6	0.8	-4.1	-19.2	-20.6	-18.0	0.3	-1.8	-19.7	-22.6	-17.5	0.7	-3.5
	2017	—	—	—	—	—	—	—	—	—	—	—	—	—	—	—
Vine Size (kg)	2015	0.76	0.15	1.61	0.33	43.3	0.61	0.10	1.16	0.19	30.7	0.66	0.20	0.96	0.18	27.6
	2016	0.61	0.18	0.97	0.15	25.2	0.43	0.20	0.61	0.09	20.1	0.49	0.14	1.03	0.24	49.9
	2017	0.69	0.17	1.29	0.22	31.7	0.52	0.15	0.83	0.11	21.4	0.66	0.35	0.99	0.14	21.5

		Site 4 (n=72)					Site 5 (n=81)					Site 6 (n=80)				
Variable	Year	Average	MIN	MAX	SD	CV(%)	Average	MIN	MAX	SD	CV(%)	Average	MIN	MAX	SD	CV(%)
NDVI	2015	0.589	0.512	0.692	0.038	6.4	0.503	0.382	0.606	0.040	8.0	0.595	0.478	0.698	0.053	8.9
	2016	0.762	0.611	0.873	0.063	8.3	0.506	0.398	0.635	0.051	10.0	0.725	0.629	0.811	0.038	5.3
	2017	0.833	0.814	0.852	0.008	1.0	0.814	0.690	0.865	0.024	2.9	0.827	0.812	0.841	0.006	0.7
Soil Moisture (%)	2015	23.2	18.2	31.1	2.8	12.0	29.9	16.4	41.8	5.6	18.8	23.2	15.6	28.5	2.4	10.5
	2016	22.8	17.1	29.2	2.7	12.0	25.9	16.9	33.9	4.0	15.5	19.3	13.6	23.4	2.0	10.5
	2017	23.6	17.4	31.3	2.5	10.6	31.1	19.9	51.2	6.2	20.1	26.6	18.1	35.5	3.6	13.4
Leaf Ψ (MPa)	2015	-1.05	-1.22	-0.80	0.10	-9.6	-1.04	-1.22	-0.85	0.06	-6.1	-1.05	-1.16	-0.91	0.04	-3.6
	2016	-1.33	-1.48	-1.03	0.07	-4.9	-1.39	-1.48	-1.32	0.03	-2.1	-1.22	-1.33	-1.02	0.04	-3.4
	2017	-0.90	-1.25	-0.57	0.14	-15.2	-0.92	-1.07	-0.78	0.06	-6.4	-0.98	-1.21	-0.85	0.05	-5.5
Gs (mmol/m²s)	2015	—	—	—	—	—	—	—	—	—	—	—	—	—	—	—
	2016	599	455	793	52	8.7	372	252	492	38	10.3	668	452	789	53	8.0
	2017	540	426	614	29	5.4	594	428	692	34	5.8	664	469	900	90	13.5
LT50 (°C)	2015	-18.5	-21.0	-16.3	0.9	-4.7	-18.1	-20.1	-15.7	0.8	-4.3	-17.9	-20.6	-16.6	0.7	-4.0
	2016	-19.3	-21.4	-17.7	0.6	-3.0	-19.2	-20.8	-16.8	0.8	-4.1	-19.7	-21.5	-17.8	0.5	-2.7
	2017	—	—	—	—	—	—	—	—	—	—	—	—	—	—	—
Vine Size (kg)	2015	0.73	0.30	1.42	0.21	29.4	0.52	0.22	0.91	0.17	32.1	0.77	0.57	1.04	0.08	10.0
	2016	0.47	0.25	1.15	0.20	41.9	0.33	0.15	0.86	0.11	32.1	0.55	0.22	0.99	0.18	32.6
	2017	0.90	0.61	1.47	0.19	20.8	0.39	0.19	0.62	0.10	26.4	0.70	0.53	0.89	0.07	10.5

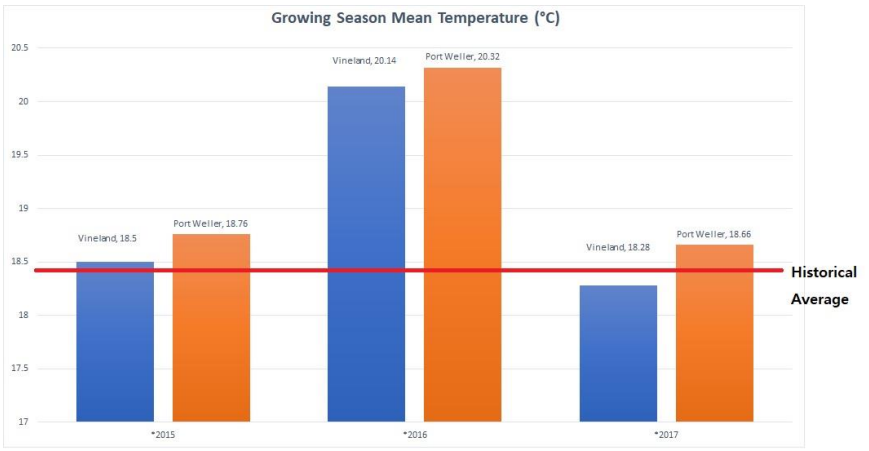

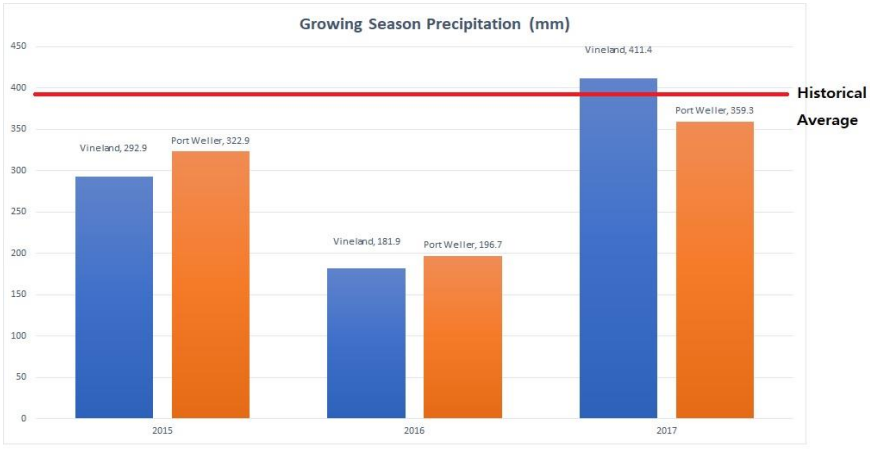

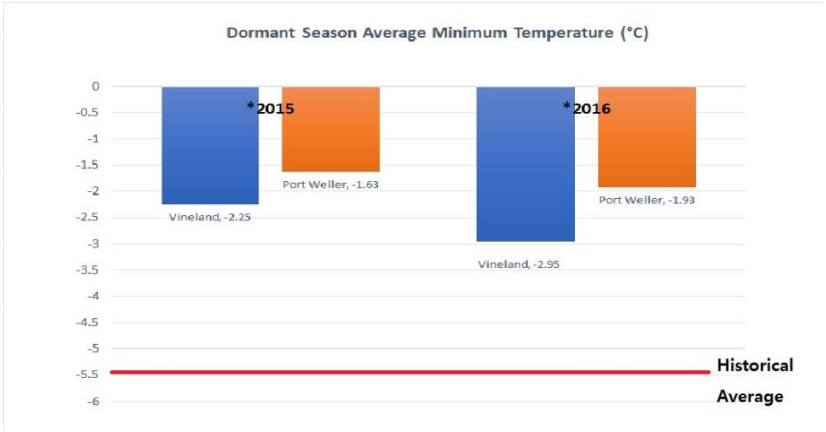

Figure 3.3. Mean growing season (May to September) temperature (°C), total growing season rainfall (mm), and average minimum dormant season (December to March) temperature (°C) from two Niagara resign locations. Port Weller AUT represented Niagara-on-the-lake vineyards and Vineland Research Station represented vineland vineyards. Historical climate normal data from St. Catharines A station 1981-2010.

The mean SM and its variation differed between sites (Table 3.2). The site with the highest SM (three years average) was site 5 (29.0 ± 5.3), followed by site 3 (25.2 ± 5.2), site 2 (23.9 ± 3.8), site 4 (23.2 ± 2.7), site 6 (23.0±2.7), with the value drop seen in site 1 (20.8 ± 3.1). The site with the highest variation in SM (three years average) was site 3 (CV%=20.6), followed by site 5 (CV%=18.1), site 2 (CV%=15.1), site 1 (CV%=14.8), with the value drop seen in site 4 (CV%=11.5) and site 6 (CV%=11.4). The three sites (site 2, 3, and 5) showed the highest variation in SM and also showed negative correlation to the remote sensing NDVI in three consecutive years (2015, 2016, 2917). Interestingly, the site 4 vineyard showed positive correlation between SM and NDVI in 2015 and 2016 and had low variation in SM. site 6 vineyard with no correlation between NDVI and SM had low variation in SM. The annual variation in SM level throughout the vineyards was also observed. The growing season was hot and dry in 2016 (Figure 3.3), and thus low SM was observed in all the vineyard sites in 2016. Overall, remote sensing NDVI could detect variation in SM at three out of six sites which had high variation in SM and showed temporal stability throughout the three consecutive years. Vineyard remote sensing NDVI had a significant negative correlation with soil moisture (SM).

3.1.2.2 Relationships between NDVI and Mid-Day Leaf Water Potential (leaf ψ)

There was a positive relationship between remote sensing NDVI and leaf ψ in two sites (site 3 and 4; Table 3.1) throughout three consecutive years (2015, 2016, and 2017). A positive relationship between leaf ψ and NDVI was also observed at site 2 in 2015 and 2017 as well as at site 5 in 2017. NDVI and leaf ψ did not show any significant correlation at site 1 and site 6. The mean leaf ψ differed between sites (Table 3.2). Previous study classified water stress levels using

leaf water potential values: severe level of -1.5 or lower, mild level of -1.5 to -0.9, and no stress level ever exceeded -0.9.[1] Water stress was lowest at site 6 with highest average leafψ (-1.08 ± 0.04), followed by site 4 (-1.09 ± 0.10), site 5 (-1.12 ± 0.05), site 1 (-1.15 ± 0.05), with the value drop seen in site 2 (-1.23 ± 0.05) and site 3 (-1.26 ± 0.08). All the sites in 2015 and 2017 fall into the mildly water stressed vine category and in 2016, hot and dry year, all the vineyards still belonged to the moderately stressed vine category and there was not severely water stressed vineyard observed in this research.

Site with the greatest variation in leaf ψ (three years average) was site 4 (CV%=9.93), followed by site 3 (CV%=6.47), with the value drop seen in site 1 (CV%=4.96), site 5 (CV%=4.86), site 6 (CV%=4.18), and site 2 (CV%=4.11). The two sites (site 3 and site 4) showed highest variation in leaf ψ and showed positive correlation to the remote sensing NDVI in three consecutive years (2015, 2016, 2917). However, site 2 vineyard even showed positive correlation between leaf ψ and NDVI in 2015 and 2017 had low variation in leaf ψ. NDVI and leaf ψ are uncorrelated in site 1 and site 6 vineyards with low variation of leaf ψ.

The annual variation in leaf ψ level throughout the vineyards had also observed. The growing season was hot and dry in 2016 (Figure 3.3), and thus during the year, all the vineyard locations showed drought-stressed vines with the low mean leaf ψ. In 2017 with highest precipitation level among three years (Figure 3.3), the highest variation (CV%) in leaf ψ had been observed throughout all six vineyards. Four out of the six sites showed statistically significant positive correlation between remote sensing NDVI and leaf ψ in 2017 while only two vineyards had the correlation in 2016.

Overall, remote sensing could detect variation in leaf ψ at two out of six sites which had high variation in leaf ψ and showed temporal stability throughout the three consecutive years. The

correlation between remote sensing NDVI and leaf ψ in vineyards was highly significant. Interestingly, the highest variation (CV%) in leaf ψ had been observed throughout all six vineyards in 2017 with ample precipitation and a positive correlation of remote sensing NDVI with leaf ψ was observed in four of six sites in 2017. Therefore, the vineyard sites showed more variation in leaf ψ and remote sensing could have more capability of detecting the variation in the year with ample precipitation.

3.1.2.3 Relationships between NDVI and stomatal conductance (Gs)

Only two years (2016 and 2017) of data for Gs was collected for this research. There was a positive relationship between remote sensing NDVI and Gs in one site (site 3, Table 3.1) throughout two consecutive years (2016 and 2017). NDVI was also positively correlated to Gs at site 1 in 2016, at site 4 in 2016, and at site 6 in 2017. However, negative correlation between NDVI and Gs observed at site 1 in 2017 and site 6 in 2016. There was no statistically significant correlation between NDVI and Gs at site 2 and site 5. Variation existed between sites in their mean Gs (Table 3.2), site 6 had highest mean Gs (666 ± 71), followed by site 4 (569 ± 41), site 2 (543 ± 39), site 5 (482 ± 36), site 1 (477 ± 56) and site 3 (415 ± 60).

The site with the highest variation in Gs (two years average) was site 3 (CV%=14.89), followed by site 1 (CV%=11.39) and site 6 (CV%=10.73), with the value drop seen in site 5 (CV%=8.05), site 2 (CV%=7.59), site 4 (CV%=7.07). Site 3 showed the highest variation in Gs and also showed positive correlation to the remote sensing NDVI in two consecutive years (2016 and 2917). Site 1 and site 6 with high variation level in Gs also showed correlation between Gs and NDVI in two years but the correlations were the opposite direction: one negative and the other positive. Site 2 and site 5 vineyards with no correlation between NDVI and Gs showed a minimum

variation in Gs across vines. The annual variation in Gs level throughout the vineyards was also observed. The growing season was hot and dry in 2016 (Figure 3.3), and thus high water stressed vines with a low mean Gs was observed in four out of six vineyard sites in the year and the other two sites showed similar level of Gs in 2016 and 2017.

Overall, remote sensing could detect variation in Gs at one out of six sites which had high variation in Gs and showed temporal stability throughout the two consecutive years. Remote sensing NDVI and Gs exhibited a significant positive correlation in the vineyard. Remote sensing NDVI had less capability of detecting the variation in Gs. The correlation between NDVI and Gs varied widely across sites and years.

3.1.2.4 Relationships between NDVI and vine size

There was a positive relationship between remote sensing NDVI and vine size (Table 3.1; site 1, 3, 5, and 6) throughout three consecutive years (2015, 2016, 2917) with only one exception of higher p-value at site 2 in 2017. The mean vine size and its variation differed between sites (Table 3.2). The site with the highest vine size (three years average) was site 4 (0.70 ± 0.20), followed by site 1 (0.69 ± 0.23), site 6 (0.68 ± 0.11), site 3(0.60 ± 0.19), with the value drop seen in site 2 (0.52 ± 0.13) and site 5 (0.42 ± 0.13).

The site with the highest variation in vine size (three years average) was site 1 (CV%=33.4) and site 3 (CV%=33.0), then site 4 (CV%=30.7), site 5 (CV%=30.2), with the value drop seen in site 2 (CV%=24.7) and site 6 (CV%=17.7). The three sites (site 1, 3, and 5) showed highest variation in vine size and showed positive correlation to the remote sensing NDVI in the consecutive years while site 6 vineyard had the lowest variation in vine size even though it showed positive relationship between NDVI and vine size in three consecutive years (2015, 2016, 2917).

The annual variation in vine size level throughout the vineyards was also observed. The growing season was hot and dry in 2016 (Figure 3.3), and thus low vine size was observed in all the vineyard sites in 2016. Interestingly, both strength of correlation (r) and variation in vine size are the highest in 2016, hot and dry year, in three out of the four sites where the positive correlation and temporal stability observed.

Overall, based on three years of data, vine size was consistently correlated with remote sensing NDVI (Table 3.1). Remote sensing could detect variation in vine size at four out of six sites where three out of the four sites had high variation in vine size and showed temporal stability throughout the three consecutive years. An NDVI-based remote sensing analysis of vine size was statistically significant in the vineyard. The overall vine vigour at a site does not appear to have an impact on its detection by remote sensing, as both positive correlation and temporal stability observed in the highest (site 1) and the lowest (site 6) vine vigour sites. Furthermore, there could be an impact of annual climate changes (mean temperature and precipitation) on its detection by remote sensing.

3.1.2.5 Relationships between NDVI and LT50 (winter hardiness)

LT50 was examined in 2015 and 2016. There was a negative correlation between remote sensing NDVI and LT50 at one site (site 3; Table 3.1) throughout two consecutive years (2015 and 2016). NDVI was also negatively correlated to LT50 at site 1, 2, and 6. There was no statistically significant correlation between NDVI and LT50 at site 4 and 5. Variation existed between sites in their mean Gs (Table 3.2), site 3 had the most winter hardy vines with the lowest mean LT50 (-18.96 ± 0.70), followed by site 4(-18.89 ± 0.72), site 6 (-18.80 ± 0.62), site 5 (-18.64 ± 0.78), site 2 (18.54 ± 0.75) and site 1 (-17.5 ± 0.79).

The site with the highest variation in LT50 (two years average) was site 1 (CV%=4.69), followed by site 5 (CV%=4.17), site 2 (CV%=4.12), site 4 (CV%=3.82), site 3 (CV%=3.72), and site 6 (CV%=3.35). Site 3 showed relatively low variation in LT50 and only showed negative correlation to the remote sensing NDVI in two consecutive years (2015 and 2026). There does not appear to be an impact of variability in LT50 and its detection by remote sensing. The annual variation in LT50 level throughout the vineyards was also observed. The dormant season was colder in 2016 (Figure 3.3), and thus winter hardier vines with the low LT50 were observed in all the six vineyard sites in the year. Four out of the six sites showed statistically significant negative correlation between remote sensing NDVI and LT50 in 2016 while only two vineyards had the correlation in 2015.

Overall, remote sensing could detect variation in LT50 at one out of six sites where there was high variation in LT50, and the site showed temporal stability throughout two consecutive years. Gs and remote sensing NDVI showed a significant negative correlation in the vineyards. Remote sensing NDVI had less capability of detecting the variation in winter hardiness. There could be an impact of dormant season minimum temperature on its detection by remote sensing.

3.1.3 Mapping and spatial autocorrelation analysis

3.1.3.1 Spatial autocorrelation analysis (Moran's I)

The spatial autocorrelation of each variable was determined by z-score (Table 3.3A), which shows clustering patterns to measure potential zonal vineyard management options when relating remote sensing data to important physiological and vine performance data.[2,3]

Table 3.3A. Moran's I analysis (z-score) results for remote sensing data and viticulturally important variables in six Niagara vineyards from 2015, 2016 and 2017 (95% confidence): blue boxes = clustered, red boxes= random, yellow boxes= dispersed, black boxes= no data collected. Abbreviations: Leaf Ψ= Leaf water potential, Gs= Stomatal conductance, LT50= Temperature that kills 50% of the primary buds.

Vineyards	NDVI	Soil Moisture	Leaf Ψ	Gs	LT50	Vine Size
2015 Site 1 (n=76)	6.0617	7.3609	9.7152		7.7740	5.9185
2016 Site 1 (n=76)	7.2130	8.4098	6.0652	6.4380	5.0463	7.9313
2017 Site 1 (n=76)	5.4303	8.5579	5.4995	9.3604		7.8400
2015 Site 2 (n=75)	4.2681	3.7051	0.8060		2.2951	-0.6489
2016 Site 2 (n=75)	2.7390	2.6266	-0.9861	5.5516	1.6954	2.2069
2017 Site 2 (n=75)	2.4997	3.2972	2.2339	0.2787		-0.3724
2015 Site 3 (n=80)	7.0372	5.1237	8.9125		1.8007	4.4566
2016 Site 3 (n=80)	6.5482	5.5526	7.5013	5.7734	7.6348	6.2326
2017 Site 3 (n=80)	6.0927	7.2624	7.9978	9.9429		6.6738
2015 Site 4 (n=72)	2.2846	7.6145	9.8197		5.1646	4.2952
2016 Site 4 (n=72)	3.3818	5.9031	8.8435	7.1454	3.5488	5.0668
2017 Site 4 (n=72)	4.8626	2.0488	8.4388	3.8995		3.1971
2015 Site 5 (n=81)	3.3973	6.9418	10.3643		7.9988	1.2430
2016 Site 5 (n=81)	6.2524	5.7277	7.6523	4.6934	11.9723	2.6576
2017 Site 5 (n=81)	3.8967	7.5388	10.7872	8.4645		2.5611
2015 Site 6 (n=80)	5.1185	2.9423	5.7679		7.0703	1.0411
2016Site 6 (n=80)	6.4873	2.4633	4.0385	3.1777	-0.1318	3.1279
2017 Site 6 (n=80)	2.2967	4.7470	4.8167	10.1531		3.1475

Table 3.3B. Moran's I analysis (Moran's Index and p-value) results for remote sensing data and viticulturally important variables in six Niagara vineyards from 2015, 2016 and 2017 (95% confidence): blue boxes = clustered, red boxes= random, yellow boxes= dispersed, black boxes= no data collected. Abbreviations: Leaf Ψ= Leaf water potential, Gs= Stomatal conductance, LT50= Temperature that kills 50% of the primary buds.

	Moran's Index						p-value					
Vineyards	NDVI	Soil Moisture	Leaf Ψ	Gs	LT50	Vine Size	NDVI	Soil Moisture	Leaf Ψ	Gs	LT50	Vine Size
2015 Site 1 (n=76)	0.6284	0.4617	0.6337		0.4670	0.3614	0.0001	0.0001	0.0001		0.0004	0.0004
2016 Site 1 (n=76)	0.7496	0.4947	0.5589	0.4372	0.2537	0.5531	0.0001	0.0001	0.0001	0.0001	0.0089	0.0001
2017 Site 1 (n=76)	0.5596	0.5860	0.3860	0.5692		0.5157	0.0001	0.0001	0.0001	0.0001		0.0001
2015 Site 2 (n=75)	0.5505	0.3919	0.0318		0.4673	-0.1343	0.0001	0.0002	0.7211		0.0001	0.3568
2016 Site 2 (n=75)	0.2315	0.2484	-0.0485	0.4818	0.1978	0.2107	0.0225	0.0127	0.7858	0.0001	0.0937	0.0395
2017 Site 2 (n=75)	0.2514	0.2607	0.2285	-0.0404		-0.1101	0.0108	0.0082	0.0244	0.8292		0.4597
2015 Site 3 (n=80)	0.7447	0.5490	0.7727		0.1782	0.4618	0.0001	0.0001	0.0001		0.1163	0.0001
2016 Site 3 (n=80)	0.8677	0.5660	0.6529	0.6023	0.6718	0.6101	0.0001	0.0001	0.0001	0.0001	0.0001	0.0001
2017 Site 3 (n=80)	0.7451	0.6723	0.7156	0.8347		0.5936	0.0001	0.0001	0.0001	0.0001		0.0001
2015 Site 4 (n=72)	0.2412	0.6218	0.9070		0.5803	0.3388	0.0170	0.0001	0.0001		0.0001	0.0016
2016 Site 4 (n=72)	0.4626	0.4578	0.9176	0.6981	0.5212	0.3591	0.0001	0.0008	0.0001	0.0001	0.0001	0.0005
2017 Site 4 (n=72)	0.6704	0.2435	0.8917	0.5269		0.4186	0.0001	0.0152	0.0001	0.0001		0.0002
2015 Site 5 (n=81)	0.3498	0.5167	0.8061		0.7447	0.0803	0.0006	0.0001	0.0001		0.0001	0.3860
2016 Site 5 (n=81)	0.6561	0.3745	0.6455	0.4187	0.8452	0.2290	0.0001	0.0003	0.0001	0.0002	0.0001	0.0244
2017 Site 5 (n=81)	0.3797	0.5370	0.7927	0.6935		0.2390	0.0003	0.0001	0.0001	0.0001		0.0182
2015 Site 6 (n=80)	0.6715	0.2923	0.6217		0.6743	0.1188	0.0001	0.0032	0.0001		0.0001	0.3129
2016Site 6 (n=80)	0.8527	0.3091	0.5086	0.3138	-0.0637	0.2336	0.0001	0.0026	0.0001	0.0015	0.6922	0.0213
2017 Site 6 (n=80)	0.2470	0.5225	0.4983	0.7119		0.2945	0.0133	0.0000	0.0001	0.0001		0.0032

Over the three-year period of measurement, NDVI from remote sensing sites was highly clustered across all six sites. The water status across sites were mostly clustered, with SM clustered in all six sites in three years, leaf ψ and Gs was clustered in five sites in three years except for site 2 vineyard where the most spatial data were randomly distributed (Table 3.3A and 3.3B). Data on

vine size was mainly grouped together in five sites in 2016 and 2017, but it was only grouped together in three locations in 2015. Winter hardiness data was highly grouped together in all six locations in 2015, but four sites were grouped in 2016. In general, remote sensing and all other variables were highly clustered variables, whereas leaf ψ and vine size in sit e2 were mostly randomly distributed.

3.1.3.2 Spatial analysis of maps

In site 1 (Figure 3.4), NDVI maps appeared to have similar spatial configurations to those of vine size in all three-year period. NDVI maps displayed negative spatial distributions with LT50 in 2016 and Gs in 2017. The remote sensing NDVI maps were identical to each other throughout all the years. In site 2 (Figure 3.4), NDVI maps showed similar distributions and high spatial heterogeneity throughout the entire site. Inverted spatial distributions were seen in maps of soil moisture over the last three years. NDVI maps appeared to have similar spatial configurations to those of leaf ψ in 2015 and 2017.

NDVI and Variables

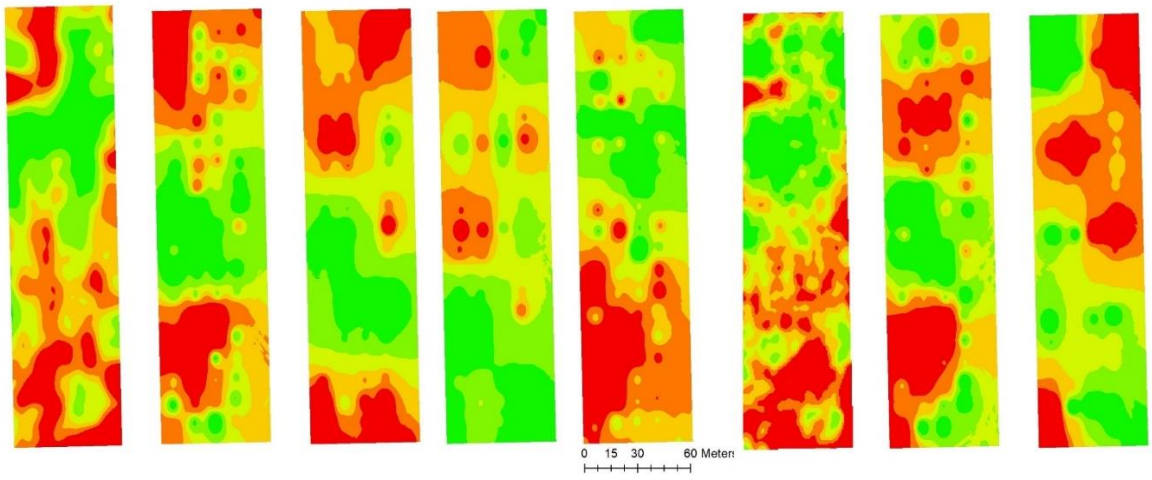

2015 Site 1 RPAS NDVI

0.485 - 0.559
0.560 - 0.573
0.574 - 0.585
0.586 - 0.601
0.602 - 0.626
0.627 - 0.706

2015 Site 1 Soil Moisture (%)

9.31 - 19.23
19.24 - 20.23
20.24 - 20.67
20.68 - 21.23
21.24 - 21.99
22.00 - 25.31

2015 Site 1 Leaf Ψ (MPa)

-1.22 - -1.17
-1.16 - -1.16
-1.15 - -1.15
-1.14 - -1.13
-1.12 - -1.11
-1.10 - -1.04

2015 Site 1 LT50 (°C)

-18.1 - -16.7
-16.6 - -16.1
-16.0 - -15.9
-15.8 - -15.6
-15.5 - -15.0
-14.9 - -13.7

2015 Site 1 Vine Size (Kg)

0.15 - 0.56
0.57 - 0.67
0.68 - 0.75
0.76 - 0.87
0.88 - 0.96
0.97 - 1.61

2016 Site 1 RPAS NDVI

0.599 - 0.707
0.708 - 0.727
0.728 - 0.747
0.748 - 0.767
0.768 - 0.787
0.788 - 0.837

2016 Site 1 Soil Moisture (%)

9.4 - 17.4
17.5 - 18.4
18.5 - 18.9
19.0 - 19.3
19.4 - 19.9
20.0 - 22.7

2016 Site 1 Leaf Ψ (MPa)

-1.42 - -1.31
-1.30 - -1.30
-1.29 - -1.29
-1.28 - -1.28
-1.27 - -1.26
-1.25 - -1.16

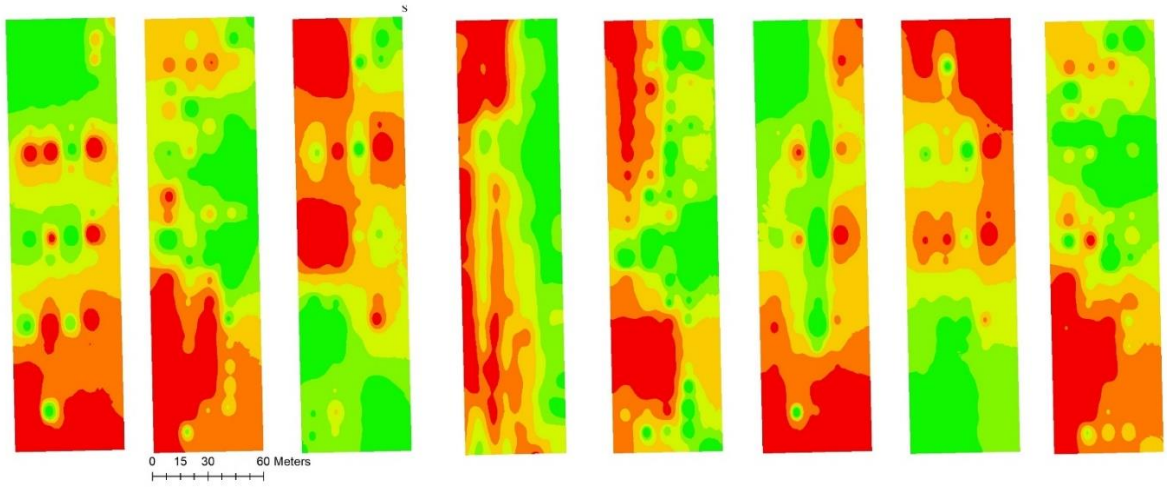

2016 Site 1 Stomatal Conductance (mmol/m² s)

298 - 390
391 - 398
399 - 407
408 - 414
415 - 434
435 - 520

2016 Site 1 Vine Size (kg)

0.18 - 0.51
0.52 - 0.59
0.60 - 0.64
0.65 - 0.68
0.69 - 0.72
0.73 - 0.97

2016 Site 1 LT50 (°C)

-18.1 - -16.1
-16.0 - -15.8
-15.7 - -15.6
-15.5 - -15.2
-15.1 - -14.9
-14.8 - -13.7

2017 Site 1 RPAS NDVI

0.657 - 0.721
0.722 - 0.735
0.736 - 0.749
0.750 - 0.767
0.768 - 0.784
0.785 - 0.812

2017 Site 1 Soil Moisture (%)

13.8 - 20.5
20.6 - 22.7
22.8 - 24.6
24.7 - 25.6
25.7 - 26.4
26.5 - 30.0

2017 Site 1 Leaf Ψ (MPa)

-1.21 - -1.06
-1.05 - -1.01
-1.00 - -0.99
-0.98 - -0.98
-0.97 - -0.95
-0.94 - -0.76

2017 Site 1 Stomatal Conductance (mmol/m² s)

350 - 488
489 - 518
519 - 542
543 - 579
580 - 607
608 - 688

2017 Site 1 Vine Size (kg)

0.17 - 0.54
0.55 - 0.63
0.64 - 0.70
0.71 - 0.78
0.79 - 0.84
0.85 - 1.29

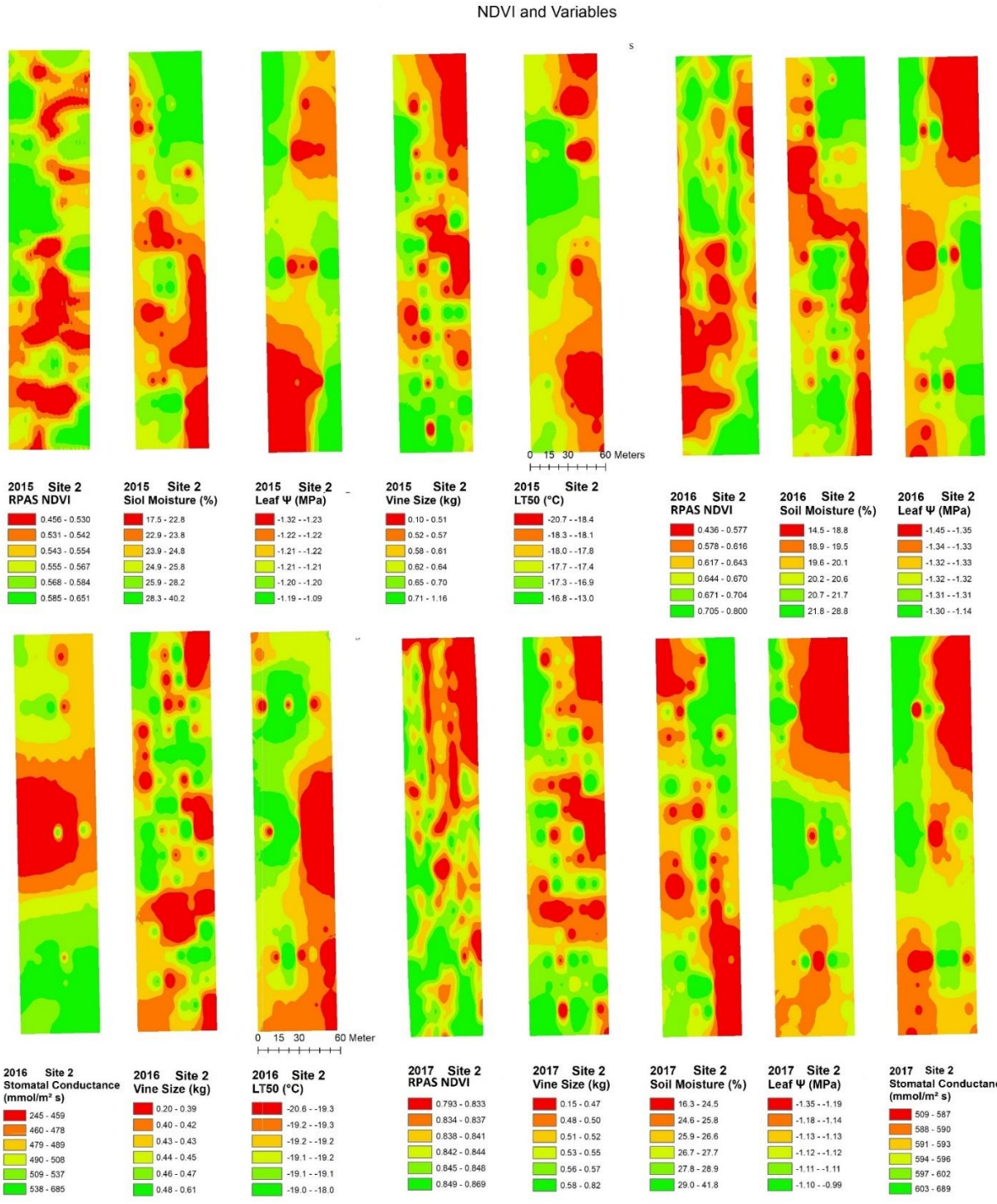

Figure 3.4. Spatial maps of vineyard variables extracted from RS data and viticulturally important variables in site 1 and 2 vineyards from 2015, 2016 and 2017. Abbreviations: NDVI= Normalized difference vegetation index, Leaf Ψ= Leaf water potential, Gs= Stomatal conductance, LT50= Temperature that kills 50% of the primary buds.

In site 3 (Figure 3.5), NDVI maps appeared to have close geographical configurations to that of vine size, leaf ψ and Gs. There were inverted spatial distributions in maps of soil moisture and LT50. The remote sensing NDVI maps were identical to each other throughout all the years. In site 4 (Figure 3.5), NDVI maps displayed an odd horizontally striated pattern, which was also seen by previous research.[4] This can be attributed to the orientation of vineyard rows in conjunction with lines of pixels, and perhaps also to the spatial-resolution utilized. The NDVI map showed close geographical configurations to that of leaf ψ, Gs, vine size, and soil moisture in all three years of the measurement. Inverted spatial distributions were seen on the map of LT50 in 2016.

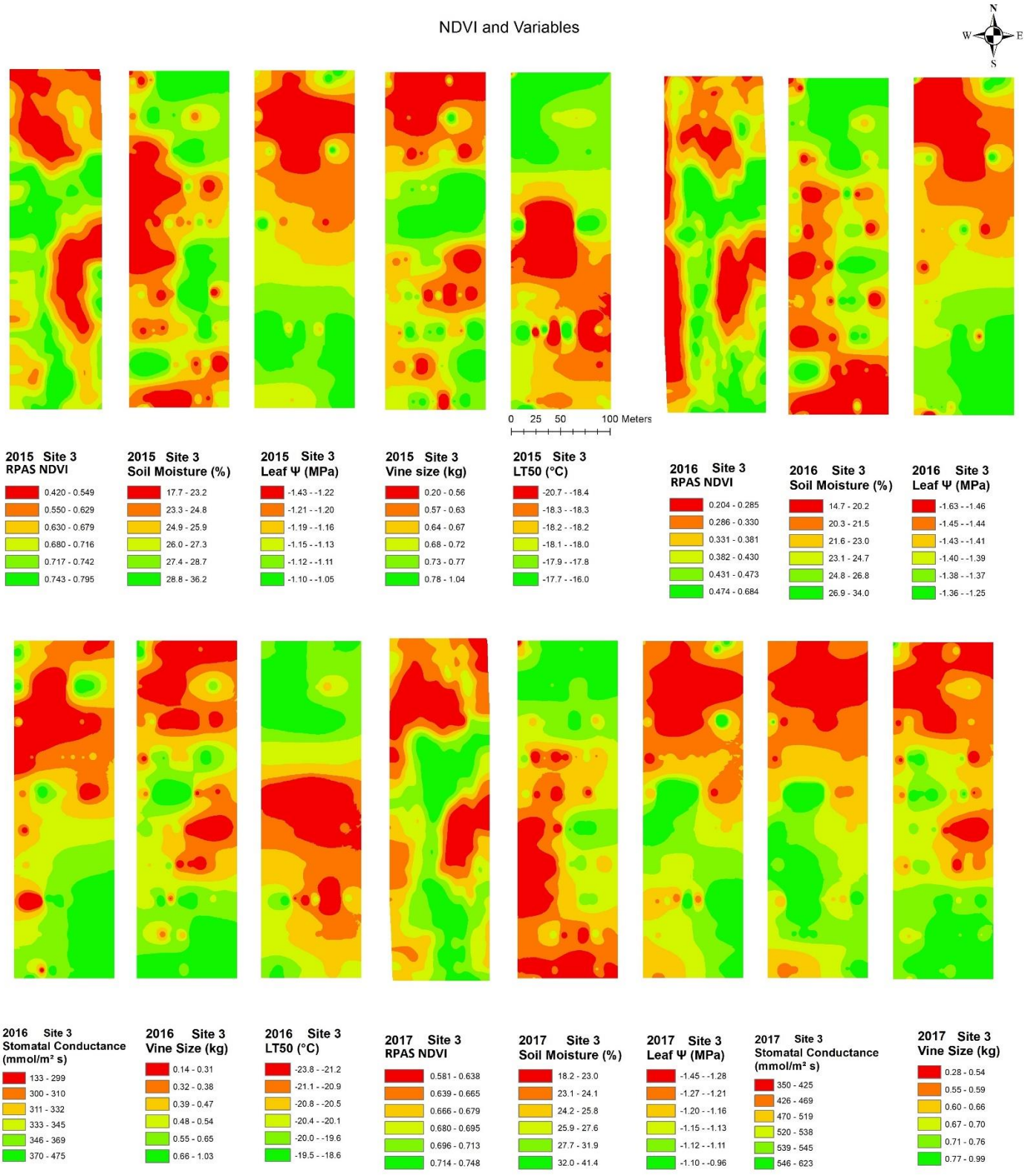
NDVI and Variables
N
W
E
S
0 25 50 100 Meters
2015 Site 3 RPAS NDVI
0.420 - 0.549
0.550 - 0.629
0.630 - 0.679
0.680 - 0.716
0.717 - 0.742
0.743 - 0.795
2015 Site 3 Soil Moisture (%)
17.7 - 23.2
23.3 - 24.8
24.9 - 25.9
26.0 - 27.3
27.4 - 28.7
28.8 - 36.2
2015 Site 3 Leaf Ψ (MPa)
-1.43 - -1.22
-1.21 - -1.20
-1.19 - -1.16
-1.15 - -1.13
-1.12 - -1.11
-1.10 - -1.05
2015 Site 3 Vine size (kg)
0.20 - 0.56
0.57 - 0.63
0.64 - 0.67
0.68 - 0.72
0.73 - 0.77
0.78 - 1.04
2015 Site 3 LT50 (°C)
-20.7 - -18.4
-18.3 - -18.3
-18.2 - -18.2
-18.1 - -18.0
-17.9 - -17.8
-17.7 - -16.0
2016 Site 3 RPAS NDVI
0.204 - 0.285
0.286 - 0.330
0.331 - 0.381
0.382 - 0.430
0.431 - 0.473
0.474 - 0.684
2016 Site 3 Soil Moisture (%)
14.7 - 20.2
20.3 - 21.5
21.6 - 23.0
23.1 - 24.7
24.8 - 26.8
26.9 - 34.0
2016 Site 3 Leaf Ψ (MPa)
-1.63 - -1.46
-1.45 - -1.44
-1.43 - -1.41
-1.40 - -1.39
-1.38 - -1.37
-1.36 - -1.25
2016 Site 3 Stomatal Conductance (mmol/m² s)
133 - 299
300 - 310
311 - 332
333 - 345
346 - 369
370 - 475
2016 Site 3 Vine Size (kg)
0.14 - 0.31
0.32 - 0.38
0.39 - 0.47
0.48 - 0.54
0.55 - 0.65
0.66 - 1.03
2016 Site 3 LT50 (°C)
-23.8 - -21.2
-21.1 - -20.9
-20.8 - -20.5
-20.4 - -20.1
-20.0 - -19.6
-19.5 - -18.6
2017 Site 3 RPAS NDVI
0.581 - 0.638
0.639 - 0.665
0.666 - 0.679
0.680 - 0.695
0.696 - 0.713
0.714 - 0.748
2017 Site 3 Soil Moisture (%)
18.2 - 23.0
23.1 - 24.1
24.2 - 25.8
25.9 - 27.6
27.7 - 31.9
32.0 - 41.4
2017 Site 3 Leaf Ψ (MPa)
-1.45 - -1.28
-1.27 - -1.21
-1.20 - -1.16
-1.15 - -1.13
-1.12 - -1.11
-1.10 - -0.96
2017 Site 3 Stomatal Conductance (mmol/m² s)
350 - 425
426 - 469
470 - 519
520 - 538
539 - 545
546 - 623
2017 Site 3 Vine Size (kg)
0.28 - 0.54
0.55 - 0.59
0.60 - 0.66
0.67 - 0.70
0.71 - 0.76
0.77 - 0.99

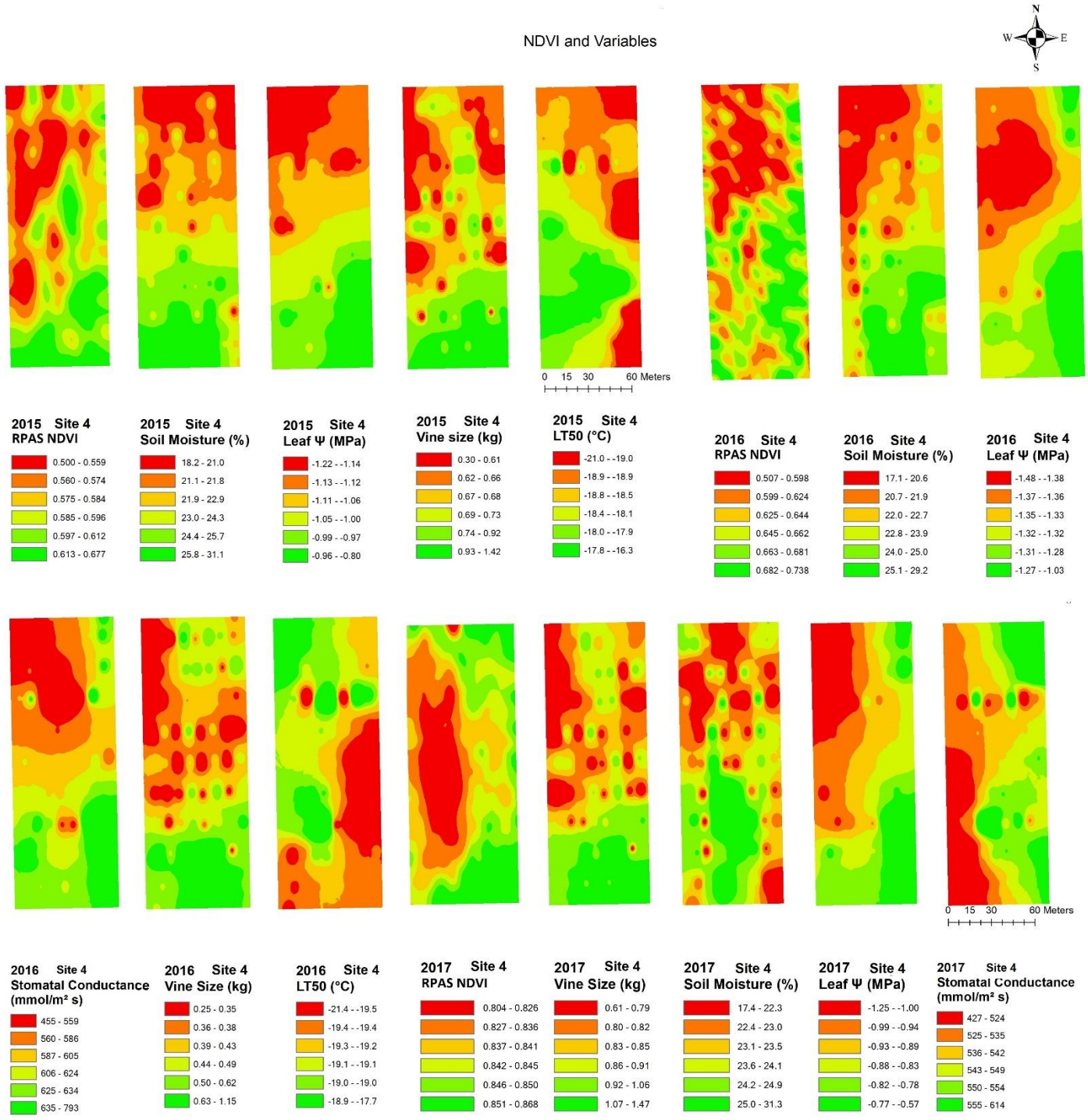

Figure 3.5. Spatial maps of vineyard variables extracted from RS data and viticulturally important variables in site 3 and 4 vineyards from 2015, 2016 and 2017. Abbreviations: NDVI= Normalized difference vegetation index, Leaf Ψ= Leaf water potential, Gs= Stomatal conductance, LT50= Temperature that kills 50% of the primary buds

In site 5 (Figure 3.6), the maps of vine size and soil moisture showed close geographical configuration in all three years of the measurement; however, the soil moisture maps displayed inverted spatial distributions. The positive correlation also observed in leaf ψ in 2017. In site 6 (Figure 3.6), NDVI maps appeared to have close geographical configuration to that of vine size in three years. LT50 exhibited inverse geographical configuration in 2015.

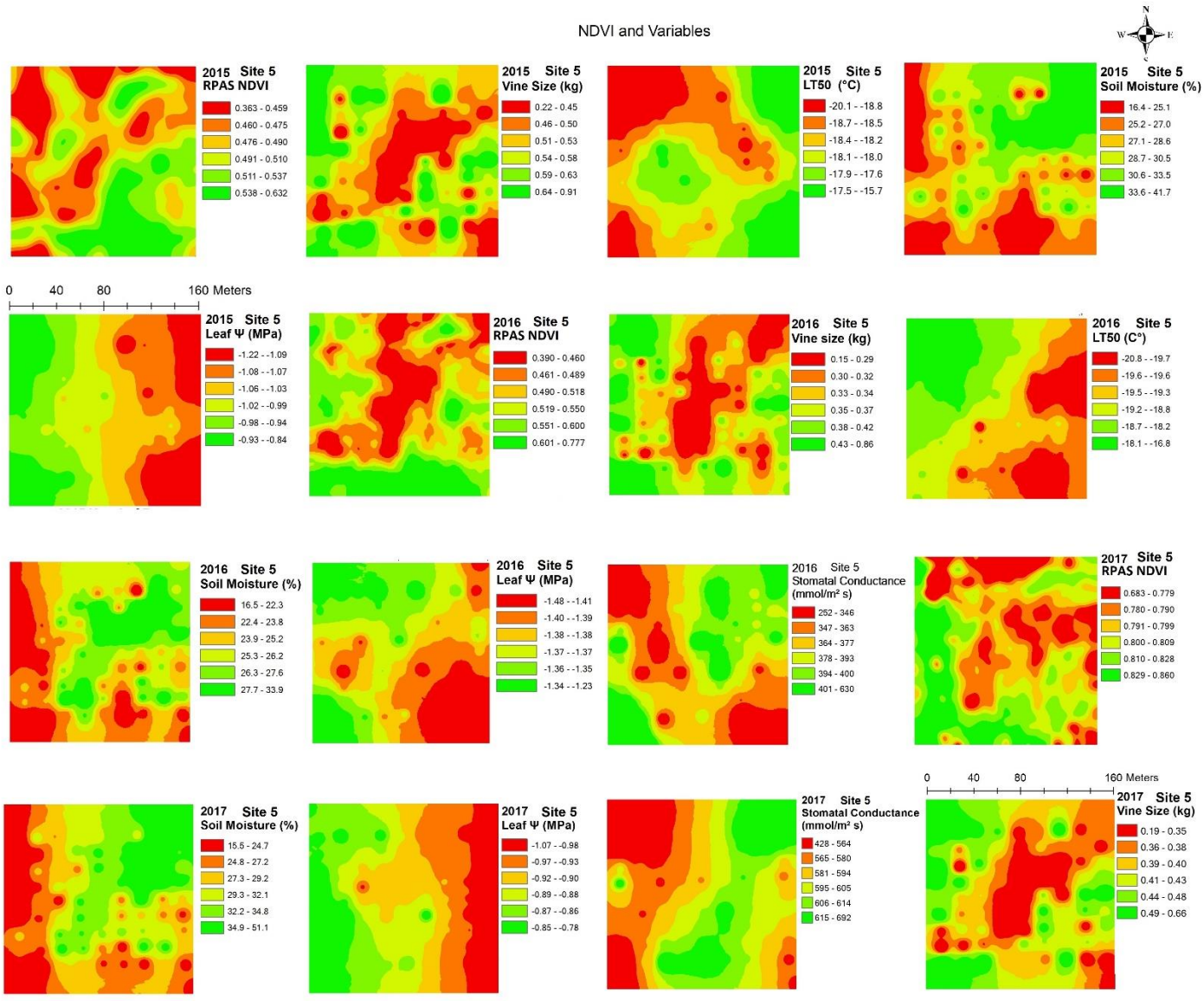

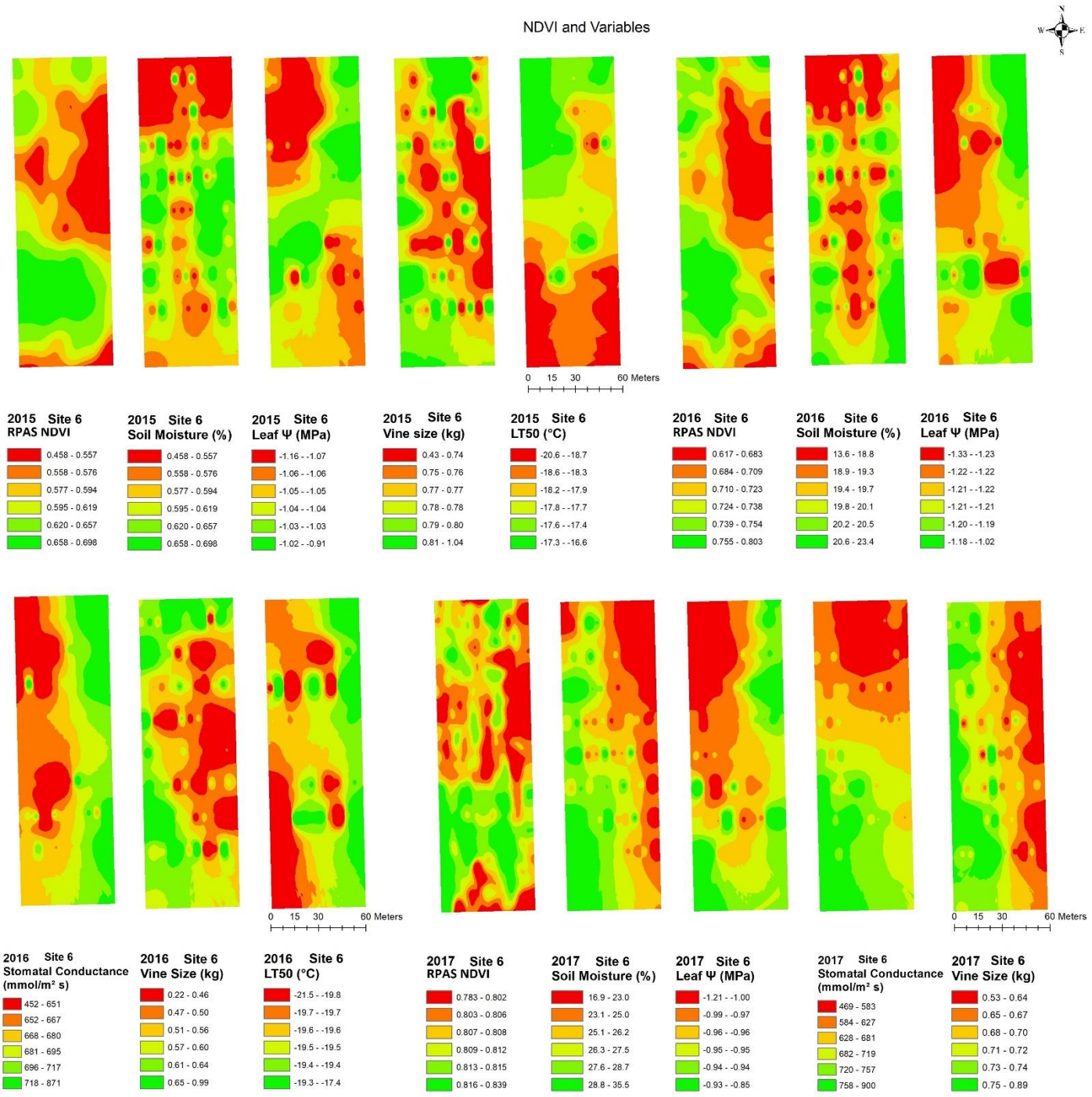

Figure 3.6. Spatial maps of vineyard variables extracted from RS data and viticulturally important variables in site 5 and 6 vineyards from 2015, 2016 and 2017. Abbreviations: NDVI= Normalized difference vegetation index, Leaf Ψ= Leaf water potential, Gs= Stomatal conductance, LT50= Temperature that kills 50% of the primary buds

Even though some sites displayed highly patchy or striped spatial patterns, the temporal consistency of spatial patterns was observed in the maps of remote sensing NDVI in most vineyards. Other variables like vine size and soil moisture also showed the temporal stability of the spatial patterns. With more clearly defined zonal differences in remote sensing variables, precision viticulture operations could be more easily conducted at those sites.

3.2 Discussion

In this study, remote sensing has indicated the ability to identify vineyard variation with temporal stability, thereby enabling the analysis of a range of viticulturally relevant variables, including water status, canopy size, and winter hardiness. Even though some sites displayed highly patchy or striped spatial patterns, the temporal consistency of spatial patterns was observed in the maps of remote sensing NDVI in most of the vineyards, as well as the spatial patterns showed stability in vine size and soil moisture through time.

NDVI was most consistently correlated with vine size at five sites each year and consistently stable for three years at four sites. This is consistent with the literature that demonstrates the feasibility of remote sensing data for detecting vegetative growth such as leaf area coefficient[5], total canopy[6], and health of vegetation[3]. In their surface canopy, plants incorporate the characteristics of their surroundings and stresses.[7] Thus, grapevine ecological condition and its level of stress are reflected in variations in vegetative growth. Additionally, the yield-to-pruning weight ratios are used to diagnose fruit quality indirectly based on balance pruning.[8] By using NDVI data, grape growers can determine variation in vegetative growth to support them in monitoring vineyard balance.[9] A precise projection of canopy size may allow

vine vegetative and reproductive balance to be altered through cluster thinning during the growing season and afterward through pruning tactics.[10]

Another interesting observation from this research was the strong inverse correlation with temporal stability between NDVI and soil moisture. Remote sensing could detect variation in SM at three out of six sites and showed temporal stability throughout the three consecutive years. SM values were very high on the sites exhibiting strong variations (CV%) across three years as well as visual evidence of water accumulation in some spots mainly caused by heavy clay soil with insufficient drainage. Interestingly, in site 4 vineyard, located in the Lincoln Lakeshore sub appellation with relatively well drained soil types (glacial till soil with high sand and stone content[11]), the NDVI was positively related to SM in 2015 and 2016. There is a possibility of using remote sensing to detect SM in sites where water drainage issues or knowingly high clay[12] can negatively impact on vegetative growth[13,14]. Remote sensing NDVI also showed inverse correlations with soil clay content and water status in the measured area.[15]

To examine the feasibility of remote sensing data for vineyard water management, it is necessary not only to establish a correlation between remote sensing data and vineyard water stress but also to survey a map of vineyard soil profiles and its soil drainage capacities since the absolute values of soil water status were not correlated to the vine health and stress level. There was a weaker correlation observed between NDVI and leaf ψ, exhibiting a positive correlation with two of the sites for three years. The level of mean leaf ψ in 2017 with ample precipitation was higher than that in 2016 with hot and dry growing season. All the mean leaf ψ in 2017 belong to mildly water stressed vine category (-1.2 to -0.9) and that in 2016 belong to moderately water stressed vine category (-1.5 to -1.2).[1] This study further observed vineyard variation of leaf conductance (Gs) in relationships with NDVI, where three sites had positive correlation in 2016 and two in

2017. During the hot and dry growing season of 2016, the lower Gs value sites showed a strong correlation between two variables.

NDVI and leaf ψ/ Gs are correlated positively in general, which is consistent with earlier studies.[16] Interestingly, the year 2016 with hot and dry growing season showed that only two sites had correlation between NDVI and leaf ψ while in the year 2017 with ample precipitation, four cites had positive correlation between the two variables. Furthermore, the highest variation (CV%) in leaf ψ also observed in 2017 while the variation (CV%) in leaf ψ, was the lowest in 2016. Therefore, leaf ψ had more variation and was more correlated to NDVI in the year with ample precipitation when higher grapevine water level could be a constraint for vegetation.[3] A change in normal stomatal behaviour caused by stress responses is possible and one can generate a new water uptake efficiency without greatly reducing biomass yield.[17] This could explain that the higher grapevine water level could be a constraint for vegetation. In 2016, the level of water stress may change the stomatal rhythm and water use efficiency toward minimizing loss of vegetative growth and lead to more uniform canopy size while in 2017, the conventional relationship between water availability and plant biomass production was applied: the vegetative growth was linearly linked with water supply and lead more variability in canopy size.

To examine the feasibility of remote sensing technologies in a vineyard for water management in terms of vine water status alone is not an easy task. Researchers agree that moderate water deficits can enhance vineyard productivity and supplemental water can remarkably boost grape production[18-21], however, there is no clear general guideline for what the level of leaf ψ belong to the moderate water deficit because it depends on site, variety, and cultural practice of specific vineyard.

In this study, NDVI correlated less with winter hardiness, exhibiting a negative correlation with temporal stability only in site 3. Four out of the six sites showed significant negative correlations between remote sensing NDVI and LT50 in 2016, colder dormant season while only two vineyards had the correlation in 2015. Winter hardier vines with the low LT50 were also observed in all the six vineyard sites in 2016. Water status[22] and pruning weight[23] can influence cold acclimation, but the lack of relationships observed in this research could be explained by the low vineyard variations in LT50 values (CV%=1.8-6.5%). Remote sensing NDVI had less capability of detecting the variation in winter hardiness. There could be an impact of dormant season minimum temperature on its detection by remote sensing.

The last, but not least, an interesting observation from this research was that site 3 vineyard was the only site where NDVI and all the viticulturally important variables correlated perfectly with temporal stability over all three years. There were three distinct cultural practices at site 3 different from other vineyards. First, the inter-row management in site 3 was topsoil cultivation while other sites planted cover crops between the rows. The inter-row spectral reflection in the data was not removed, so the NDVI data extracted from the vineyards could be affected.[4,24,25] Secondly, pruning practice and training system in this vineyard were distinct from other vineyard sites. A canopy-based NDVI measurement can be greatly affected by a cultural practice such as pruning and training systems.[26] The spur-pruned cordon systems with stronger horizontal profiles in this site could be more appropriate for airborne monitoring. There would need to be further research on the effect of training systems on the performance of remote sensing data. Lastly, the application of heavy copper spray was observed through the growing season in site 3. The heavy copper spray created a blue colour background layer as the RPAS flight performed to get

NDVI data. There would also need to be further research on the effect of background colour on the performance of remote sensing data.

When evaluating the possibility of applying remote sensing data to measure vineyard variations, it is necessary to produce reliable and precise maps that illustrate areas of the variables to implement precision viticulture. In Moran's I analysis, viticulturally significant variables and remote sensing data were highly clustered, and zonal vineyard management such as selective shoot thinning or precise spraying based on the clustering across the vineyards, may be feasible.[27] However, when vineyards have numerous environmental factors affecting canopy areas, such as soil profile[28], micro climate[29], water status[30], nutrient deficiency[31], and other variables, it can be challenging to determine the correlations between remote sensing data and the variables. Plants often experience multiple stress conditions simultaneously in a field, rather than a single stress condition.[32] Stress-induced symptoms can be magnified when these stresses interact, impacting plant vegetative and reproductive processes in further ways.[32,33] There is a need for further research aimed at understanding how remote sensing data detects these variables as plants are stressed in the field under various circumstances.

3.3 Conclusions

Even though the biological relevance of remote sensing data per site and per vintage should still be evaluated through ground truthing of sampled vines and in many cases, it was difficult for remote sensing NDVI to detect agriculturally significant variables between sites and vintages, this study still verified that remote sensing NDVI could be feasible to detect variations across vineyards for several agriculturally relevant variables. The variable that most correlated with remote sensing NDVI and the most temporally stable was vine size. The NDVI data can be used to project canopy

size accurately and help growers determine an ideal balance of plant vegetation and reproduction, which can be adjusted through thinning of clusters during the growing season and pruning afterward. The analysis of vineyard variables and remote sensing data can also lead to zonal quality management programs such as vine phytosanitary and canopy management, as well as ensuring the quality of the finished product. A strong inverse correlation with temporal stability between NDVI and soil moisture was also observed. There was evidence in these correlation sites of considerable standing water in some spots with inadequate water drainage, indicating SM in areas with drainage concerns can be detected by remote sensing.

Furthermore, site 3 vineyard showed perfect correlation of NDVI and all the viticulturally important variables with temporal stability of all three years measurements. There were some distinct cultural practices at site 3 different from other vineyards. Further investigation of the relationships between the remote sensing detectability and the vineyard cultural practices will promote an accuracy and usefulness of remote sensing data to identify variabilities in spectral behaviour of grapevine leaves and will expand knowledge of the spatiotemporal dynamics of plant physiology in vineyards.

3.4 References

1. Williams, L.; Araujo, F. Correlations among predawn leaf, midday leaf, and midday stem water potential and their correlations with other measures of soil and plant water status in Vitis vinifera. *Journal of the American Society for Horticultural Science* **2002**, *127*, 448-454.

2. Pringle, M.J.; McBratney, A.B.; Whelan, B.M.; Taylor, J.A. A preliminary approach to assessing the opportunity for site-specific crop management in a field, using yield monitor data. *Agricultural Systems* **2003**, *76*, 273-292, doi:10.1016/s0308-521x(02)00005-7.

3. Acevedo-Opazo, C.; Tisseyre, B.; Guillaume, S.; Ojeda, H. The potential of high spatial resolution information to define within-vineyard zones related to vine water status. *Precision Agriculture* **2008**, *9*, 285-302.

4. Lamb, D.; Hall, A.; Louis, J.J.A.G.; Winemaker. Airborne remote sensing of vines for canopy variability and productivity. **2001**, 89-94.

5. Johnson, L.F. Temporal stability of an NDVI-LAI relationship in a Napa Valley vineyard. *Australian Journal of Grape and Wine Research* **2003**, *9*, 96-101.

6. Debuisson, S.; Germain, C.; Garcia, O.; Panigai, L.; Moncomble, D.; Le Moigne, M.; Fadaili, E.; Evain, S.; Cerovic, Z. Using Multiplex® and Greenseeker™ to manage spatial variation of vine vigour in Champagne. In Proceedings of the 10th International Conference on Precision Agriculture. Denver, Colorado, **2010**.

7. Wiegand, C.; Richardson, A.J.A.J. Leaf Area, Light Interception, and Yield Estimates from Spectral Components Analysis 1. **1984**, *76*, 543-548.

8. Smart, R.; Robinson, M. *Sunlight into wine: a handbook for winegrape canopy management*; Winetitles: **1991**.

9. Hall, A.; Lamb, D.; Holzapfel, B.; Louis, J. Optical remote sensing applications in viticulture-a review. *Australian journal of grape and wine research* **2002**, *8*, 36-47.

10. Dobrowski, S.; Ustin, S.; Wolpert, J.J.A.J.o.G.; Research, W. Grapevine dormant pruning weight prediction using remotely sensed data. **2003**, *9*, 177-182.

11. Kingston, M.S.; Presant, E. *The soils of the regional municipality of Niagara*; Ministry of Agriculture and Food: **1989**.

12. Koundouras, S.; Marinos, V.; Gkoulioti, A.; Kotseridis, Y.; van Leeuwen, C. Influence of vineyard location and vine water status on fruit maturation of nonirrigated cv. Agiorgitiko (Vitis vinifera L.). Effects on wine phenolic and aroma components. *Journal of Agricultural and Food Chemistry* **2006**, *54*, 5077-5086.

13. Myburgh, P.; Moolman, J. Ridging—a soil preparation practice to improve aeration of vineyard soils. *South African Journal of Plant and Soil* **1991**, *8*, 189-193.

14. Lambert, J.; Anderson, M.; Wolpert, J. Vineyard nutrient needs vary with rootstocks and soils. *California agriculture* **2008**, *62*, 202-207.

15. Ledderhof, D.; Brown, R.; Reynolds, A.; Jollineau, M. Using remote sensing to understand Pinot noir vineyard variability in Ontario. *Canadian journal of plant science* **2016**, *96*, 89-108.

16. Baluja, J.; Diago, M.P.; Balda, P.; Zorer, R.; Meggio, F.; Morales, F.; Tardaguila, J. Assessment of vineyard water status variability by thermal and multispectral imagery using an unmanned aerial vehicle (UAV). *Irrigation Science* **2012**, *30*, 511-522.

17. Jones, H.G. *Plants and microclimate: a quantitative approach to environmental plant physiology*; Cambridge university press: **2013**.

18. Matthews, M.; Anderson, M.; SCHULT, H.J.V. Phenologic and growth responses to early and late season. **1987**, *26*, 147-160.

19. Matthews, M.A.; Anderson, M.M.J.A.J.o.E.; Viticulture. Reproductive development in grape (Vitis vinifera L.): responses to seasonal water deficits. **1989**, *40*, 52-60.

20. Reynolds, A.G.; Naylor, A.P. Pinot noir'andRiesling'Grapevines Respond to Water Stress Duration and Soil Water-holding Capacity. *HortScience* **1994**, *29*, 1505-1510.

21. Santos, T.P.; Lopes, C.M.A.; Rodrigues, M.; Souza, C.R.d.; Maroco, J.; Pereira, J.S.; Silva, J.R.; Chaves, M.M.J.F.P.B. Partial rootzone drying: effects on growth and fruit quality of field-grown grapevines (Vitis vinifera). **2003**, *30*, 663-671.

22. Basinger, A.R.; Hellman, E.W. Evaluation of regulated deficit irrigation on grape in Texas and implications for acclimation and cold hardiness. *International journal of fruit science* **2007**, *6*, 3-22.

23. Howell, G.S.; Stergios, B.G.; Stackhouse, S. Interrelation of productivity and cold hardiness of Concord grapevines. *American Journal of Enology and Viticulture* **1978**, *29*, 187-191.

24. Ledderhof, D. Using GPS, GIS & remote sensing to understand Niagara Terroir: Pinot noir in the Four Mile Creek & St. David's Bench sub-appellations. **2012**.

25. Hall, A.; Louis, J.; Lamb, D.W. Low-resolution remotely sensed images of winegrape vineyards map spatial variability in planimetric canopy area instead of leaf area index. *Australian journal of grape and wine research* **2008**, *14*, 9-17.

26. Roberts, D.A.; Roth, K.L.; Perroy, R.L. hyperspectral vegetation indices. *Hyperspectral remote sensing of vegetation.* **2016**, 309.

27. Arnó Satorra, J.; Martínez Casasnovas, J.A.; Ribes Dasi, M.; Rosell Polo, J.R. Precision viticulture. Research topics, challenges and opportunities in site-specific vineyard management. *Spanish Journal of Agricultural Research* **2009**, *7*, 779-790.

28. Reynolds, A.G.; Rezaei, J.H. Spatial variability in Ontario Cabernet Franc vineyards: I. Interrelationships among soil composition, soil texture, soil and vine water status. *Journal of Applied Horticulture* **2014**, *16*.

29. Battany, M.; Grismer, M.J.H.p. Rainfall runoff and erosion in Napa Valley vineyards: effects of slope, cover and surface roughness. **2000**, *14*, 1289-1304.

30. Taylor, J.A.; Acevedo-Opazo, C.; Ojeda, H.; Tisseyre, B. Identification and significance of sources of spatial variation in grapevine water status. *Australian Journal of Grape and Wine Research* **2010**, *16*, 218-226.

31. Schreiner, R.P.J.P.; soil. Spatial and temporal variation of roots, arbuscular mycorrhizal fungi, and plant and soil nutrients in a mature Pinot noir (Vitis vinifera L.) vineyard in Oregon, USA. **2005**, *276*, 219-234.

32. Atkinson, N.J.; Urwin, P.E.J.J.o.e.b. The interaction of plant biotic and abiotic stresses: from genes to the field. **2012**, *63*, 3523-3543.

33. Suzuki, N.; Rivero, R.M.; Shulaev, V.; Blumwald, E.; Mittler, R.J.N.P. Abiotic and biotic stress combinations. **2014**, *203*, 32-43.

CHAPTER 4: RESULTS AND DISCUSSION – FEASIBILITY STUDY OF REMOTE SENSING TECHNOLOGIES TO MONITOR YIELD AND FRUIT QUALITIES

The short-term objective of this chapter was to examine the feasibility of using remote sensing technologies to monitor yield and fruit quality. We hypothesize that remote sensing data-analysis (NDVI, thermal, other indices) would correlate with yield and berry composition and vegetative growth in different stages of growing season could have different impact on yield and fruit quality.

4.1 Results

The vineyard canopy reflectance data from GreenSeeker® and RPAS flights were compared with harvest data (yield, number of clusters, berry weight) and berry composition data (Brix, pH, TA, phenols, and anthocyanin). RPAS flights with multispectral and thermal sensors were performed at veraison in 2015 and 2016. Proximal sensing (GreenSeeker®) readings were taken at three different times in 2015 and 2016 at the berry set, lag phase, and veraison and, twice in 2017 at lag phase and veraison. Basic statistics for RPAS /GreenSeeker® data and grape yield/quality along with the average values and their variations across the sites and years were provided in Table 4.1.

Table 4.1. Summary of the statistical analysis of data from the RPAS flight/proximal sensing, yield components, and berry composition in six Niagara vineyards from 2015, 2016 and 2017. Abbreviations: RPAS= Remotely Piloted Aircraft System, NDVI= Normalized difference vegetation index, P-NDVI= Proximal sensing NDVI, MIN= Minimum, MAX- Maximum, SD= Standard deviation, CV%= Coefficient of variation.

Site 1 (n=76)							Site 2 (n=75)						
Variable	Year	Average	MIN	MAX	SD	CV(%)	Variable	Year	Average	MIN	MAX	SD	CV(%)
RPAS NDVI	2015	0.588	0.505	0.676	0.042	7.1	RPAS NDVI	2015	0.655	0.396	0.807	0.093	14.2
	2016	0.738	0.655	0.819	0.039	5.2		2016	0.783	0.599	0.900	0.057	7.3
	2017	—	—	—	—	—		2017	—	—	—	—	—
RPAS Thermal (°C)	2015	26.75	25.55	27.59	0.50	1.9	RPAS Thermal (°C)	2015	31.61	29.94	32.49	0.50	1.6
	2016	27.53	26.93	28.03	0.25	0.9		2016	35.19	33.17	36.83	0.89	2.5
	2017	—	—	—	—	—		2017	—	—	—	—	—
P-NDVI	2015	0.714	0.641	0.754	0.025	3.5	P-NDVI	2015	0.804	0.774	0.825	0.013	1.6
	2016	0.741	0.708	0.771	0.014	1.9		2016	0.786	0.760	0.806	0.010	1.3
	2017	0.723	0.668	0.778	0.025	3.5		2017	0.839	0.820	0.851	0.007	0.8
Clusters	2015	20	5	49	10	49.6	Clusters	2015	19	3	43	8	40.9
	2016	46	12	83	14	31.5		2016	22	3	37	6	28.5
	2017	34	11	51	7	20.6		2017	22	9	43	6	28.3
Yield (kg)	2015	2.04	0.46	4.77	1.00	49.1	Yield (kg)	2015	2.56	0.40	5.96	0.97	38.0
	2016	4.34	0.44	8.92	1.66	38.3		2016	1.94	0.33	3.53	0.68	35.0
	2017	3.49	0.58	5.73	1.02	29.2		2017	2.42	0.68	4.52	0.86	35.4
Berry Wt. (g)	2015	1.27	0.85	1.57	0.17	13.2	Berry Wt. (g)	2015	1.10	0.82	1.67	0.12	11.3
	2016	1.25	1.00	1.48	0.12	9.3		2016	1.08	0.75	1.29	0.10	9.4
	2017	1.06	0.75	1.42	0.18	17.2		2017	1.10	0.89	1.40	0.11	9.6
Brix	2015	20.9	16.8	25.1	2.5	11.9	Brix	2015	24.6	22.6	26.1	0.9	3.5
	2016	20.9	15.0	24.5	1.8	8.6		2016	25.2	21.6	27.1	0.9	3.7
	2017	23.6	16.5	26.9	2.3	9.9		2017	24.1	21.4	27.4	1.1	4.7
pH	2015	3.48	3.19	5.53	0.26	7.6	pH	2015	3.59	3.45	3.76	0.07	1.9
	2016	3.44	3.10	3.69	0.12	3.5		2016	3.57	3.40	3.77	0.07	2.0
	2017	3.46	3.17	3.70	0.10	2.9		2017	3.59	3.36	3.76	0.09	2.4
TA (g/L)	2015	6.11	4.50	8.08	0.76	12.5	TA (g/L)	2015	5.66	4.59	6.71	0.47	8.2
	2016	5.90	4.79	8.57	0.75	12.7		2016	5.30	4.73	6.18	0.19	3.6
	2017	7.10	5.16	9.21	0.87	12.2		2017	6.57	5.08	10.00	0.65	9.9
Phenols (mg/L)	2015	1334	504	2440	474	35.5	Phenols (mg/L)	2015	2144	1027	3576	703	32.8
	2016	1524	370	3382	718	47.1		2016	1813	1078	3054	489	27.0
	2017	1388	623	2668	433	31.2		2017	1817	1104	3063	412	22.7
Anthocyanins (mg/L)	2015	266	66	636	154	57.9	Anthocyanins (mg/L)	2015	621	210	1099	244	39.4
	2016	411	70	1038	190	46.1		2016	648	281	1060	174	26.8
	2017	370	37	675	114	30.8		2017	625	227	1039	156	25.0
Site 3 (n=80)							**Site 4 (n=72)**						
Variable	Year	Average	MIN	MAX	SD	CV(%)	Variable	Year	Average	MIN	MAX	SD	CV(%)
RPAS NDVI	2015	0.655	0.396	0.807	0.093	14.2	RPAS NDVI	2015	0.589	0.512	0.692	0.038	6.4
	2016	0.426	0.204	0.684	0.106	29.9		2016	0.762	0.611	0.873	0.063	8.3
	2017	—	—	—	—	—		2017	—	—	—	—	—
RPAS Thermal (°C)	2015	21.52	20.57	21.88	0.25	1.1	RPAS Thermal (°C)	2015	24.17	23.86	24.50	0.12	0.5
	2016	33.48	31.64	35.57	1.07	3.2		2016	30.73	29.83	31.84	0.48	1.6
	2017	—	—	—	—	—		2017	—	—	—	—	—
P-NDVI	2015	0.769	0.727	0.810	0.021	2.7	GS NDVI	2015	0.828	0.803	0.843	0.007	0.8
	2016	0.796	0.741	0.828	0.023	2.9		2016	0.834	0.815	0.855	0.010	1.2
	2017	0.748	0.666	0.801	0.028	3.8		2017	0.833	0.814	0.852	0.008	1.0
Clusters	2015	—	—	—	—	—	Clusters	2015	34	12	49	8	22.5
	2016	34	14	60	10	31.0		2016	34	14	55	8	24.2
	2017	23	5	43	7	32.0		2017	37	22	49	5	14.7
Yield (kg)	2015	—	—	—	—	—	Yield (kg)	2015	5.33	0.41	9.08	1.44	27.0
	2016	2.65	0.82	5.81	1.03	38.9		2016	3.80	1.45	8.34	1.48	39.0
	2017	2.88	0.85	6.44	1.22	42.4		2017	5.67	3.36	8.87	1.14	20.1
Berry Wt. (g)	2015	—	—	—	—	—	Berry Wt. (g)	2015	1.21	0.91	1.59	0.17	14.1
	2016	1.02	0.42	1.43	0.22	21.8		2016	1.38	0.98	1.72	0.15	11.2
	2017	1.18	0.87	1.57	0.12	10.2		2017	1.07	0.87	1.48	0.10	9.6
Brix	2015	—	—	—	—	—	Brix	2015	20.4	15.4	23.1	1.5	7.2
	2016	25.1	19.7	27.6	1.8	7.2		2016	21.2	17.1	24.5	1.6	7.7
	2017	24.2	16.6	27.8	2.6	10.7		2017	22.3	15.8	25.6	2.3	10.4
pH	2015	—	—	—	—	—	pH	2015	3.33	3.16	3.44	0.06	1.9
	2016	3.66	3.44	3.88	0.10	2.7		2016	3.26	2.94	3.46	0.10	3.1
	2017	3.54	3.21	3.74	0.12	3.4		2017	3.38	3.21	3.56	0.07	2.1
TA (g/L)	2015	—	—	—	—	—	TA (g/L)	2015	7.16	5.78	8.79	0.51	7.1
	2016	6.61	5.76	7.92	0.39	5.9		2016	7.28	6.06	9.84	0.74	10.2
	2017	6.97	5.30	9.50	0.92	13.2		2017	7.23	5.43	9.52	0.70	9.7
Phenols (mg/L)	2015	—	—	—	—	—	Phenols (mg/L)	2015	1372	504	3075	575	41.9
	2016	2025	1000	3804	644	31.8		2016	1533	329	2880	618	40.3
	2017	1963	800	3400	643	32.8		2017	1301	504	2754	350	26.9
Anthocyanins (mg/L)	2015	—	—	—	—	—	Anthocyanins (mg/L)	2015	481	163	918	160	33.2
	2016	750	240	1385	202	26.9		2016	506	108	938	188	37.3
	2017	711	154	1427	248	34.9		2017	432	183	577	109	25.2

Site 5 (n=81)							Site 6 (n=80)						
Variable	Year	Average	MIN	MAX	SD	CV(%)	Variable	Year	Average	MIN	MAX	SD	CV(%)
RPAS NDVI	2015	0.503	0.382	0.606	0.040	8.0	RPAS NDVI	2015	0.595	0.478	0.698	0.053	8.9
	2016	0.506	0.398	0.635	0.051	10.0		2016	0.725	0.629	0.811	0.038	5.3
	2017	—	—	—	—	—		2017	—	—	—	—	—
RPAS Thermal (°C)	2015	31.20	30.41	32.10	0.43	1.4	RPAS Thermal (°C)	2015	25.06	23.04	26.20	0.98	3.9
	2016	32.76	30.69	34.00	0.70	2.1		2016	32.56	31.02	34.19	0.81	2.5
	2017	—	—	—	—	—		2017	—	—	—	—	—
P-NDVI	2015	0.798	0.747	0.827	0.017	2.1	P-NDVI	2015	0.795	0.731	0.822	0.017	2.2
	2016	0.739	0.612	0.778	0.025	3.4		2016	0.832	0.806	0.855	0.011	1.3
	2017	0.814	0.690	0.865	0.024	2.9		2017	0.827	0.812	0.841	0.006	0.7
Clusters	2015	33	4	64	12	37.5	Clusters	2015	32	18	54	7	22.3
	2016	30	12	49	9	29.5		2016	34	16	56	8	24.7
	2017	25	21	27	1	4.9		2017	30	13	49	8	24.8
Yield (kg)	2015	3.40	0.49	6.03	1.23	36.1	Yield (kg)	2015	3.23	1.28	5.15	0.88	27.3
	2016	1.92	0.55	4.30	0.78	40.4		2016	3.52	1.09	6.91	1.04	29.6
	2017	2.98	0.30	6.37	1.19	40.1		2017	3.23	1.24	4.74	0.83	25.6
Berry Wt. (g)	2015	1.12	0.79	1.45	0.15	13.3	Berry Wt. (g)	2015	1.21	1.01	1.49	0.10	8.4
	2016	0.94	0.74	1.16	0.10	11.1		2016	1.25	1.05	1.40	0.07	5.6
	2017	1.08	0.87	1.40	0.10	9.3		2017	1.03	0.80	1.63	0.12	11.6
Brix	2015	23.8	20.7	26.5	1.4	5.8	Brix	2015	24.6	22.2	26.4	1.1	4.6
	2016	25.2	20.0	27.5	1.4	5.7		2016	24.3	18.6	26.4	1.5	6.0
	2017	24.8	21.2	27.4	1.2	4.9		2017	24.9	17.9	28.1	2.1	8.3
pH	2015	3.49	3.28	3.81	0.11	3.2	pH	2015	3.51	3.34	3.65	0.07	1.9
	2016	3.34	3.05	3.56	0.09	2.7		2016	3.47	3.26	3.73	0.10	2.9
	2017	3.50	3.23	3.71	0.11	3.0		2017	3.50	3.28	3.70	0.10	2.8
TA (g/L)	2015	6.04	4.92	7.18	0.39	6.5	TA (g/L)	2015	5.64	4.80	6.68	0.33	5.8
	2016	7.26	6.10	8.53	0.48	6.7		2016	6.76	5.18	8.50	0.73	10.8
	2017	5.99	4.74	7.44	0.63	10.5		2017	6.85	5.15	10.07	0.91	13.2
Phenols (mg/L)	2015	2037	801	3931	725	35.6	Phenols (mg/L)	2015	1913	705	4176	776	40.6
	2016	2379	1067	3690	595	25.0		2016	2357	899	4415	762	32.3
	2017	2082	800	3388	551	26.4		2017	2099	801	3683	436	20.7
Anthocyanins (mg/L)	2015	719	200	1564	288	40.0	Anthocyanins (mg/L)	2015	731	280	1607	293	40.1
	2016	901	405	1321	176	19.6		2016	850	275	1390	276	32.5
	2017	770	281	1361	210	27.4		2017	802	265	1342	217	27.0

4.1.1 Principal component analysis (PCA) between NDVIs and grape yield/fruit quality

Principal component analysis (PCA) results for NDVIs and grape yield/quality are presented in Figure 4.1 and 4.2. PCA results were built based on the first two factors, which explained between 40 to 64% of the data (Figure 4.1 and 4.2). In site 1 2015, 2016, and 2017 (Figure 4.1), the analysis described 49.80%, 51.38%, and 57.07% of the data and demonstrated that NDVIs from proximal sensing and from the RPAS flight positively correlated to phenols and berry weight in 2015 but phenols and berry weights were derived from relatively short vectors, so visual correlations were difficult to establish. The vector for yield and NDVIs in 2016 and 2017 were relatively long and showed positive correlation to each other. Other variables like pH, TA, Brix, and clusters were also derived from relatively short vectors, so visual correlations were

difficult to establish. The NDVIs were clustered together through the years and negatively correlated to the thermal in 2015.

In site 2 2015, 2016, and 2017 (Figure 4.1), the analysis described 51.26%, 46.74%, and 49.36% of the data and demonstrated that proximal sensing NDVI (P-NDVI) negatively correlated to anthocyanins and phenols in the three-year period while NDVI from the RPAS flight was derived from relatively short vectors, so visual correlations were difficult to establish. Thermal imaging from the RPAS flight was positively correlated to phenols, anthocyanin, Brix, and pH and negatively correlated to the NDVIs in 2016.

In site 3 2016 and 2017 (Figure 4.1), the analysis described 64.37% and 53.51% of the data and demonstrated that P-NDVI and NDVI had an inverse relationship with yield, clusters, and berry weight and had a positive relationship with anthocyanins, phenols, brix, and pH in 2016. P-NDVI somewhat positively correlated to berry weight, yield, and clusters in 2017 but the vectors for the variables were relatively short and thus there does not appear to be clear in the PCA chart.

In site 4 2015, 2016, and 2017 (Figure 4.2), the analysis described 45.19%, 51.00%, and 39.40% of the data and demonstrated that P-NDVIs had a positive relationship with berry weight and yield and had an inverse relationship with anthocyanin in 2015 and 2016 while NDVI was derived from relatively short vectors, so visual correlations were difficult to establish. In 2017, phenols, anthocyanins, and brix were negatively correlated to P-NDVI while yield and berry weight were somewhat positively correlated to P-NDVIs but the vectors for the variables were relatively short and thus there does not appear to be clear in the PCA chart. Thermal was negatively correlated with the NDVIs and positively correlated to anthocyanin, phenols, pH, and Brix in 2016.

In site 5 2015, 2016, and 2017 (Figure 4.2), the analysis described 48.84%, 50.75%, and 47.28% of the data and demonstrated that P-NDVIs negatively correlated to phenols, anthocyanins,

and brix and positively correlated to yield and clusters throughout the three-year period. NDVI showed somewhat similar correlation to P-NDVIs, but NDVI was derived from relatively short vectors, so visual correlations were difficult to establish. Thermal had a negative relationship with the NDVIs and positively correlated to phenols, anthocyanins, and brix in both years.

In site 6 2015, 2016, and 2017 (Figure 4.2), the analysis described 46.09%, 50.81%, and 44.16% of the data and showed NDVI and TA were positively correlated, and an inverse correlation between NDVI and pH was found in 2015 and 2016 but those had short vectors and thus there does not appear to be clear in the PCA chart. In 2017, there does not appear to be clear relationships in the PCA chart, and some vectors were short.

Overall, observing the short vectors for some variables, Pearson's correlations should be used to test whether other factors are adequately explaining some variable. It was found that the NDVIs and yield/berry weight are positively correlated, while phenols and anthocyanins level in the grapes is inversely correlated to them.

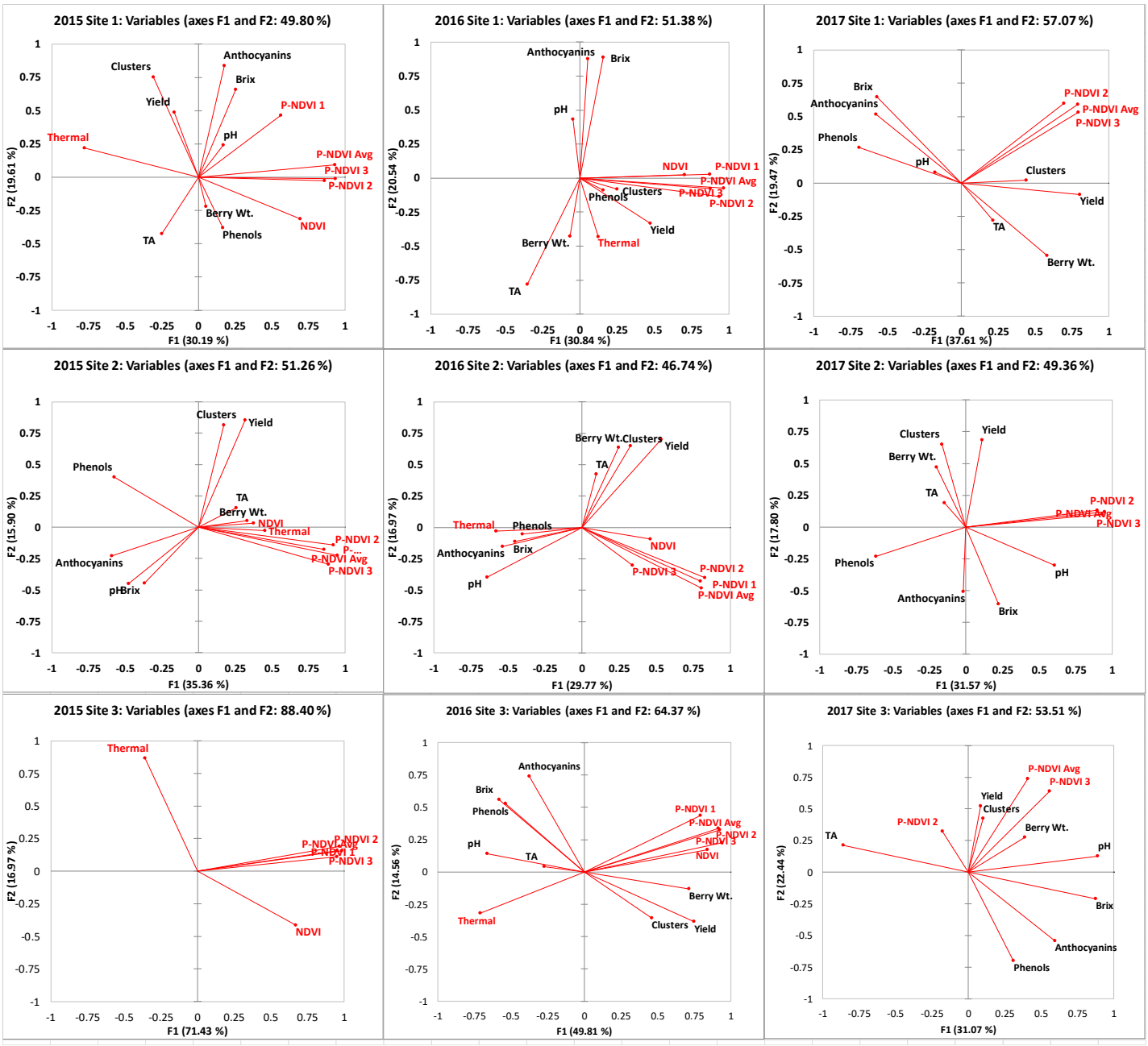

Figure 4.1. PCA results among data from proximal sensing and RPAS flight, vineyard yield and berry composition in site 1, 2, and 3 vineyards from 2015, 2016 and 2017. No harvest data collected at site 3 vineyard in 2015. Abbreviations: NDVI= Normalized difference vegetation index, Clusters= Number of clusters, Berry WT= Berry weight, TA= Titratable acidity, P-NDVI 1= Proximal NDVI at berry set, P-NDVI 2= Proximal NDVI at lag phase, P-NDVI 3= Proximal NDVI at veraison, NDVI= NDVI from RPAS flight at veraison, Thermal= Thermal imaging from RPAS flight at veraison.

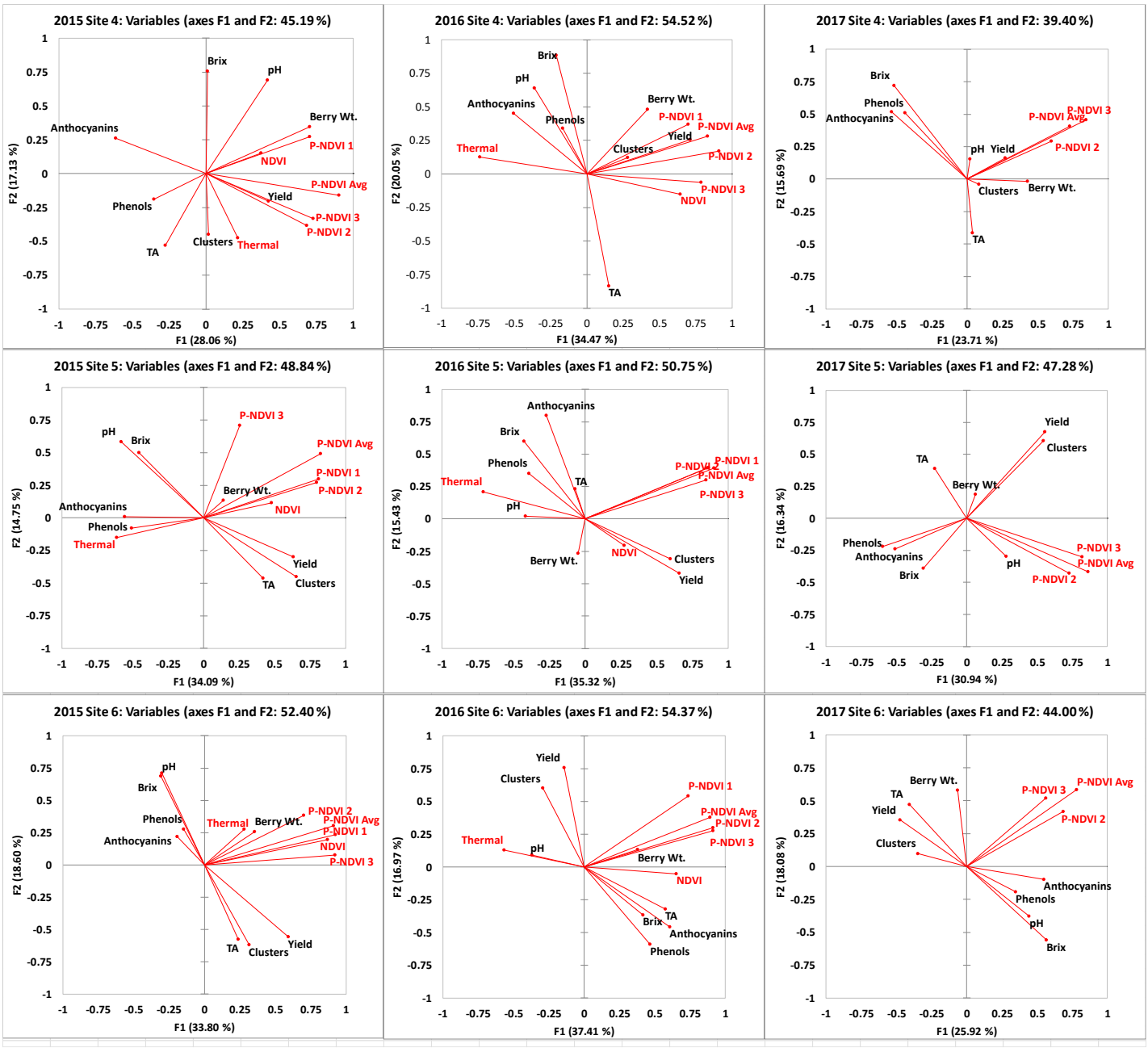

Figure 4.2. PCA results among data from proximal sensing and from RPAS flight, vineyard yield and berry composition in site 4, 5, and 6 vineyards from 2015, 2016 and 2017. No harvest data was collected at site 3 vineyard in 2015. Abbreviations: NDVI= Normalized difference vegetation index, Clusters= Number of clusters, Berry WT= Berry weight, TA= Titratable acidity, P-NDVI 1= Proximal NDVI at berry set, P-NDVI 2= Proximal NDVI at lag phase, P-NDVI 3= Proximal NDVI at veraison, NDVI= NDVI from RPAS flight at veraison, Thermal= Thermal imaging from RPAS flight at veraison.

4.1.2 Pearson's correlation between proximal sensing and grape yield/fruit quality

4.1.2.1 Relationships between proximal sensing NDVIs and yield

Table 4.2 indicated that P-NDVIs were positively correlated to yield in multiple sites throughout the consecutive years. The measurement at berry set (P-NDVI 1) showed the most correlation with yield. All the sites except for site 2 indicated a positive relationship between P-NDVI 1 and yield. The P-NDVI measurement at lag phase and veraison also indicated positive correlation to the yield but some negative correlation observed between the two variables.

The mean yield and its variation differed between sites (Table 4.1). The site with the highest yield (three years average) was site 4 (4.93 ± 1.35), followed by site 6 (3.32 ± 0.92), site 1 (3.29 ± 1.23), with the value drop seen in site 5 (2.77 ± 1.07), site 3 (2.77 ± 1.13), and site 2 (2.31 ± 0.84). The site with the highest variation in yield (three years average; Table 4.1) was site 3 (CV%=40.64), site 1 (CV%=38.87), site 5 (CV%=38.88), and site 2 (CV%=36.10) with the value drop seen in site 4 (CV%=28.70) and site 6 (CV%=27.50).

Table 4.2. Pearson's correlation results between proximal sensing NDVI vs yield and berry composition data in six Niagara vineyards from 2015, 2016 and 2017. Those variables with significant (95% confidence) were listed in bold, with blank cells representing no correlation: blue boxes= positive correlation with NDVI, red boxes= negative correlation with NDVI, black boxes= no data collected. Abbreviations: Clusters= Number of clusters, Berry Wt= Berry weight, TA= Titratable acidity.

Proximal Sensing NDVI 1 (Fruit Set)-Correlation matrix

Vineyards	Clusters	Yield	Berry Wt.	Brix	pH	TA	Phenols	Anthocyanins
2015 Site 1	0.118	0.055	-0.194	**0.330**	0.151	-0.125	-0.062	**0.437**
2016 Site 1	0.099	**0.255**	-0.177	0.090	-0.150	**-0.266**	0.023	0.078
2015 Site 2	0.064	0.111	**0.237**	-0.131	**-0.325**	0.223	**-0.487**	**-0.420**
2016 Site 2	0.060	0.209	0.002	**-0.249**	**-0.346**	-0.136	-0.207	**-0.244**
2015 Site 3								
2016 Site 3	**0.221**	**0.416**	**0.370**	**-0.317**	**-0.379**	-0.145	-0.178	-0.040
2015 Site 4	-0.057	**0.259**	**0.403**	0.152	**0.396**	-0.106	**-0.337**	**-0.339**
2016 Site 4	-0.077	**0.431**	**0.256**	0.142	-0.147	-0.085	**0.243**	-0.155
2015 Site 5	**0.396**	**0.334**	0.087	-0.155	**-0.353**	**0.232**	-0.197	-0.167
2016 Site 5	**0.359**	**0.322**	-0.108	-0.139	**-0.260**	-0.047	**-0.238**	0.008
2015 Site 6	0.101	**0.385**	**0.369**	-0.147	-0.087	0.105	-0.100	-0.114
2016 Site 6	-0.013	0.200	**0.224**	0.130	-0.129	0.159	0.018	**0.222**

Proximal Sensing NDVI 1 (Fruit Set)-p-values

Vineyards	Clusters	Yield	Berry Wt.	Brix	pH	TA	Phenols	Anthocyanins
2015 Site 1	0.310	0.639	0.093	**0.004**	0.192	0.282	0.592	**0.000**
2016 Site 1	0.396	**0.026**	0.127	0.439	0.196	**0.020**	0.846	0.501
2015 Site 2	0.585	0.342	**0.041**	0.263	**0.004**	0.054	**0.000**	**0.000**
2016 Site 2	0.607	0.072	0.985	**0.031**	**0.002**	0.245	0.075	**0.035**
2015 Site 3								
2016 Site 3	**0.049**	**0.000**	**0.001**	**0.004**	**0.001**	0.198	0.114	0.724
2015 Site 4	0.635	**0.028**	**0.000**	0.201	**0.001**	0.377	**0.004**	**0.004**
2016 Site 4	0.522	**0.000**	**0.030**	0.233	0.217	0.479	**0.040**	0.194
2015 Site 5	**0.000**	**0.002**	0.440	0.166	**0.001**	**0.037**	0.078	0.135
2016 Site 5	**0.001**	**0.003**	0.337	0.215	**0.019**	0.677	**0.033**	0.941
2015 Site 6	0.371	**0.000**	**0.001**	0.194	0.441	0.354	0.379	0.316
2016 Site 6	0.907	0.076	**0.046**	0.249	0.253	0.160	0.876	**0.048**

Proximal Sensing NDVI 2 (Lag Phase)-Correlation matrix

Vineyards	Clusters	Yield	Berry Wt.	Brix	pH	TA	Phenols	Anthocyanins
2015 Site 1	-0.211	-0.070	-0.097	0.085	0.052	-0.063	0.065	0.120
2016 Site 1	0.084	**0.362**	-0.006	0.018	-0.124	-0.203	0.100	-0.061
2017 Site 1	0.138	**0.402**	0.018	-0.085	-0.216	0.173	**-0.331**	-0.095
2015 Site 2	0.092	0.166	**0.242**	-0.222	**-0.339**	**0.321**	**-0.438**	**-0.397**
2016 Site 2	-0.018	0.180	-0.002	**-0.312**	**-0.291**	-0.125	-0.214	**-0.256**
2017 Site 2	0.032	0.119	-0.189	0.028	**0.322**	-0.220	**-0.351**	0.026
2015 Site 3								
2016 Site 3	**0.333**	**0.545**	**0.519**	**-0.383**	**-0.507**	-0.179	**-0.292**	-0.136
2017 Site 3	-0.042	-0.082	0.037	-0.166	-0.103	**0.258**	-0.109	-0.146
2015 Site 4	0.001	0.172	0.169	-0.097	0.096	0.055	0.128	-0.180
2016 Site 4	0.059	**0.602**	**0.352**	-0.039	**-0.250**	0.090	0.004	**-0.385**
2017 Site 4	0.062	0.140	0.224	-0.162	**0.294**	0.085	-0.004	-0.113
2015 Site 5	**0.398**	**0.370**	0.104	-0.173	**-0.345**	0.153	**-0.255**	**-0.274**
2016 Site 5	**0.360**	**0.432**	-0.033	-0.113	**-0.273**	-0.034	-0.191	0.033
2017 Site 5	0.135	0.099	-0.008	-0.127	0.026	-0.202	**-0.242**	**-0.223**
2015 Site 6	0.058	0.194	0.161	0.064	-0.012	0.025	0.120	0.075
2016 Site 6	-0.144	-0.019	**0.292**	**0.283**	**-0.229**	**0.381**	**0.229**	**0.376**
2017 Site 6	-0.201	**-0.268**	0.093	0.113	0.008	-0.041	0.130	**0.303**

Proximal Sensing NDVI 2 (Lag Phase)-p-values

Vineyards	Clusters	Yield	Berry Wt.	Brix	pH	TA	Phenols	Anthocyanins
2015 Site 1	0.067	0.548	0.404	0.468	0.653	0.589	0.576	0.303
2016 Site 1	0.471	**0.001**	0.960	0.876	0.287	0.079	0.391	0.600
2017 Site 1	0.235	**0.000**	0.875	0.466	0.061	0.136	**0.003**	0.413
2015 Site 2	0.430	0.154	**0.037**	0.056	**0.003**	**0.005**	**0.000**	**0.000**
2016 Site 2	0.879	0.122	0.985	**0.006**	**0.011**	0.285	0.066	**0.027**
2017 Site 2	0.788	0.310	0.104	0.813	**0.005**	0.058	**0.002**	0.826
2015 Site 3								
2016 Site 3	**0.003**	**0.000**	**0.000**	**0.000**	**0.000**	0.111	**0.008**	0.228
2017 Site 3	0.711	0.467	0.744	0.140	0.362	**0.021**	0.335	0.197
2015 Site 4	0.996	0.148	0.156	0.418	0.423	0.645	0.283	0.131
2016 Site 4	0.622	**0.000**	**0.002**	0.745	**0.034**	0.454	0.976	**0.001**
2017 Site 4	0.604	0.241	0.058	0.175	**0.012**	0.479	0.972	0.344
2015 Site 5	**0.000**	**0.001**	0.355	0.122	**0.002**	0.172	**0.022**	**0.013**
2016 Site 5	**0.001**	**0.000**	0.772	0.313	**0.014**	0.763	0.087	0.772
2017 Site 5	0.231	0.380	0.942	0.257	0.815	0.070	**0.029**	**0.046**
2015 Site 6	0.611	0.084	0.153	0.576	0.914	0.825	0.288	0.509
2016 Site 6	0.203	0.864	**0.009**	**0.011**	**0.041**	**0.000**	**0.041**	**0.001**
2017 Site 6	0.074	**0.016**	0.411	0.320	0.941	0.716	0.251	**0.006**

Proximal Sensing NDVI 3 (Varaison)-Correlation matrix

Vineyards	Clusters	Yield	Berry Wt.	Brix	pH	TA	Phenols	Anthocyanins
2015 Site 1	-0.207	-0.022	0.013	0.012	0.089	0.017	0.089	0.155
2016 Site 1	0.044	**0.267**	0.102	0.116	0.094	**-0.253**	0.225	-0.092
2017 Site 1	**0.291**	**0.544**	0.215	-0.121	0.000	-0.035	**-0.421**	-0.206
2015 Site 2	-0.044	0.066	0.171	-0.210	-0.225	0.207	**-0.607**	**-0.384**
2016 Site 2	0.091	0.028	-0.061	-0.059	-0.048	-0.131	-0.033	**-0.273**
2017 Site 2	-0.072	0.131	-0.135	0.112	**0.377**	-0.129	**-0.467**	0.024
2015 Site 3								
2016 Site 3	**0.378**	**0.633**	**0.582**	**-0.383**	**-0.520**	**-0.314**	**-0.378**	-0.218
2017 Site 3	0.110	0.216	**0.281**	**0.309**	**0.508**	**-0.226**	-0.194	-0.014
2015 Site 4	0.031	0.206	**0.375**	-0.063	0.131	-0.146	-0.020	**-0.355**
2016 Site 4	0.207	**0.438**	**0.232**	-0.126	**-0.250**	0.163	-0.165	**-0.297**
2017 Site 4	-0.044	0.138	0.106	-0.064	-0.191	-0.066	-0.159	-0.156
2015 Site 5	-0.159	-0.002	-0.060	0.087	**0.291**	-0.082	**-0.330**	**-0.311**
2016 Site 5	**0.224**	**0.332**	0.027	-0.152	-0.195	-0.068	**-0.272**	-0.072
2017 Site 5	**0.272**	**0.302**	-0.019	-0.046	**0.356**	-0.106	**-0.369**	**-0.237**
2015 Site 6	0.211	**0.453**	**0.312**	**-0.229**	-0.208	0.164	-0.105	-0.151
2016 Site 6	-0.185	-0.037	**0.311**	**0.284**	**-0.258**	**0.356**	**0.225**	**0.354**
2017 Site 6	0.028	0.068	0.181	0.071	0.200	-0.121	0.053	0.160

Proximal Sensing NDVI 3 (Varaison)-p-values

Vineyards	Clusters	Yield	Berry Wt.	Brix	pH	TA	Phenols	Anthocyanins
2015 Site 1	0.073	0.851	0.914	0.915	0.443	0.886	0.445	0.181
2016 Site 1	0.708	**0.020**	0.380	0.319	0.420	**0.027**	0.050	0.431
2017 Site 1	**0.011**	**0.000**	0.063	0.297	0.999	0.767	**0.000**	0.075
2015 Site 2	0.705	0.575	0.142	0.070	0.052	0.074	**0.000**	**0.001**
2016 Site 2	0.437	0.811	0.601	0.613	0.684	0.263	0.777	**0.018**
2017 Site 2	0.539	0.263	0.249	0.340	**0.001**	0.271	**0.000**	0.836
2015 Site 3								
2016 Site 3	**0.001**	**0.000**	**0.000**	**0.000**	**0.000**	**0.005**	**0.001**	0.052
2017 Site 3	0.331	0.055	**0.012**	**0.005**	**0.000**	**0.044**	0.092	0.902
2015 Site 4	0.796	0.083	**0.001**	0.597	0.273	0.220	0.843	**0.002**
2016 Site 4	0.081	**0.000**	**0.050**	0.290	**0.034**	0.172	0.166	**0.011**
2017 Site 4	0.716	0.246	0.375	0.591	0.108	0.581	0.182	0.192
2015 Site 5	0.156	0.988	0.596	0.442	**0.008**	0.469	**0.003**	**0.005**
2016 Site 5	**0.044**	**0.002**	0.807	0.175	0.081	0.545	**0.014**	0.524
2017 Site 5	**0.014**	**0.006**	0.868	0.685	**0.001**	0.345	**0.001**	**0.033**
2015 Site 6	0.061	**0.000**	**0.005**	**0.041**	0.064	0.147	0.353	0.180
2016 Site 6	0.100	0.742	**0.005**	**0.011**	**0.021**	**0.001**	**0.045**	**0.001**
2017 Site 6	0.806	0.547	0.109	0.531	0.075	0.286	0.640	0.157

The annual variation in yield level throughout the vineyards was also observed. The mean temperature (°C) and precipitation (mm) data from 2015 to 2017 in Niagara, Ontario were shown in Figure 4.3. As illustrated in Figure 4.3, in 2016, the mean temperatures were about 1.5 °C above the historical average while the growing season precipitation was about 200 mm below the historical average. Both mean temperatures and precipitation were similar to the historical average in 2015 and 2017. Interestingly, in the regular growing season (i.e., 2015 and 2017), the yield level was consistent but in hot and dry years (i.e., 2016), the yield level shifted to higher yield in site 1 and 6 while shifted to lower yield in site 2, 3, 4, and 5.

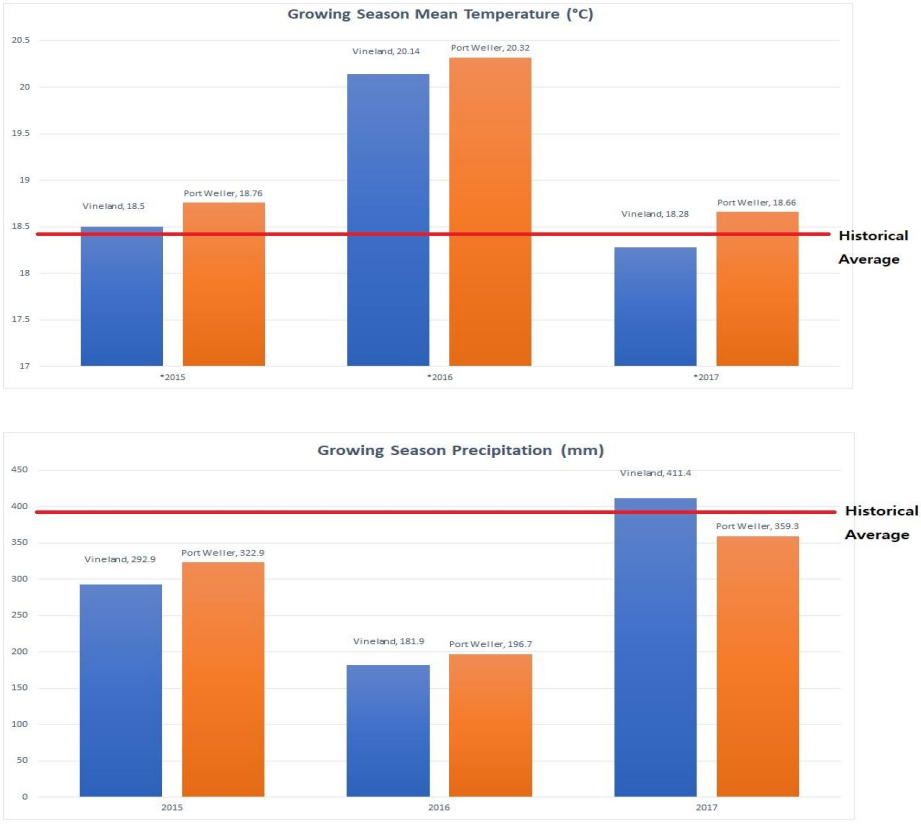

Figure 4.3. Mean growing season (May to September) temperature (°C) and total growing season rainfall (mm) from two Niagara resign locations. Port Weller AUT represented Niagara-on-the-lake vineyards and Vineland Research Station represented vineland vineyards. Historical climate normal data from St. Catharines A station 1981-2010.

Overall, proximal sensing measurement at fruit set could detect variation in yield at five out of six sites where three out of the three sites had high variation and showed temporal stability throughout the consecutive years. Vineyard yield was positively correlated with NDVI. Detecting local yield variation by proximal sensing does not appear to have an impact, because positive correlation was observed in low (site 4) and high (site 3 and 5) yield variation sites. However, the observation of better positive correlation level between P-NDVI and yield at fruit set stage indicated a possible temporal vegetation impact on yield. Furthermore, there could be an impact of annual climate changes (mean temperature and precipitation) on yield in the vineyard, but the impact could be either positive or negative.

4.1.2.2 Relationships between proximal sensing NDVI and clusters/berry weight

P-NDVIs were not associated with number of clusters in five vineyards, with only site 5 vineyards displaying consistent positive correlations through the years (Table 4.2). While P-NDVIs were not associated with clusters in most sites, NDVI and berry weight were more closely correlated. The P-NDVI at fruit set had a positive relationship with the weight of berry in four sites (Table 4.2) and three sites showed temporal stability of two consecutive years data. Variation occurred across sites in the mean berry weight (Table 4.1), with the largest mean weight per berry (g) being in site 4 (1.22 ± 0.14), then site 1 (1.19 ± 0.15), site 6 (1.16 ± 0.10), with the value drop seen in site 3 (1.10 ± 0.17), site 2 (1.09 ± 0.11), and site 5 (1.05 ± 0.12). Additionally, the overall variability of yield varied between vineyards, with the biggest variation in site 3 (16.00%), then site 1 (13.23%), site 4 (11.26%), site 5 (11.24%), site 2 (10.11%), and the least in site 6 (8.54%).

Overall, proximal sensing could detect variation in weight of single berry at three vineyard sites with temporal stability throughout the consecutive years. The NDVI from the RPAS flight and berry weight showed a significant positive correlation. The lowest variation site (site 6) showed both positive correlation and temporal stability, but the highest variation sites (site 1) did not show any correlation between the two variables. Detecting local yield variation by proximal sensing does not appear to have an impact. Higher positive correlation level between P-NDVI and yield at fruit set stage was also observed and indicated a possible temporal vegetation impact on yield.

4.1.2.3 Relationships between proximal sensing NDVIs and anthocyanins

P-NDVIs were negatively correlated to anthocyanins in two sites (site 2 and 5; Table 4.2) while site 6 site showed positive correlations. The measurements at lag phase (P-NDVI 2) and veraison (P-NDVI 3) showed a better correlation with anthocyanins than that of fruit set measurement. The average of the P-NDVI also negatively correlated to anthocyanins level. The mean anthocyanins level and its variation differed between sites (Table 4.1). The site with the highest anthocyanins level (three years average) was site 5 (796 ± 224), followed by site 6 (794 ± 262), site 3 (730 ± 225), site 2 (631 ± 191), with the value drop seen in site 4 (472 ± 152) and site 1 (348 ± 152). The site with the highest variation in anthocyanins (three years average; Table 4.1) was site 1 (CV%=44.96), followed by site 6 (CV%=33.21), with the value drop seen in site 4 (CV%=31.89), site 3 (CV%=30.92), site 2 (CV%=30.38) and site 5 (CV%=28.97). The annual variation in anthocyanins level throughout the vineyards was also observed. Interestingly, in Figure 4.3, the growing season was hot and dry in 2016, and a high anthocyanins level was observed in all the vineyard sites in 2016.

Overall, proximal sensing could detect variation in anthocyanins level at three out of six sites and showed some temporal stability throughout the consecutive years. The level of anthocyanins in vineyards was negatively correlated with the NDVI observed from the RPAS flights. The vegetation at lag phase and at veraison (P-NDVI 3) could have more impacts on accumulation of anthocyanins level in berry since the P-NDVI measurements at lag phase and veraison showed the better correlation with anthocyanins than that of fruit set measurement. There does not appear to be an impact of variation of anthocyanins level and its detection by proximal sensing, because both negative correlation and temporal stability observed in the high (site 6) and the low (site 5) variation in anthocyanins level. As in the case of yield, seasonal differences with respect to temperature and precipitation impacted the level of anthocyanins in the berries.

4.1.2.4 Relationships between proximal sensing NDVI and phenols

P-NDVIs were negatively correlated to phenols with some temporal consistency observed through the years (site 2, 3, and 5; Table 4.2). The measurements at veraison (P-NDVI 3) showed better correlation with phenols than that of fruit set (P-NDVI 1) and lag phase (P-NDVI 2) measurement. The average of the P-NDVI also negatively correlated to phenols level. The mean phenols level and its variation differed between sites (Table 4.1). The site with the highest phenols level (three years average) was site 5 (2166 ± 623), followed by site 6 (2123 ± 658), site 3 (1993 ± 643), site 2 (1924 ± 534), with the value drop seen in site 1 (1415 ± 541) and site 4 (1401 ± 152). The site with the highest variation in phenols (three years average; Table 4.1) was site 1 (CV%=37.92), followed by site 4 (CV%=36.38), with the value drop seen in site 3 (CV%=32.28), site 6 (CV%=31.22), site 5 (CV%=29.02), and site 2 (CV%=27.48). The annual variation in phenols level throughout the vineyards was also observed. Interestingly, the growing season was

hot and dry in 2016 (Figure 4.3), and a high phenols level was observed in almost all the vineyard sites in 2016, which also observed in anthocyanins level in the berries.

Overall, proximal sensing could detect variation in phenols level at three out of six sites in 2017 and these relationships were consistent and stable in time. The level of phenols in vineyards was negatively correlated with the NDVI from the RPAS flight. There does not appear to be a relationship between NDVI from the RPAS flight and the variation in phenol levels. However, the observation of better positive correlation level between P-NDVI and phenols at veraison indicated a possible temporal vegetation impact on yield. Furthermore, there could be an impact of growing season on the total level of phenols, same pattern observed in anthocyanins in the berries.

4.1.2.5 Relationships between proximal sensing NDVI and Brix/titratable acidity (TA)/pH

There were only weak correlations observed between P-NDVIs and other berry composition values (Brix, TA, and pH) and a lack of consistency in the correlations was evident throughout the sites and years (Table 4.2). However, P-NDVI measurement at lag phase showed a strong negative correlation to the pH in most of sites in 2016, a hot and dry year (Table 4.2). P-NDVI at fruit set also negatively correlated in three sites in 2016. The site with the highest Brix level (three years average; Table 4.1) was site 2 (24.64 ± 0.97), site 3 (24.66 ± 2.19), site 5 (24.62 ± 1.34), site 6 (24.57 ± 1.56), with the value drop seen in site 1 (21.80 ± 2.21) and site 4 (21.32 ± 1.81).

The site with the highest variation in Brix (three years average; Table 4.1) was site 1 (CV%=10.15), followed by site 3 (CV%=8.92), and site 4 (CV%=8.43), with the value drop seen site 6 (CV%=6.33), site 5 (CV%=5.47), and site 2 (CV%=3.95). The site with the highest TA level was site 4 (7.22 ± 0.65), followed by site 3 (6.79 ± 0.65), site 5 (6.43 ± 0.65), site 6 (6.42 ± 0.50),

and site 1 (6.37 ± 0.79) with the value drop seen in site 2 (5.84 ± 0.44). The site with the highest variation in Brix was site 1 (CV%=12.47), followed by site 6 (CV%=9.95), site 3 (CV%=9.51), site 4 (CV%=9.01), with the value drop seen in site 5 (CV%=7.22), and site 2 (CV%=7.25). The site with the highest pH level was site 3 (3.6 ± 0.11), site 2 (3.58 ± 0.08), with the value drop seen in site 6 (3.48 ± 0.09), site 1 (3.46 ± 0.16), site 5 (3.44 ± 0.10), and site 4 (3.32 ± 0.08). Site 1 had the highest pH variation (CV%=4.67), then in site 3 (CV%=3.08), site 5 (CV%=3.00), site 6 (CV%=2.96), and with the value drop seen site 4 (CV%=2.34), and site 2 (CV%=2.12).

Overall, proximal sensing NDVI was least capable of detecting variation in other berry compositions (Brix, TA, and pH) in all vineyard sites and years. P-NDVI did not appear to be affected by Brix, TA, or pH values for any of the sites, or variations in those values. However, P-NDVI at lag phase with a strong capability to detect variations in pH in all vineyard sites in 2016 and P-NDVI at fruit set also negatively correlated in three sites in 2016. Therefore, there could be an impact of annual climate changes (mean temperature and precipitation) on its detection by proximal sensing in particularly, earlier stage of berry development. Furthermore, there was no specific pattern found to show an impact of annual climate changes (mean temperature and precipitation) on the level of Brix, TA, and pH of the berry samples.

4.1.3 Pearson's correlation between NDVI/thermal from the RPAS flight and grape yield/fruit quality

4.1.3.1 Relationships between NDVI/thermal from the RPAS flight and yield (kg)/berry weight(g)

Table 4.3 indicated that NDVI had a positive correlation with yield in most of sites and site 5 showed temporal stability throughout the consecutive years. However, there were only weak correlations observed between thermal and yield with consistent negative relationships between

the two variables in 2016. Interestingly, the annual variation in the correlation matrix between NDVI from the RPAS flight and yield throughout the vineyards had indicated with more capability of detecting the correlation in the year with hot and dry growing season like 2016 (Figure 4.3), and thus the statistically significant positive correlations between the NDVI and yield were observed in five of six sites in 2016 while only two vineyards had the correlation in 2015.

Table 4.3. Pearson's correlation results between NDVI/thermal from the RPAS flight vs yield and berry composition data in six Niagara vineyards from 2015, 2016 and 2017. Those variables with significant (95% confidence) were listed in bold, with blank cells representing no correlation: blue boxes= positive correlation with NDVI, red boxes= negative correlation with NDVI, black boxes= no data collected. Abbreviations: Clusters= Number of clusters, Berry Wt= Berry weight, TA= Titratable acidity.

Remote Sensing NDVI (Correlation matrix)

Vineyards	Clusters	Yield	Berry Wt.	Brix	pH	TA	Phenols	Anthocyanins
2015 Site 1	**-0.392**	-0.131	**0.264**	0.129	0.055	**-0.272**	0.220	-0.222
2016 Site 1	0.226	**0.410**	-0.197	0.042	-0.157	**-0.247**	0.022	0.091
2015 Site 2	0.049	0.181	**0.238**	**-0.238**	-0.002	0.107	-0.053	-0.047
2016 Site 2	**0.243**	**0.241**	0.033	-0.032	-0.064	0.095	-0.047	0.095
2015 Site 3								
2016 Site 3	**0.304**	**0.512**	**0.462**	**-0.432**	**-0.513**	-0.213	**-0.355**	-0.220
2015 Site 4	0.035	0.117	**0.328**	-0.021	0.131	0.055	-0.181	**-0.232**
2016 Site 4	**0.252**	**0.390**	**0.297**	**-0.262**	-0.195	0.148	-0.176	**-0.263**
2015 Site 5	0.137	**0.233**	**0.293**	-0.107	**-0.294**	**0.268**	**-0.384**	-0.192
2016 Site 5	0.134	**0.234**	0.141	-0.105	0.031	**-0.328**	0.059	-0.151
2015 Site 6	0.056	**0.309**	**0.362**	-0.162	-0.142	0.089	-0.124	-0.202
2016 Site 6	**-0.220**	0.023	**0.321**	0.164	**-0.296**	**0.512**	**0.294**	**0.406**

Remote Sensing NDVI (p-values)

Vineyards	Clusters	Yield	Berry Wt.	Brix	pH	TA	Phenols	Anthocyanins
2015 Site 1	**0.000**	0.259	**0.021**	0.267	0.635	**0.017**	0.056	0.054
2016 Site 1	0.049	**0.000**	0.088	0.717	0.177	**0.032**	0.848	0.435
2015 Site 2	0.679	0.120	**0.040**	**0.040**	0.984	0.361	0.654	0.687
2016 Site 2	**0.049**	**0.048**	0.781	0.784	0.583	0.420	0.688	0.419
2015 Site 3								
2016 Site 3	**0.006**	**0.000**	**0.000**	**0.000**	**0.000**	0.058	**0.001**	0.050
2015 Site 4	0.769	0.328	**0.005**	0.864	0.274	0.646	0.127	**0.049**
2016 Site 4	**0.033**	**0.001**	**0.011**	**0.026**	0.101	0.214	0.139	**0.025**
2015 Site 5	0.222	**0.037**	**0.008**	0.343	**0.008**	**0.016**	**0.000**	0.086
2016 Site 5	0.233	**0.035**	0.210	0.349	0.783	**0.003**	0.600	0.179
2015 Site 6	0.623	**0.005**	**0.001**	0.151	0.209	0.433	0.273	0.073
2016 Site 6	**0.050**	0.837	**0.004**	0.145	**0.008**	**0.000**	**0.008**	**0.000**

Remote Sensing Thermal (Correlation matrix)

Vineyards	Clusters	Yield	Berry Wt.	Brix	pH	TA	Phenols	Anthocyanins
2015 Site 1	**0.300**	0.143	-0.083	-0.130	-0.035	0.218	-0.201	0.087
2016 Site 1	-0.119	0.032	**0.352**	**-0.238**	**0.247**	0.112	0.160	**-0.438**
2015 Site 2	0.029	0.053	0.097	-0.090	**-0.354**	0.124	-0.186	-0.216
2016 Site 2	-0.085	-0.194	-0.097	0.034	**0.485**	-0.212	**0.254**	0.177
2015 Site 3								
2016 Site 3	-0.093	**-0.348**	**-0.712**	**0.233**	**0.539**	0.145	0.196	0.047
2015 Site 4	-0.106	-0.003	0.096	**-0.281**	-0.115	0.014	0.155	-0.165
2016 Site 4	**-0.236**	**-0.451**	**-0.284**	0.167	**0.265**	-0.095	**0.351**	**0.411**
2015 Site 5	**-0.299**	-0.171	0.007	**0.299**	**0.310**	-0.162	0.094	**0.346**
2016 Site 5	**-0.381**	**-0.470**	0.004	**0.427**	**0.277**	0.162	**0.303**	**0.237**
2015 Site 6	0.056	0.171	0.039	0.180	0.085	-0.118	0.018	-0.015
2016 Site 6	0.139	0.132	-0.181	-0.184	**0.311**	**-0.337**	**-0.355**	**-0.262**

Remote Sensing Thermal (p-values)

Vineyards	Clusters	Yield	Berry Wt.	Brix	pH	TA	Phenols	Anthocyanins
2015 Site 1	**0.008**	0.217	0.474	0.263	0.762	0.058	0.082	0.455
2016 Site 1	0.304	0.784	**0.002**	**0.039**	**0.032**	0.334	0.168	**0.000**
2015 Site 2	0.808	0.653	0.408	0.442	**0.002**	0.289	0.110	0.063
2016 Site 2	0.469	0.096	0.409	0.772	**0.000**	0.068	**0.028**	0.128
2015 Site 3								
2016 Site 3	0.411	**0.002**	**0.000**	**0.038**	**0.000**	0.198	0.081	0.676
2015 Site 4	0.378	0.979	0.420	**0.017**	0.334	0.907	0.193	0.165
2016 Site 4	**0.046**	**0.000**	**0.016**	0.162	**0.025**	0.426	**0.002**	**0.000**
2015 Site 5	**0.007**	0.128	0.948	**0.007**	**0.005**	0.150	0.405	**0.002**
2016 Site 5	**0.000**	**0.000**	0.973	**0.000**	**0.012**	0.147	**0.006**	**0.033**
2015 Site 6	0.620	0.131	0.733	0.109	0.454	0.296	0.875	0.898
2016 Site 6	0.220	0.242	0.109	0.102	**0.005**	**0.002**	**0.001**	**0.019**

NDVI from the RPAS flight showed a strong positive correlation to the berry weight in most of sites and four sites showed temporal stability throughout the consecutive years (Table 4.3).

There also were only weak relationships found between thermal and berry weight and a lack of consistency in the correlations was evident throughout the sites and years (Table 4.3).

Overall, NDVI could detect variation in yield and berry weight in most of sites where four sites showed temporal stability in berry weight throughout the consecutive years. In general, NDVI from the RPAS flight and yield were positively correlated. There could be an annual climate impact on yield values and its detection by NDVI from the RPAS flight, because significantly more correlations between the NDVI and yield were detected in 2016, a hot and dry year, over 2015 with ample precipitation. Therefore, NDVI from the RPAS flight could have more capability of detecting the variation of yield in the year with hot and dry condition.

4.1.3.2 Relationships between NDVI/thermal from the RPAS flight and anthocyanins/phenols

There were only weak correlations found between NDVI from the RPAS flight and anthocyanins/phenols and a lack of consistency in the correlations was evident throughout the sites and years (Table 4.3). NDVI was somewhat negatively correlated to anthocyanins and phenols and positively correlated between thermal imaging and anthocyanins/phenols. Overall, NDVI and thermal from the RPAS flight had low capability of detecting variation in anthocyanins and phenols in all vineyard sites and years.

4.1.3.3 Relationships between NDVI/thermal from the RPAS flight and other berry compositions (Brix, titratable acidity (TA), and pH)

There were only weak correlations observed between NDVI/thermal and Brix/TA and a lack of consistency in the correlations was evident throughout the sites and years (Table 4.3). However, thermal showed a strong positive correlation to the pH in most of sites and site 5 showed

temporal stability throughout the consecutive years (Table 4.3). Interestingly, strong positive correlations between the two variables were observed throughout the sites (six of six sites) in 2016, a hot and dry year, while only one vineyard had the correlation in 2015.

Overall, NDVI and thermal from the RPAS flight was least capable of detecting variation in Brix and TA but thermal data showed a strong capability to detect variations in pH in all vineyard sites in 2016, a relatively hot and dry year. Therefore, NDVI and thermal emission data were not reliable for detecting variation for primary fruit composition except for pH. However, heat units and precipitation can impact its level of detection, limiting their feasibility.

4.1.4 Correlation analysis between other indices from the RPAS flight and grape yield/fruit quality

Several vegetation indices (VIs) are applied in viticulture to measure a variety of plant characteristics, for example, leaf colour intensity, area index of leaves, plant physiology, and nutrient deficiency.[1] Plant canopy VIs, including NDVI, are less effective at identifying differences in berry compositions than other indicators responsive to leaf pigments.[2] These biochemical indicators were also more closely linked to measures of wine colour intensity.[2] Numerous remote sensing indices can be calculated from the green, red, red edge, and NIR regions of EM reflectance to detect reproductive growth and potential grape quality. Therefore, this study investigated other VIs to detect the variations of plant yield and quality production and to compare the correlation results to NDVI from proximal sensing and from the RPAS flight. The feature indices (Table 4.4) in the study were referred to the indices to characterize the plant yield and quality production according to previous studies.[3-6]

Table 4.4. Other vegetation indices (VIs) to characterize the plant yield and quality production.

Remote sensing Indices	Equation
CI green (green Chlorophyll Index)	(NIR/Green) – 1
CI red edge (Red Edge Chlorophyll Index)	(NIR/Red Edge) − 1
NDRE (Red Edge Normalized Difference Vegetation Index)	(NIR − Red Edge)/ (NIR + Red Edge)
GNDVI (NDVI Green)	(NIR – Green)/ (NIR + Green)
GRVI (Green-Red Vegetation Index)	(Green – Red)/ (Green + Red)
RVI (Ratio Vegetation Index)	NIR/Red

4.1.4.1 Principal component analysis (PCA) of other indices from the RPAS flight and grape yield/fruit quality

PCA results were built based on the first two factors, which explained between 50 to 62% of the data (Figure 4.4). In site 1 (Figure 4.4), the analysis described 49.16% of the data and showed that NIR and red edge positively correlated to clusters, anthocyanins, and brix and negatively correlated to TA and berry weight. Ratio vegetation index (RVI) showed a strong positive correlation to the yield and NDVI green (GNDVI) and green chlorophyll index (CI green) also positively correlated to vine size. However, due to the relatively short vector other variables, it was difficult to visually interpret the relationship. A significant correlation between indices is also observed with clustering of green and red; red edge and NIR; red edge normalized difference vegetation index (NDRE) and red edge chlorophyll index (CI red edge); RVI, GNDVI, and CI green. A slight negative correlation observed between NIR and green/red.

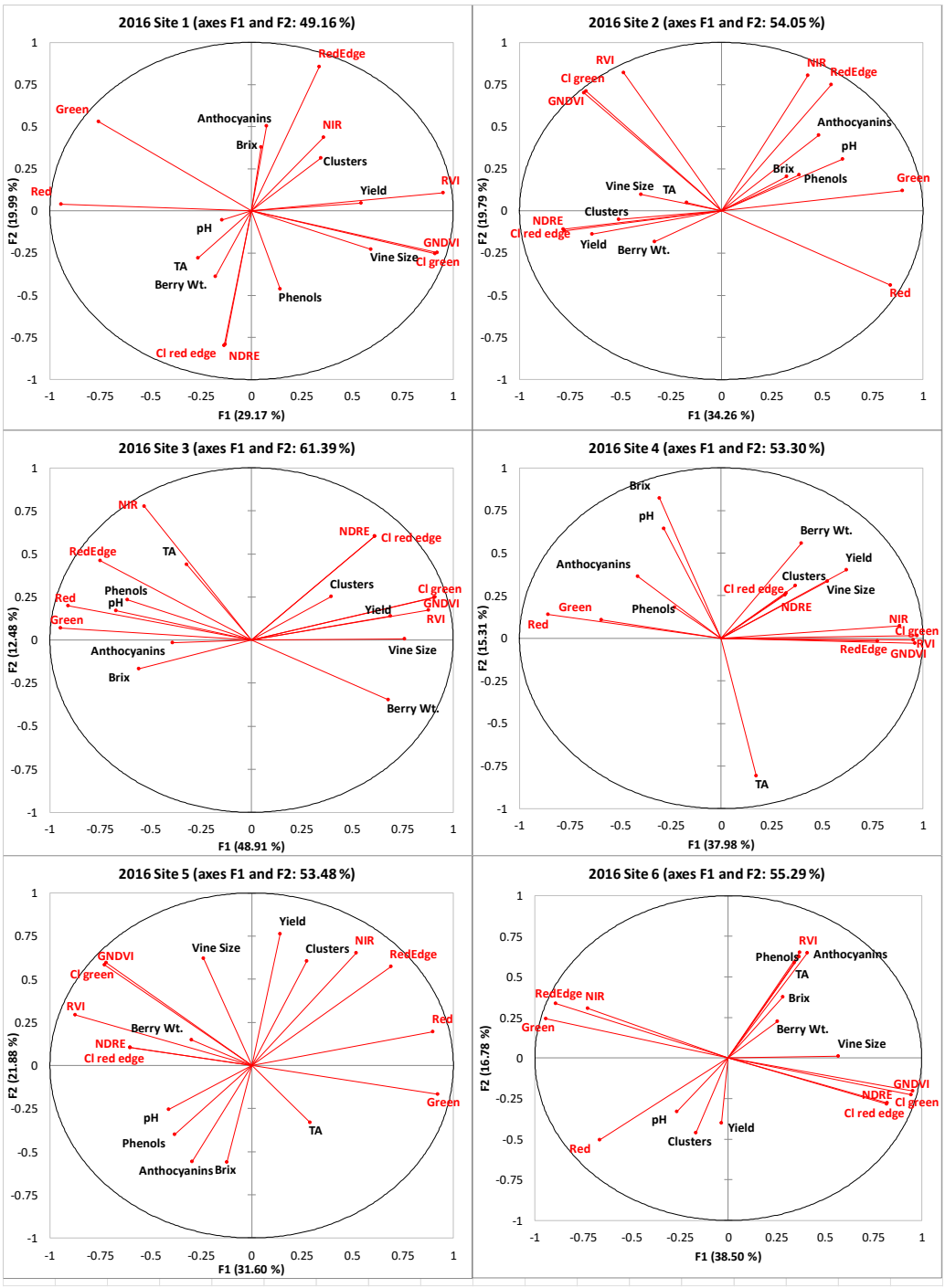

Figure 4.4. PCA results among indices from the RPAS flight, vineyard yield and berry composition in six Niagara vineyards from 2016. Variables include data in six Ontario vineyards in 2016. Abbreviations: Berry WT= Berry weight, TA= Titratable acidity, CI green= Green chlorophyll index, CI red edge= Red edge chlorophyll index, NDRE= Red edge normalized difference vegetation index, GNDVI= NDVI green, RVI= Ratio vegetation index.

In site 2 (Figure 4.4), the analysis described 54.05% of the data and showed that NDRE, CI red edge, vine size, yield, clusters, and berry weight were clustered together while green, red edge, NIR, anthocyanins, phenols, pH, and Brix were clustered together in the other plane even though the vectors for some variables such as TA, Brix, and berry weight were relatively short and thus there does not appear to be clear in the PCA chart. NIR and red edge exhibit a strong positive correlation.

In site 3 (Figure 4.4), the analysis described 61.39% of the data and showed that NDRE, CI red edge, CI green, GNDVI, RVI, vine size, yield, and clusters were clustered together while green, red, red edge, NIR, anthocyanins, phenols, pH, TA and Brix were clustered together in the other plane even though the vectors for some variables such as TA, anthocyanins, and clusters were relatively short and thus there does not appear to be clear in the PCA chart. A significant positive correlation between indices was also observed with clustering of green, red, red edge and NIR.

In site 4 (Figure 4.4), the analysis described 53.30% of the data and showed that NDRE, CI red edge, CI green, red edge, NIR, GNDVI, RVI, vine size, yield, clusters, and berry weight were clustered together while green, red, anthocyanins, phenols, pH, and Brix were clustered together in the other plane even though the vectors for some variables such as phenols, clusters, NDRE, and CI red edge were relatively short and thus there does not appear to be clear in the PCA chart. A significant correlation between indices observed with clustering of green and red; red edge and NIR. A strong negative correlation was also observed between red edge/NIR and green/red.

In site 5 (Figure 4.4), the analysis described 53.48% of the data and showed that NIR, red edge, yield, and clusters were clustered together while no clustering was observed between indices from the RPAS flight and berry compositions. Brix, pH, phenols, and anthocyanins were

negatively correlated to red edge and NIR. A significant positive correlation between indices was also observed with clustering of green, red, red edge and NIR.

In site 6 (Figure 4.4), the analysis described 55.29% of the data and showed that red somewhat positively correlated to yield, clusters, and pH but those had short vectors and thus there does not appear to be clear in the PCA chart. On the other plane, RVI, anthocyanins, phenols, TA, and Brix were clustered together. Other indices were not correlated to the yield and berry compositions. A significant positive correlation between indices was also observed with clustering of green, red edge and NIR.

Overall, yield and vine size indicated a positive correlation with CI green, GNDVI, and RVI while these were inversely correlated to green and red in four of six sites. It was observed that berry compositions did not correlate well with other indices from the RPAS flight. In site 2 and 3, pH and phenols were positively correlated to the green, red, red edge, and NIR. A positive correlation was also observed between anthocyanins and green/red edge/NIR in site 2 and between anthocyanins and green/red in site 3. The negative correlations observed between anthocyanins and green/red edge/NIR in site 2 and between anthocyanins and green/red in site 3. However, pH and phenols were inversely correlated to green, red, red edge, and NIR in site 5. As shown in their short vectors, berry weight, Brix, pH, and TA could not be well explained by the first two factors. Pearson's correlation should be used to confirm relationships.

4.1.4.2 Pearson's correlation analysis of other indices from the RPAS flight and grape yield/fruit quality

i. Relationships between other indices and yield components

CI green was positively correlated to vine size in all six sites, to yield in five sites, and to both clusters and berry weight in two sites in Table 4.5 and 4.6. In site 3 and 4, positive correlations were observed between CI green and all four yield components. CI red edge also showed positive correlations to yield and vine size in three of six sites while clusters and yield were inversely correlated to the CI red edge in site 1. Similar to CI green, strong positive correlations were observed between GNDVI and yield components with correlation to vine size in all six sites, to yield in five sites. Green was negatively correlated to vine size in five of six sites and to yield in four of six sites. Negative correlations were observed between green and all four yield components in site 3.

Green was also negatively correlated to berry weight in three of six sites. Negative correlations were observed between red and all four yield components in site 3 while clusters positively correlated to red in site 5 and 6. NDRE showed the same pattern of correlations as the CI red edge. NIR and red edge indicated some correlation to the yield components. NIR and red edge were positively correlated to clusters and yield in site 4 and 5 and to vine size and berry weight in site 4 while these were inversely correlated to clusters and yield in site 2 and to vine size and berry weight in site 3. Positive correlations were observed between NIR/red edge and all four yield components in site 4. RVI had a positive relationship with vine size in five of six sites, with berry weight in four sites, and with yield in three sites. In site 3 and 4, positive correlations were observed between RVI and all four yield components.

Table 4.5. Pearson's correlation results sorted **by indices** between indices from the RPAS flight vs yield and berry composition data in six Niagara vineyards from 2016. The indices from the RPAS flight included green, red, red edge, NIR, CI green, CI red edge, NDRE, GNDVI and RVI. Those variables with significant (95% confidence) were listed in bold, with blank cells representing no correlation: blue boxes= positive correlation with indices, red boxes= negative correlation with indices, black boxes= no data collected. Abbreviations: Berry WT= Berry weight, TA= Titratable acidity, CI green= Green chlorophyll index, CI red edge= Red edge chlorophyll index, NDRE= Red edge normalized difference vegetation index, GNDVI= NDVI green, RVI= Ratio vegetation index.

Variables	Vineyards	Clusters	Yield	Vine Size	Berry Wt.	Brix	pH	TA	Phenols	Anthocyanins
CI green	Site 1	0.059	**0.272**	**0.438**	-0.165	-0.002	-0.078	**-0.231**	0.162	0.017
	Site 2	0.222	**0.253**	**0.255**	0.025	-0.084	-0.192	0.144	-0.158	-0.042
	Site 3	**0.314**	**0.538**	**0.648**	**0.472**	**-0.462**	**-0.518**	-0.186	**-0.373**	**-0.239**
	Site 4	**0.267**	**0.523**	**0.437**	**0.345**	**-0.242**	-0.227	0.118	-0.129	**-0.285**
	Site 5	0.130	**0.242**	**0.438**	0.158	-0.073	0.064	**-0.338**	0.070	-0.129
	Site 6	-0.088	0.017	**0.501**	0.163	0.147	-0.167	0.207	0.159	0.199
CI red edge	Site 1	**-0.338**	**-0.265**	-0.008	0.184	-0.021	0.184	0.021	0.218	-0.183
	Site 2	0.204	**0.308**	0.080	0.055	**-0.293**	**-0.385**	-0.027	**-0.228**	**-0.440**
	Site 3	**0.227**	**0.344**	**0.457**	0.169	**-0.263**	**-0.221**	-0.048	**-0.270**	-0.135
	Site 4	0.097	**0.386**	**0.449**	0.085	-0.093	-0.026	0.061	0.050	-0.060
	Site 5	-0.110	-0.070	0.031	-0.035	-0.006	-0.002	-0.004	**0.247**	0.189
	Site 6	-0.047	-0.035	**0.305**	0.093	0.205	-0.050	0.120	0.159	0.157
GNDVI	Site 1	0.075	**0.302**	**0.455**	-0.165	-0.007	-0.084	-0.224	0.176	0.023
	Site 2	**0.244**	**0.280**	**0.277**	0.050	-0.052	-0.202	0.124	-0.126	-0.017
	Site 3	**0.339**	**0.541**	**0.655**	**0.477**	**-0.441**	**-0.527**	-0.187	**-0.371**	-0.212
	Site 4	**0.244**	**0.474**	**0.388**	**0.330**	**-0.245**	-0.216	0.120	-0.111	**-0.251**
	Site 5	0.134	**0.234**	**0.429**	0.141	-0.105	0.031	**-0.328**	0.059	-0.151
	Site 6	-0.102	0.011	**0.506**	0.199	0.179	-0.152	0.217	0.186	0.218
Green	Site 1	-0.035	**-0.319**	**-0.484**	0.033	0.138	0.112	0.104	**-0.378**	0.088
	Site 2	**-0.368**	**-0.445**	**-0.260**	-0.212	0.159	**0.506**	-0.088	**0.358**	**0.385**
	Site 3	**-0.292**	**-0.520**	**-0.656**	**-0.580**	**0.404**	**0.613**	**0.315**	**0.470**	**0.228**
	Site 4	-0.070	**-0.289**	-0.145	-0.034	**0.250**	0.210	-0.106	-0.047	-0.098
	Site 5	0.111	0.027	**-0.266**	-0.214	-0.120	**-0.219**	**0.225**	**-0.249**	0.054
	Site 6	0.109	-0.003	**-0.493**	-0.166	-0.161	0.176	-0.191	-0.181	**-0.221**
NDRE	Site 1	**-0.346**	**-0.271**	-0.011	0.188	-0.023	0.195	0.021	0.222	-0.187
	Site 2	0.206	**0.312**	0.082	0.058	**-0.290**	**-0.394**	-0.024	**-0.235**	**-0.436**
	Site 3	**0.225**	**0.343**	**0.456**	0.170	**-0.266**	**-0.221**	-0.050	**-0.273**	-0.136
	Site 4	0.090	**0.379**	**0.443**	0.079	-0.100	-0.034	0.067	0.048	-0.060
	Site 5	-0.111	-0.073	0.031	-0.042	-0.006	-0.004	-0.004	**0.251**	0.191
	Site 6	-0.052	-0.039	**0.306**	0.101	0.213	-0.049	0.124	0.167	0.164
NIR	Site 1	0.065	-0.018	-0.018	**-0.228**	0.216	0.045	**-0.227**	**-0.334**	0.176
	Site 2	**-0.233**	**-0.279**	-0.063	-0.200	0.126	**0.393**	0.030	**0.300**	**0.430**
	Site 3	0.029	-0.161	**-0.324**	**-0.502**	0.104	**0.473**	**0.446**	**0.435**	0.131
	Site 4	**0.303**	**0.469**	**0.452**	**0.437**	-0.157	-0.150	0.083	-0.210	**-0.455**
	Site 5	**0.407**	**0.425**	0.205	-0.148	**-0.398**	**-0.364**	-0.104	**-0.373**	-0.166
	Site 6	0.080	-0.002	**-0.377**	-0.039	-0.058	0.205	-0.083	-0.099	-0.162
Red	Site 1	**-0.226**	**-0.455**	**-0.508**	0.133	0.029	0.192	0.196	-0.135	-0.033
	Site 2	**-0.353**	**-0.381**	**-0.308**	-0.149	0.109	**0.308**	-0.100	0.221	0.147
	Site 3	**-0.238**	**-0.474**	**-0.602**	**-0.570**	**0.380**	**0.600**	**0.349**	**0.457**	**0.232**
	Site 4	-0.209	**-0.331**	-0.224	-0.197	**0.291**	0.206	-0.159	0.152	0.154
	Site 5	**0.294**	0.170	-0.106	**-0.278**	**-0.320**	**-0.425**	0.141	**-0.333**	-0.092
	Site 6	**0.237**	-0.020	**-0.509**	**-0.321**	-0.184	**0.357**	**-0.520**	**-0.326**	**-0.452**
RedEdge	Site 1	**0.295**	0.189	-0.001	**-0.283**	0.156	-0.121	-0.160	**-0.384**	**0.245**
	Site 2	**-0.249**	**-0.311**	-0.071	-0.193	0.170	**0.439**	0.030	**0.328**	**0.475**
	Site 3	-0.068	**-0.293**	**-0.490**	**-0.533**	0.205	**0.531**	**0.435**	**0.516**	0.180
	Site 4	**0.276**	**0.330**	**0.290**	**0.414**	-0.117	-0.136	0.056	**-0.240**	**-0.434**
	Site 5	**0.418**	**0.419**	0.179	-0.130	**-0.373**	**-0.341**	-0.093	**-0.437**	**-0.220**
	Site 6	0.083	0.019	**-0.408**	-0.080	-0.148	0.161	-0.119	-0.154	-0.194
RVI	Site 1	0.214	**0.376**	**0.423**	-0.208	0.036	-0.158	**-0.250**	-0.004	0.069
	Site 2	0.131	0.128	0.211	-0.021	-0.081	-0.016	0.147	-0.100	0.056
	Site 3	**0.289**	**0.513**	**0.591**	**0.450**	**-0.453**	**-0.495**	-0.209	**-0.359**	**-0.242**
	Site 4	**0.294**	**0.482**	**0.396**	**0.329**	**-0.254**	-0.216	0.138	-0.214	**-0.331**
	Site 5	-0.050	0.124	**0.345**	**0.259**	0.118	**0.314**	**-0.308**	0.179	-0.006
	Site 6	-0.219	0.038	**0.359**	**0.321**	0.158	**-0.283**	**0.486**	**0.263**	**0.400**

Table 4.6. Pearson's correlation results sorted **by sites** between indices from the RPAS flight vs yield and berry composition data in six Niagara vineyards from 2016. The indices from the RPAS flight included green, red, red edge, NIR, CI green, CI red edge, NDRE, GNDVI and RVI. Those variables with significant (95% confidence) were listed in bold, with blank cells representing no correlation: blue boxes= positive correlation with indices, red boxes= negative correlation with indices, black boxes= no data collected. Abbreviations: Berry WT= Berry weight, TA= Titratable acidity, CI green= Green chlorophyll index, CI red edge= Red edge chlorophyll index, NDRE= Red edge normalized difference vegetation index, GNDVI= NDVI green, RVI= Ratio vegetation index.

Vineyards	Variables	Clusters	Yield	Vine Size	Berry Wt.	Brix	pH	TA	Phenols	Anthocyanins
Site 1	Green	-0.035	**-0.319**	**-0.484**	0.033	0.138	0.112	0.104	**-0.378**	0.088
	Red	**-0.226**	**-0.455**	**-0.508**	0.133	0.029	0.192	0.196	-0.135	-0.033
	RedEdge	**0.295**	0.189	-0.001	**-0.283**	0.156	-0.121	-0.160	**-0.384**	**0.245**
	NIR	0.065	-0.018	-0.018	**-0.228**	0.216	0.045	**-0.227**	**-0.334**	0.176
	Cl green	0.059	**0.272**	**0.438**	-0.165	-0.002	-0.078	**-0.231**	0.162	0.017
	Cl red edge	**-0.338**	**-0.265**	-0.008	0.184	-0.021	0.184	0.021	0.218	-0.183
	NDRE	**-0.346**	**-0.271**	-0.011	0.188	-0.023	0.195	0.021	0.222	-0.187
	GNDVI	0.075	**0.302**	**0.455**	-0.165	-0.007	-0.084	-0.224	0.176	0.023
	RVI	0.214	**0.376**	**0.423**	-0.208	0.036	-0.158	**-0.250**	-0.004	0.069
Site 2	Green	**-0.368**	**-0.445**	**-0.260**	-0.212	0.159	**0.506**	-0.088	**0.358**	**0.385**
	Red	**-0.353**	**-0.381**	**-0.308**	-0.149	0.109	**0.308**	-0.100	0.221	0.147
	RedEdge	**-0.249**	**-0.311**	-0.071	-0.193	0.170	**0.439**	0.030	**0.328**	**0.475**
	NIR	**-0.233**	**-0.279**	-0.063	-0.200	0.126	**0.393**	0.030	**0.300**	**0.430**
	Cl green	0.222	**0.253**	**0.255**	0.025	-0.084	-0.192	0.144	-0.158	-0.042
	Cl red edge	0.204	**0.308**	0.080	0.055	**-0.293**	**-0.385**	-0.027	**-0.228**	**-0.440**
	NDRE	0.206	**0.312**	0.082	0.058	**-0.290**	**-0.394**	-0.024	**-0.235**	**-0.436**
	GNDVI	**0.244**	**0.280**	**0.277**	0.050	-0.052	-0.202	0.124	-0.126	-0.017
	RVI	0.131	0.128	0.211	-0.021	-0.081	-0.016	0.147	-0.100	0.056
Site 3	Green	**-0.292**	**-0.520**	**-0.656**	**-0.580**	**0.404**	**0.613**	**0.315**	**0.470**	**0.228**
	Red	**-0.238**	**-0.474**	**-0.602**	**-0.570**	**0.380**	**0.600**	**0.349**	**0.457**	**0.232**
	RedEdge	-0.068	**-0.293**	**-0.490**	**-0.533**	0.205	**0.531**	**0.435**	**0.516**	0.180
	NIR	0.029	-0.161	**-0.324**	**-0.502**	0.104	**0.473**	**0.446**	**0.435**	0.131
	Cl green	**0.314**	**0.538**	**0.648**	**0.472**	**-0.462**	**-0.518**	-0.186	**-0.373**	**-0.239**
	Cl red edge	**0.227**	**0.344**	**0.457**	0.169	**-0.263**	**-0.221**	-0.048	**-0.270**	-0.135
	NDRE	**0.225**	**0.343**	**0.456**	0.170	**-0.266**	**-0.221**	-0.050	**-0.273**	-0.136
	GNDVI	**0.339**	**0.541**	**0.655**	**0.477**	**-0.441**	**-0.527**	-0.187	**-0.371**	-0.212
	RVI	**0.289**	**0.513**	**0.591**	**0.450**	**-0.453**	**-0.495**	-0.209	**-0.359**	**-0.242**
Site 4	Green	-0.070	**-0.289**	-0.145	-0.034	**0.250**	0.210	-0.106	-0.047	-0.098
	Red	-0.209	**-0.331**	-0.224	-0.197	**0.291**	0.206	-0.159	0.152	0.154
	RedEdge	**0.276**	**0.330**	**0.290**	**0.414**	-0.117	-0.136	0.056	**-0.240**	**-0.434**
	NIR	**0.303**	**0.469**	**0.452**	**0.437**	-0.157	-0.150	0.083	-0.210	**-0.455**
	Cl green	**0.267**	**0.523**	**0.437**	**0.345**	**-0.242**	-0.227	0.118	-0.129	**-0.285**
	Cl red edge	0.097	**0.386**	**0.449**	0.085	-0.093	-0.026	0.061	0.050	-0.060
	NDRE	0.090	**0.379**	**0.443**	0.079	-0.100	-0.034	0.067	0.048	-0.060
	GNDVI	**0.244**	**0.474**	**0.388**	**0.330**	**-0.245**	-0.216	0.120	-0.111	**-0.251**
	RVI	**0.294**	**0.482**	**0.396**	**0.329**	**-0.254**	-0.216	0.138	-0.214	**-0.331**
Site 5	Green	0.111	0.027	**-0.266**	-0.214	-0.120	**-0.219**	**0.225**	**-0.249**	0.054
	Red	**0.294**	0.170	-0.106	**-0.278**	**-0.320**	**-0.425**	0.141	**-0.333**	-0.092
	RedEdge	**0.418**	**0.419**	0.179	-0.130	**-0.373**	**-0.341**	-0.093	**-0.437**	**-0.220**
	NIR	**0.407**	**0.425**	0.205	-0.148	**-0.398**	**-0.364**	-0.104	**-0.373**	-0.166
	Cl green	0.130	**0.242**	**0.438**	0.158	-0.073	0.064	**-0.338**	0.070	-0.129
	Cl red edge	-0.110	-0.070	0.031	-0.035	-0.006	-0.002	-0.004	**0.247**	0.189
	NDRE	-0.111	-0.073	0.031	-0.042	-0.006	-0.004	-0.004	**0.251**	0.191
	GNDVI	0.134	**0.234**	**0.429**	0.141	-0.105	0.031	**-0.328**	0.059	-0.151
	RVI	-0.050	0.124	**0.345**	**0.259**	0.118	**0.314**	**-0.308**	0.179	-0.006
Site 6	Green	0.109	-0.003	**-0.493**	-0.166	-0.161	0.176	-0.191	-0.181	**-0.221**
	Red	**0.237**	-0.020	**-0.509**	**-0.321**	-0.184	**0.357**	**-0.520**	**-0.326**	**-0.452**
	RedEdge	0.083	0.019	**-0.408**	-0.080	-0.148	0.161	-0.119	-0.154	-0.194
	NIR	0.080	-0.002	**-0.377**	-0.039	-0.058	0.205	-0.083	-0.099	-0.162
	Cl green	-0.088	0.017	**0.501**	0.163	0.147	-0.167	0.207	0.159	0.199
	Cl red edge	-0.047	-0.035	**0.305**	0.093	0.205	-0.050	0.120	0.159	0.157
	NDRE	-0.052	-0.039	**0.306**	0.101	0.213	-0.049	0.124	0.167	0.164
	GNDVI	-0.102	0.011	**0.506**	0.199	0.179	-0.152	0.217	0.186	0.218
	RVI	-0.219	0.038	**0.359**	**0.321**	0.158	**-0.283**	**0.486**	**0.263**	**0.400**

Overall, CI green and GNDVI showed the most capability of detecting variation in yield and vine size in most of sites with statistically significant positive correlation. Green and red also showed a good negative correlation to yield and vine size. The relationship between RVI and berry weight was also positive in four out of six sites. NIR and red edge showed the least correlation to the yield components. Site 3 and 4 showed the most correlation between other indices and yield components while other indices in site 6 only showed the significant correlation to berry weight.

ii. Relationships between other indices from the RPAS flight and berry compositions

There were some correlations observed between other indices from the RPAS flight and berry compositions, and only three sites (site 2, 3, and 5) had some correlations between the two variables (Table 4.5 and 4.6). Interestingly, green, red edge and NIR were positively correlated to pH, phenols, and anthocyanins while these were inversely correlated to yield and clusters in in site 2. Similar correlations were also seen in site 3 that green, red, red edge and NIR were positively correlated to pH, phenols, TA, and anthocyanins while these were inversely correlated to yield components. An inverse correlation was shown between CI red edge/NDRE and Brix/pH/phenols/anthocyanins in site 2 and between CI green/ CI red edge/NDRE/GNDVI/RVI and Brix/pH/phenols in site 3. These indices in both sites also showed positive correlation to yield components. In site5, a reverse correlation pattern from site 3 and site 2 was observed that red, red edge, NIR were negatively correlated to brix, pH, and phenols while these were positively correlated to clusters and yield. Site 4 site with the strong positive correlation between indices from the RPAS flight and yield components indicated a negative correlation between CI green/GNDVI/RVI and brix/anthocyanins.

Overall, CI green, CI red edge, GNDVI, and NDRE were negatively correlated to Brix, pH, TA, phenols, and anthocyanins in some sites while the nature of the relationships in the other indices varied between sites. The correlations between indices from the RPAS flight and berry compositions were site specific and two sites showed an identical correlation between the two variables while inverse correlation observed in another site. The other three sites only indicated weak correlations between the two variables, which varied between sites. Interestingly, the indices were strongly correlated to berry composition such as brix, pH, phenols, anthocyanins in some sites while these correlations were inverse pattern to yield components at the same site.

4.1.5 Mapping and spatial autocorrelation analysis

4.1.5.1 Spatial autocorrelation analysis (Moran's I)

The spatial autocorrelation of each variable was determined by z-score (Table 4.7A), which shows clustering patterns to measure zonal vineyard management options.[7-9] All EM reflectance data analysis (NDVIs and other Vis) and thermal emission data were highly clustered across the six sites throughout the years. The number of clusters in 2015 and 2016 showed generally random distribution, being clustered at only two sites in each year and clustered only one sites in 2017. Dispersed pattern also appeared at site 4 in 2016. Yield was mostly clustered in 2016 with five out of six sites being clustered, only site 1 was randomly distributed. However, only two sites showed a clustering pattern, and the other sites were randomly distributed or dispersed in 2017. There was no clustering pattern observed in 2015, and the yield was randomly distributed in all the vineyards. There was a strong clustering of berry weight and basic berry composition across sites.

Overall, indices from the RPAS flight, berry phenols, and anthocyanin level showed high clustering, whereas clusters and yields were predominantly random. There was moderate

clustering of berry weight and composition, with spatial orientations relaying strongly on the site and year.

Table 4.7A. Moran's I analysis results (z-score) for data from the RPAS flight /proximal sensing, yield, and berry composition data in six Niagara vineyards from 2015, 2016 and 2017 (95% confidence): blue boxes= clustered, red boxes= random, yellow boxes= dispersed, black boxes= no data collected. Abbreviations: NDVI= Normalized difference vegetation index, P-NDVI= Proximal NDVI, Clusters = Number of clusters, Berry WT= Berry weight, TA= Titratable acidity.

Vineyards	NDVI	Thermal	PNDVI Avg	Clusters	Yield	Berry Wt.	Brix	pH	TA	Phenols	Anthocyanins
2015 Site 1 (n=76)	6.0617	7.9863	7.1601	2.0338	-0.5719	0.7205	2.4373	0.6190	2.6179	1.9107	5.2621
2016 Site 1 (n=76)	7.2130	4.8483	5.6752	0.8022	0.0027	3.7264	1.8987	0.3316	1.6603	5.7378	2.2707
2017 Site 1 (n=76)			5.4303	2.4816	4.3632	3.4735	2.7145	1.9304	0.5598	2.3823	1.8573
2015 Site 2 (n=75)	4.2681	5.3533	5.2768	-0.5758	0.2740	1.3604	1.9080	3.4863	0.1223	0.7864	0.3780
2016 Site 2 (n=75)	2.7390	5.2274	2.6147	1.0149	1.7665	2.5659	3.9504	3.2227	-1.4321	0.6443	3.7295
2017 Site 2 (n=75)			2.4997	0.4936	0.9892	3.0366	0.8023	1.9965	-0.4950	1.6264	1.1532
2015 Site 3 (n=80)	6.2152	6.4905	6.2152								
2016 Site 3 (n=80)	7.0372	6.9643	6.5482	0.6361	2.6756	6.6569	2.7873	3.5517	1.9396	4.5423	1.6671
2017 Site 3 (n=80)			6.0927	0.2710	-0.0867	2.0948	1.0797	3.4308	2.1172	0.0115	0.8964
2015 Site 4 (n=72)	2.2846	5.8056	4.1695	-1.0165	-0.7471	4.4183	1.3093	0.7637	0.2841	0.7014	1.8670
2016 Site 4 (n=72)	3.3818	5.5484	5.2513	-1.6860	2.1123	1.7563	1.7939	1.8991	0.0500	3.3689	4.3048
2017 Site 4 (n=72)			4.8626	0.4881	-1.0049	3.4903	1.2793	0.8943	-0.4684	1.9413	1.0183
2015 Site 5 (n=81)	3.3973	6.4341	2.6433	2.7220	-0.0273	3.5509	3.2872	6.5300	2.0402	1.7011	5.5350
2016 Site 5 (n=81)	6.2524	6.8356	3.5233	4.5448	4.5815	1.9210	6.6947	4.3985	1.8582	2.7014	2.5670
2017 Site 5 (n=81)			3.8967	1.7598	1.3014	0.9018	-0.2729	4.8438	1.9527	6.0737	0.0535
2015 Site 6 (n=80)	5.1185	7.1593	5.8291	-0.2032	0.6685	-0.3805	1.4997	0.1566	-0.4067	2.9453	3.0871
2016 Site 6 (n=80)	6.4873	5.1600	6.7888	2.4548	2.2780	1.2555	-0.1585	0.8938	3.5924	1.6528	3.6199
2017 Site 6 (n=80)			2.2967	-0.4960	-1.6948	-0.2936	1.0437	1.9468	1.3128	-0.1789	3.7179

Table 4.7B. Moran's I analysis results (Moran's Index and p-value) for data from the RPAS flight /proximal sensing, yield, and berry composition data in six Niagara vineyards from 2015, 2016 and 2017 (95% confidence): blue boxes= clustered, red boxes= random, yellow boxes= dispersed, black boxes= no data collected. Abbreviations: NDVI= Normalized difference vegetation index, P-NDVI= Proximal NDVI, Clusters = Number of clusters, Berry WT= Berry weight, TA= Titratable acidity.

	Moran's Index											p-value									
Vineyards	NDVI	P-NDVI	Thermal	Clusters	Yield	Berry Wt.	Brix	pH	TA	Phenols	Anthocyanins	NDVI	P-NDVI	Thermal	Clusters	Yield	Berry Wt.	Brix	pH	TA	Phenols	Anthocyanins
2015 Site 1 (n=76)	0.6284	0.7388	0.8308	0.1833	-0.0335	0.0072	0.2353	0.0022	0.2199	0.1478	0.4094	0.0001	0.0001	0.0001	0.0600	0.8480	0.8456	0.0201	0.8088	0.0269	0.1257	0.0000
2016 Site 1 (n=76)	0.7496	0.5875	0.4990	-0.0170	0.1490	0.2992	0.1879	-0.0114	0.1785	0.4415	0.2608	0.0001	0.0001	0.0001	0.9712	0.1222	0.0030	0.0550	0.9854	0.0660	0.0000	0.0080
2017 Site 1 (n=76)		0.5596		0.2100	0.3944	0.2743	0.3138	0.1540	0.0080	0.3075	0.0797		0.0001		0.0320	0.0001	0.0066	0.0018	0.1112	0.8395	0.0020	0.3749
2015 Site 2 (n=75)	0.5505	0.6813	0.6819	-0.1493	0.0088	0.1385	0.1385	0.3476	-0.0120	-0.0640	-0.1030	0.0001	0.0001	0.0001	0.3000	0.2328	0.2233	0.2328	0.0012	0.9905	0.7023	0.4991
2016 Site 2 (n=75)	0.2315	0.3310	0.6762	0.1013	0.2407	0.3109	0.3583	0.4281	-0.2295	-0.0148	0.2929	0.0225	0.0089	0.0001	0.3799	0.0170	0.0023	0.0004	0.0001	0.0884	0.9923	0.0032
2017 Site 2 (n=75)		0.2514		0.0040	0.0511	0.3799	0.0478	0.3041	-0.1470	0.1834	0.0860		0.0108		0.8935	0.6243	0.0003	0.6403	0.0032	0.2759	0.1319	0.4488
2015 Site 3 (n=80)	0.7450	0.7650	0.7829									0.0001	0.0001	0.0001								
2016 Site 3 (n=80)	0.8677	0.8037	0.8585	0.1407	0.2960	0.6133	0.2864	0.3890	0.1844	0.4918	0.2477	0.0001	0.0001	0.0001	0.2182	0.0031	0.0001	0.0032	0.0002	0.1104	0.0001	0.0124
2017 Site 3 (n=80)		0.7451		0.1016	0.0067	0.2621	0.0524	0.3663	0.2377	-0.0355	0.0500		0.0001		0.3559	0.8754	0.0083	0.5999	0.0002	0.0184	0.8546	0.6133
2015 Site 4 (n=72)	0.2412	0.5599	0.7988	-0.1248	-0.1096	0.3223	0.0361	0.0390	0.0398	0.0227	0.1677	0.0170	0.0001	0.0001	0.4304	0.4920	0.0022	0.7187	0.7015	0.7015	0.7927	0.1955
2016 Site 4 (n=72)	0.4626	0.7276	0.7691	-0.3332	0.2435	0.2018	0.1868	0.2503	-0.0765	0.3122	0.3354	0.0001	0.0001	0.0001	0.0230	0.0152	0.1235	0.1529	0.0115	0.6511	0.0021	0.0024
2017 Site 4 (n=72)		0.6704		0.0203	-0.1928	0.4134	0.0616	0.1763	-0.1156	0.2261	0.0664		0.0001		0.8058	0.2041	0.0002	0.5890	0.1761	0.4631	0.0805	0.5690
2015 Site 5 (n=81)	0.3498	0.2380	0.6784	0.2277	-0.0273	0.2277	0.3498	0.4994	0.0706	0.1553	0.4684	0.0006	0.0188	0.0001	0.0247	-0.0273	0.0248	0.0006	0.0001	0.4328	0.1167	0.0000
2016 Site 5 (n=81)	0.6561	0.3452	0.7187	0.2992	0.2986	0.0902	0.3473	0.3050	0.1488	0.3043	0.2330	0.0001	0.0006	0.0001	0.0035	0.0034	0.3378	0.0007	0.0028	0.1300	0.0031	0.0219
2017 Site 5 (n=81)		0.3797		0.1627	0.1355	0.0491	0.0027	0.3000	0.1512	0.4138	-0.0066		0.0003		0.1011	0.1660	0.5626	0.8867	0.0034	0.1257	0.0001	0.6109
2015 Site 6 (n=80)	0.6715	0.7540	0.9481	-0.0490	0.0044	-0.1596	0.1275	0.0685	-0.0822	0.4372	0.3143	0.0001	0.0001	0.0001	0.7837	0.8982	0.2698	0.2948	0.5415	0.5984	0.0001	0.0028
2016 Site 6 (n=80)	0.8527	0.8951	0.6785	0.2690	0.2350	0.1146	-0.0363	0.0296	0.3706	0.1987	0.3235	0.0001	0.0001	0.0001	0.0082	0.0207	0.3377	0.8559	0.7513	0.0001	0.1118	0.0021
2017 Site 6 (n=80)		0.2470		-0.0877	-0.1688	-0.0495	0.0625	0.1227	0.0607	-0.0508	0.2813		0.0133		0.5732	0.2412	0.6280	0.5700	0.3117	0.5797	0.7724	0.0045

4.1.5.2 Spatial analysis of maps

It is imperative that reliable maps are produced that show areas of substantial variation to determine if data from the RPAS flight will be useful in detecting vineyard variability. Figure 4.5 indicated maps of NDVIs derived from the data of the RPAS flight and proximal sensing, yield, and berry compositions in three consecutive years data and showed maps of other VIs, yield, and berry compositions in 2016 at site 4 vineyard. The maps were created by ArcGIS 10.6 (ESRI 2011).

2015 Spatial Maps of Remote and Proximal Sensing, Yield, and Berry Compositions

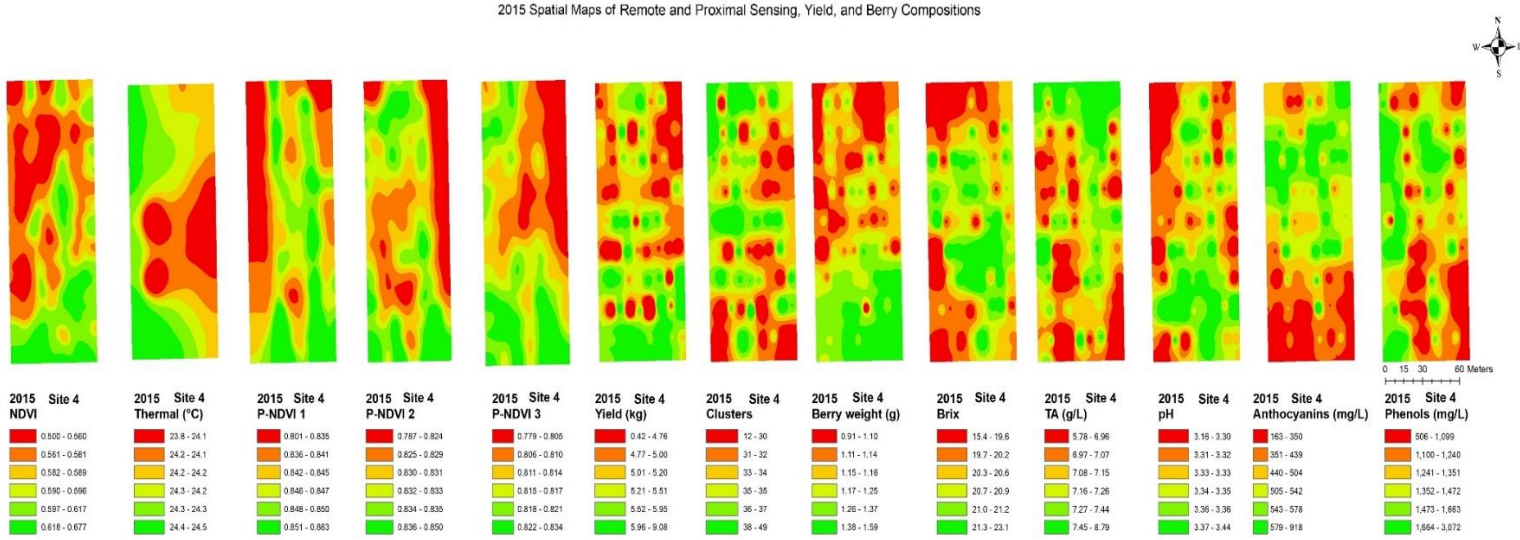

2017 Spatial Maps of Remote and Proximal Sensing, Yield, and Berry Compositions

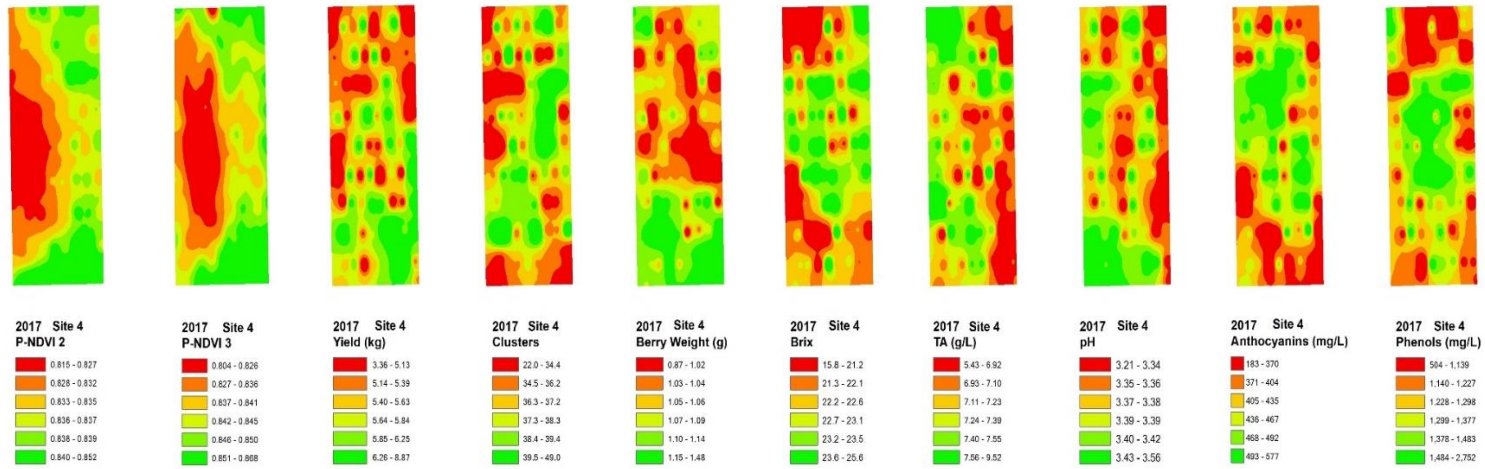

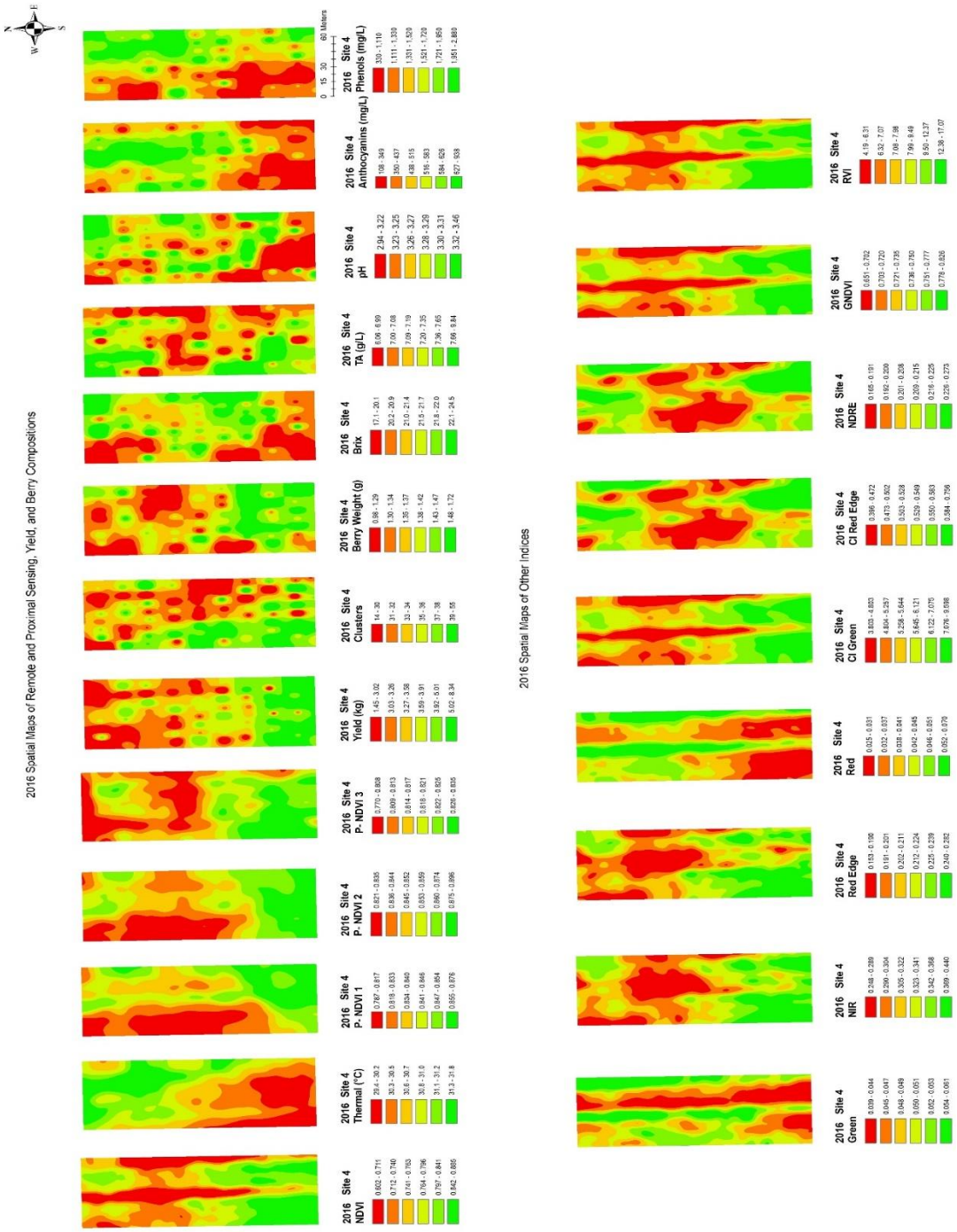

Figure 4.5. Spatial maps of data from proximal sensing and from the RPAS flight, vineyard yield and berry composition at site 4 vineyard from 2015, 2016 and 2017. Abbreviations: NDVI= Normalized difference vegetation index, P-NDVI1= Proximal sensing NDVI measured at fruit set, P-NDVI2= Proximal sensing NDVI measured at lag phase, P-NDVI3= Proximal sensing NDVI measured at veraison, TA= Titratable acidity.

In site 4 (Figure 4.5), the NDVI maps displayed an odd horizontally striated pattern, which was also seen by previous research.[10] This can be attributed to the orientation of vineyard rows in conjunction with lines of pixels, and perhaps also to the spatial-resolution utilize. The proximal NDVI maps showed different spatial patterns between fruits set and lag phase/veraison in 2015 while similar spatial patterns to those NDVIs in 2016 and 2017. The proximal NDVI at lag phase/veraison and NDVI maps from the RPAS flight were similar to each other throughout the years. The thermal emission maps only showed inverse correlation to the NDVI maps from proximal sensing and from the RPAS flight in 2016 while it displayed two unusual big circle patterns in the middle of the site in 2015. Yield and berry weight indicated a positive correlation to the NDVIs through the years. In the 2016 site 4 maps, the yield components had a similar spatial cluster pattern to red edge, NIR, CI green, CI red edge, NDRE, GNDVI, and RVI with higher values in the south end and the northeastern of the block while yield was inversely correlated to green and red with north-south striped pattern. In the berry compositions, the inverted spatial distributions to the NDVI maps were also seen in maps of anthocyanins, where the values were lower at the southern edge of the map. In the 2016 site 4 maps, the anthocyanins had an inverse spatial cluster pattern to red edge, NIR, CI green, GNDVI, RVI while Brix had a similar clustering pattern to green and red.

In site 1, the spatial correlation between the sensing data and berry compositions was weak and limited. However, some other VIs like red edge and NIR in the 2016 site 1 map were inversely correlated to TA and phenols. In site 2, yield components indicated a weak positive correlation to the NDVIs. An inverse correlation of green, red edge, and NIR to yield components was also observed while yield showed similar spatial pattern to CI green, CI red edge, NDRE, and GNDVI.

There was no temporal stability observed between the berry compositions and NDVIs. In the 2016 site 2 maps, green, red edge, and NIR indicated a clear spatial clustering and showed positive correlation to brix, pH, phenols, and anthocyanins. In site 3, the NDVI maps from the RPAS flight and proximal sensing were identical to each other throughout the growing season and years and NDVI maps appeared to have close spatial configurations to that of clusters, berry weight and yield. In the 2016 site 3 maps, the yield components had a similar spatial cluster pattern to CI green, CI red edge, NDRE, GNDVI, and RVI while berry weight and yield had an inverse relationship with green, red edge, and NIR. The Inverted spatial distributions to the NDVI maps were also found in maps of pH, TA, Brix, phenols, and anthocyanins while brix, pH, and phenols were inversely correlated to CI green, CI red edge, NDRE, GNDVI, and RVI. In site 5, yield and berry weight indicated a positive correlation to the NDVIs through the years. In the 2016 site 5 maps, clusters and yield had a similar spatial cluster pattern to red edge and NIR and the similar spatial patterns to the thermal emission maps were seen in maps of Brix, pH, phenols, and anthocyanins while these had an inverse spatial cluster pattern to green, red, red edge. In site 6, there was no temporal stability observed in the yield and berry compositions maps. The maps of TA, phenols, and anthocyanins positively correlated to RVI map while inversely correlated to red map.

Overall, the proximal sensing maps at fruit set had similar clustering patterns to yield in five out of six sites with showing temporal stability throughout the consecutive years in three sites and these clustering also observed in weight of single berry at three vineyard sites with the temporal stability. The other proximal sensing maps at lag phase and veraison also showed similar clustering patterns to yield and berry wight but no temporal stability observed throughout the consecutive years. There were inverse clustering patterns observed between proximal sensing and

phenols/anthocyanins in three of six sites with some temporal stability through the consecutive years. The proximal sensing maps at lag phase and at veraison indicated more correlations than these maps of fruit set thus the vegetation at the latter growing season could have more impacts on accumulation of phenols and anthocyanins level in berry.

As a result of Moran's I analysis, these maps are less accurate due to the many variables showing random distribution results of the spatial analysis and there were only weak correlations observed between proximal sensing maps and other berry compositions (Brix, TA, and pH) maps. However, proximal sensing measurement at fruit set and lag phase showed a strong negative correlation to the pH in most of sites in 2016, hot and dry year. The NDVI maps from the RPAS flight indicated similar clustering patterns to yield and berry weight in most of sites where four sites showed temporal stability in berry weight throughout the consecutive years while in the berry composition maps, ability to compare spatial patterns and relationships across the variables varied by site and year.

The thermal emission maps from the RPAS flight showed less correlation to the yield component maps but these indicated better correlation to the berry composition maps. Especially, the thermal emission maps showed a strong positive correlation to the pH in most of sites and site 5 showed temporal stability throughout the consecutive years. CI green and GNDVI maps showed the most similar clustering patterns to yield and vine size and a positive relationship also found between RVI and berry weight in four of six sites while green and red showed a weak inverse correlation to yield and vine size. NIR and red edge showed the least correlation to the yield.

Maps from site 3 and 4 showed the most correlation between other indices and yield components while maps of other indices in site 6 only showed the significant correlation to berry weight. The correlations between indices from the RPAS flight and berry compositions were site

specific and two sites showed an identical correlation between the two variables while inverse correlation observed in another site. The other three sites only indicated weak correlations between the two variables, which varied between sites. CI red edge and NDRE had inverse clustering patterns to Brix, pH, TA, phenols, and anthocyanins while green, red, red edge, NIR had similar clustering patterns to pH, phenols, and anthocyanins in the two sites. The inverse clustering patterns were also observed between Brix/pH/phenols and green/red/red edge/NIR in another site. The maps of berry composition were inversely correlated to yield components in the sites with the high correlations.

4.2 Discussion

This study demonstrated the viability of using the RPAS flight and proximal sensing methods for predicting vineyard productivity and fruit quality in cool-climate Cabernet franc vineyards. Neither of the NDVIs were associated with number of clusters in five vineyards, with only site 5 vineyard displaying positive correlations in 2016 and 2017 (Table 4.2 and 4.3). This result could be caused by cluster thinning practice since all six sites performed cluster thinning in the growing seasons and it caused the uniform number of clusters throughout the vineyard. However, more relationships were seen between the NDVIs and measure of yield and berry weight. Previous studies confirmed the results showed that NDVI positively correlated to yield and berry weight.[1,8]

Interestingly, there could be an impact of annual climate changes (mean temperature and precipitation) on yield in the vineyards. In a regular growing season like 2015 or 2017 (Figure 4.3) the yield level was consistent. In a hot and dry year (2016, Figure 4.3) the yield shifted to a higher level in site 1, 2, and 6 while it shifted to a lower level in site 3, 4, and 5. Furthermore, the annual

variation in the correlation matrix between NDVI from the RPAS flight and yield throughout the vineyards had indicated more capability of detecting the correlation in a year with a hot and dry growing season as in 2016. Thus, lower water content and subsequent stress could be a limiting factor for reproductive process.[11] Vine size has been demonstrated to significantly affect berry composition and yield in previous studies[12,13] and with stomata operating at full capacity most of the time, biomass production is linearly correlated with water consumption[8]. This may explain that lower grapevine water status could be a constraint for reproductive process.

Variations of yield level in different sites were also observed in the dry year. This could explain that in some vineyard sites, the presence of water stress may alter the normal cycle of stomatal closure, causing an improved performance in water usage, no longer having an impact on vegetative and reproductive growth[14] while in the other sites, the conventional relationship between water availability and plant reproductive production was applied.

Another interesting observation in this study is the possibility of seasonal vegetation impacts on yield. The proximal sensing measurement at fruit set indicated more correlations than measurements at lag phase and veraison, thus the vegetation at earlier growing season could have more impacts on the reproductive process. It has been demonstrated that water stress affects yield greatly during critical phenological periods.[15] Previous studies also indicated a possibility of seasonal water deficit and vegetation impacts on yield that a positive correlation was found between NDVI and yield when the site experienced water stress prior to veraison.[15,16] Water stress during the early stages of growth can cause canopy reduction, berry cell division, changing the source-sink balance, and potentially leading to smaller yield.[17-19] Both NDVIs represented an activity of photosynthetic radiation absorbed by the plant and therefore, in early developmental

stages, reproductive growth was also influenced by variation in light-induced biomass production under water stress.[15]

In general, there were only weak correlations observed between NDVIs from the RPAS flight and from proximal sensing and berry compositions (Table 4.2 and 4.3). Several factors may have influenced the lack of temporal stability between NDVI from the RPAS flight and fruit quality data in this research, including the variability in harvest dates between blocks and years. This lack of stability has been observed in previous research as well.[8,15,20,21] Differences in fruit quality from the different NDVI zones fluctuated across years.[8] Brix, TA, pH, and phenol concentrations were not related to NDVI data.[20,21] Interestingly, a strong trend for a positive correlation between thermal emission data from the RPAS flight and pH was seen throughout the sites in 2016 (dry year). Inverse trends were also observed between early developmental stages of proximal NDVI measurements and pH.

Evidence for an inverse correlation between phenols/anthocyanins level and NDVIs was also seen, in three sites (site 1, 4, and 5; Table 4.2 and 4.3) throughout three consecutive years (2015, 2016, 2917). This result confirms the previous study that berry composition variables, especially phenolic accumulation, are inversely impacted by vigorous leaf canopies via fruit exposure to sunlight to the flavonoid biosynthesis.[22-24] The annual variation in anthocyanins level throughout the vineyards had also observed. Interestingly, the growing season was hot and dry in 2016 (Figure 4.3), and a high anthocyanin concentration was observed throughout the sites in 2016.

Furthermore, this study confirms that mild drought stress after veraison did not influence the berry compositions but altered phenols and anthocyanins levels of the fruit.[25] Interestingly, the proximal NDVI measurements around veraison showed better correlation with phenols and

anthocyanins than measurements at fruit set and therefore, the vegetation at the latter growing season could have more impacts on accumulation of phenols and anthocyanins level in berries. It confirmed a previous finding that by severely reducing water availability from veraison to maturity, stress-induced biosynthesis was increased and produced more phenolic compounds.[26]

Numerous indices from the RPAS flight data can be calculated from the green, red, red edge, and NIR regions of EM reflectance to detect reproductive growth and potential grape quality.[2] The factors contributing to the different level of reflectance in green, red, red edge, and NIR peaks are very diverse. Leaf reflectance in green and red is usually controlled by plant pigments while in the NIR range, variations in reflectance might be influenced by alterations in leaf structure and/or thickness that affect leaf absorbance and reflectance.[27] The red edge peak is in the boundary between visible and NIR spectrums and the peak is employed to determine foliar composition such as chlorophyll content.[28] Chlorophyll is the primary molecules that absorb the light energy and convert the energy for photosynthesis and is also a critical barometer of the plant health and growth.[29] Chlorophyll content is negatively correlated to the red reflectance peak because chlorophyll strongly absorbs red radiation for the electron transitions for photosynthesis at the magnesium component of the photoactive site.[29] Therefore, red reflectance could be a reliable candidate for estimating plant chlorophyll content and photosynthesis activity. However, the measurements of red reflectance are very sensitive to the effects of various other variables such as solar irradiance, presence of other pigment molecules, background soil, and the geometrical arrangement of the scene.[27,30] Reflectance at the red edge is less relying on these variables since it marks the boundary between leaf inner cellular scattering in NIR peak and chlorophyll absorption in red peak.[31]

This study examined the feature indices (Table 4.4) such as green, red, red edge, NIR, green chlorophyll index (CI green), red edge chlorophyll index (CI red edge), red edge normalized difference vegetation index (NDRE), NDVI green (GNDVI) and ratio vegetation index (RVI) to characterize the plant yield and quality production according to previous studies.[3-6]

From the results of this study, CI green and GNDVI showed the most capability of detecting variation in yield and vine size in most of sites with statistically significant positive correlation. Both CI green and GNDVI are derived from the ratio of green and NIR portion of the electromagnetic reflectance spectra. The formula of CI green is ' $\frac{NIR}{Green}$ – 1' and GNDVI is $\frac{(NIR-Green)}{(NIR+Green)}$. There has been extensive evidence that leaf chlorophyll concentrations and nitrogen levels of maize are intimately associated, as are nitrogen levels and maize productivity.[32,33] Changes in leaf nitrogen concentration alter the photosynthetic membranes that is predominantly chlorophyll.[32-34] Many studies found that the green chlorophyll index (CI green) was reliable and consistent indicator of canopy chlorophyll and nitrogen levels.[3,6,34-39] GNDVI was another key index to monitor the variation in yield and vine canopy. GNDVI and CI green were proved to be identical to each other with high Pearson's correlation coefficient (R) values. Green and red also showed a good negative correlation to yield and vine size. NIR and red edge showed the least correlation to the yield components.

The correlations between indices from the RPAS flight and berry compositions were less significant than these between the indices and yield components. For berry compositions, the correlations were also in a random pattern such that two sites showed an identical correlation between the two variables while an inverse correlation was observed in another site. CI red edge and NDRE indicated the inverse correlation to most of the variables like Brix, pH, phenols, and anthocyanins and green, red edge, and NIR were also positively correlated to pH, phenols, and

anthocyanins while Brix, pH, phenols, and anthocyanins were negatively correlated to CI red edge and NDRE in site 2. Both CI red edge and NDRE are derived from the ratio of red edge and NIR portions of the electromagnetic reflectance spectra. In site 3, green and red positively correlated to all the berry composition variables and CI green and RVI also showed the high inverse correlations to Brix, pH, phenols, and anthocyanins.

Interestingly, in site 5 vineyard, an inverse correlation-matrix to site 2 and site 3 were observed between the indices and berry compositions. Red edge indicated an inverse correlation to most of the variables like Brix, pH, phenols, and anthocyanins and red and NIR also showed the inverse correlations to Brix, pH, and phenols. CI red edge and NDRE were only positively correlated to level of phenols. In site 4, CI green, GNDVI, and RVI were inversely correlated to brix and anthocyanins. The formular of CI red edge is ' $\frac{NIR}{Red\ Edge} - 1$' and GNDVI is $\frac{(NIR-Red\ edge)}{(NIR+Red\ Edge)}$. Many previous studies only focused on the relationship between leaf red edge reflectance and canopy structure such as leaf chlorophyll and N contents[28,35,40,41] and the negative impacts on photosynthesis and plant growth with reduction of red edge peak were observed as of the reduction in chlorophyll concentration in stressed leaves[42-44]. However, the prediction of the correlations between photosynthetically active biomass with stress and the fruit quality would be difficult since in some cases, a mild stress can boost the fruit quality in the vineyard.

Grape quality, particularly that of red grape varieties, is largely dependent on secondary metabolites such as the accumulation of phenols and anthocyanins.[45] Lack of vine water influx reduces vegetative and reproductive growth while increases colour intensity.[46,47] However, extensive water stress risk production and quality loss[26] and therefore, controlling the balance of grapevine vegetative and reproductive growth with limiting the water supply has been a key issue

in the vineyard management practice and the balance is in site and time specific manner[19,45,48-50].

To examine the feasibility of remote sensing technologies in a vineyard quality management program in terms of controlling yield and grape quality is not an easy task. Even though many scientists agree that moderate water deficits are beneficial for vineyard productivity and additional water with relatively small quantities can boost grape yield significantly [18,51-53], there is no clear general guideline for what the level of water stress can be assigned to the moderate water deficit because it depends on site, variety, and cultural practice of specific vineyard. However, remote sensing technology could be a tool to discover the balanced grapevine water level for optimum wine production. Vineyard soil map and its drainage potential are essential since a soil type impacts soil and leaf water potential.[45]

The noteworthy observation from the results were that the yield components and berry compositions were inversely correlated to each other in the three sites (site 2, 3, and 5) with high correlation rate observed. The other three sites only indicated no or weak correlations between the two variables, which varied between sites. These could be explained that application of mild stress in the three sites with high correlation limited the vine growth, reduced the yield components and increased berry anthocyanins and phenol contents.[46,47] However, the excessive water deficit stress applied in the other three sites and lead to yield and quality losses.[26]

Using remote sensing data to predict grape quality and productivity, it is necessary to produce reliable and precise maps that illustrate areas of the variables to implement zonal vineyard management. This study found that spatial patterns in the maps indicate a strong relationship between remote sensing data and vineyard yield and some quality indicators, resulting in the potential use of remote sensing maps to pinpoint target areas in a single vineyard.[54] In Moran's I

analysis, yield/berry composition and data from the RPAS flight/proximal sensing were highly clustered in 2016 (dry year), and a selective harvesting based on these parameters may be feasible in single vineyard blocks.

4.3 Conclusions

According to the findings of this study, data analysis from the RPAS flight and from proximal sensing data have some potential for predicting grape quality and productivity but site and variable growing season conditions can limit its reliability. Even though NDVI and other remote sensing data analysis tools were not associated with number of variables in quantity and quality of grape production, a strong trend of a positive correlation for NDVI from the RPAS flight and from early-stage proximal sensing NDVI to yield and berry weight was still seen throughout the sites and years. The vegetation earlier in the growing season could have more impact on the reproductive process.[15]

The other strong trend for a positive correlation between thermal emission data from the RPAS flight and pH was seen throughout the sites and years, especially in 2016 (dry year), all sites showed positive correlation between the two variables, which also indicated that variation in a crop canopy temperature could be a key determinant of pH under water stress condition. There was also possible inverse correlation between late season proximal NDVI and phenols/anthocyanins level in three of six sites and the vegetation at the latter growing season could have more impacts on accumulation of phenols and anthocyanins level in berry. One important message from the results is that a remote sensing data acquisition timeline could be a critical factor to incorporate remote sensing technologies into vineyard management decision

making. Further research will be required to confirm the impacts of vegetation in different timelines on the fruit yield and quality.

4.4 References

1. Rey-Caramés, C.; Diago, M.; Martín, M.; Lobo, A.; Tardaguila, J. Using RPAS multi-spectral imagery to characterise vigour, leaf development, yield components and berry composition variability within a vineyard. *Remote Sensing* **2015**, *7*, 14458-14481.

2. Meggio, F.; Zarco-Tejada, P.J.; Núñez, L.C.; Sepulcre-Cantó, G.; González, M.; Martín, P. Grape quality assessment in vineyards affected by iron deficiency chlorosis using narrow-band physiological remote sensing indices. *Remote Sensing of Environment* **2010**, *114*, 1968-1986.

3. Wang, F.-M.; Huang, J.-F.; Tang, Y.-L.; Wang, X.-Z.J.R.S. New vegetation index and its application in estimating leaf area index of rice. **2007**, *14*, 195-203.

4. Wu, D.; Feng, L.; Zhang, C.; He, Y.J.T.o.t.A. Early detection of Botrytis cinerea on eggplant leaves based on visible and near-infrared spectroscopy. **2008**, *51*, 1133-1139.

5. Kayad, A.; Sozzi, M.; Gatto, S.; Marinello, F.; Pirotti, F.J.R.S. Monitoring Within-Field Variability of Corn Yield using Sentinel-2 and Machine Learning Techniques. **2019**, *11*, 2873.

6. Motohka, T.; Nasahara, K.N.; Oguma, H.; Tsuchida, S.J.R.S. Applicability of green-red vegetation index for remote sensing of vegetation phenology. **2010**, *2*, 2369-2387.

7. Pringle, M.J.; McBratney, A.B.; Whelan, B.M.; Taylor, J.A. A preliminary approach to assessing the opportunity for site-specific crop management in a field, using yield monitor data. *Agricultural Systems* **2003**, *76*, 273-292, doi:10.1016/s0308-521x(02)00005-7.

8. Acevedo-Opazo, C.; Tisseyre, B.; Guillaume, S.; Ojeda, H. The potential of high spatial resolution information to define within-vineyard zones related to vine water status. *Precision Agriculture* **2008**, *9*, 285-302.

9. Naidu, R.A.; Perry, E.M.; Pierce, F.J.; Mekuria, T. The potential of spectral reflectance technique for the detection of Grapevine leafroll-associated virus-3 in two red-berried wine grape cultivars. *Computers and Electronics in Agriculture* **2009**, *66*, 38-45.

10. Lamb, D.; Hall, A.; Louis, J.J.A.G.; Winemaker. Airborne remote sensing of vines for canopy variability and productivity. **2001**, 89-94.

11. Arnó, J.; Rosell, J.; Blanco, R.; Ramos, M.; Martínez-Casasnovas, J. Spatial variability in grape yield and quality influenced by soil and crop nutrition characteristics. *Precision Agriculture* **2012**, *13*, 393-410.

12. Smart, R.E. Principles of grapevine canopy microclimate manipulation with implications for yield and quality. A review. *American Journal of Enology and Viticulture* **1985**, *36*, 230-239.

13. Terry, D.B.; Kurtural, S.K. Achieving vine balance of Syrah with mechanical canopy management and regulated deficit irrigation. *American journal of enology and viticulture* **2011**, *62*, 426-437.

14. Jones, H.G. *Plants and microclimate: a quantitative approach to environmental plant physiology*; Cambridge university press: **2013**.

15. González-Flor, C.; Serrano, L.; Gorchs, G.; Pons, J.M. Assessment of grape yield and composition using reflectance-based indices in rainfed vineyards. *Agronomy Journal* **2014**, *106*, 1309-1316.

16. Serrano, L.; González-Flor, C.; Gorchs, G. Assessment of grape yield and composition using the reflectance based Water Index in Mediterranean rainfed vineyards. *Remote sensing of environment* **2012**, *118*, 249-258.

17. Van Leeuwen, C.; Trégoat, O.; Choné, X.; Bois, B.; Pernet, D.; Gaudillère, J.-P. Vine water status is a key factor in grape ripening and vintage quality for red Bordeaux wine. How can it be assessed for vineyard management purposes. *OENO One* **2009**, *43*, 121-134.

18. Matthews, M.; Anderson, M.; SCHULT, H.J.V. Phenologic and growth responses to early and late season. **1987**, *26*, 147-160.

19. Ojeda, H.; Deloire, A.; Carbonneau, A.J.V.-G.-. Influence of water deficits on grape berry growth. **2001**, *40*, 141-146.

20. Urretavizcaya, I.; Santesteban, L.G.; Tisseyre, B.; Guillaume, S.; Miranda, C.; Royo, J.B. Oenological significance of vineyard management zones delineated using early grape sampling. *Precision Agriculture* **2013**, *15*, 111-129, doi:10.1007/s11119-013-9328-3.

21. Ledderhof, D.; Brown, R.; Reynolds, A.; Jollineau, M. Using remote sensing to understand Pinot noir vineyard variability in Ontario. *Canadian journal of plant science* **2016**, *96*, 89-108.

22. Drissi, R.; Goutouly, J.-P.; Forget, D.; Gaudillere, J.-P. Nondestructive measurement of grapevine leaf area by ground normalized difference vegetation index. *Agronomy Journal* **2009**, *101*, 226-231.

23. Lamb, D.W.; Weedon, M.; Bramley, R. Using remote sensing to predict grape phenolics and colour at harvest in a Cabernet Sauvignon vineyard: Timing observations against vine phenology and optimising image resolution. *Australian Journal of Grape and Wine Research* **2004**, *10*, 46-54.

24. Stamatiadis, S.; Taskos, D.; Tsadilas, C.; Christofides, C.; Tsadila, E.; Schepers, J.S. Relation of ground-sensor canopy reflectance to biomass production and grape color in two Merlot vineyards. *American Journal of Enology and viticulture* **2006**, *57*, 415-422.

25. Kennedy, J.A.; Matthews, M.A.; Waterhouse, A.L.J.A.J.o.E.; Viticulture. Effect of maturity and vine water status on grape skin and wine flavonoids. **2002**, *53*, 268-274.

26. Ojeda, H.; Andary, C.; Kraeva, E.; Carbonneau, A.; Deloire, A.J.A.j.o.E.; Viticulture. Influence of pre-and postveraison water deficit on synthesis and concentration of skin phenolic compounds during berry growth of Vitis vinifera cv. Shiraz. **2002**, *53*, 261-267.

27. Curran, P.J.J.R.s.o.e. Remote sensing of foliar chemistry. **1989**, *30*, 271-278.

28. Curran, P.J.; Dungan, J.L.; Gholz, H.L.J.T.p. Exploring the relationship between reflectance red edge and chlorophyll content in slash pine. **1990**, *7*, 33-48.

29. Danks, S.M.; Evans, E.H.; Whittaker, P.A. *Photosynthetic systems: structure, function, and assembly*; John Wiley & Sons: **1983**.

30. Curran, P.J.P.T.o.t.R.S.o.L.S.A., Mathematical; Sciences, P. Multispectral remote sensing for the estimation of green leaf area index. **1983**, *309*, 257-270.

31. Horler, D.; DOCKRAY, M.; Barber, J.J.I.j.o.r.s. The red edge of plant leaf reflectance. **1983**, *4*, 273-288.

32. Evans, J.R.J.O. Photosynthesis and nitrogen relationships in leaves of C 3 plants. **1989**, *78*, 9-19.

33. Baret, F.; Houlès, V.; Guerif, M.J.J.o.E.B. Quantification of plant stress using remote sensing observations and crop models: the case of nitrogen management. **2007**, *58*, 869-880.

34. Schlemmer, M.; Gitelson, A.; Schepers, J.; Ferguson, R.; Peng, Y.; Shanahan, J.; Rundquist, D.J.I.J.o.A.E.O.; Geoinformation. Remote estimation of nitrogen and chlorophyll contents in maize at leaf and canopy levels. **2013**, *25*, 47-54.

35. Gitelson, A.A.; Viña, A.; Verma, S.B.; Rundquist, D.C.; Arkebauer, T.J.; Keydan, G.; Leavitt, B.; Ciganda, V.; Burba, G.G.; Suyker, A.E.J.J.o.G.R.A. Relationship between gross primary production and chlorophyll content in crops: Implications for the synoptic monitoring of vegetation productivity. **2006**, *111*.

36. Gitelson, A.A.; Merzlyak, M.N.J.J.o.p.p. Signature analysis of leaf reflectance spectra: algorithm development for remote sensing of chlorophyll. **1996**, *148*, 494-500.

37. Gitelson, A.A.; Gritz, Y.; Merzlyak, M.N.J.J.o.p.p. Relationships between leaf chlorophyll content and spectral reflectance and algorithms for non-destructive chlorophyll assessment in higher plant leaves **2003**, *160*, 271-282.

38. Yoder, B.J.; Pettigrew-Crosby, R.E.J.R.s.o.e. Predicting nitrogen and chlorophyll content and concentrations from reflectance spectra (400–2500 nm) at leaf and canopy scales. **1995**, *53*, 199-211.

39. Zagajewski, B.; Kycko, M.; Tømmervik, H.; Bochenek, Z.; Wojtun, B.; Bjerke, J.W.; Klos, A. Feasibility of hyperspectral vegetation indices for the detection of chlorophyll concentration in three high Arctic plants: Salix polaris, Bistorta vivipara, and Dryas octopetala. **2018**.

40. Gitelson, A.A.; Merzlyak, M.N.; Lichtenthaler, H.K.J.J.o.p.p. Detection of red edge position and chlorophyll content by reflectance measurements near 700 nm. **1996**, *148*, 501-508.

41. Chang-Hua, J.; Yong-Chao, T.; Xia, Y.; Wei-Xing, C.; Yan, Z.; Hannaway, D.J.P. Estimating leaf chlorophyll content using red edge parameters. **2010**, *20*, 633-644.

42. Cabaleiro, C.; Segura, A.; Garcia-Berrios, J.J.A.J.o.E.; Viticulture. Effects of grapevine leafroll-associated virus 3 on the physiology and must of Vitis vinifera L. cv. Albarino following contamination in the field. **1999**, *50*, 40-44.

43. Bertamini, M.; Muthuchelian, K.; Nedunchezhian, N.J.J.o.P. Effect of grapevine leafroll on the photosynthesis of field grown grapevine plants (Vitis vinifera L. cv. Lagrein). **2004**, *152*, 145-152.

44. Endeshaw, S.T.; Sabbatini, P.; Romanazzi, G.; Schilder, A.C.; Neri, D.J.S.H. Effects of grapevine leafroll associated virus 3 infection on growth, leaf gas exchange, yield and basic fruit chemistry of Vitis vinifera L. cv. Cabernet Franc. **2014**, *170*, 228-236.

45. Chaves, M.M.; Santos, T.P.; Souza, C.d.; Ortuño, M.; Rodrigues, M.; Lopes, C.; Maroco, J.; Pereira, J.S. Deficit irrigation in grapevine improves water-use efficiency while controlling vigour and production quality. *Annals of Applied Biology* **2007**, *150*, 237-252.

46. Matthews, M.A.; Anderson, M.M.J.A.J.o.e.; Viticulture. Fruit ripening in Vitis vinifera L.: responses to seasonal water deficits. **1988**, *39*, 313-320.

47. Koundouras, S.; Marinos, V.; Gkoulioti, A.; Kotseridis, Y.; van Leeuwen, C. Influence of vineyard location and vine water status on fruit maturation of nonirrigated cv. Agiorgitiko (Vitis vinifera L.). Effects on wine phenolic and aroma components. *Journal of Agricultural and Food Chemistry* **2006**, *54*, 5077-5086.

48. Girona, J.; Mata, M.; Del Campo, J.; Arbonés, A.; Bartra, E.; Marsal, J.J.I.S. The use of midday leaf water potential for scheduling deficit irrigation in vineyards. **2006**, *24*, 115-127.

49. Salón, J.L.; Chirivella, C.; Castel, J.R. Response of cv. Bobal to timing of deficit irrigation in Requena, Spain: water relations, yield, and wine quality. *American Journal of Enology and Viticulture* **2005**, *56*, 1-8.

50. Basinger, A.R.; Hellman, E.W. Evaluation of regulated deficit irrigation on grape in Texas and implications for acclimation and cold hardiness. *International journal of fruit science* **2007**, *6*, 3-22.

51. Matthews, M.A.; Anderson, M.M.J.A.J.o.E.; Viticulture. Reproductive development in grape (Vitis vinifera L.): responses to seasonal water deficits. **1989**, *40*, 52-60.

52. Reynolds, A.G.; Naylor, A.P. Pinot noir'andRiesling'Grapevines Respond to Water Stress Duration and Soil Water-holding Capacity. *HortScience* **1994**, *29*, 1505-1510.

53. Santos, T.P.; Lopes, C.M.A.; Rodrigues, M.; Souza, C.R.d.; Maroco, J.; Pereira, J.S.; Silva, J.R.; Chaves, M.M.J.F.P.B. Partial rootzone drying: effects on growth and fruit quality of field-grown grapevines (Vitis vinifera). **2003**, *30*, 663-671.

54. Arnó Satorra, J.; Martínez Casasnovas, J.A.; Ribes Dasi, M.; Rosell Polo, J.R. Precision viticulture. Research topics, challenges and opportunities in site-specific vineyard management. *Spanish Journal of Agricultural Research* **2009**, *7*, 779-790.

CHAPTER 5: RESULTS AND DISCUSSION - FEASIBILITY STUDY OF REMOTE SENSING NDVI ANALYSIS TO DETECT OENOLOGICALLY RELEVANT VINEYARD ZONES

The objective of this chapter was to investigate the zonal effect of remote sensing NDVI on wine sensory and chemical attributes. It was hypothesized that if vineyard blocks were harvested based on zones corresponding to low and high NDVI, resulting wines would differ in their chemical and sensory attributes.

5.1 Results

5.1.1 Vineyard zoning and must analysis

Each vineyard site was divided into two NDVI zones with three field replicates based on the 2016 RPAS NDVI (remote sensing) interpolated maps: high NDVI zone: green colour and low NDVI zone: red colour (Figure 2.2). To maintain consistency between the years (2016 and 2017), the NDVI zonal maps were the same in both years. The impacts of the different NDVI zones on wine chemical and sensory attributes within a site were investigated in this chapter.

In Figure 5.1, a chemical analysis of the grape-must showed that some berry compositions differed significantly between low and high NDVIs (95%). Overall, grape-must composition did not vary between treatments, other than anthocyanins, which varied in multiple sites in both years. The anthocyanin content of treatment wines differed in all six sites in 2016 and in four sites in 2017. Remote sensing NDVI had an inverse relationship with anthocyanins in three sites (site 1, 4, and 5) throughout the consecutive years (2016 and 2017) while site 6 showed positive correlations through the years (Figure 5.1).

There were some other chemical components showing distinct differences between NDVI zones such as brix and phenols. Site 4 and 5 had an inverse relationship between NDVI and phenols concentration while site 2 and 6 had a positive relationship between the two variables. Site 5 and 3 had an inverse relationship between NDVI and Brix while site 2 and 6 had a positive relationship between the two variables (Figure 5.1).

Overall, anthocyanin levels in grape must analysis differentiated for low and high NDVI at three out of six sites showed temporal stability throughout the consecutive years. There was statistically significant difference with negative correlation between remote sensing NDVI and anthocyanins level in the sites. There were some other chemical components showing distinct differences between NDVI values, but the degree and direction of differences differed depending on the year and the location.

Figure 5.1. Comparison of grape must analysis results from 2016 and 2017 Low vs High NDVI in the six vineyard sites. * p-values of significantly different between the treatments ($p<0.05$).

5.1.2 Wine chemical analysis

In Figure 5.2, a chemical analysis of the wines showed that some wine chemistry differed significantly between low and high NDVIs (95%) and the pattern of the difference was similar to grape must analysis. Overall, wine chemistry did not differ in NDVI variations, other than anthocyanins, which varied in multiple sites in both years. The anthocyanin content of treatment wines differed in all six sites in 2016 and in four sites in 2017. Remote sensing NDVI had an inverse relationship with anthocyanins in three sites (site 1, 4, and 5; Figure 5.2) throughout the consecutive years (2016 and 2017). There were some other chemical components showing distinct differences between the NDVI zones such as % alcohol level and phenols. Site 2 and 5 had an inverse relationship between NDVI and phenols concentration in 2017. However, site 6 had a positive relationship between NDVI and phenols concentration in 2016. In 2017, site 2, 3, and 6 had a positive relationship between NDVI and % alcohol while in 2016, site 3 and 5 had an inverse relationship between NDVI and % alcohol (Figure 5.2).

There was a significant difference with negative correlation between remote sensing NDVI and anthocyanins level in the vineyards. Overall, anthocyanin levels in wine chemical analysis at three of six vineyards differentiated by low and high NDVI zones showed temporal stability throughout the consecutive years.

Figure 5.2. Comparison of wine analysis results from 2016 and 2017 Low vs High NDVI in in the six vineyard sites. * p-values of significantly different between the treatments ($p<0.05$).

5.1.3 Sensory sorting test

In all MDS Kruskal stress tests, the stress score was acceptable levels (<0.2) (Figure 5.3 and 5.4) and agglomerative hierarchical clustering (AHC) dendrogram for Cabernet franc wines from the six sites in Figure 5.5 and 5.6. In four sites, panelists sorted 2016 and 2017 wines by their NDVI levels (Figure 5.5 and 5.6). In particular, they were able to group all replicates by NDVI levels in 2017. As shown in Figure 5.5, in both years, site 3 considered it to have the lowest sorting rate. Overall, the panel was able to sort different NDVI treatments in both years, but it was especially successful in 2017, with full sorting of different NDVI treatments in each replicate at four out of six sites.

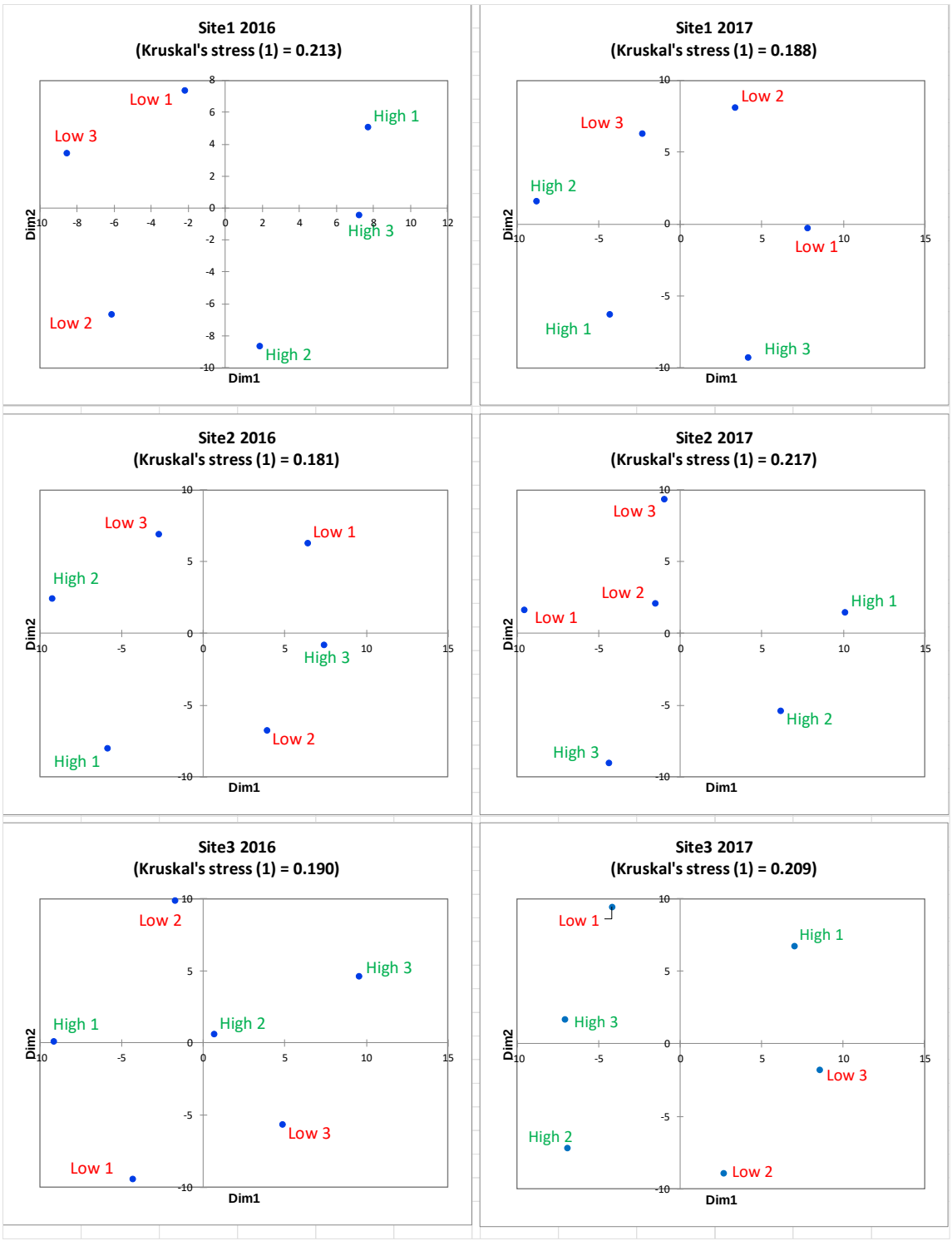

Figure 5.3. MDS Kruskal stress test results in Cabernet Franc wines from site 1, 2 and 3 vineyards. A co-occurrence matrix was generated from the results of the wine sorting test.

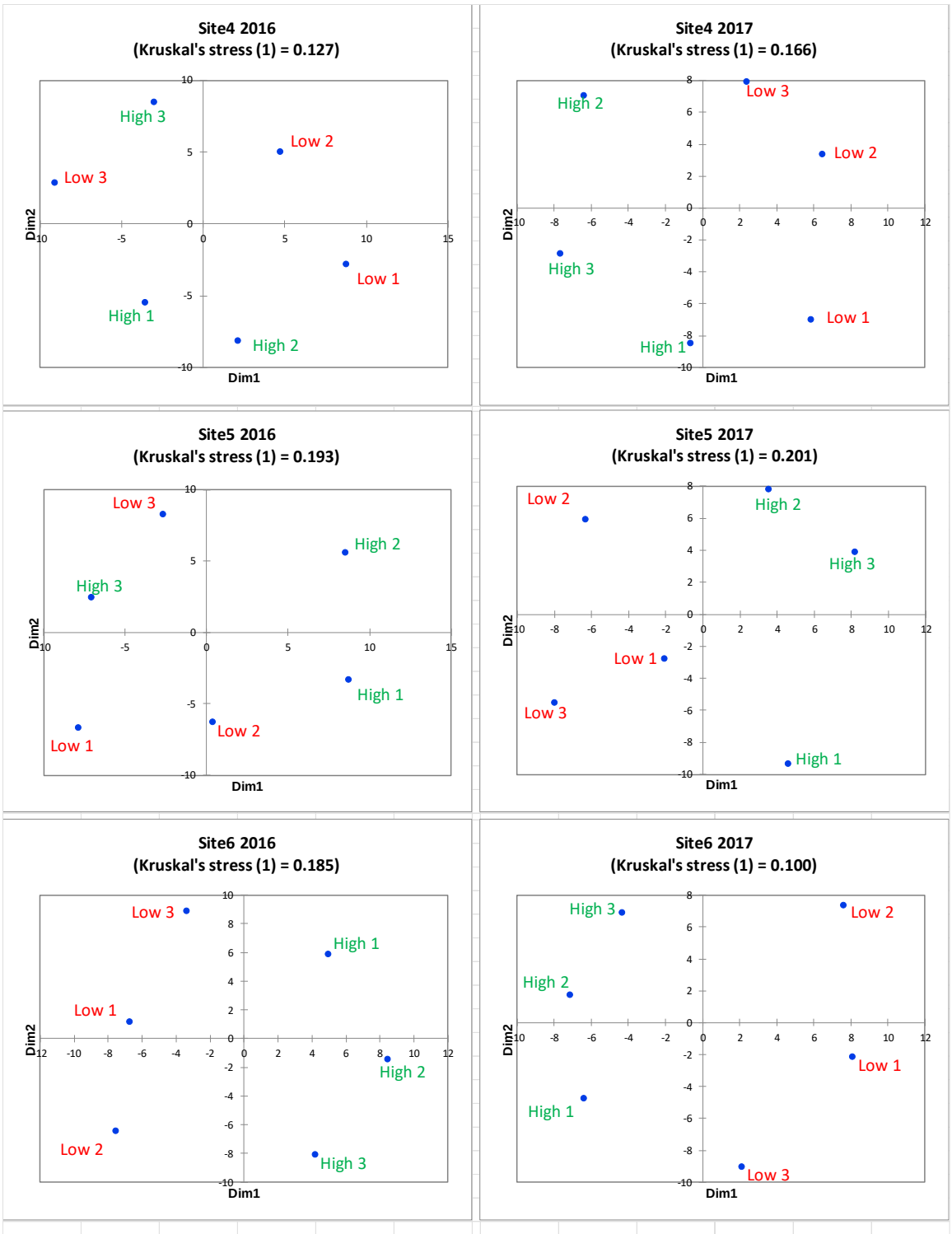

Figure 5.4. MDS Kruskal stress test results in Cabernet Franc wines from site 4, 5, and 6 vineyards. A co-occurrence matrix was generated from the results of the wine sorting test.

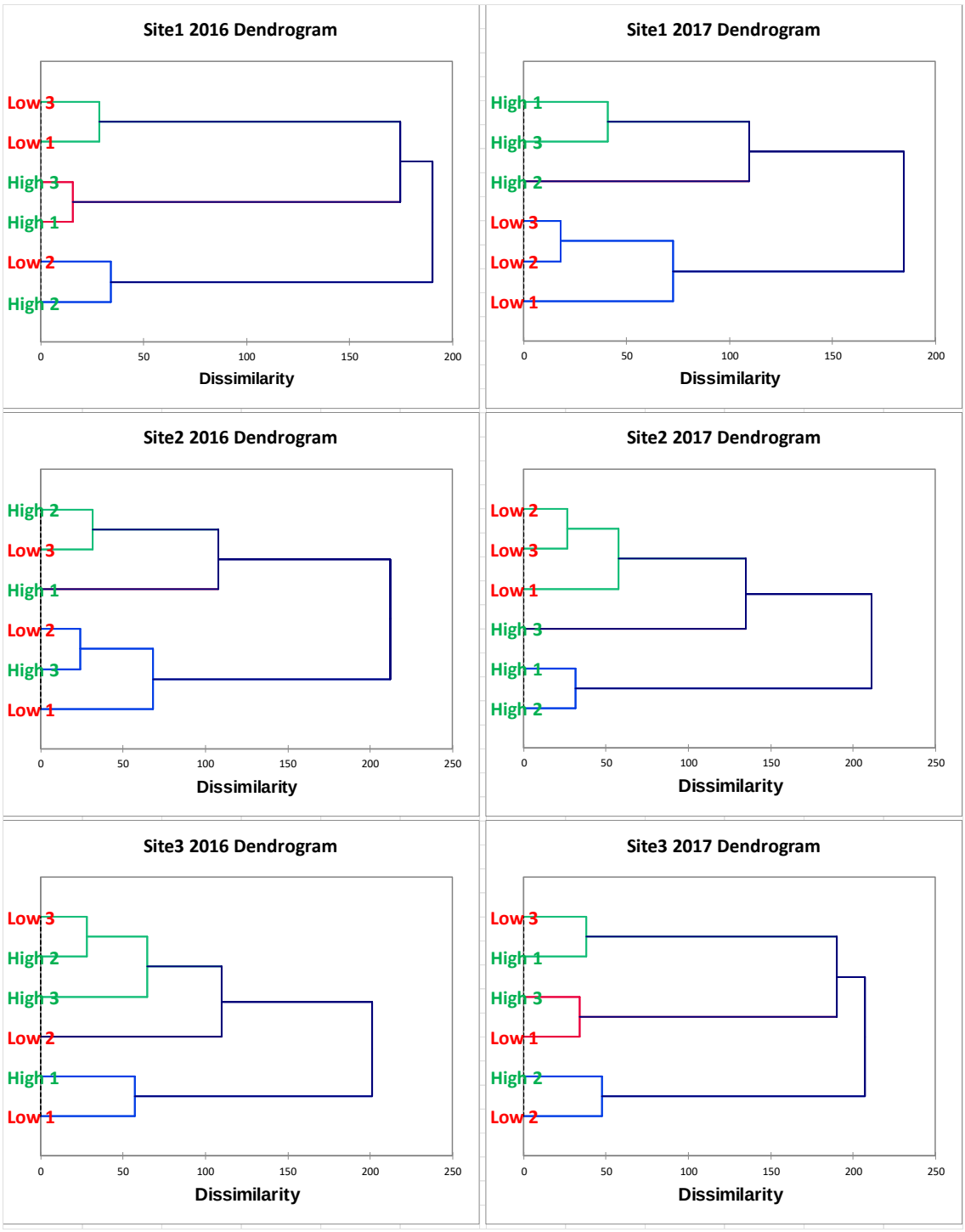

Figure 5.5. AHC results in Cabernet Franc wines from site 1, 2 and 3 vineyards. The dendrograms illustrated the hierarchical division of categories according to the level of difference.

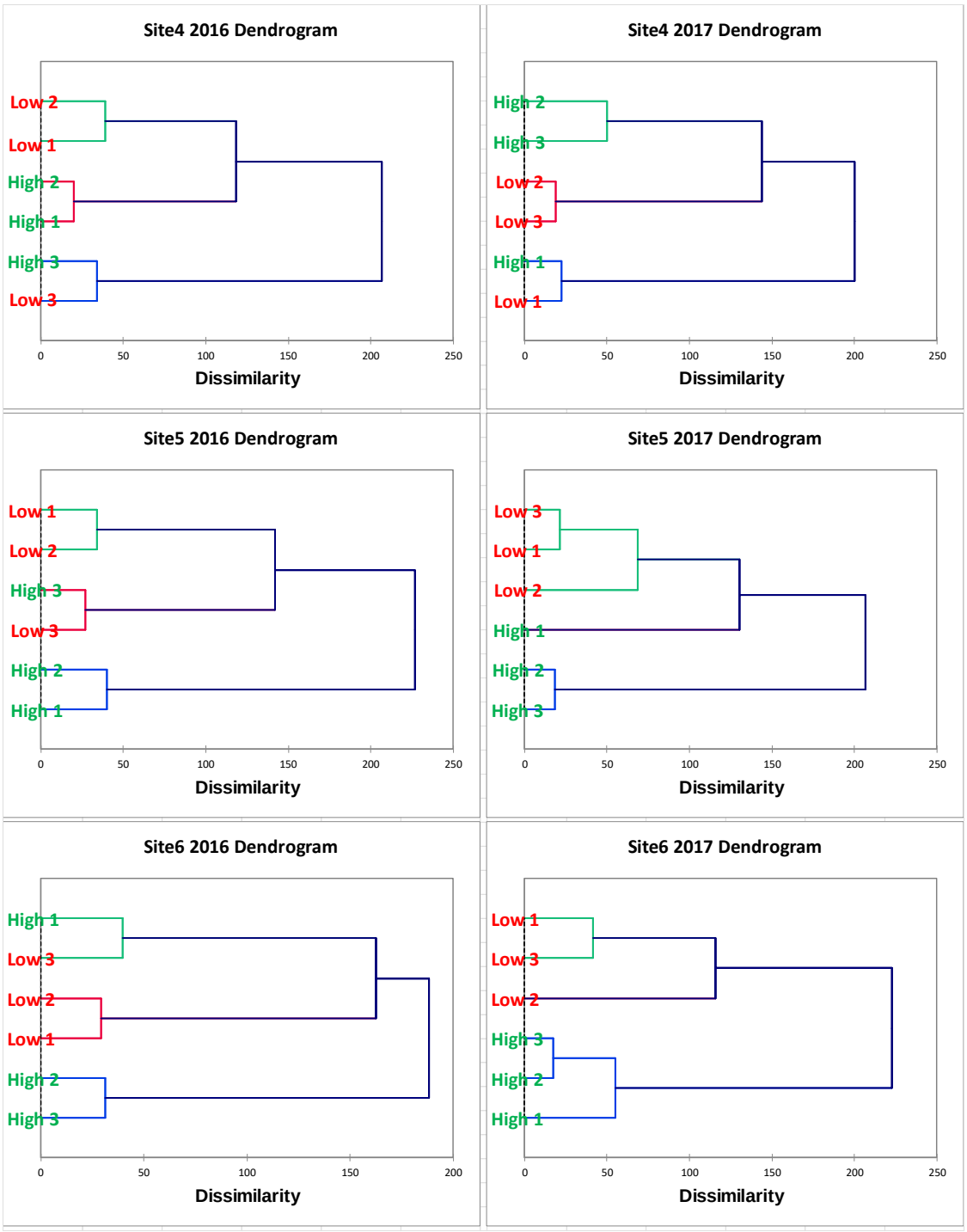

Figure 5.6. AHC results in Cabernet Franc wines from site 4, 5, and 6 vineyards. The dendrograms illustrated the hierarchical division of categories according to the level of difference.

5.1.4 Wine aromatic compounds analysis (GC-MS)

GC-MS was performed to analyze the levels of major odor active compounds in the Cabernet franc wines from two different NDVI zones (low and high NDVI) with triplicates and the results showed that the Cabernet franc wines have high concentration of Ethyl lactate and Diethyl succinate while cis-Rose oxide, Ethyl cinnamate, and γ-Decalactone were low in concentration. From the results of two-sample t-test in Figure 5.7 and 5.8, various odor active compounds showed significantly different concentration levels in high and low NDVI throughout the vineyard sites.

In 2016, only site 6 vineyard showed significantly different concentration level of various key odor active aroma compounds in high and low NDVI, and other vineyard sites didn't show any significant difference in the level of aroma compounds between low and high NDVI zones (Figure 5.7). In 2017, five of the six sites had statistically significant difference in concentrations of 1-Heptanol in wines from low and high NDVI zones (Figure 5.8). Levels of cis-3-Hexenol [(Z)-3-hexenol], 1-Hexanol, Ethyl hexanoate, Diethyl succinate, 2-Phenylethanol, and Eugenol also showed the significant difference (four of six sites) in wines from low and high NDVI zones.

Furthermore, concentration level of terpenes such as α-Terpineol, Geraniol, and Linalool showed a significant difference (three of six sites) while Isobutyl acetate, Ethyl butanoate, Isoamyl acetate, Acetic acid, Hexyl acetate, Citronellol, β-Damascenone, Ethyl decanoate, Ethyl cinnamate, Decanoic acid, and γ-Decalactone showed the least significant difference in wines from low and high NDVI zones throughout the six sites.

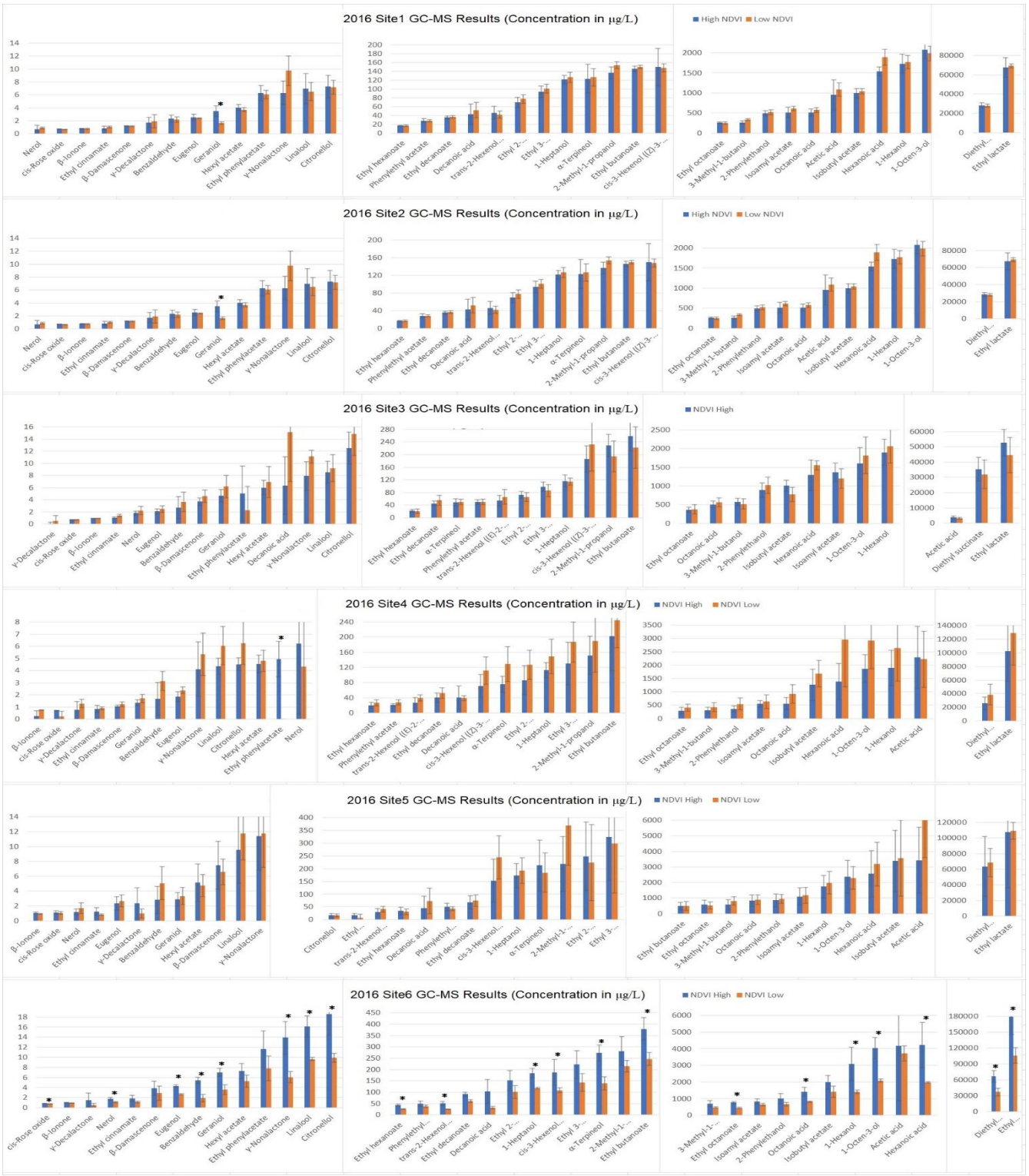

Figure 5.7. Significance of difference in the concentrations(µg/L) of key odor active aroma compounds in the 2016 Cabernet franc wines from two different NDVI zones (low and high NDVI) using a t-test with two samples: * significant p-values (95% confidence).

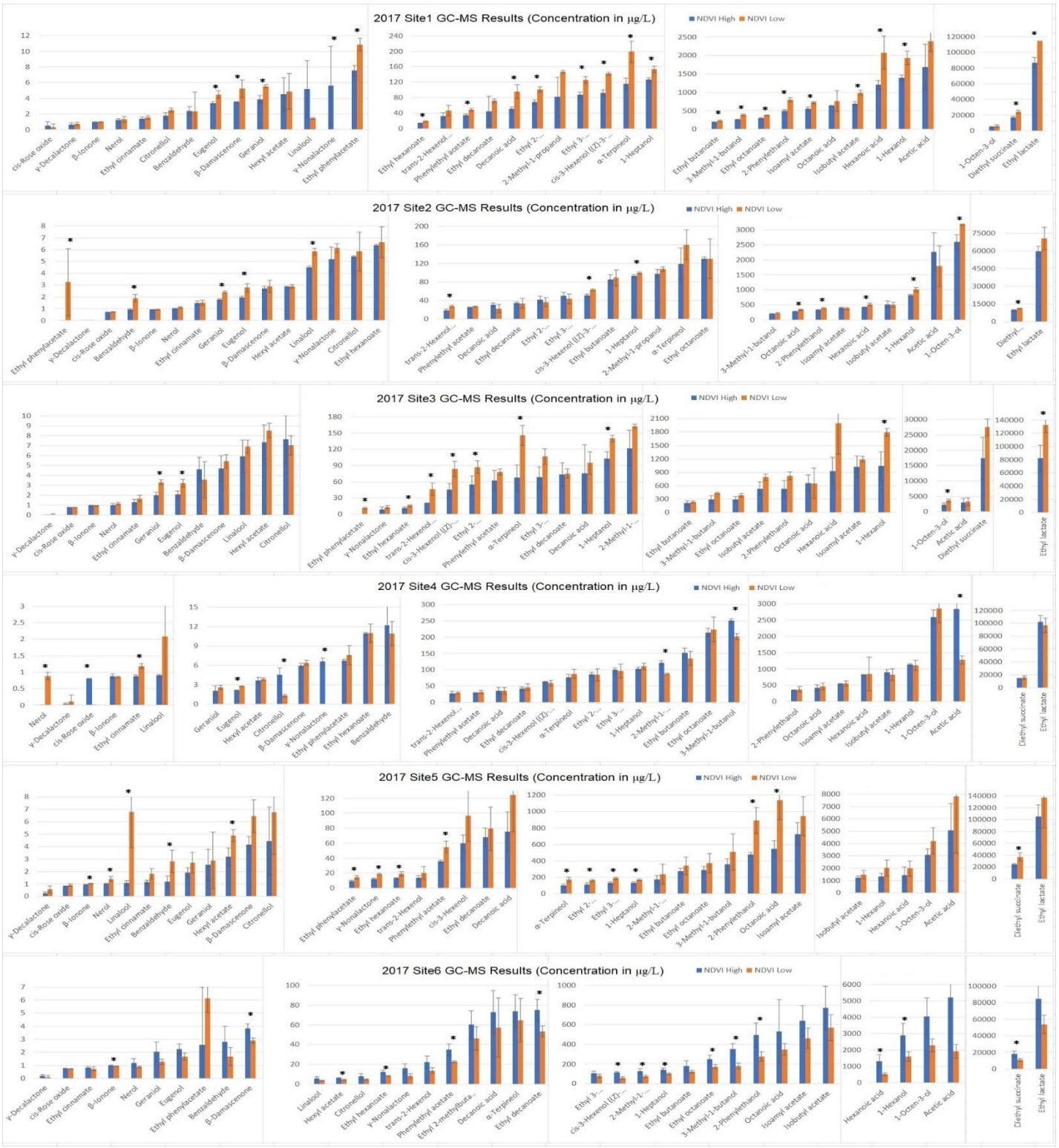

Figure 5.8. Significance of difference in the concentrations(µg/L) of key odor active aroma compounds in the 2017 Cabernet franc wines from two different NDVI zones (low and high NDVI) using a t-test with two samples: * significant p-values (95% confidence).

A seasonal variation of key odor active aroma compounds between 2016 and 2017 vintages was also detected in Figure 5.9 using two-sample t-test. All the six sites had statistically significant difference between 2016 and 2017 in concentrations of Diethyl succinate and Citronellol with higher concentration in 2016. Levels of Isobutyl acetate, Ethyl hexanoate, and Linalool also showed the significant difference (five of six sites) with higher concentration in 2016.

The other vineyards not showing the significant difference still showed strong seasonal variation in Isobutyl acetate (site 3, p-value=0.061) and Linalool (site 2, p-value=0.098) concentrations (Figure 5.9). 2-Methyl-1-propanol, 3-Methyl-1-butanol, Ethyl 3-methylbutanoate, cis-3-Hexenol ((Z)-3-hexenol), Ethyl octanoate were other distinct aroma compounds with higher concentration in 2016 vintages while concentration of 1-Octen-3-ol indicated higher concentration in 2017 vintages (significantly different concentration level in four of six sites) (Figure 5.9). Concentration of cis-3-Hexenol [(Z)-3-hexenol] in site 1 (p-value=0.076) and site 4 (p-value=0.080) still showed strong seasonal variation with higher concentration in 2016 vintages (Figure 5.9). Concentration of γ-Decalactone also showed strong seasonal variation with higher concentration in 2016 vintages (significantly different concentration level in three of six sites) (Figure 5.9). The concentration level of Isoamyl acetate, Acetic acid, Hexyl acetate, Benzaldehyde, Ethyl decanoate, Octanoic acid, γ-Nonalactone, β-Ionone, and Decanoic acid indicated the least significant difference in concentration level between 2016 and 2017 wines throughout the six sites (Figure 5.9).

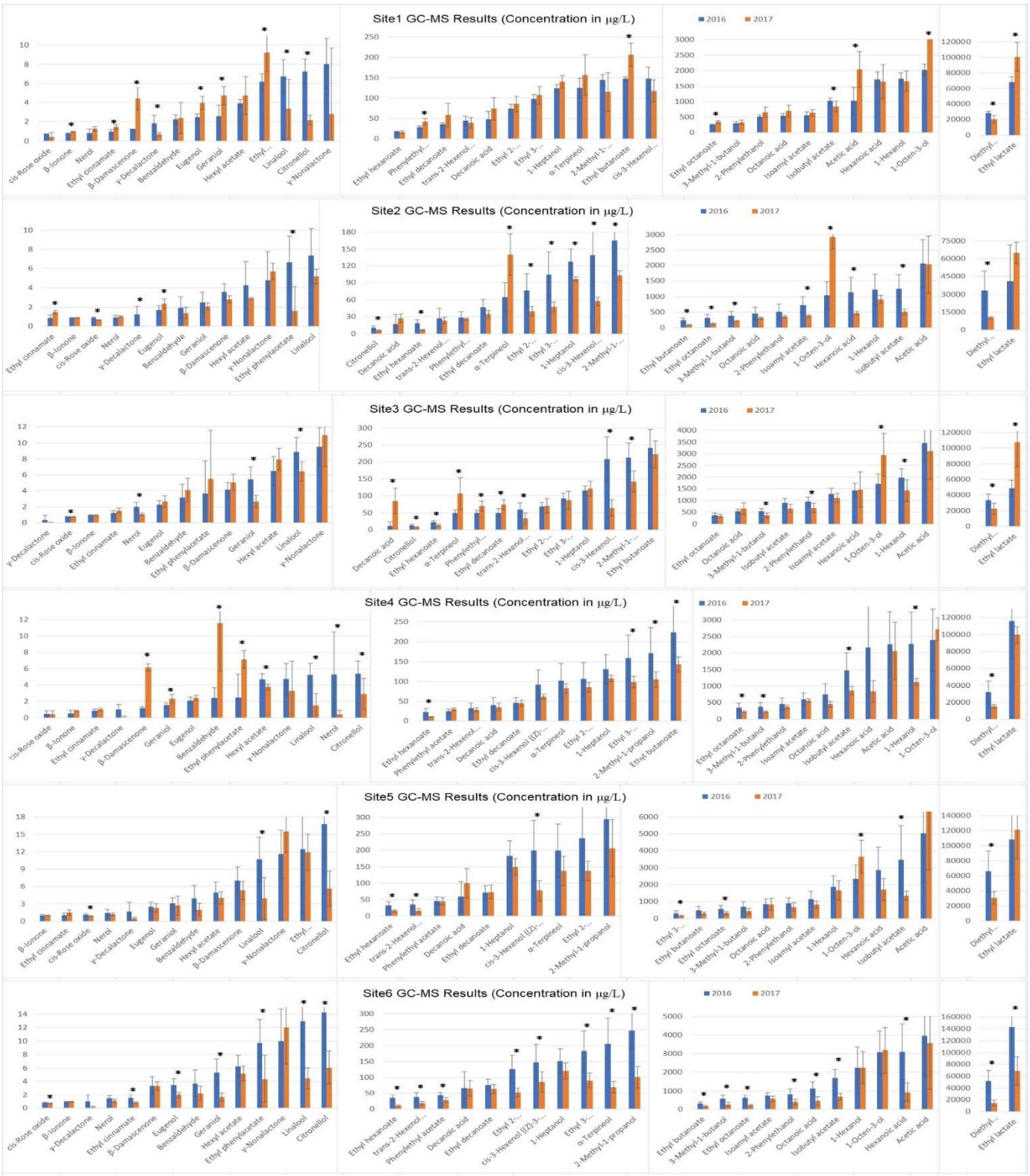

Figure 5.9. Comparison of mean concentrations (µg/L) of key odor active aroma compounds between 2016 and 2017 vintage Cabernet franc wines from the six Niagara vineyards using a t-test with two samples: * significant p-values (95% confidence).

Overall, various key odor active aroma compounds showed significantly different concentration level in high and low NDVI throughout the vineyard sites in 2017 include 1-Heptanol, cis-3-Hexenol ((Z)-3-hexenol), 1-Hexanol, Ethyl hexanoate, Diethyl succinate, 2-Phenylethanol, Eugenol, α-Terpineol, Geraniol, and Linalool. However, in 2016, almost all vineyard sites except for site 6 didn't show any significant difference in the level of aroma compounds between low and high NDVI zones. A seasonal variation of the key odor active aroma compounds between 2016 and 2017 vintages was also detected in different concentrations of Diethyl succinate, Citronellol, Isobutyl acetate, Ethyl hexanoate, and Linalool.

5.1.5 Sensory descriptive analysis (DA)

The sensory descriptive analysis for 2016 vintages was performed in spring of 2018, two years after the wine was bottled. According to each DA result, the first two factors in PCA accounted for between 60 and 72% of the data (Figure 5.10 and 5.11). In site 1, the analysis described 64% of the data and presented a similar grouping pattern to the sorting results in aroma descriptors, low 1 and low 3 were in the same group as descriptors of dry fruit, dark fruit, vegetal and spicy nose, and herbaceous flavor and high 1 and high 3 were closely grouped nearby descriptors of floral, earthy nose and vegetal flavor. However, wine colour and mouthfeel descriptors were not sorted by different NDVIs in the sorting test, though the low 1 and low 3 were still closely grouped near descriptor of colour intensity. In site 2 for aroma descriptors, as with the sorting outputs, the low 1 and low 2 were closely sorted nearby descriptive notes of dried fruit, spice, and vegetal nose. The colour and mouthfeel descriptors were also as with the sorting outputs.

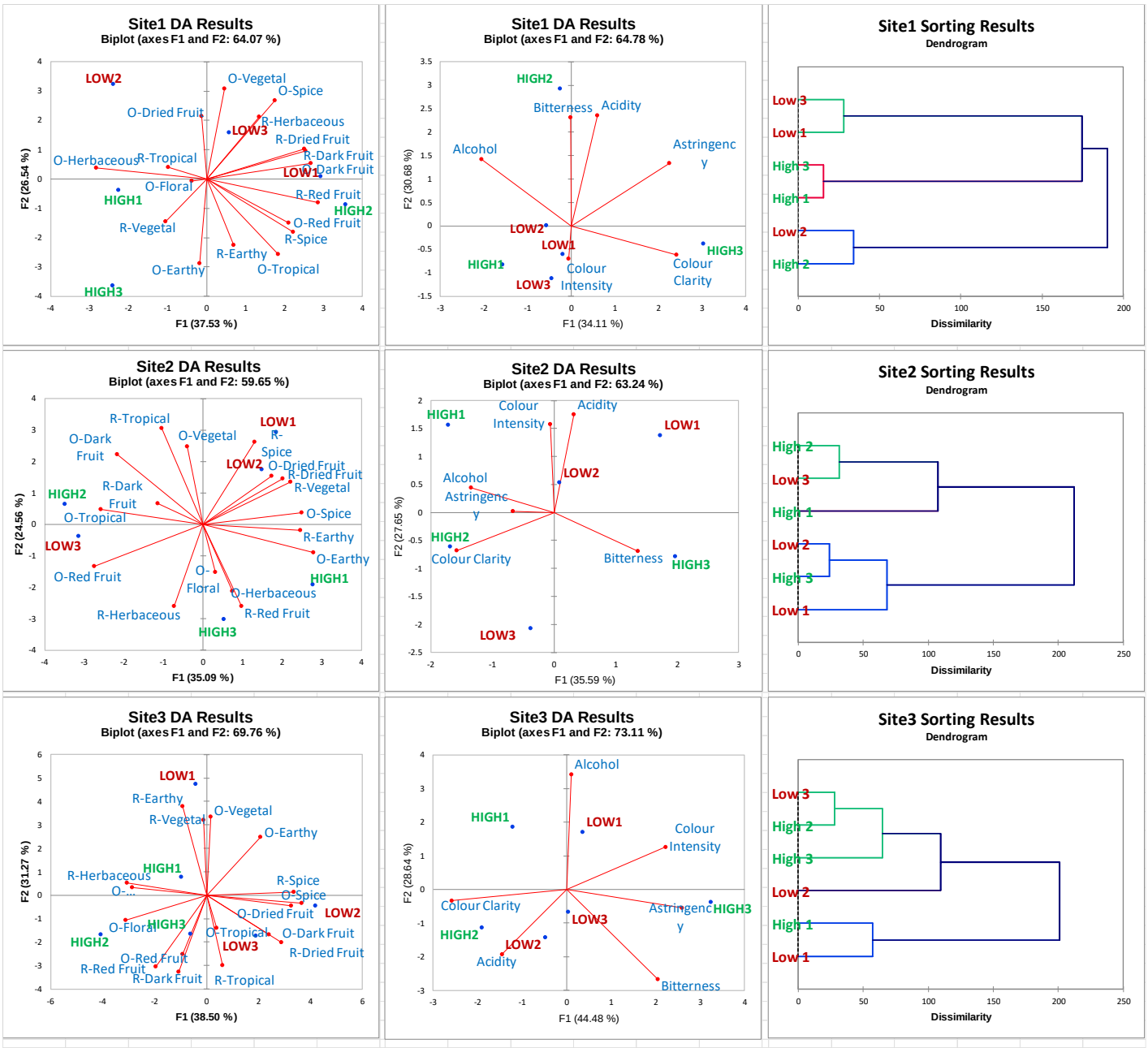

Figure 5.10. PCA results of sensory descriptive analysis (DA) for Cabernet Franc wines from site 1, 2, and 3 vineyards. Left: PCA results of orthonasal- and retronasal-sensory descriptors for low NDVI vs high NDVI, middle: PCA results of colour and mouthfeel sensory descriptors for low NDVI vs high NDVI, and right: Sensory sorting results in the agglomerative hierarchical clustering dendrogram.

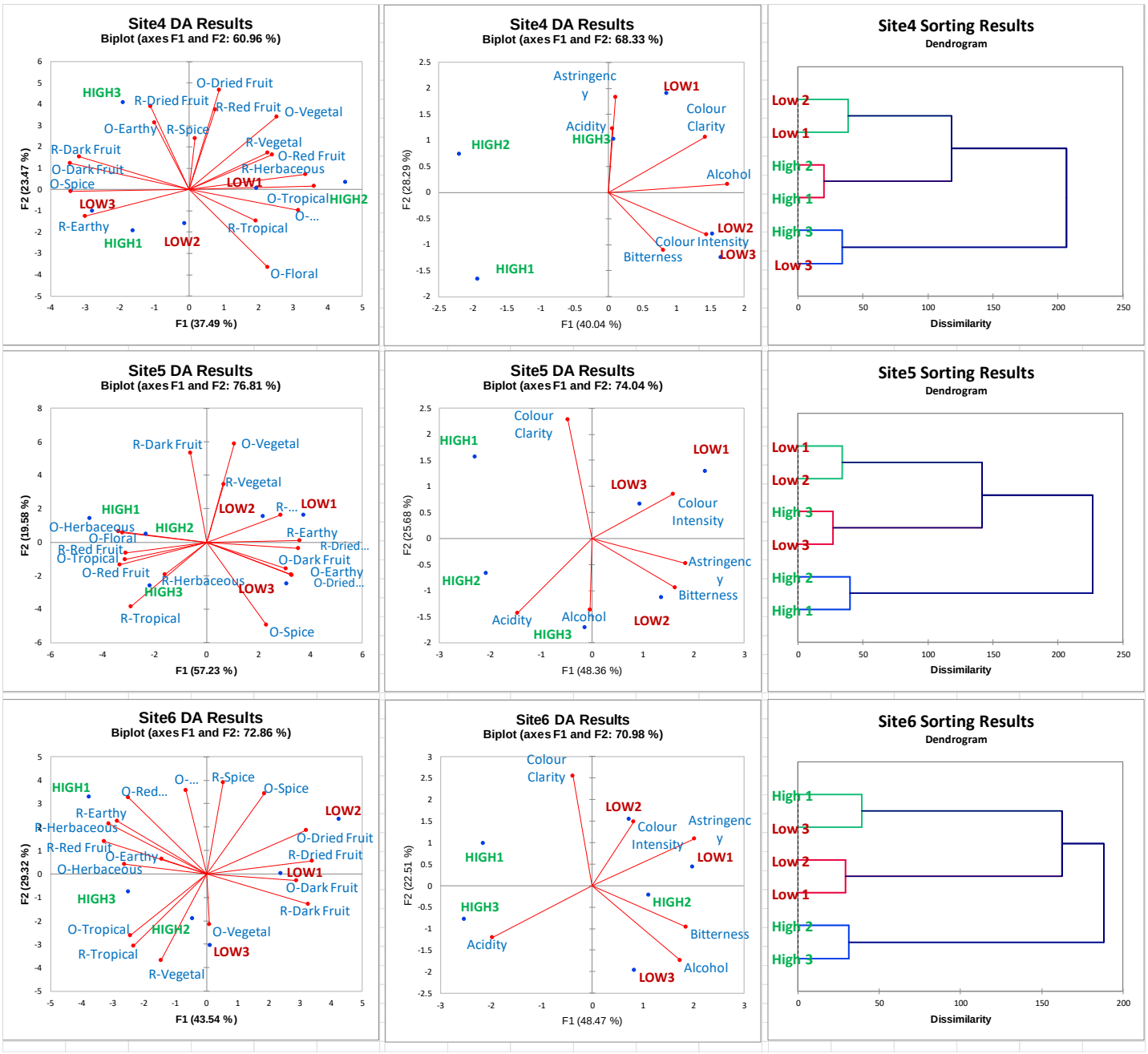

Figure 5.11. PCA results of sensory descriptive analysis (DA) for Cabernet Franc wines from site 4, 5, and 6 vineyards. Left: PCA results of orthonasal- and retronasal-sensory descriptors for low NDVI vs high NDVI, middle: PCA results of colour and mouthfeel sensory descriptors for low NDVI vs high NDVI, and right: Sensory sorting results in the agglomerative hierarchical clustering dendrogram.

In the site 3, PCA projection in aroma descriptors, as with the sorting outputs, high 2 and high 3 were closely sorted nearby descriptive notes of red fruit, dark fruit, and floral nose and the low1 and high1 also clustered together in the quadrant near earthy, herbaceous, and vegetal descriptors. The colour and mouthfeel descriptors were also as with the sorting outputs. The low 1 and high 2 were closely grouped nearby high alcohol descriptor and the low 2 and low 3 also cluster together with high acidity and high bitterness.

The PCA result differs from the sorting outputs for sensory descriptors in site 4. According to the sorting results, high1/high2 and low1/low2 were grouped together, however they appear a long way apart in the PCA map. Despite being close on a PCA map, low 2 and low 3 were far apart on the sorting matrix. In the colour and mouthfeel descriptors PCA map; low 2 and low 3 were closely grouped nearby descriptors of higher colour intensity and bitterness. Interestingly, the high1 and high 2 were clustered together separated from other treatment with less intensity for all the descriptors.

In site 5, the model most highly explained the data (75%) and demonstrated similar grouping pattern to the sorting outputs in aroma descriptors, low 1 and low 2 were closely sorted with descriptive notes of dry fruit, dark fruit, vegetal and spicy nose, and herbaceous flavor and high 1 and high 3 were closely grouped nearby the descriptors of vegetal, spicy, and earthy favor. However, wine colour and mouthfeel descriptors were not sorted by different NDVIs in the sorting test, though the high 1 and high2 were still clustered together in the edge of the quadrant away from other treatment with less intensity for all the descriptors. On the PCA map for site 5, treatments were categorized with high NDVIs nearby descriptive notes of floral, red fruit, tropical fruit, and herbaceous with high acidity, and low NDVIs nearby dried fruit, dark fruit, spicy, earthy, and vegetal with higher colour intensity, astringency, and bitterness.

In site 6, the model highly explained the data (72%) and demonstrated similar grouping pattern to the sorting outputs in sensory descriptors, low 1 and low 2 were closely sorted with descriptive notes of dry fruit, dark fruit, and spice and high 2 and high 3 were closely sorted nearby the descriptive notes of red fruit, tropical, herbaceous, and earthy. Wine colour and mouthfeel descriptors were also sorted by different NDVIs in the sorting test, though the high 1 and high 2 were clustered together in the edge of the quadrant away from other treatment with less intensity for all the descriptors except for the acidity and low1 and low 2 were grouped together with high colour intensity and astringency. On the PCA map for site 6, treatments were categorized with high NDVIs nearby descriptive notes of red fruit, tropical, herbaceous, and earthy with high acidity, and low NDVIs near of dry fruit, dark fruit, and spice with higher colour intensity and astringency.

Overall, wines with high NDVI were characterized as floral, red fruit, tropical fruit, herbaceous, and high acidity, and the majority of the low NDVI wines were characterized as vegetable, dry fruit, dark fruit, and spice with high colour intensity, bitterness, and astringency.

5.1.6 Partial least squares regression (PLSR) analyses

Since there was no significant correlation detected in the level of the key aroma compounds between low and high NDVI zones in 2016, the grouping results of sorting test in 2016 (Figure 5.5 and 5.6) were applied. It was indicated grouping of low 1,3 and high 1,3 in site 1; low 1,2 and high 1,2 in site 2; low 1,2 and high 1,2 in site 4; low 1,2 and high 1,2 in site 5; and low 1,2 and high 2,3 in site 6. The significant difference in concentration of various key odor aroma compounds in high and low NDVI were indicated in Figure 5.12.

Three of the five sites had statistically significant difference in concentrations of trans-2-Hexenol ((E)-2-hexenol), Linalool, Geraniol, and Eugenol in wines from low and high NDVI

zones. Levels of 3-Methyl-1-butanol, Ethyl hexanoate, Ethyl octanoate, α-Terpineol, and Diethyl succinate also showed the significant difference (two of five sites) in wines from low and high NDVI zones while concentration level of cis-3-Hexenol ((Z)-3-hexenol), Hexyl acetate, β-Damascenone, β-Ionone, Decanoic acid, and γ-Decalactone did not show any significant difference in wines from low and high NDVI zones throughout the six sites (Figure 5.12).

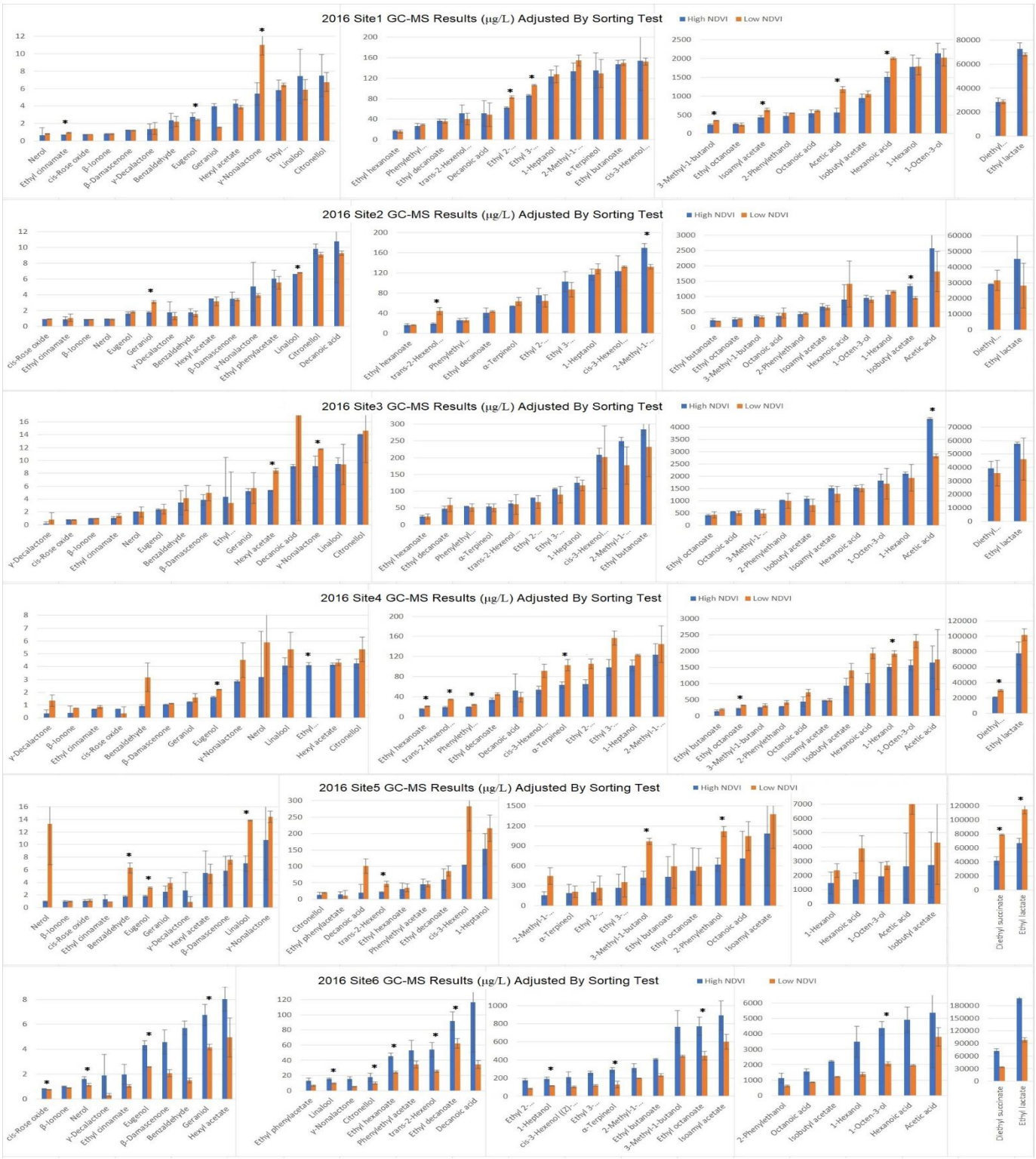

Figure 5.12. Significance of difference in the concentrations (µg/L) of key odor active aroma compounds from sorted NDVI replicates in the 2016 Cabernet franc wines using a t-test with two samples: * significant p-values (95% confidence).

Partial least squares regression (PLSR) analyses were performed to confirm the correlations among the NDVI treatments, the key odor active volatile compounds, and the aroma attributes from the sensory DA for each treatment and the results are in Figure 5.13.

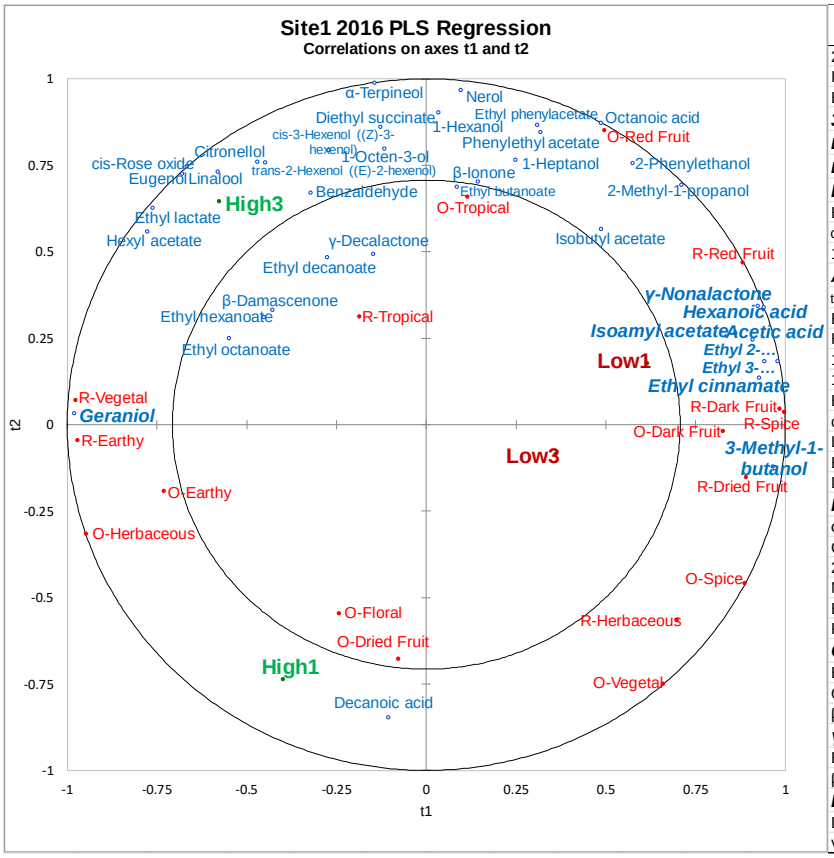

Variable	p-values
2-Methyl-1-propanol	0.267
Isobutyl acetate	0.341
Ethyl butanoate	0.709
3-Methyl-1-butanol	**0.023**
Ethyl 2-methylbutanoate	**0.010**
Ethyl 3-methylbutanoate	**0.008**
Isoamyl acetate	**0.049**
Ethyl lactate	0.348
cis-3-Hexenol ((Z)-3-hexenol)	0.959
1-Hexanol	0.970
Acetic acid	**0.023**
trans-2-Hexenol ((E)-2-hexenol)	0.522
Ethyl hexanoate	0.755
Hexyl acetate	0.351
1-Heptanol	0.806
1-Octen-3-ol	0.698
Benzaldehyde	0.880
cis-Rose oxide	0.423
Linalool	0.573
Ethyl octanoate	0.645
Diethyl succinate	0.923
Hexanoic acid	**0.033**
α-Terpineol	0.856
Citronellol	0.726
2-Phenylethanol	0.307
Nerol	0.771
Ethyl phenylacetate	0.540
Phenylethyl acetate	0.526
Geraniol	**0.008**
Ethyl decanoate	0.940
Octanoic acid	0.435
β-Damascenone	0.781
γ-Nonalactone	**0.044**
Eugenol	0.382
β-Ionone	0.935
Ethyl cinnamate	**0.014**
Decanoic acid	0.924
γ-Decalactone	0.927

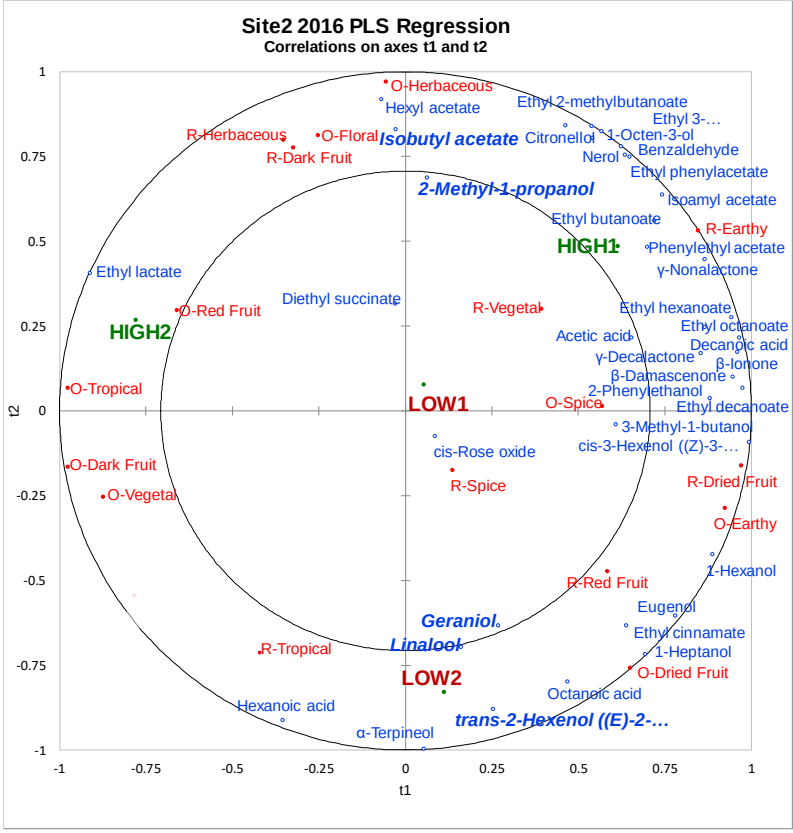

Variable	p-values
2-Methyl-1-propanol	**0.032**
Isobutyl acetate	**0.016**
Ethyl butanoate	0.437
3-Methyl-1-butanol	0.626
Ethyl 2-methylbutanoate	0.495
Ethyl 3-methylbutanoate	0.465
Isoamyl acetate	0.775
Ethyl lactate	0.584
cis-3-Hexenol ((Z)-3-hexenol)	0.726
1-Hexanol	0.423
Acetic acid	0.484
trans-2-Hexenol ((E)-2-hexeno	**0.039**
Ethyl hexanoate	0.934
Hexyl acetate	0.544
1-Heptanol	0.390
1-Octen-3-ol	0.639
Benzaldehyde	0.645
cis-Rose oxide	0.296
Linalool	**0.003**
Ethyl octanoate	0.765
Diethyl succinate	0.638
Hexanoic acid	0.503
α-Terpineol	0.217
Citronellol	0.266
2-Phenylethanol	0.582
Nerol	0.558
Ethyl phenylacetate	0.628
Phenylethyl acetate	0.913
Geraniol	**0.017**
Ethyl decanoate	0.753
Octanoic acid	0.561
β-Damascenone	0.887
γ-Nonalactone	0.662
Eugenol	0.317
β-Ionone	0.831
Ethyl cinnamate	0.697
Decanoic acid	0.902
γ-Decalactone	0.700

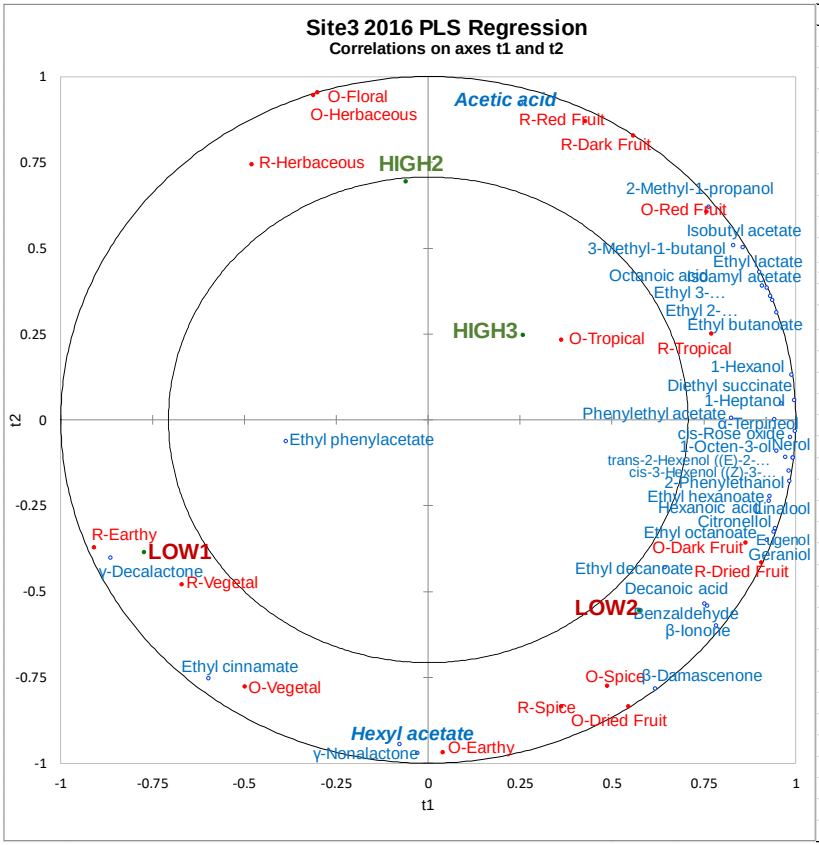

Variable	p-values
2-Methyl-1-propanol	0.217
Isobutyl acetate	0.295
Ethyl butanoate	0.503
3-Methyl-1-butanol	0.329
Ethyl 2-methylbutanoat	0.492
Ethyl 3-methylbutanoat	0.450
Isoamyl acetate	0.414
Ethyl lactate	0.416
cis-3-Hexenol ((Z)-3-hexen	0.922
1-Hexanol	0.697
Acetic acid	**0.002**
trans-2-Hexenol ((E)-2-hexen	0.905
Ethyl hexanoate	0.913
Hexyl acetate	**0.008**
1-Heptanol	0.677
1-Octen-3-ol	0.808
Benzaldehyde	0.741
cis-Rose oxide	0.831
Linalool	0.969
Ethyl octanoate	0.862
Diethyl succinate	0.690
Hexanoic acid	0.944
α-Terpineol	0.721
Citronellol	0.881
2-Phenylethanol	0.965
Nerol	0.981
Ethyl phenylacetate	0.882
Phenylethyl acetate	0.766
Geraniol	0.808
Ethyl decanoate	0.550
Octanoic acid	0.472
β-Damascenone	0.406
γ-Nonalactone	0.146
Eugenol	0.852
β-Ionone	0.635
Ethyl cinnamate	0.252
Decanoic acid	0.540
γ-Decalactone	0.535

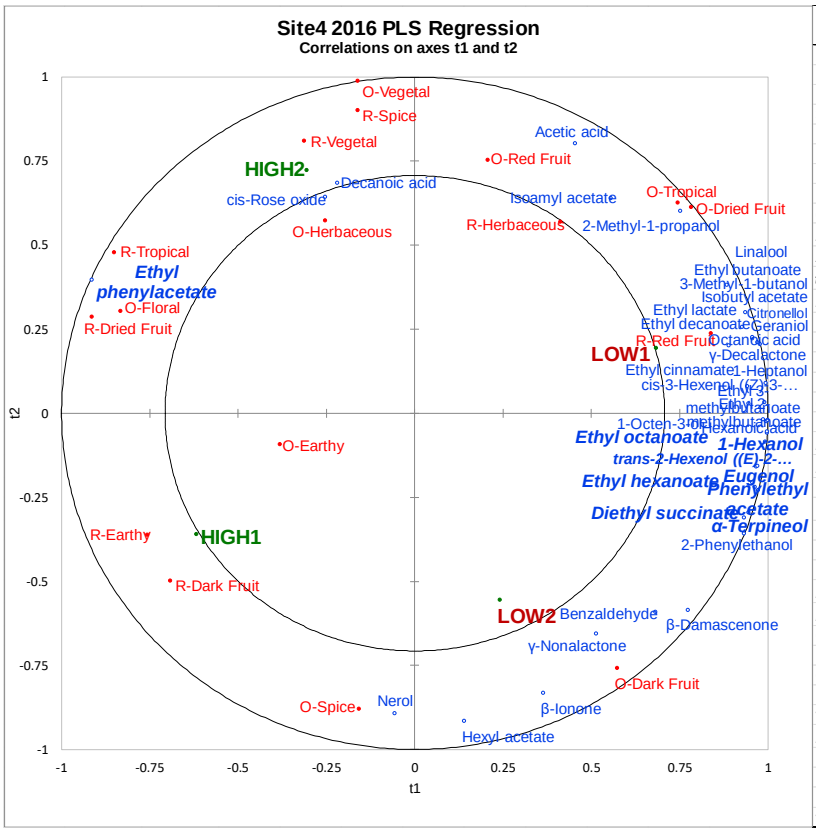

Variable	p-values
2-Methyl-1-propanol	0.557
Isobutyl acetate	0.166
Ethyl butanoate	0.222
3-Methyl-1-butanol	0.219
Ethyl 2-methylbutanoate	0.051
Ethyl 3-methylbutanoate	0.060
Isoamyl acetate	0.784
Ethyl lactate	0.176
cis-3-Hexenol ((Z)-3-hexenol)	0.073
1-Hexanol	**0.041**
Acetic acid	0.918
trans-2-Hexenol ((E)-2-hexenol)	**0.011**
Ethyl hexanoate	**0.017**
Hexyl acetate	0.492
1-Heptanol	0.118
1-Octen-3-ol	0.054
Benzaldehyde	0.103
cis-Rose oxide	0.444
Linalool	0.354
Ethyl octanoate	**0.025**
Diethyl succinate	**0.015**
Hexanoic acid	0.062
α-Terpineol	**0.047**
Citronellol	0.271
2-Phenylethanol	0.070
Nerol	0.674
Ethyl phenylacetate	**0.001**
Phenylethyl acetate	**0.011**
Geraniol	0.301
Ethyl decanoate	0.080
Octanoic acid	0.165
β-Damascenone	0.102
γ-Nonalactone	0.220
Eugenol	**0.003**
β-Ionone	0.413
Ethyl cinnamate	0.176
Decanoic acid	0.633
γ-Decalactone	0.123

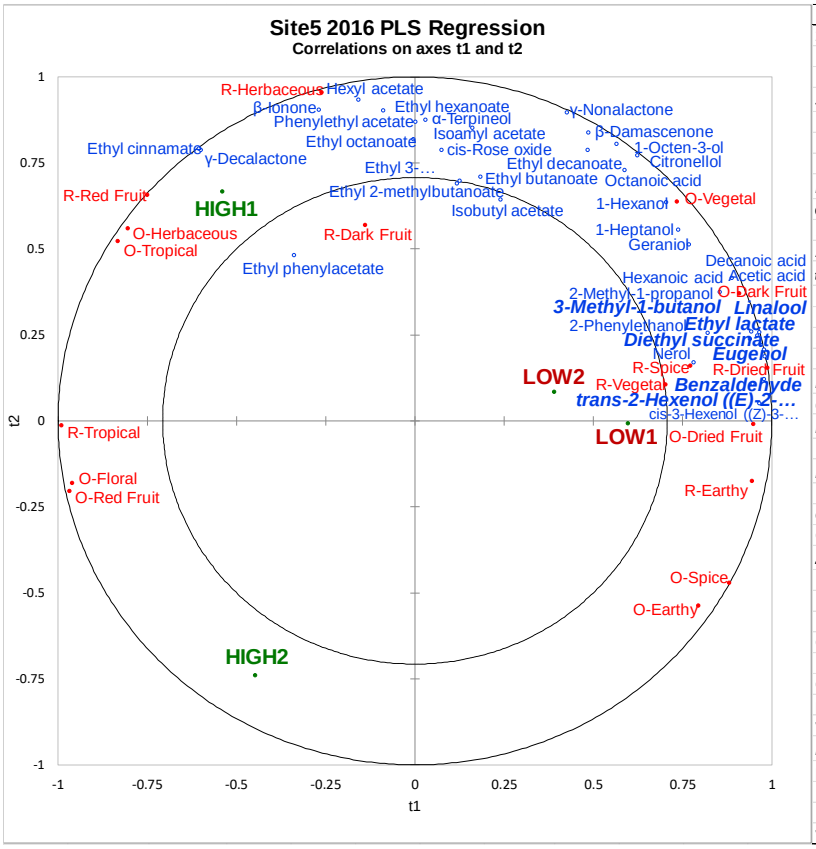

Variable	p-values
2-Methyl-1-propanol	0.097
Isobutyl acetate	0.611
Ethyl butanoate	0.669
3-Methyl-1-butanol	**0.020**
Ethyl 2-methylbutanoate	0.729
Ethyl 3-methylbutanoate	0.724
Isoamyl acetate	0.705
Ethyl lactate	**0.017**
cis-3-Hexenol ((Z)-3-hexenol)	0.078
1-Hexanol	0.303
Acetic acid	0.119
trans-2-Hexenol ((E)-2-hexeno	**0.049**
Ethyl hexanoate	0.836
Hexyl acetate	0.961
1-Heptanol	0.284
1-Octen-3-ol	0.406
Benzaldehyde	**0.015**
cis-Rose oxide	0.780
Linalool	**0.015**
Ethyl octanoate	0.860
Diethyl succinate	**0.011**
Hexanoic acid	0.091
α-Terpineol	0.863
Citronellol	0.344
2-Phenylethanol	**0.030**
Nerol	0.131
Ethyl phenylacetate	0.817
Phenylethyl acetate	0.959
Geraniol	0.258
Ethyl decanoate	0.408
Octanoic acid	0.414
β-Damascenone	0.421
γ-Nonalactone	0.494
Eugenol	**0.010**
β-Ionone	0.850
Ethyl cinnamate	0.447
Decanoic acid	0.077
γ-Decalactone	0.477

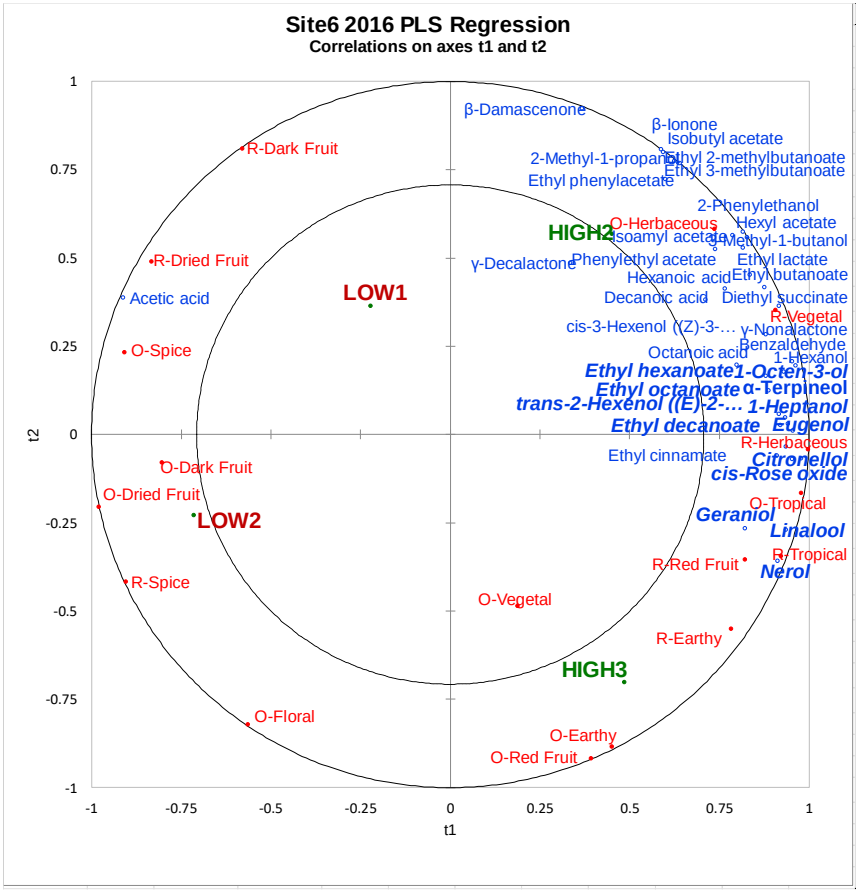

Variable	p-values
2-Methyl-1-propanol	0.541
Isobutyl acetate	0.528
Ethyl butanoate	0.157
3-Methyl-1-butanol	0.232
Ethyl 2-methylbutanoate	0.582
Ethyl 3-methylbutanoate	0.505
Isoamyl acetate	0.420
Ethyl lactate	0.177
cis-3-Hexenol ((Z)-3-hexenol)	0.090
1-Hexanol	0.054
Acetic acid	0.138
trans-2-Hexenol ((E)-2-hexenc	**0.007**
Ethyl hexanoate	**0.049**
Hexyl acetate	0.315
1-Heptanol	**0.013**
1-Octen-3-ol	**0.042**
Benzaldehyde	0.064
cis-Rose oxide	**0.012**
Linalool	**0.014**
Ethyl octanoate	**0.017**
Diethyl succinate	0.138
Hexanoic acid	0.179
α-Terpineol	**0.021**
Citronellol	**0.003**
2-Phenylethanol	0.336
Nerol	**0.034**
Ethyl phenylacetate	0.645
Phenylethyl acetate	0.515
Geraniol	**0.031**
Ethyl decanoate	**0.015**
Octanoic acid	0.094
β-Damascenone	0.813
γ-Nonalactone	0.064
Eugenol	**0.011**
β-Ionone	0.553
Ethyl cinnamate	0.231
Decanoic acid	0.193
γ-Decalactone	0.987

Figure 5.13. PLSR analysis results of Cabernet Franc wines from low and high NDVI zone at the six vineyard sites in 2016 based on sensory attributes from DA and key odor active aroma compounds concentration from GC-MS. The p-values represent a significant difference in value of variables for low and high NDVI ($P \leq 0.05$ in bold).

In site 1, PLSR analysis showed better clustering in the low NDVI wines grouped together with descriptors of dry fruit, dark fruit, red fruit and spicy flavor, and dark fruit nose. The low NDVI also associated with the aromatic compounds of 3-Methyl-1-butanol, Ethyl 2-methylbutanoate, Ethyl 3-methylbutanoate, Isoamyl acetate, Acetic acid, Hexanoic acid, γ-Nonalactone, and Ethyl cinnamate. While the high NDVI wines with more dispersed pattern

grouped together with descriptors of earthy and herbaceous nose, and vegetal and earthy flavor, which were correlated with higher levels of Geraniol (Figure 5.13).

In site 2, PLSR analysis showed a dispersed pattern of clustering in the high NDVI wines grouped together with descriptors of herbaceous and floral nose, and dark fruit, vegetal, and herbaceous flavor which were correlated with higher levels of 2-methyl-1-propanol and isobutyl acetate. The low NDVI wines also showed a dispersed pattern grouped together with descriptors of dried fruit nose, and red fruit, spice, and tropical flavor. The low NDVI also associated with the aromatic compounds of trans-2-Hexenol ((E)-2-hexenol), Linalool, and Geraniol (Figure 5.13).

In site 3, PLSR analysis showed a dispersed pattern of clustering in the high NDVI wines grouped together with descriptors of floral and herbaceous nose, and red fruit, dark fruit, and herbaceous flavor. The high NDVI was also associated with high concentration of Acetic acid. The low NDVI wines also showed a dispersed pattern grouped together with descriptors of vegetal, earthy, spice and dried fruit nose, and vegetal, earthy, and spice flavor which were correlated with higher levels of Hexyl acetate (Figure 5.13).

In site 4, PLSR analysis showed some clustering in the low NDVI wines grouped together with descriptors of dark fruit, tropical and dried fruit nose, and red fruit flavor. The low NDVI also associated with the key aroma compounds include 1-Hexanol, trans-2-Hexenol ((E)-2-hexenol), Ethyl hexanoate, Ethyl octanoate, Diethyl succinate, α-terpineol, Phenylethyl acetate and Eugenol. While the high NDVI wines with more dispersed pattern grouped together with descriptors of earthy, floral, vegetal, and herbaceous nose, and vegetal, spice, earthy, dark fruit, dried fruit, and tropical flavor, which were correlated with higher levels of ethyl phenylacetate (Figure 5.13).

In site 5, PLSR analysis showed better clustering in the low NDVI wines closely grouped with descriptors of vegetal, dark fruit, and dried fruit nose and vegetal, earthy, dark fruit, and dried

fruit flavor which were correlated with higher levels of 3-Methyl-1-butanol, Ethyl lactate, trans-2-Hexenol ((E)-2-hexenol), Benzaldehyde, Linalool, Diethyl succinate, 2-Phenylethanol and Eugenol. While the low NDVI wines with more dispersed pattern grouped together with descriptors of red fruit, floral, tropical, and herbaceous nose and red fruit, tropical, and herbaceous flavor with no case of significantly different concentration level of odor active volatile compounds (Figure 5.13).

In site 6, PLSR analysis showed more dispersed clustering in the high NDVI wines grouped together with descriptors of herbaceous and tropical nose and red fruit, tropical, earthy, herbaceous, and vegetal flavor. The high NDVI associated with almost all key order active volatile compounds (except for Acetic acid) with significantly different concentration level of trans-2-Hexenol ((E)-2-hexenol), Ethyl hexanoate, 1-Heptanol, 1-Octen-3-ol, Ethyl octanoate, α-Terpineol, Cis-rose oxide, Linalool, Nerol, Geraniol, Citronellol, Eugenol and Ethyl decanoate. The low NDVI wines showed some clustering with descriptors of spice, dark fruit, and dried fruit nose and spice, dark fruit, and dried fruit flavor with no case of significantly different concentration level of odor active volatile compound (Figure 5.13).

In general, PLSR indicated better clustering of each treatment than PCA results with similar patterns of correlation between NDVI and sensory descriptors as the PCA. Groups of wine replicates with low NDVI were frequently described as vegetal, dry fruit, dark fruit, and spice with higher concentrations of 3-Methyl-1-butanol, trans-2-Hexenol ((E)-2-hexenol), Linalool, Diethyl succinate, and Eugenol. High NDVI wine groups were characterized as floral, red fruit, tropical fruit, and herbaceous with higher concentrations of Geraniol.

5.2 Discussion

The vineyard variables such as water status, soil structure, and canopy size affect the chemistry and sensory characteristics of fruit and wine. Vegetative growth varies over time, and plant stress is determined by the physiological status of vegetation[1], nutrient deficiency, and plant disease[2]. Wines from different vineyard zones by water status were distinguishable for its aroma, taste, and mouthfeel profiles.[3-7] There was also a noticeable difference between wines from different vigour areas with respect to anthocyanin and colour contents.[8-10] Previous research indicated that remote sensing NDVI have been positively correlated with vine water status, leaf area, vine vigour, and yield while negatively correlated with fruity quality (low brix and aroma compounds, high TA).[3-5,7,10,11]

One hypothesis of this study was that variation in NDVI data from remote sensing would correspond to the spatial variation in viticulturally important vineyard variables, yield, and berry composition. Additionally, NDVI zonal maps could allow several distinctive wine products in a single vineyard block. To confirm the hypothesis, both chemical and sensory analysis of wines from two separate NDVI zones (low NDVI vs high NDVI) were performed.

Primarily, chemical analysis completed on the grape musts and wines found that basic chemical compositions did not vary between treatments, other than anthocyanins, which varied in multiple sites in both years. The anthocyanin content of treatment wines differed in all six sites in 2016 and in four sites in 2017. Remote sensing NDVI was negatively correlated to anthocyanins in three sites throughout the years.

Research from previous years has indicated that fruits grown in a variety of vigour zones vary in their anthocyanin and colour compounds[8], a descriptive analysis found that low vigour

zones had higher sensory profiles than higher vigour zones[9], and differences in the composition of berries such as Brix, pH, and TA were not associated with NDVI zones[12].

While variations in wine chemistry can influence winemaking and sensory attributes, they appear to be linked more to volatile aroma compounds than to differences in typical wine chemistry.[4,7] The sensory sorting results indicated better differentiation of wines from different NDVI levels than that of wine chemical analysis results and In 2017, sorting of NDVI-treated wines was more effective than in 2016. In 2017, panelists were able to sort out all three replicates together by low and high NDVI in four of six sites and two replicates together by the treatments in one site; however, in 2016, this was not the case in 2016 (Figure 5.5 and 5.6) since no complete sorting of the three replicates was seen.

Wine aromatic compounds analysis by GC-MS was also consistent with the wine sorting test results. Various key odor active aroma compounds showed significantly different concentration level in high and low NDVI throughout the vineyard sites in 2017 while most vineyard sites didn't show any significant difference in the level of aroma compounds between low and high NDVI zones in 2016 (Figure 5.7 and 5.8). A vintage variation of key odor active aroma compounds between 2016 and 2017 vintages was also detected from all the six vineyard sites (Figure 5.9).

The primary candidates of key order compounds causing the vintage variation were Diethyl succinate, Citronellol, Isobutyl acetate, Ethyl hexanoate, and Linalool with higher concentration in 2016 while level of 1-Octen-3-ol indicated higher concentration in 2017 vintages. Wine aromas have shown to be highly versatile, as evidenced by the seasonal variation of key odor active compounds.[13] Previous research suggests that glycoconjugates of aroma compounds in wines differ seasonally, especially for volatile compounds.[4]

Variations in climate are more likely to be responsible for inconsistent results in sorting and aroma compounds analysis between different wine vintages. It was hot and wet in 2016 and relatively mild in 2017 during the growing season. Previous studies indicated that different years differ in climatic conditions, sun exposure and water status, resulting in different aroma compounds accumulation[14,15] and under stress conditions, differences in wine chemistry and sensory attributes were more evident in wines made from areas of differing water stress levels[3,4]. However, in this study, due to the consistently low rainfall and high temperatures seen in 2016, variation in wine quality may have been affected less by water stress since vineyards were more evenly stressed. A change in normal stomatal behaviour caused by stress responses is possible and one can generate a new water uptake efficiency without greatly reducing biomass yield[16] and this could explain that the higher grapevine water level could be a constraint for the variation in vegetative and reproductive growth. Interestingly, the previous chapter of the correlation between vine vigour (NDVI) and leaf water potential (leaf ψ) indicated the same result that a year with hot and dry growing season showed more variations and correlations than a regular growing season. From the results, this study assumed that the higher grapevine water level could be a limiting factor for variations in vegetative growth, grape and wine quality.

Another possible explanation of the vintage differences was that 2016 and 2017 vintages were aged in bottles differently as the analysis was completed during the same week in both vintages. Young wines exhibit vintage characteristics that are altered by bottle aging as they develop their particular flavors.[17] During bottle aging, fermentation and fresh fruity notes in wine also disappear, resulting in an aging flavor.[18-20] Thus, the loss in fresh fruity aroma and development of homogeneous complex aroma compounds during wine bottle aging could strongly impact distinguishability between the different vintage wines.

Sensory descriptive analysis has been conducted for 2016 vintage wines to better understand the variations in odour and flavour intensity between NDVI zonal wines. Based on the analysis, a similar sorting pattern emerged compared to the sorting result with low NDVI wines describing as vegetable, dry fruit, dark fruit, and spice with higher intensity, bitterness, and astringency, and high NDVI wines describing as floral, tropical fruit, and herbaceous with high acidity (Figure 5.10 and 5.11). According to a previous study, red wines from higher vegetative growth areas had higher intensities of green/vegetable flavors, while those from lower vegetative growth areas had stronger fruit flavors.[21] Interestingly, the trend of low NDVI wines having higher colour intensity, bitterness and astringency descriptors was consistent with a tendency of negative correlation between anthocyanins level and NDVI in the previous chapter. The berry composition variables, especially phenolic accumulation (e.g., anthocyanins), are negatively influenced by vigorous canopies via fruit exposure to sunlight to the flavonoid biosynthesis.[22-24]

Aroma developed in wine is a combination of many volatile compounds and rarely comes from one substance alone.[25] The volatile compounds can be detected at concentrations between a few hundred g/L to smaller concentrations in ng/L.[25] It would be beneficial to compare the prime aroma compounds of Cabernet franc wines from different NDVI zones for a better understanding of the chemistry behind descriptors of wines. The Cabernet franc wine aromatic compound analysis by GC-MS indicated that various key odor active aroma compounds showed significantly different concentration level in high and low NDVI throughout the vineyard sites in 2017 include 1-Heptanol, cis-3-Hexenol ((Z)-3-hexenol), 1-Hexanol, Ethyl hexanoate, Diethyl succinate, 2-Phenylethanol, Eugenol, α-Terpineol and Geraniol (Figure 5.8).

A group of fusel alcohols (1-Heptanol) and ethyl esters (Ethyl hexanoate) are commonly recognized as by-products of yeast alcoholic fermentation and Malo-lactic fermentation. Most of

the ethyl esters and minor alcohols formed during fermentation are produced by *Saccharomyces cerevisiae* and its related enzyme.[25,26] Fatty acid esters include Diethyl succinate are also a by-product of Malo-lactic fermentation. Previous researches reported that the concentration of ethyl esters like diethyl succinate increased because of MLF.[27,28] During MLF, esters are synthesized and hydrolyzed through the metabolism of lactic acid bacteria. A result of the metabolism of microbial α-ketoglutarate, diethyl succinate is formed by esterifying succinic acid.[27] Those minor alcohol and esters are byproducts of fermentation process, thus the impacts of grapevine vegetative status on these aromatic compounds could be limited. However, grape berry aroma compounds or compounds produced by precursors such as C6 alcohol, aromatic alcohols, terpenes, and aromatic phenols could be important odor compounds distinct from different NDVI levels.

In this study, four of the six sites in 2017 had statistically significant differences in concentration of cis-3-Hexenol ((Z)-3-hexenol) and 1-Hexanol in wines from low and high NDVI zones with three sites (site 1, 2, and 3) showing negatively correlated to NDVI and site 6 indicating positive correlation (Figure 5.8). The C6 alcohols include cis-3-Hexenol ((Z)-3-hexenol) and 1-Hexanol have been described as key aroma compounds in Bordeaux red wines and has a herbaceous aroma and may enhance green notes in wine.[29] It has been observed that level of cis-3-Hexenol ((Z)-3-hexenol) significantly decreased during berry ripening while it seems to be stable under fermentation conditions.[29-32] Furthermore, it could be assumed that one potential source of cis-3-Hexenol ((Z)-3-hexenol) and 1-Hexanol was the polyunsaturated fatty acids in grape metabolized via a series of enzymatic complexes, which are commonly observed in plants grown under cool climate region due to a close relationship between concentration of unsaturated fatty acids and plant cold tolerance.[32-35] Thus, especially cool climate grape growing area like

the Niagara region, cis-3-Hexenol ((Z)-3-hexenol) and 1-Hexanol could be a critical odor active aroma compound for indicating significant differences in wine quality from different NDVI levels.

The other compounds distinct from NDVI level were aromatic alcohols (2-Phenylethanol) and terpenes (Terpineol and Geraniol). These compounds in lower amounts can be found in Bordeaux red grape varieties as well as aromatic grapes.[36] It had been widely reported that the sensory thresholds of these terpene compounds are generally at µg/L levels with contributing to the fruity and berry flavours of a red wine.[37] In this study, in 2017, concentration of 2-Phenylethanol showed a significant difference (four of six sites) in wines from low and high NDVI with three sites (site 1, 2, and 5) showing negatively correlated to NDVI and site 6 indicating positive correlation (Figure 5.8). Level of terpenes (α-Terpineol and Geraniol) also indicate a significant difference (three of six sites) in wines with all three sites showing negatively correlated to NDVI (Figure 5.8).

Finally, volatile phenols such as Eugenol (2-Methoxy-4-(2-propenyl) phenol) were found to be altered between NDVI treatments and may contribute attractive flavours to a wine's bouquet depending on grape variety. In addition to being extracted from burned wood and grape glycosides, eugenol is also a product of the shikimic acid process in plants.[25,38] Since no oak was used in this research, the difference in Eugenol concentration was only acid degradation, enzyme degradation, or bacteria metabolizing hydroxycinnamic acids during fermentation.[39]

The concentration of Eugenol in wines from low and high NDVI zones differed significantly in four of the six sites in 2017 with all four sites showing negative correlation to NDVI (Figure 5.8). In 2016, most vineyard sites except for site 6 didn’t show any significant difference in the level of aroma compounds between low and high NDVI zones (Figure 5.7). The sorting test results indicated that NDVI zonation still influenced wine quality in 2016, even though

variations in levels of odour active compounds were not easily detected by NDVI in most cases, and there could have been possible spatial links between these variables and other remote sensing indices. In 2016 vintages, variation in the key odor aroma compounds between high and low NDVI wines would have provided more distinct treatment difference and a significantly different concentration level of various key odor active aroma compounds in high and low NDVI were indicated in all five sites if some of the field replicates were removed by sorting test results (Figure 5.12). Concentrations of trans-2-Hexenol ((E)-2-hexenol), Linalool, Geraniol, and Eugenol in wines from low and high NDVI zones showed the most significant difference (Figure 5.12).

Partial least squares regression (PLSR) was performed to determine the links among the NDVI treatments, wine odour active compounds, and the sensory profiles from DA for each treatment in 2016 vintages and indicated better clustering of each treatment than PCA results with similar patterns of correlation between NDVI and sensory descriptors as the PCA. Low NDVI wines tend to be characterized as vegetal, dry fruit, dark fruit, and spice associated with higher concentrations of 3-Methyl-1-butanol (Isoamyl alcohol), trans-2-Hexenol ((E)-2-hexenol), Linalool, Diethyl succinate, and Eugenol. High NDVI wines tend to be identified as floral, red fruit, tropical fruit, and herbaceous associated with higher concentrations of Geraniol (Figure 5.13). As the esters breakdown, 3-Methyl-1-butanol (Isoamyl alcohol) is produced and released by *Saccharomyces cerevisiae* and its related enzyme.[25,26] The diethyl succinate also increased as a results of Malo-lactic fermentation (MLF).[27,28] They are by-products of fermentation process, thus the impacts of grapevine vegetative status on these aromatic compounds could be limited.

Furthermore, the aromatic compounds which are released directly from fruits or from their precursors such as C6 alcohols, terpenes, and aromatic phenols could be important odor

compounds distinct from different NDVI levels. Trans-2-Hexenol ((E)-2-hexenol) is an isomer of cis-3-Hexenol ((Z)-3-hexenol) and these isomers are resulted from the lipoxygenase (LOX) pathway and short-chain alcohols resulted from the LOX pathway are in the Z conformation. However, they can be isomerized to the E form by spontaneous isomerization depending on the conditions of their environment (pH, temperature) or by a isomerization enzyme.[40] Trans-2-Hexenol ((E)-2-hexenol) could be the other critical odor active aroma compound for indicating significant difference in wine quality from different NDVI levels since it may derive from grape polyunsaturated fatty acids through a cool climate specific cascade of enzymatic reactions (LOX).

Other important odor compounds distinct from different NDVI level in 2016 wines were terpenes and eugenol. The results in significantly high concentration level of C6 alcohol, terpenes, and eugenol from Low NDVI wines were consistent with the results from the key odor compounds analysis of different NDVI wines in 2017 (Figure 5.8).

5.3 Conclusions

Even though chemical analysis completed on the grape musts and wines found that basic chemical compositions did not vary between treatments, the results of sensory analysis were clearly discerned the differences between the zonal wines, as a series of sites were sorted separately in both years according to the different NDVI levels. The NDVI zone-specific wines have different chemical and sensory characteristics. Zonal differences were not significant based on juice chemistry but did show differences based on aromatic wine composition. Additionally, the results indicate significant year-to-year variations in outcomes of the sorting test and aromatic compounds analysis due to the considerable climate alterations between the vintages and variations in wine aging. This study also suggested that in cool climate grape growing area like the Niagara region,

cis-3-Hexenol ((Z)-3-hexenol) and 1-Hexanol could be critical odor active aroma compounds for indicating significant differences in wine quality from different NDVI levels.

Overall, this study indicated some important findings to develop future research for use of remote sensing data to detect oenologically relevant vineyard zones for selective harvest, but it is necessary to develop more robust vegetative indices that can be used for selective harvest and zonal winemaking in single vineyard blocks.

5.4 References

1. Jackson, R.D. Remote sensing of biotic and abiotic plant stress. *Annual review of Phytopathology* **1986**, *24*, 265-287.

2. Larcher, W. *Physiological plant ecology: ecophysiology and stress physiology of functional groups*; Springer Science & Business Media: **2003**.

3. Ledderhof, D.; Reynolds, A.G.; Manin, L.; Brown, R. Influence of water status on sensory profiles of Ontario Pinot noir wines. *LWT-Food Science and Technology* **2014**, *57*, 65-82.

4. Koundouras, S.; Marinos, V.; Gkoulioti, A.; Kotseridis, Y.; van Leeuwen, C. Influence of vineyard location and vine water status on fruit maturation of nonirrigated cv. Agiorgitiko (Vitis vinifera L.). Effects on wine phenolic and aroma components. *Journal of Agricultural and Food Chemistry* **2006**, *54*, 5077-5086.

5. Willwerth, J.; Reynolds, A.; Lesschaeve, I. Sensory analysis of Ontario Riesling wines from various water status zones. *OENO One* **2018**, *52*, 145-171.

6. Marciniak, M.; Reynolds, A.G.; Brown, R. Influence of water status on sensory profiles of Ontario Riesling wines. *Food research international* **2013**, *54*, 881-891.

7. CHAPMAN, D.M.; ROBY, G.; EBELER, S.E.; GUINARD, J.X.; MATTHEWS, M.A. Sensory attributes of Cabernet Sauvignon wines made from vines with different water status. *Australian Journal of Grape and Wine Research* **2005**, *11*, 339-347.

8. Cortell, J.M.; Halbleib, M.; Gallagher, A.V.; Righetti, T.L.; Kennedy, J.A. Influence of vine vigor on grape (Vitis vinifera L. cv. Pinot noir) anthocyanins. 2. Anthocyanins and pigmented polymers in wine. *Journal of agricultural and food chemistry* **2007**, *55*, 6585-6595.

9. Cortell, J.M.; Sivertsen, H.K.; Kennedy, J.A.; Heymann, H. Influence of vine vigor on Pinot noir fruit composition, wine chemical analysis, and wine sensory attributes. *American journal of enology and viticulture* **2008**, *59*, 1-10.

10. Reynolds, A.G.; Senchuk, I.V.; van der Reest, C.; De Savigny, C. Use of GPS and GIS for elucidation of the basis for terroir: Spatial variation in an Ontario Riesling vineyard. *American Journal of Enology and Viticulture* **2007**, *58*, 145-162.

11. Marciniak, M.; Brown, R.; Reynolds, A.G.; Jollineau, M. Use of remote sensing to understand the terroir of the Niagara Peninsula. Applications in a Riesling vineyard. *OENO One* **2015**, *49*, 1-26.

12. Acevedo-Opazo, C.; Tisseyre, B.; Guillaume, S.; Ojeda, H. The potential of high spatial resolution information to define within-vineyard zones related to vine water status. *Precision Agriculture* **2008**, *9*, 285-302.

13. Hjelmeland, A.K.; Ebeler, S.E.J.A.J.o.E.; Viticulture. Glycosidically bound volatile aroma compounds in grapes and wine: a review. **2015**, *66*, 1-11.

14. Ristic, R.; Downey, M.O.; Iland, P.G.; Bindon, K.; Francis, I.L.; Herderich, M.; Robinson, S.P.J.A.J.o.G.; Research, W. Exclusion of sunlight from Shiraz grapes alters wine colour, tannin and sensory properties. **2007**, *13*, 53-65.

15. De Orduna, R.M.J.F.R.I. Climate change associated effects on grape and wine quality and production. **2010**, *43*, 1844-1855.

16. Jones, H.G. *Plants and microclimate: a quantitative approach to environmental plant physiology*; Cambridge university press: **2013**.

17. Picard, M.; Tempere, S.; de Revel, G.; Marchand, S.J.F.Q.; Preference. A sensory study of the ageing bouquet of red Bordeaux wines: A three-step approach for exploring a complex olfactory concept. **2015**, *42*, 110-122.

18. Villamor, R.R.; Harbertson, J.F.; Ross, C.F.J.A.J.o.E.; Viticulture. Influence of tannin concentration, storage temperature, and time on chemical and sensory properties of Cabernet Sauvignon and Merlot wines. **2009**, *60*, 442-449.

19. Loscos, N.; Hernández-Orte, P.; Cacho, J.; Ferreira, V.J.F.c. Evolution of the aroma composition of wines supplemented with grape flavour precursors from different varietals during accelerated wine ageing. **2010**, *120*, 205-216.

20. Ugliano, M.J.J.o.a.; chemistry, f. Oxygen contribution to wine aroma evolution during bottle aging. **2013**, *61*, 6125-6136.

21. Bramley, R.; Ouzman, J.; Boss, P.K. Variation in vine vigor, grape yield and vineyard soils and topography as indicators of variation in the chemical composition of grapes, wine and

wine sensory attributes. *Australian Journal of Grape and Wine Research* **2011**, *17*, 217-229.

22. Drissi, R.; Goutouly, J.-P.; Forget, D.; Gaudillere, J.-P. Nondestructive measurement of grapevine leaf area by ground normalized difference vegetation index. *Agronomy Journal* **2009**, *101*, 226-231.

23. Lamb, D.W.; Weedon, M.; Bramley, R. Using remote sensing to predict grape phenolics and colour at harvest in a Cabernet Sauvignon vineyard: Timing observations against vine phenology and optimising image resolution. *Australian Journal of Grape and Wine Research* **2004**, *10*, 46-54.

24. Stamatiadis, S.; Taskos, D.; Tsadilas, C.; Christofides, C.; Tsadila, E.; Schepers, J.S. Relation of ground-sensor canopy reflectance to biomass production and grape color in two Merlot vineyards. *American Journal of Enology and viticulture* **2006**, *57*, 415-422.

25. Ebeler, S.E.J.F.r.i. Analytical chemistry: Unlocking the secrets of wine flavor. **2001**, *17*, 45-64.

26. Tao, Y.; Li, H.; Wang, H.; Zhang, L.J.J.o.F.C.; Analysis. Volatile compounds of young Cabernet Sauvignon red wine from Changli County (China). **2008**, *21*, 689-694.

27. Pozo-Bayón, M.; G-Alegría, E.; Polo, M.; Tenorio, C.; Martín-Álvarez, P.; Calvo De La Banda, M.; Ruiz-Larrea, F.; Moreno-Arribas, M.J.J.o.A.; Chemistry, F. Wine volatile and amino acid composition after malolactic fermentation: effect of Oenococcus oeni and Lactobacillus plantarum starter cultures. **2005**, *53*, 8729-8735.

28. Maicas, S.; Gil, J.-V.; Pardo, I.; Ferrer, S.J.F.R.I. Improvement of volatile composition of wines by controlled addition of malolactic bacteria. **1999**, *32*, 491-496.

29. Kotseridis, Y.; Baumes, R.J.J.o.A.; Chemistry, F. Identification of impact odorants in Bordeaux red grape juice, in the commercial yeast used for its fermentation, and in the produced wine. **2000**, *48*, 400-406.

30. Joslin, W.; Ough, C.J.A.J.o.E.; Viticulture. Cause and fate of certain C6 compounds formed enzymatically in macerated grape leaves during harvest and wine fermentation. **1978**, *29*, 11-17.

31. Yang, C.; Wang, Y.; Wu, B.; Fang, J.; Li, S.J.F.C. Volatile compounds evolution of three table grapes with different flavour during and after maturation. **2011**, *128*, 823-830.

32. Kalua, C.; Boss, P.K.J.A.J.o.G.; Research, W. Comparison of major volatile compounds from Riesling and Cabernet Sauvignon grapes (Vitis vinifera L.) from fruitset to harvest. **2010**, *16*, 337-348.

33. García, E.; Chacón, J.; Martínez, J.; Izquierdo, P.J.F.s.; international, t. Changes in volatile compounds during ripening in grapes of Airén, Macabeo and Chardonnay white varieties grown in La Mancha region (Spain). **2003**, *9*, 33-41.

34. Watkins, P.; Wijesundera, C.J.T. Application of zNose™ for the analysis of selected grape aroma compounds. **2006**, *70*, 595-601.

35. Vilanova, M.; Genisheva, Z.; Bescansa, L.; Masa, A.; Oliveira, J.M.J.P. Changes in free and bound fractions of aroma compounds of four Vitis vinifera cultivars at the last ripening stages. **2012**, *74*, 196-205.

36. Fan, W.; Xu, Y.; Jiang, W.; Li, J.J.J.o.f.s. Identification and quantification of impact aroma compounds in 4 nonfloral Vitis vinifera varieties grapes. **2010**, *75*, S81-S88.

37. Ribéreau-Gayon, P.; Boidron, J.; Terrier, A.J.J.o.A.; Chemistry, F. Aroma of Muscat grape varieties. **1975**, *23*, 1042-1047.

38. Fang, Y.; Qian, M.C.J.J.o.a.; chemistry, f. Quantification of selected aroma-active compounds in Pinot noir wines from different grape maturities. **2006**, *54*, 8567-8573.

39. Parker, M.; Capone, D.L.; Francis, I.L.; Herderich, M.J.J.J.o.a.; chemistry, f. Aroma precursors in grapes and wine: Flavor release during wine production and consumption. **2017**, *66*, 2281-2286.

40. Grechkin, A.J.P.L.R. Recent developments in biochemistry of the plant lipoxygenase pathway. **1998**, *37*, 317-352.

CHAPTER 6: RESULTS AND DISCUSSION – FEASIBILITY STUDY OF REMOTE SENSING TECHNOLOGIES TO DETECT GRAPEVINE VIRUS PRESENCE

The objective of this study was to examine the effects of grapevine leafroll-associated virus 3 (GLRaV3) infection and its symptoms on electromagnetic reflectance of grapevine leaf. We hypothesized that the presence of grapevine virus and its infected leaves have unique electromagnetic signatures which could be detected by a narrow-band, hyperspectral spectrometer.

6.1 Results

6.1.1 Detection of grapevine leafroll associated virus (GLRaV)-1,2,3 infection by Real Time qPCR

In this study, two Niagara Peninsula Cabernet franc vineyard sites were examined for the presence of GLRaV-1, -2, -3. In Table 6.1, no samples were infected by GLRaV-1 and only one vine was infected by GLRaV-2 across the sites, so all statistical analyses were confined to determining GLRaV-3 presence only. Near the time of the RPAS flight, a random sample was taken of upper, middle, and lower leaves of Cabernet franc vines in September 2016.

Table 6.1. Real-Time qPCR results in the presence of GLRaV-2 and -3 for grapevine leaf samples collected from two study sites. "-"indicated negative result, "+" indicated cycle threshold (CT) value in the range of 36 to 38, "++" indicated CT value below 35.

Site	Row	Panel	GLRaV-2	GLRaV-3	Site	Row	Panel	GLRaV-2	GLRaV-3
Site 1	3	9	–	–	Site 2	4	12	–	–
	3	24	–	–		4	37	–	+
	3	39	–	–		7	37	–	–
	7	39	–	++		7	22	–	–
	7	24	–	+		7	7	–	++
	7	9	–	–		10	12	–	–
	11	9	–	++		10	37	–	+
	11	24	–	–		13	37	–	–
	11	39	–	+		13	22	–	+
	15	39	–	+		13	7	–	–
	15	24	–	–		16	12	–	–
	15	9	+	++		16	37	–	–
	19	9	–	–		19	37	–	–
	19	24	–	++		19	22	–	–
	19	39	–	+		19	7	–	–
						22	12	–	++
						22	37	–	–
						25	37	–	–
						25	22	–	++
						25	7	–	++

6.1.2 Spectral measurements of healthy and GLRaV3 infected leaves by the hand-held spectrometer

A total of 150 leaf samples comprising 75 leaf samples from each site (25 from healthy vines, 25 from asymptomatic vines, and 25 from symptomatic vines) were measured from the two different GLRaV3 infected sites and were pictured in the photos shown in Figure 2.1. The virus-positive Cabernet franc leaves demonstrated common signs of GLRaV-3 during scouting spectral measurements by the hand-held spectrometer in September 2017 [Figure 2.1 (a)]. Previous study indicated that a visual symptom of GLRaV infection was distinct at later season.[1,2] Therefore, the late growing season measurements were used to distinguish asymptomatic leaves from symptomatic leaves. On the leaf blades of infected grapevines, the interveinal spaces contained

purple pigmentation and veins appeared to have a slight band of greenish tissue on both sides. However, some GLRaV-3 positive vines remained asymptomatic [Figure 2.1 (b)]. All grapevines that tested negative for GLRaV-3 had healthy leaves without any virus symptoms [Figure 2.1 (c)]. The series of mean electromagnetic (EM) spectra (n=75) for leaves from healthy and GLRaV-3-infected grapevines from each site are shown in Figure 6.1 and 6.2.

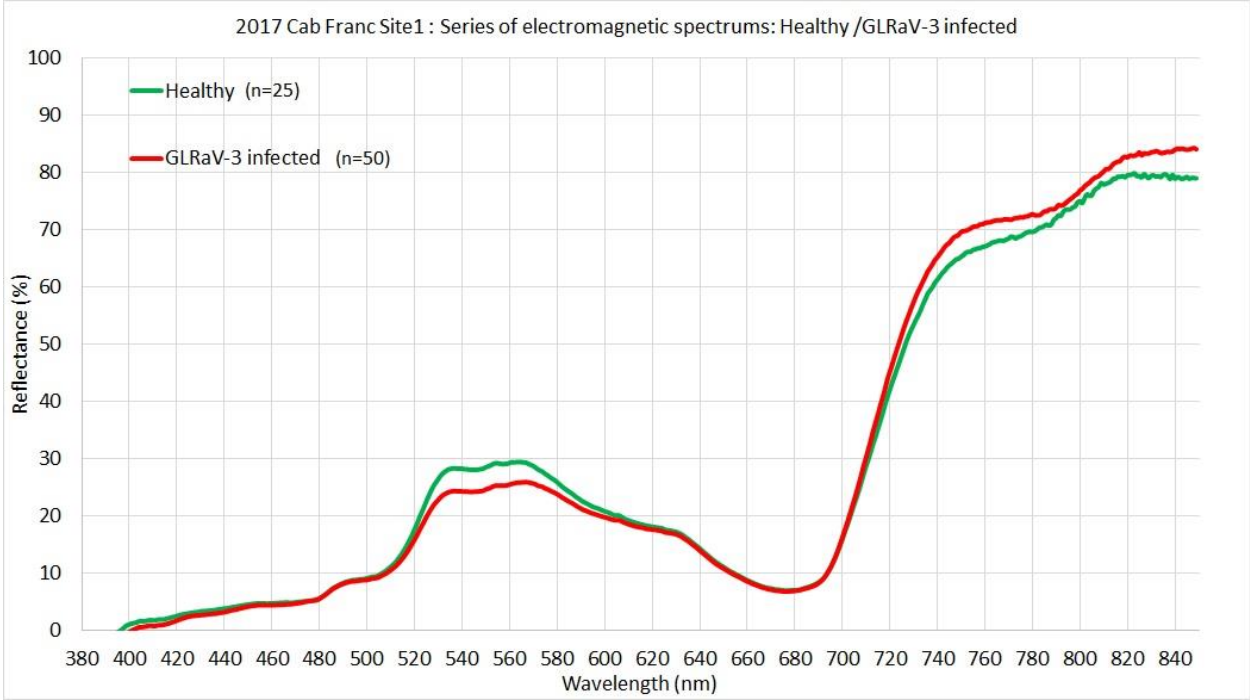

Figure 6.1. The series of electromagnetic spectra from healthy and GLRaV-3 infected Cabernet franc leaves measured by hand-held spectrometer at site 1.

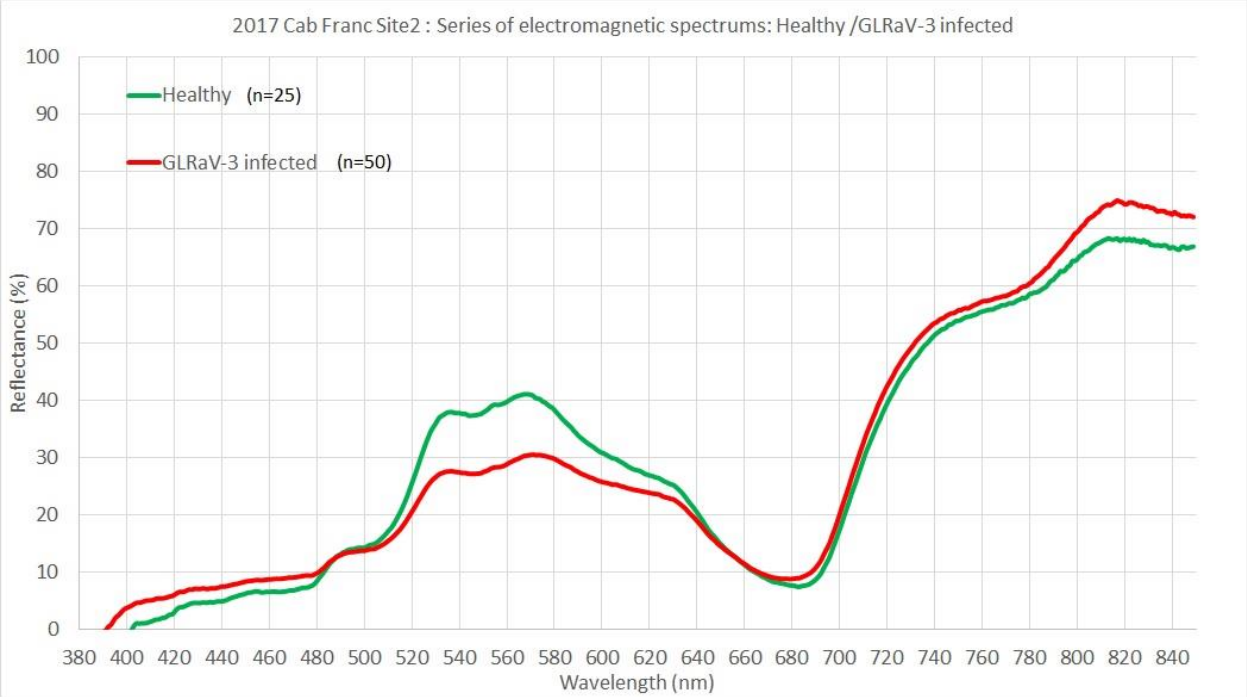

Figure 6.2. The series of electromagnetic spectra from healthy and GLRaV-3 infected Cabernet franc leaves measured by hand-held spectrometer at site 2.

A difference was seen in the reflectance of GLRaV-3-virus infected leaves and healthy leaves in four wavelength bands: green (500-600 nm), red (630-700 nm), red edge (701-740 nm), and near infrared (NIR) (741-849 nm). In the visible range of the EM reflectance, higher reflectance levels were observed in healthy leaves in the green peak region while there was minimal difference in the red trough with only a slightly higher reflectance level in GLRaV-3 infected leaves in site 2 (Figure 6.2).

Interestingly, GLRaV-3-infected grapevines had a higher level of reflectance at the red edge peak. This trend continued extending into the NIR region with a bigger gap between healthy and infected vines in both sites (Figure 6.1 and 6.2). The t-test results also confirmed that there were significantly different reflectance levels in these peaks between healthy and GLRaV-3 infected leaves (Figure 6.3).

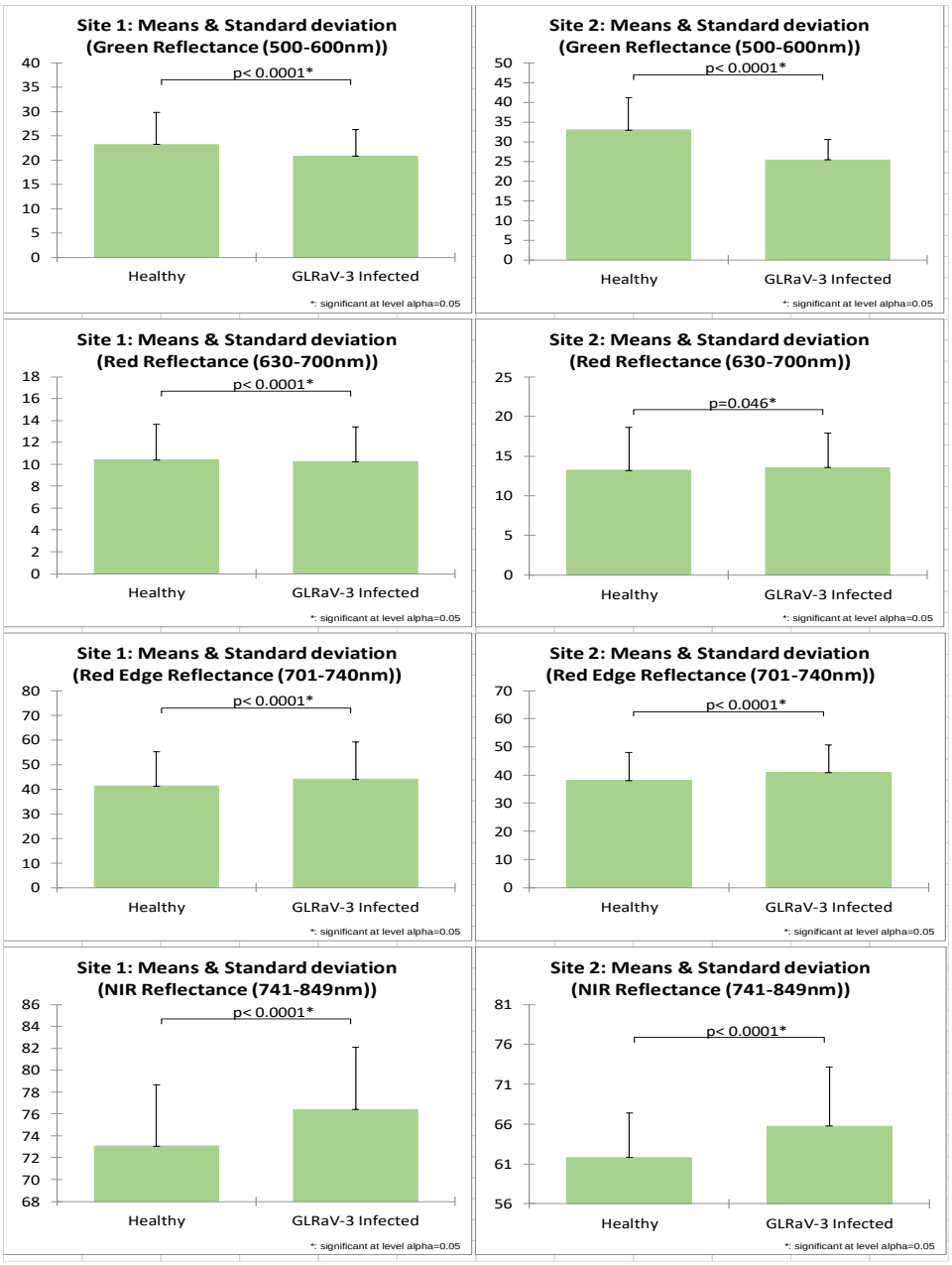

Figure 6.3. Comparison of mean reflectance (%) of EM spectrums of green, red, red edge, and NIR peaks from healthy (n=25) and GLRaV-3 infected (n=50) Cabernet Franc leaves measured by hand-held spectrometer in both site 1 and site 2 using a t-test with two samples: * significant p-values (95% confidence).

To determine if visible symptoms affected the remote sensing indices and wavelength bands, the electromagnetic spectrum of symptomatic and asymptomatic GLRaV-3-infected leaves

were presented separately. EM reflectance differences between asymptomatic and healthy leaves were observed throughout the spectra (Figure 6.4 and 6.5). The different EM reflectance peaks were segregated based on the inflection point of each band from Figure 6.4: the green (500-600 nm), the red (630-700 nm), the red edge (701-740 nm), and the NIR (741-849 nm). The EM reflectance differences between symptomatic and asymptomatic leaves were more prominent than the differences between symptomatic and healthy leaves in at the green and red wavelengths (Figure 6.4 and 6.5). GLRaV-3 asymptomatic leaves also had substantially higher light reflectance levels than those of healthy and symptomatic leaves throughout the visible (green and red), red edge, and NIR regions (Figure 6.4 and 6.5). The reflectance in GLRaV-3 symptomatic leaves had substantially lower light reflectance levels than these of healthy and symptomatic leaves at green and red regions. The symptomatic leaves had a reflectance hike at the red edge peak. This trend continued extending into the NIR region with a bigger increase (Figure 6.4 and 6.5). The t-test results also confirmed that different reflectance levels occurred in these regions among symptomatic, asymptomatic, and healthy leaves (Figure 6.6 and 6.7).

Red edge spectral shifts from these leaf samples were also investigated. Red edge inflection point (REIP), also known as red edge position (REP) is the maximum first derivative of red edge reflectance and was based on the formula[3-6]: REIP=MAX(nm) $\frac{R(n+1)-R(n)}{WAVELENGTH(n+1)-WAVELENGTH(n)}$ = MAX(nm) $\frac{R(n+1)-R(n)}{1}$ = Max R(x)′.

Rn = reflectance value at wavelength n, R(n+1) = reflectance value at wavelength n+1.

R(x)’ = first derivative of reflectance change (slope of reflectance graph).

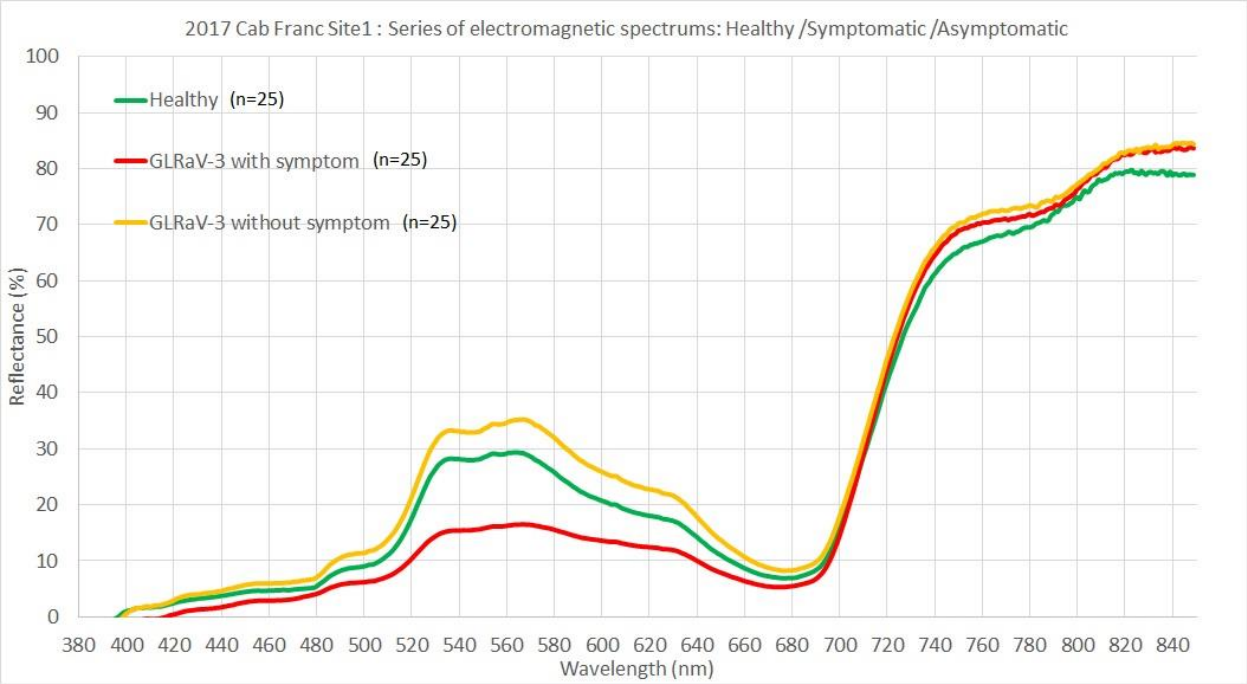

Figure 6.4. The series of electromagnetic spectra from healthy and GLRaV-3 symptomatic and asymptomatic Cabernet franc leaves measured by hand-held spectrometer at site 1.

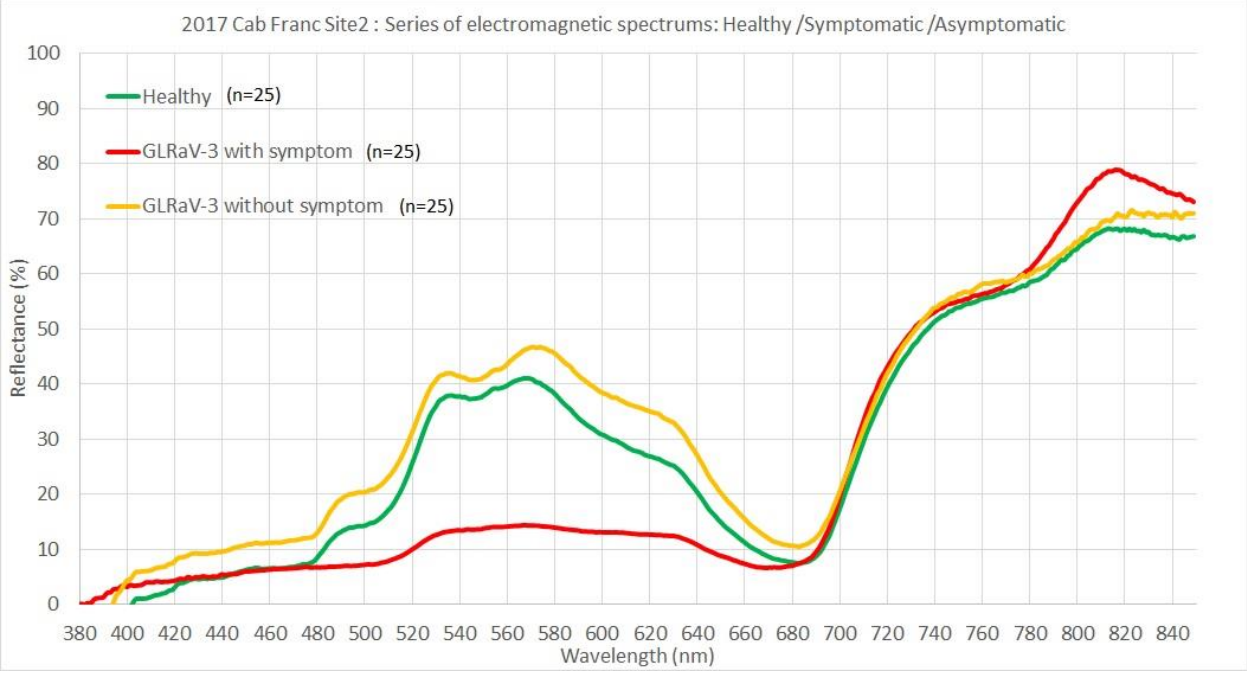

Figure 6.5. The series of electromagnetic spectra from healthy and GLRaV-3 symptomatic and asymptomatic Cabernet franc leaves measured by hand-held spectrometer at site 2.

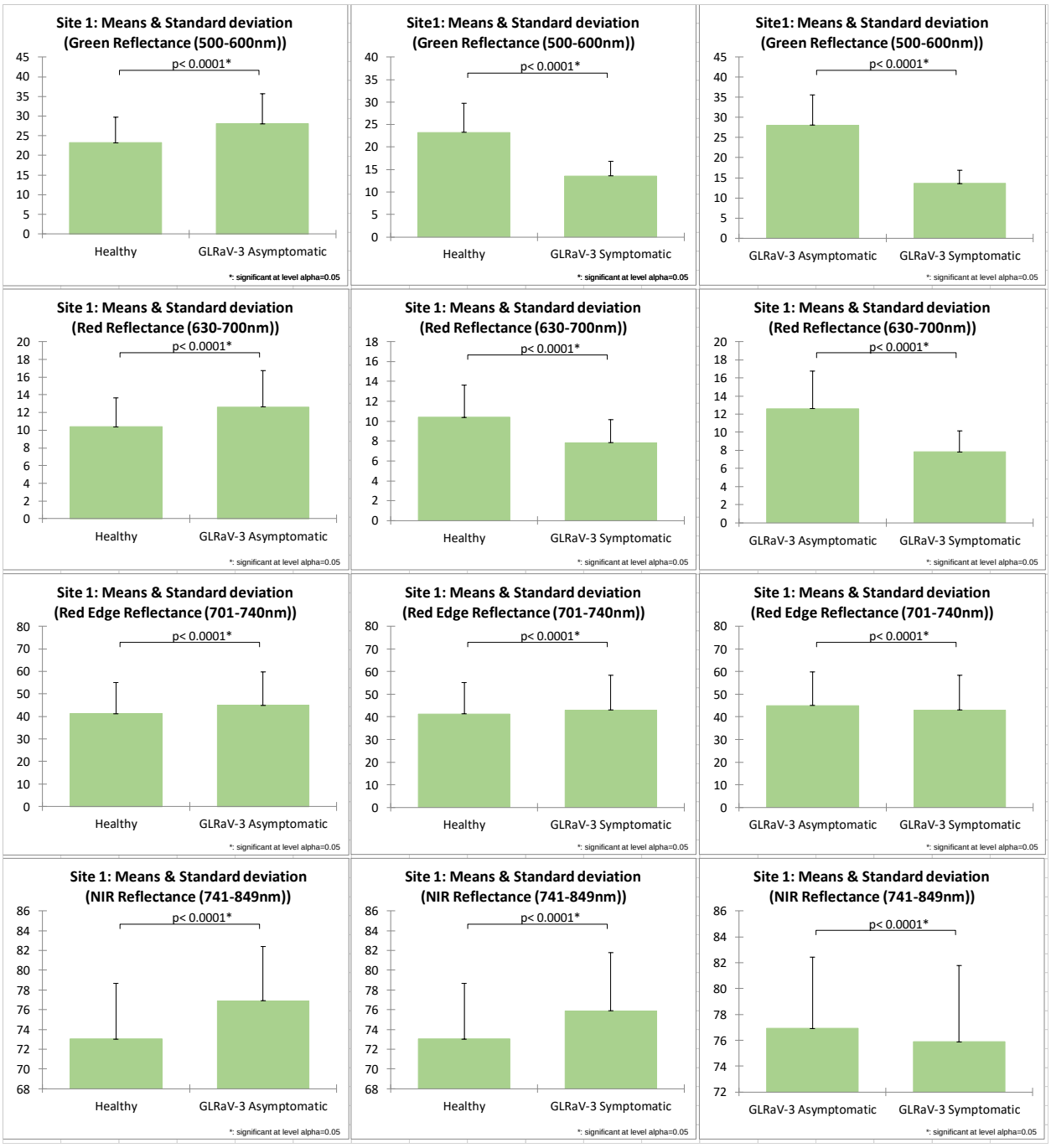

Figure 6.6. Comparison of mean reflectance (%) of EM spectrums of green, red, red edge, and NIR peaks from healthy (n=25), asymptomatic (n=25) and symptomatic (n=25) GLRaV-3 infected Cabernet Franc leaves measured by hand-held spectrometer at site 1 using a t-test with two samples: * significant p-values (95% confidence).

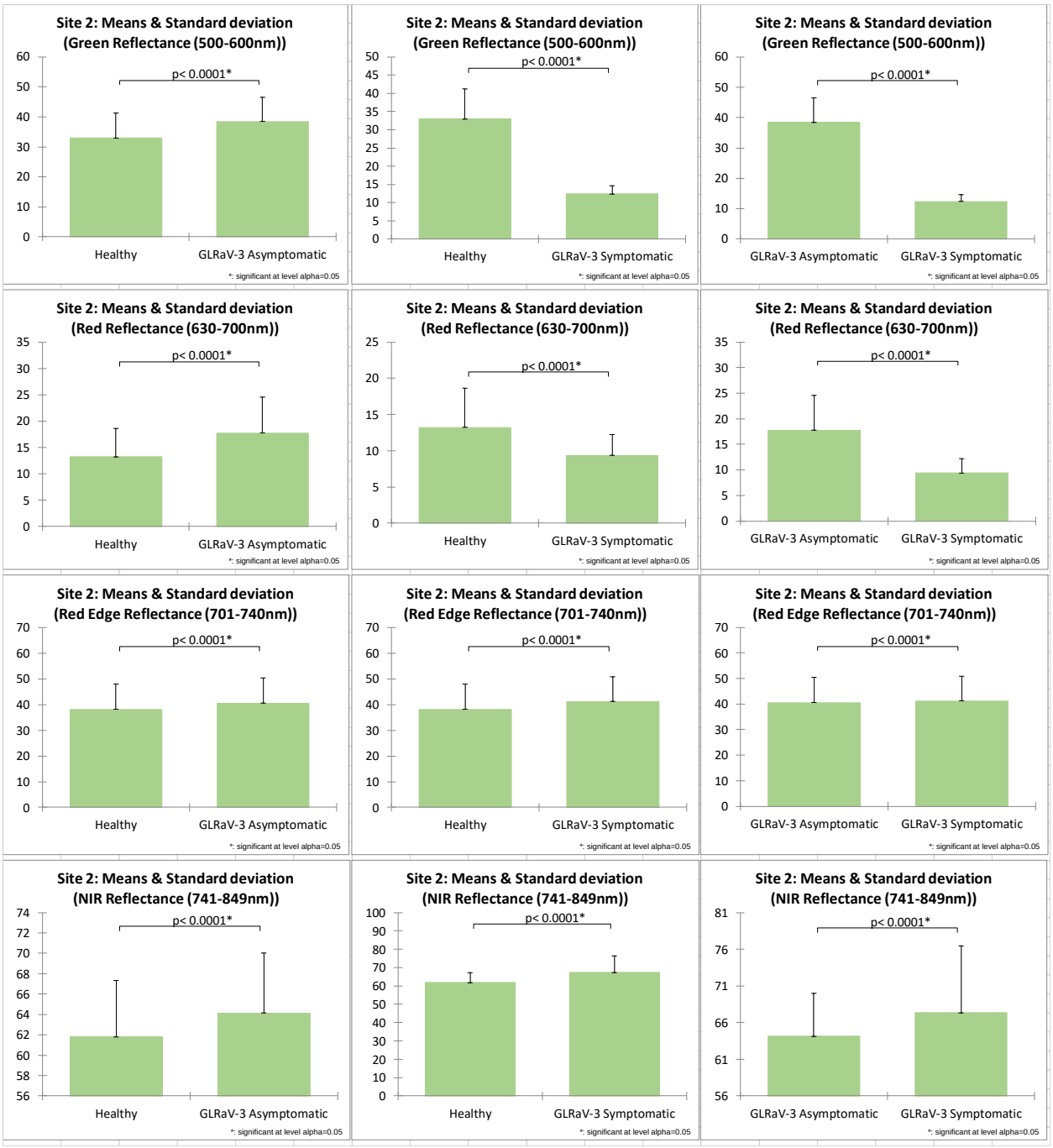

Figure 6.7. Comparison of mean reflectance (%) of EM spectrums of green, red, red edge, and NIR peaks from healthy (n=25), asymptomatic (n=25) and symptomatic (n=25) GLRaV-3 infected Cabernet Franc leaves measured by hand-held spectrometer at site 2 using a t-test with two samples: * significant p-values (95% confidence).

The REIP results are shown in Figure 6.8 and 6.9, which indicate that both in site 1 and site 2, virus symptomatic leaves had the lowest REIP while asymptomatic and healthy leaves showed the REIP shifted to higher wavelength. In the red and red edge regions, the maximum value of relative reflectance changes (MaxΔRn) was determined for the different treatments to observe the rate of change based on reflectance values at each wavelength. The relative reflectance change (ΔRn) from one wavelength to another was calculated from the formula[7]:

$$\Delta Rn = \frac{R(n)'}{R(n)} = \ln(R(n))' = \frac{d\ln(R(n))}{dn} = \lim_{h-1} \frac{\ln(R(n+h)) - \ln(R(n))}{h} = \ln(R(n+1)) - \ln(R(n)).$$

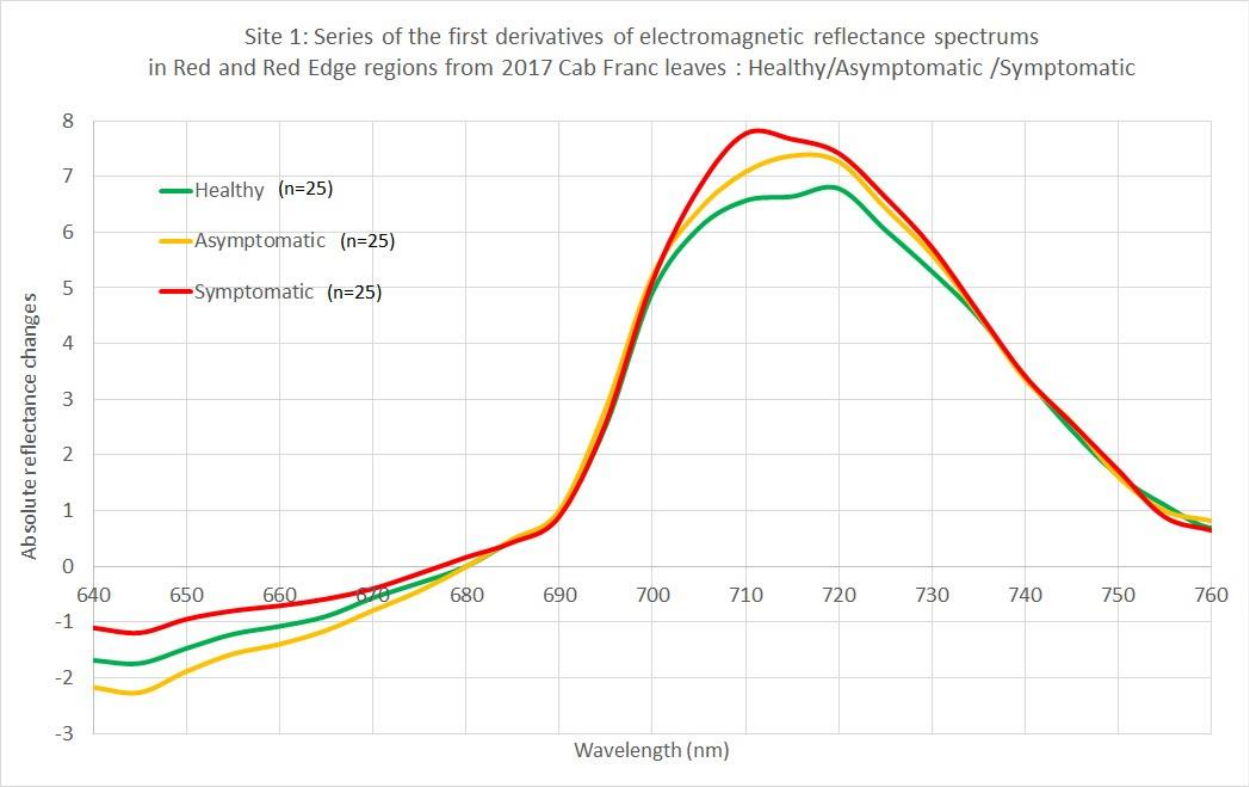

Figure 6.8. The series of the first derivative values of electromagnetic reflectance spectra in red and red edge regions from healthy and GLRaV-3 symptomatic and asymptomatic Cabernet Franc leaves measured by hand-held spectrometer at site 1.

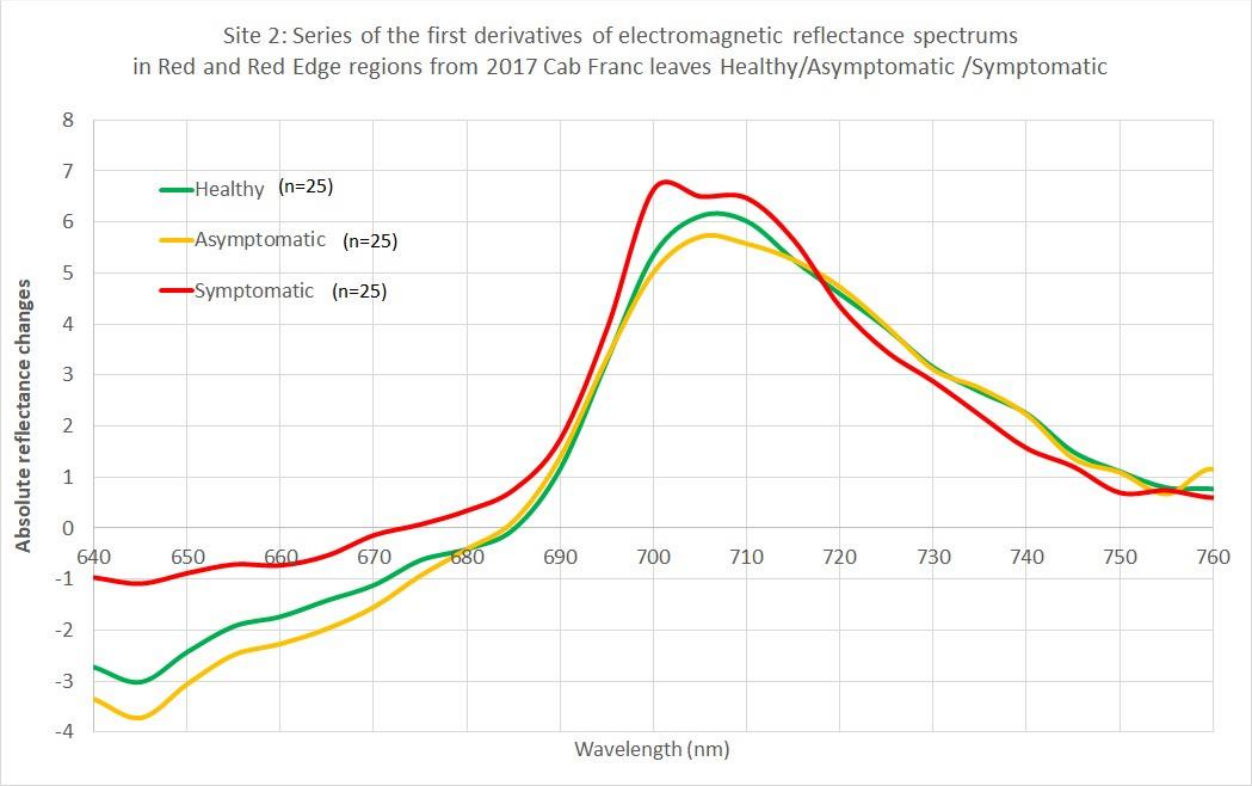

Figure 6.9. The series of the first derivative values of electromagnetic reflectance spectra in red and red edge regions from healthy and GLRaV-3 symptomatic and asymptomatic Cabernet franc leaves measured by hand-held spectrometer at site 2.

The MaxΔRn results are shown in Figure 6.10 and 6.11, which indicate a smooth and clear trend at the inflection point for all three treatments with the same inflection point at 698 nm in site 1 and at 697 nm in site 2. Despite the different position of the inflection point between REIP and MaxΔRn, the lowest red reflectance peak, where the slopes changed negative to positive, were consistent between the two formulae at the wavelength of 676 nm (symptomatic) and 677 nm (healthy and asymptomatic) in site 1 and of 670 nm (symptomatic), 683 nm (healthy), and 683 nm (asymptomatic) in site 2.

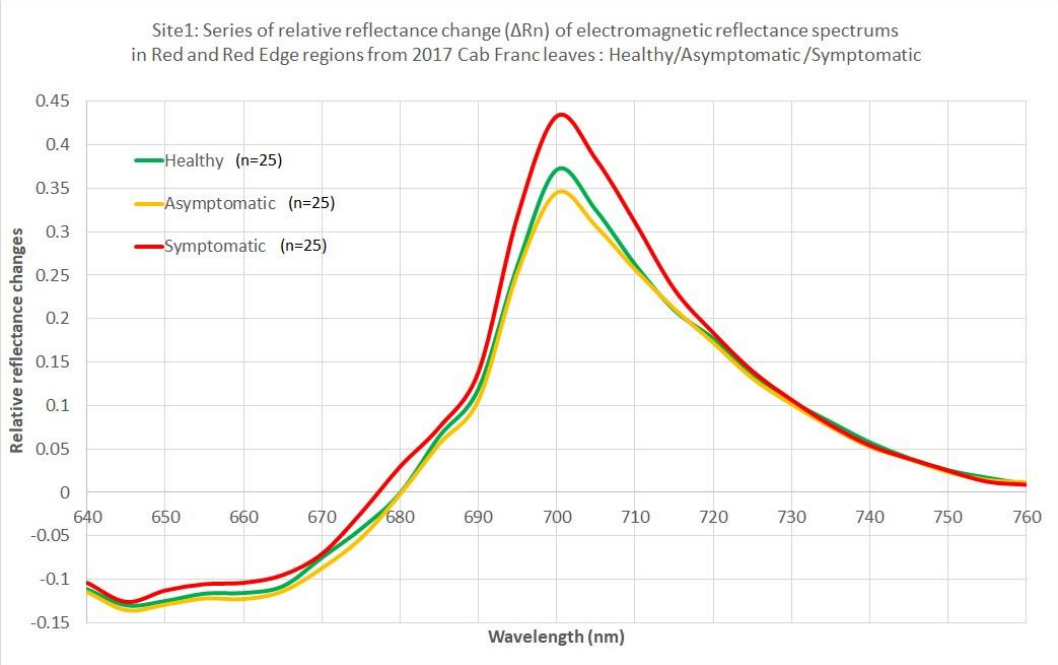

Figure 6.10. The series of relative reflectance change (ΔRn) of EMS in red and red edge regions from healthy, GLRaV-3 symptomatic and asymptomatic Cabernet franc leaves measured by hand-held spectrometer at site 1.

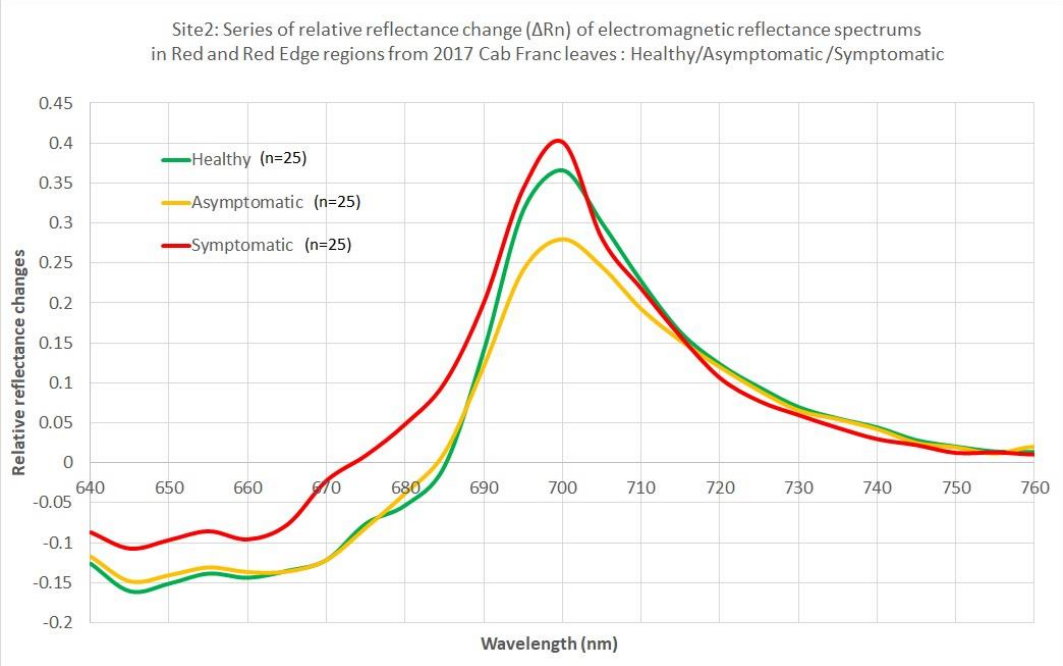

Figure 6.11. The series of relative reflectance change (ΔRn) of EMS in red and red edge regions from healthy, GLRaV-3 symptomatic, and asymptomatic Cabernet franc leaves measured by hand-held spectrometer at site 2.

Overall, the spectral measurements of EM reflectance found in healthy and GLRaV-3-infected grapevine leaves showed that the higher light reflectance level in healthy leaves occurred in the green peak while GLRaV-3 infected grapevines reflected more light in the regions of red edge, and NIR peaks.

The results from the effect of the visible symptoms of GLRaV-3 infection on the EM spectra indicated that GLRaV-3 asymptomatic leaves had higher light reflectance levels than those of healthy leaves throughout the visible (green and red), red edge, and NIR spectra. Secondly, GLRaV-3 symptomatic leaves had lower light reflectance (high light absorbance) levels than these of healthy leaves at the visible (green and red) region, however, it had reflectance spikes at red edge and NIR. Thirdly, the virus-symptomatic leaves had lower REIP values than these of asymptomatic and healthy leaves in both sites, indicating that the lowest chlorophyll concentration occurred in the virus-symptomatic leaves and higher chlorophyll concentrations were found in the healthy and asymptomatic leaves.[8-10] Lastly, the relative inflection point (MaxΔRn) was consistent at 700 nm throughout the sites and treatments and the relative data indicated that the relative reflectance difference between the wavelengths was lower in virus asymptomatic leaves than these in virus symptomatic and healthy leaves at the inflection point.

6.1.3 Relationships between remote sensing data and GLRaV-3infection

6.1.3.1 Remote sensing indices for GLRaV-3 infected vine detection

From the hand-held spectrometer measurements, healthy plants apparently had higher reflectance in the green peak, while virus infected vines indicated higher reflectance in red edge and NIR peaks. Consequently, multiple remote sensing indices can be calculated based on the

green, red edge, and NIR regions of multispectral imagery to determine whether vines are infected with viruses. In Table 6.2, feature indices were constructed using the earlier spectral measurements of grape leaves by the hand-held spectrometer with additional indices to characterize virus detection according to previous studies.[11,12]

Table 6.2. Remote sensing indices to characterize vine health and virus infections.

Remote sensing Indices	Equation
NDRE (Red Edge Normalized Difference Vegetation Index)	(NIR − Red Edge)/ (NIR + Red Edge)
GNDVI (NDVI Green)	(NIR – Green)/ (NIR + Green)
GRVI (Green-Red Vegetation Index)	(Green – Red)/ (Green + Red)
MTCI (MERIS Terrestrial Chlorophyll Index)	(NIR − Red Edge)/ (Red Edge + Red)
RTVI core (Core Red Edge Triangular Vegetation Index)	100(NIR – Red Edge) − 10(NIR − Green)

6.1.3.2 Principal component analysis (PCA) and Pearson's correlation analysis

According to Figure 6.12, over 83% of the data for GLRaV-3 detection in each site was explained by PCA models based on the first two factors. The GLRaV-3 infection positively correlated to NDRE in site 1 and to RTVIcore in site 2 but in both sites, vectors for GLRaV-3 infection were short, making visual comparisons challenging (Figure 6.12).

Pearson's correlation analysis did not detect a correlation between the remote sensing indices and GLRaV-3 infection (Table 6.3).

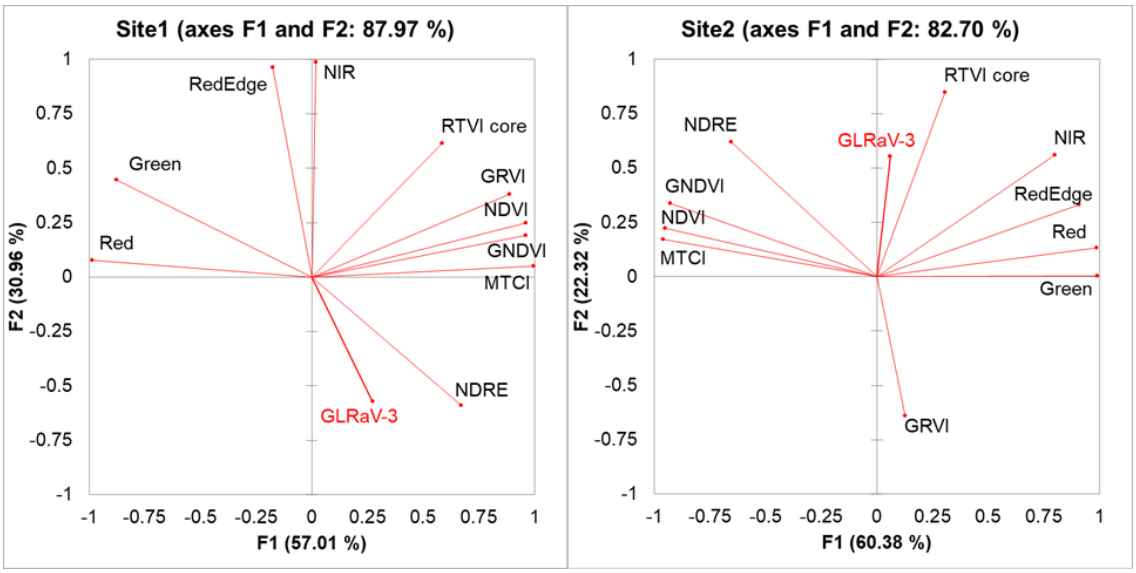

Figure 6.12. PCA results for GLRaV-3 presence vs. remote sensing indices including green, red, red edge, NIR, NDVI, NDRE, GNDVI, GRVI, MTCI, and RTVI core. Abbreviations: NIR= Near infrared, NDVI= Normalized difference vegetation Index, NDRE= Red edge normalized vegetation index, GNDVI= NDVI green, GRVI= Green-red vegetation index, MTCI= MERIS terrestrial chlorophyll index, RTVI core= Core red edge triangular vegetation index.

Table 6.3. Pearson's correlation results between GLRaV-3 presence and remote sensing indices in the two virus infected vineyards. Abbreviations: NIR= Near infrared, NDVI= Normalized difference vegetation Index, NDRE= Red edge normalized vegetation index, GNDVI= NDVI green, GRVI= Green-red vegetation index, MTCI= MERIS terrestrial chlorophyll index, RTVI core= Core red edge triangular vegetation index.

	Correlation matrix		p-values	
Variables	Site1	Site2	Site1	Site2
Green	-0.449	0.016	0.093	0.948
Red	-0.295	0.076	0.286	0.750
RedEdge	-0.471	0.272	0.076	0.246
NIR	-0.443	0.323	0.098	0.164
NDVI	0.140	0.064	0.618	0.787
NDRE	0.393	0.075	0.147	0.755
MTCI	0.213	0.064	0.445	0.789
RTVI core	-0.173	0.258	0.538	0.272
GNDVI	0.190	0.138	0.498	0.561
GRVI	-0.014	-0.291	0.962	0.213

6.2 Discussion

In addition to photosynthesis being drastically reduced[13,14], anthocyanin production and soluble solid levels in berries are being affected by GLRaV-3 infection[13,15]. Grapevine virus infected leaves expressed up-regulated soluble solid transporters and senescence-associated genes.[16] Plants may have biotic stresses that cause spectral differences that can be detected in the visible and NIR peaks of the EM reflection. It is possible to determine a plant's virus infection using these differences. In previous studies, researchers demonstrated that asymptomatic phases of early disease symptoms were characterized by EM reflectance in red edge and NIR peaks based on a lower chlorophyll level.[17,18]

In this study, the results of portable spectrometer readings indicated that the GLRaV-3 infected grapevines had a higher level of reflectance at red edge peak and this trend continued extending to the NIR region with a bigger gap between healthy and the virus infected leaves (Figure 6.1 and 6.2). Different factors have a profound impact on the reflectance levels in the visible, red edge, and NIR peaks. The visible region of the reflectance is influenced by pigment molecules, while changes in NIR spectrum are affected by variations in leaf arrangement and density.[19] The red edge peak is in the boundary between visible and NIR spectra and the peak is applied to calculate plant composition such as chlorophyll contents.[20] Previous research proved that chlorophyll concentration is negatively correlated to the EM reflectance spectra at the red edge range and an increase in chlorophyll concentration shifts the inflection point of entering red edge region to higher wavelength.[8-10]

Chlorophylls are the primary molecules that absorb the light energy and convert the energy for photosynthesis and also provide a valuable insight into the health of plant vegetation.[21]

Chlorophyll concentration is negatively correlated to the red reflectance peak because chlorophyll strongly absorbs red radiation for the electron transitions for photosynthesis at the magnesium component of the photoactive site.[21] Therefore, red reflectance could be a reliable candidate for estimating plant chlorophyll concentration and photosynthesis activity. However, the measurements of red reflectance are very sensitive to the effects of various other variables such as solar irradiance, presence of other pigment molecules, background soil, and the geometrical arrangement of the scene.[19,22] Reflectance at the red edge is less affected by these factors because it marks a line that separates the absorption of chromophores in the red peak and leaf inner cells dispersing in the NIR peak.[9] Virus infection is predicted to negatively correlate with red edge and NIR peaks due to a reduction in chlorophyll in virus-infected leaves and a negative impact on photosynthesis and plant growth.[23-25] However, the abnormality between the reflectance of red edge/NIR and the virus infection in this study may be caused by disorganization of the structure of the mesophyll cell via accumulations of anthocyanins and carbohydrates from plant defense responses against GLRaV-3 infections.

An observation on the phenotypic changes induced by GLRaV-3 infection shows two distinct features: late season reddening of foliar tissues and interveinal reddening (primary veins remain green). The virus-infected leaves turn red primarily as a result of anthocyanin deposition.[13,26] During veraison, grapevines require a substantial transport of photosynthesis products from leaves to fruits, and phloem in the inferior vein pass through structural and functional modifications to become the major channels of long-range soluble solids transport within these leaves.[27] Disease symptoms may appear in the ripening period as a result of source-sink dynamics that interfere with carbohydrates being transported from the leaves to the berry tissues, leading to accumulation of carbohydrates in the leaves.[28,29] Carbohydrate accumulation

in mesophyll cells inhibits photosynthesis and promote the accumulation of flavanols and anthocyanins for mitigating photo-oxidative damage via upregulated expression of MYB type transcription factors.[30,31] Transformation of the vein areas in stressed leaves is also expected from the dilution effect of carbohydrate buildup and the accumulation of flavanols and anthocyanins in mesophyll cells.

The leaf reflectance emanates from the three sources: a direct specular refection from the surface of the leaf, an internal refraction by the interior leaf tissue pigment, and a diffuse reflection by refractive discontinuity in leaf cellular structures.[32] Radiation has a tendency of scattering in the leaf cell as it confronts different cellular structures at each refractive discontinuity and an diffuse reflectance is the scattered radiation directed back to the leaf surface.[32,33] The reflectance in NIR and red edge peaks in leaves is affected by leaf structure, and leaf reflectance arises from the orientation of the cell walls, as well as differences in the refractive cell walls and air in the pore spaces.[34,35] The cell reorientation results in increased number of cell wall-air interface and multiple scattering of radiation and leads a higher reflectance level in red edge and NIR peaks.[36,37]

There is difficulty in identifying organic compounds from leaf spectra due to the overtones of photosynthetically active chlorophyll and other pigments in the visible and NIR range, and therefore, a correlation between leaf reflectance and chemical concentration in some wavelengths may not indicate a sole chemical compound but rather is the result of a strong inter correlation between several chemicals.[19,38] Previous studies found that the reflectance and its derivatives between red edge and NIR (low 800 nm wavelengths) indicated an evidence of responses related to the phenolic concentrations in leaves and the organic matter in soil.[38-40] Therefore, it was hypothesized that the results of the reflectance spikes at red edge and NIR spectral regions in the

GLRaV-3 infected leaves in this study could be caused by transformation of electromagnetic discontinuity and consequent increase in outflux of scattering events of radiation in the vein areas due to the high level of carbohydrates and anthocyanins.

An investigation of the effect of visible symptoms of GLRaV-3 on EM spectra was also carried out in this study, and the results indicated that GLRaV-3 asymptomatic leaves had substantially higher light reflectance levels than these of healthy and symptomatic leaves throughout the visible (green and red), and red edge spectra. Due to the role of pigment molecules in plant photosynthesis and productivity, leaf pigment concentration provides an indication of plant health and its ability to photosynthesis.[41] Stresses such as water, nutrients, and viral infection have demonstrated physical symptoms associated with changes in leaf colour and patterns, indicative of changes in their pigment concentration.[41-43] These changes would further impact the specific wavelengths of light being absorbed and utilized by the plant, and those being reflected. Pathogenic attacks initiate biochemical pathways, and the plant defense system responds to the threat of infection by pathogens in two different ways.[44]

First, defenses are initiated by inducible mechanisms when pathogens are perceived as a threat and cause induction of defense pathways, even in the undamaged leaves of pest infested plants soon after attack.[45] The inducible defenses are still not completely understood, but changes and accumulations of papillae are observed as a physical barrier to prevent pathogens from accessing the inner cells of the plant.[46] The cell wall associated defense system acts early to stop invading pathogens, removing the potential for expensive defense mechanisms, known as the hypersensitive response (HR).[44] Cell wall structures like glycoproteins, pectin, and xyloglucans are part of the papillae accumulation process, along with callose, lignin, phenolic polymers, and reactive oxygen species (ROS).[47] Some of the compounds are considered to form a physical

barrier through hardening the wall to prevent degradation from pathogen attacks.[47,48] Plant leaf surfaces are at the front line to fight against any biotic stresses with altering its cell wall structure and providing a protection against pathogens.[49] The first defense system of plants is induced by infection with GLRaV-3, resulting in hardening of leaf surfaces to stop invading pathogens. Hence, the odd observation of higher light reflectance in asymptomatic leaves with GLRaV-3 infection in this study may be associated with the hardening of the leaf surface walls at an early stage of infection, preventing light penetration and absorption.

Another distinct result from the investigation of the visible symptoms of GLRaV-3 infection on the EM spectra was that the EM reflectance in GLRaV-3 symptomatic leaves had substantially lower light reflectance levels than these of healthy and asymptomatic leaves in the visible (green and red) regions where the leaf reflectance is dominated by ability of absorbing light energy by leaf pigments.[37] Since the symptomatic leaves indicated the reduction in chlorophyll concentration and its negative impacts on absorbing red light for photosynthesis, the higher reflectance level was expected in the symptomatic leaves in the red trough.[21] The abnormality between the reflectance of red peak and the virus symptomatic leaves in this study could be explained by presence of the second mode of plant defense system, known as hypersensitive response (HR), in the GLRaV-3 symptomatic leaves. HR is involved in defense mechanisms against pathogen infected cells limiting further pathogen multiplication and spread.[50] The GLRaV-3 symptomatic leaves were at the later stage of the virus infection and triggered HR dominated plant defense response against the virus infection. Stress activates the HR predominantly through reactive oxygen species (ROS) that oxidize polyunsaturated fatty acids, alter permeability, and alter essential proteins, DNA, and affect the structural integrity of

cells.[51,52] In addition, the accelerated cell death in an HR induced by bacteria reduced chlorophyll concentration as well.[53,54]

The leaf reflectance in the visible ranges is mostly affected by direct specular refection from the surface of the leaf and internal refraction by the interior leaf tissue pigment.[32] The specular reflectance from the leaf surface has a characteristic of linear polarization of incident light in visible and NIR ranges and differentiated by leaf surface structures so that there is no interaction with pigments or inner cellular structures.[55] The magnitude of the reflectance is determined in part by surface undulations, which may cause masking or shadowing of the specular refection.[56] The direct specular reflectance on leaf surface is an important element of optical properties at the wavebands of high absorption, especially in the red peak.[57] Therefore, the HR may induce a structural change at the leaf surface, which diminishes the specular reflectance as each ray of the beam encounters different geometric angles in the red region.

Radiation incident on a leaf may be transmitted into the leaf, reflected at the leaf surface, or absorbed in the interior tissue. The conservation of energy by the Kirchoff's radiation law requires that the sum of light reflectance, transmittance, and absorbance should be equal to 1.[58] It was also assume that the intra-cellular structural changes induced by HR destroyed the refractive discontinuities in the interior leaf and more radiation internally scattered by the leaf transmitted through the leaf.[32,33] Previous studies also confirmed that increases in leaf transmittance and decreases in leaf absorbance levels in the EM spectrum were observed in the stressed plants.[59,60] Therefore, it can be hypothesized that the degradation of chlorophyll and other organ cells on the surface and interior of the leaves by HR in the virus symptomatic leaves induced the decline in ability to absorb and reflect the light energy and more light energy were transmitted through the leaves in the visible EM ranges.

Another notable spectral observation of the GLRaV-3 infected leaves was the symptomatic leaves had a reflectance hike at the red edge peak. This trend continued extending into the NIR region with a bigger increase. Previous studies indicated that chlorophyll fluorescence light emission occurs in red edge and NIR peaks[10] and the increasing light emission rate of the chlorophyll fluorescence in the virus symptomatic leaves may cause the reflectance increase in red edge and NIR regions. Chlorophyll fluorescence is an emitted light energy in photosynthetic tissues upon excitation with natural or artificial illumination in the red and red edge peak to disperse the excessive photosynthesis energy and to protect the chloroplast from oxidative damage.[61,62] Chlorophyll molecules in leaves can either facilitate photosynthesis, release heat or emit fluorescence, and these three processes are competitive, such that any increase in output in one affects the yield in the other two.[61-64] Therefore, chlorophyll fluorescence is inversely related to photosynthetic rates and the symptomatic leaves with severe stress conditions may trigger activation of HR and induce a collapse of chlorophyll activity and decrease in photosynthesis rates.[65,66]

The last notable observation of spectral measurements by the hand-held spectrometer was from the investigation of changes in the first derivative EM reflectance by GLRaV-3 infection. The degradation of chlorophyll in the virus symptomatic leaves was observed by comparing the red edge inflection point (REIP) index extracted from the EM reflectance of three virus infection treatments.[8-10] The REIP is based on calculation of absolute reflectance changes to get the inflection point at the red edge spectrum. The virus symptomatic leaves had the lower REIP value than these of asymptomatic and healthy leaves in both sites indicating the lowest chlorophyll concentration in the virus symptomatic leaves and the higher chlorophyll concentration in the healthy and asymptomatic leaves.[8-10]

Effects of relative reflectance changes (ΔRn, rate of changes from the original value) on calculation of the inflection point were also investigated. Both REIP and MaxΔRn measured the changes in reflectance at red edge peak; however, the nature of the data was different from each other. The REIP calculated by an absolute difference between the reflectance per each wavelength unit (1 nm) while MaxΔRn calculated by a relative rate change from the original reflectance. Mathematically, the former is the slope of the reflectance graph, $R(n)' = \lim_{h-1} \frac{R(n+h)-R(n)}{h}$, and the latter is logarithmic reflectance difference between the wavelengths, $\frac{R(n)'}{R(n)} = \ln(R(n))' = \frac{d\ln(R(n))}{dn} = \lim_{h-1} \frac{\ln(R(n+h))-\ln(R(n))}{h} = \ln(R(n+1)) - \ln(R(n))$. Since logarithmic conversion transfers an exponential scale into a linear scale, the relative values could be a useful concept to compare numerical variables with quantities growing exponentially in the red edge peak.[67] The concept of relative difference also allows to understanding of the comparative ratio of two numbers that gives us a direct insight into the true scale of difference between the treatments.[67]

Interestingly, the relative rate changes of reflectance at red edge region were the highest (inflection point) at certain wavelength (700 nm) throughout the treatments and sites and one could assume that a significant spectral incidence occurred at the inflection point (700 nm) in terms of the relative changes for the treatments. Results also indicated that the relative reflectance difference between the wavelengths was significantly lower in virus asymptomatic leaves and higher in virus symptomatic leaves at 700 nm (Figure 6.10 and 6.11). The significant difference in rate increment of reflectance change between the asymptomatic and symptomatic leaves at 700 nm may be induced by the chlorophyll fluorescence effect. Photosystem II (PSII), a solar energy-harvesting component in higher plants, is regulated by external environmental factors.[68] Nonphotochemical quenching (NPQ) occurs when moderately excess light occurs without

damaging PSII reaction centers. Unwanted energy is harmlessly released as heat while the photochemical quenching system is engaged.[69] Therefore, chlorophyll fluorescence is inversely related to photosynthetic rates in normal condition however, when stress initiated, it can plummet even at low photosynthesis rate due to an intensified protective quench. This causes the plant to produce more heat to disperse surplus energy, decreasing chlorophyll fluorescence.[70] Moreover, if HR is activated, severe stress conditions may reduce PSII functionally, and the chlorophyll fluorescence emission rate would increase with decreased NPQ activity.[65,66] In summary, the significant high-rate increment of reflectance change at 700 nm in the virus symptomatic leaves would lead the assumption that a severe stress condition with activation of hypersensitive response (HR) might also induce a collapse of the photosystem II activity, and the emission rate of chlorophyll fluorescence would increase with decreasing the NPQ activity and subsequent spike of the relative increment rate of EM reflectance observed at the certain peak (700 nm) in red edge range.

Remote sensing indices from the multi-spectral data of the RPAS flight were extracted and examined to characterize vine health and virus detection. The correlation coefficient test indicated that there were no significant correlations found among any of the RPAS remote-sensing indices and the occurrence of the GLRaV-3 virus (Table 6.3). The absence of any correlation between the virus infections and remote sensing indices could be caused by limitations of spatial and spectral resolution of the multi-spectral sensor measurement from RPAS flight. Multispectral sensors have spectrally broad bands with integration of tens of nanometers into one band leaving gaps between different bands and therefore, they are not able to reconstruct a detailed continual reflectance of plant canopy.[71] The light weight and low cost, multispectral sensors is a benefit for airborne and satellite applications. However, they provide less data complexity and information content than to

the spectrometers which corresponds more precisely to the specie's spectral signatures under particular conditions.[72]

This research also examined the correlations between grapevine red blotch associated virus (GRBV) infection and remote sensing indices from the multi-spectral data of the RPAS flight since the virus became an issue of concern in the region during this study. An end-point PCR test was performed on the same blocks in 2019 although the spectral analysis was done a few years prior. A total of six Cabernet franc vineyard blocks were analyzed for GRBV contamination in the Niagara wine region. However, GRBV infection was not detected at three of these sites, so they were excluded from analysis and are not represented in appendix Table A2. In the blocks that were evaluated, random samples of two mature canes from the bottom portion of the canopy of the Cabernet franc vines were collected in February 2019. The RPAS flight data were collected in September 2016. According to appendix Figure A1, over 81% of the data for GRBV detection in each site was explained by PCA models based on the first two factors. In site 1, the PCA model demonstrated that GRBV presence negatively correlated to NIR, red edge, and GRVI while red, NDRE, and RTVIcore were showing positive correlation but vectors for GRBV infection were short, making visual comparisons challenging (Figure A1). Pearson's correlation analysis did not detect a correlation between the remote sensing indices and GRBV infection (Table A3). In site 2, the virus presence positively correlated to RTVIcore but the vectors for GRBV infection were short, making visual comparisons challenging (Figure A1). Pearson's correlation analysis did not detect a correlation between the remote sensing indices and GRBV infection (Table A3). In site 3, the PCA model demonstrated that red edge, NIR, and GRVI were positively clustered together with GRBV infection (Figure A1). However, the correlation coefficient (r) values only showed a significant positive correlation between GRBV infection and NIR (Table A3). There was no

significant correlation between remote sensing indices and GRBV presence in most of the sites (Table A3). Only site 3 showed a positive correlation between GRBV presence and NIR (Table A3). The absence of any correlation between the virus infections and remote sensing indices could be caused by the temporal gap between the two measurements. There is over a 2-year gap from when the RPAS flight data was collected, and when the virus testing was done. This leads to a recommendation for further study in the area of application of this technology where the PCR testing and spectral analysis are done at the same time.

6.3 Conclusions and recommendations

Even though there were some experimental challenges such as visual assessment of virus symptoms, limited sample size, and time gaps between measurements, this study suggested that the response of individual foliar electromagnetic (EM) reflectance may differ due to an absence or presence of visible symptoms of infected leaves. The relative rate of reflectance changes at 700 nm could be an indicator for a dynamic light harvesting mechanism between energy utilization and dissipation in different stages of virus infection progress.

None of the conventional spectral indices investigated were consistent or robust enough to predict GLRaV-3 infection from the RPAS multi-spectral data. However, the hyperspectral spectrometer data showed consistent and significant differences among the spectra of healthy, asymptomatic, and symptomatic leaves. This finding leads to a recommendation for further study in a much more comprehensive investigation since there appears to be potential for development of a narrow-band hyperspectral index for grapevine virus detection. For instance, a combination of hyperspectral sensor and chlorophyll fluorescence sensors may detect changes in leaf reflectance and emission from GLRaV-3 infection. This may warrant to interpolate suspect

wavebands into ratios or indices. Concurrent virus titer and reflectance measurements along with much larger sample sizes and a more controlled environment would also be required.

6.4 References

1. Naidu, R.A.; Maree, H.J.; Burger, J.T. Grapevine leafroll disease and associated viruses: a unique pathosystem. *Annual Review of Phytopathology* **2015**, *53*, 613-634.

2. Maree, H.J.; Almeida, R.P.; Bester, R.; Chooi, K.M.; Cohen, D.; Dolja, V.V.; Fuchs, M.F.; Golino, D.A.; Jooste, A.E.; Martelli, G.P. Grapevine leafroll-associated virus 3. *Frontiers in microbiology* **2013**, *4*, 82.

3. Tian, Y.; Yao, X.; Yang, J.; Cao, W.; Zhu, Y.J.P.p.s. Extracting red edge position parameters from ground-and space-based hyperspectral data for estimation of canopy leaf nitrogen concentration in rice. **2011**, *14*, 270-281.

4. Gholizadeh, A.; Mišurec, J.; Kopačková, V.; Mielke, C.; Rogass, C.J.F. Assessment of red-edge position extraction techniques: A case study for norway spruce forests using hymap and simulated sentinel-2 data. **2016**, *7*, 226.

5. Baranoski, G.; Rokne, J.J.I.J.o.R.S. A practical approach for estimating the red edge position of plant leaf reflectance. **2005**, *26*, 503-521.

6. Dong, T.; Liu, J.; Shang, J.; Qian, B.; Ma, B.; Kovacs, J.M.; Walters, D.; Jiao, X.; Geng, X.; Shi, Y.J.R.S.o.E. Assessment of red-edge vegetation indices for crop leaf area index estimation. **2019**, *222*, 133-143.

7. Lendar, M.; Aissat, A.; Cazaunau, M.; Daële, V.; Mellouki, A.J.C.P.L. Absolute and relative rate constants for the reactions of OH and Cl with pentanols. **2013**, *582*, 38-43.

8. Ustin, S.; Martens, S.; Curtiss, B.; Vanderbilt, V. Use of high spectral resolution sensors to detect air pollution injury in conifer forests. In *Remote sensing Applications of Acid Deposition*; EPA: **1988**; pp. 72-85.

9. Horler, D.; DOCKRAY, M.; Barber, J.J.I.j.o.r.s. The red edge of plant leaf reflectance. **1983**, *4*, 273-288.

10. Gitelson, A.A.; Merzlyak, M.N.; Lichtenthaler, H.K.J.J.o.p.p. Detection of red edge position and chlorophyll content by reflectance measurements near 700 nm. **1996**, *148*, 501-508.

11. Wang, F.-M.; Huang, J.-F.; Tang, Y.-L.; Wang, X.-Z.J.R.S. New vegetation index and its application in estimating leaf area index of rice. **2007**, *14*, 195-203.

12. Wu, D.; Feng, L.; Zhang, C.; He, Y.J.T.o.t.A. Early detection of Botrytis cinerea on eggplant leaves based on visible and near-infrared spectroscopy. **2008**, *51*, 1133-1139.

13. Gutha, L.R.; Casassa, L.F.; Harbertson, J.F.; Naidu, R.A. Modulation of flavonoid biosynthetic pathway genes and anthocyanins due to virus infection in grapevine (Vitis viniferaL.) leaves. *BMC Plant Biology* **2010**, *10*, 187.

14. Mannini, F.; Mollo, A.; Credi, R. Field performance and wine quality modification in a clone of Vitis vinifera cv. Dolcetto after GLRaV-3 elimination. *American journal of enology and viticulture* **2012**, *63*, 144-147.

15. Vega, A.; Gutiérrez, R.A.; Pena-Neira, A.; Cramer, G.R.; Arce-Johnson, P. Compatible GLRaV-3 viral infections affect berry ripening decreasing sugar accumulation and anthocyanin biosynthesis in Vitis vinifera. *Plant Molecular Biology* **2011**, *77*, 261.

16. Espinoza, C.; Medina, C.; Somerville, S.; Arce-Johnson, P. Senescence-associated genes induced during compatible viral interactions with grapevine and Arabidopsis. *Journal of Experimental Botany* **2007**, *58*, 3197-3212.

17. Polischuk, V.; Shadchina, T.; Kompanetz, T.; Budzanivskaya, I.; Boyko, A.; Sozinov, A. Changes in reflectance spectrum characteristic of Nicotiana debneyi plant under the influence of viral infection. **1997**.

18. Delalieux, S.; Van Aardt, J.; Keulemans, W.; Schrevens, E.; Coppin, P.J.E.J.o.A. Detection of biotic stress (Venturia inaequalis) in apple trees using hyperspectral data: Non-parametric statistical approaches and physiological implications. **2007**, *27*, 130-143.

19. Curran, P.J.J.R.s.o.e. Remote sensing of foliar chemistry. **1989**, *30*, 271-278.

20. Curran, P.J.; Dungan, J.L.; Gholz, H.L.J.T.p. Exploring the relationship between reflectance red edge and chlorophyll content in slash pine. **1990**, *7*, 33-48.

21. Danks, S.M.; Evans, E.H.; Whittaker, P.A. *Photosynthetic systems: structure, function, and assembly*; John Wiley & Sons: **1983**.

22. Curran, P.J.P.T.o.t.R.S.o.L.S.A., Mathematical; Sciences, P. Multispectral remote sensing for the estimation of green leaf area index. **1983**, *309*, 257-270.

23. Cabaleiro, C.; Segura, A.; Garcia-Berrios, J.J.A.J.o.E.; Viticulture. Effects of grapevine leafroll-associated virus 3 on the physiology and must of Vitis vinifera L. cv. Albarino following contamination in the field. **1999**, *50*, 40-44.

24. Bertamini, M.; Muthuchelian, K.; Nedunchezhian, N.J.J.o.P. Effect of grapevine leafroll on the photosynthesis of field grown grapevine plants (Vitis vinifera L. cv. Lagrein). **2004**, *152*, 145-152.

25. Endeshaw, S.T.; Sabbatini, P.; Romanazzi, G.; Schilder, A.C.; Neri, D.J.S.H. Effects of grapevine leafroll associated virus 3 infection on growth, leaf gas exchange, yield and basic fruit chemistry of Vitis vinifera L. cv. Cabernet Franc. **2014**, *170*, 228-236.

26. Springob, K.; Nakajima, J.-i.; Yamazaki, M.; Saito, K.J.N.p.r. Recent advances in the biosynthesis and accumulation of anthocyanins. **2003**, *20*, 288-303.

27. Turgeon, R.; Wolf, S.J.A.r.o.p.b. Phloem transport: cellular pathways and molecular trafficking. **2009**, *60*, 207-221.

28. Zhang, X.-Y.; Wang, X.-L.; Wang, X.-F.; Xia, G.-H.; Pan, Q.-H.; Fan, R.-C.; Wu, F.-Q.; Yu, X.-C.; Zhang, D.-P.J.P.p. A shift of phloem unloading from symplasmic to apoplasmic pathway is involved in developmental onset of ripening in grape berry. **2006**, *142*, 220-232.

29. Lee, D.-K.; Ahn, S.; Cho, H.Y.; Yun, H.Y.; Park, J.H.; Lim, J.; Lee, J.; Kwon, S.W.J.S.r. Metabolic response induced by parasitic plant-fungus interactions hinder amino sugar and nucleotide sugar metabolism in the host. **2016**, *6*, 1-11.

30. Wan, H.; Zhang, J.; Song, T.; Tian, J.; Yao, Y.J.F.i.p.s. Promotion of flavonoid biosynthesis in leaves and calli of ornamental crabapple (Malus sp.) by high carbon to nitrogen ratios. **2015**, *6*, 673.

31. Close, D.C.; Beadle, C.L.J.T.B.R. The ecophysiology of foliar anthocyanin. **2003**, *69*, 149-161.

32. Woolley, J.T.J.P.p. Reflectance and transmittance of light by leaves. **1971**, *47*, 656-662.

33. Grant, L.J.R.S.o.E. Diffuse and specular characteristics of leaf reflectance. **1987**, *22*, 309-322.

34. Gausman, H.W.J.P.E. Leaf reflectance of near-infrared. **1974**, *40*, 183-191.

35. Gausman, H.; Allen, W.J.P.p. Optical parameters of leaves of 30 plant species. **1973**, *52*, 57-62.

36. Daughtry, C.; Biehl, L.L. Changes in spectral properties of detached leaves. **1984**.

37. Knipling, E.B.J.R.s.o.e. Physical and physiological basis for the reflectance of visible and near-infrared radiation from vegetation. **1970**, *1*, 155-159.

38. Ben-Dor, E.; Inbar, Y.; Chen, Y.J.R.S.o.E. The reflectance spectra of organic matter in the visible near-infrared and short wave infrared region (400–2500 nm) during a controlled decomposition process. **1997**, *61*, 1-15.

39. Ferwerda, J.G.; Skidmore, A.K.; Stein, A.J.I.J.o.R.S. A bootstrap procedure to select hyperspectral wavebands related to tannin content. **2006**, *27*, 1413-1424.

40. Krishnan, P.; Alexander, J.D.; Butler, B.; Hummel, J.W.J.S.S.S.o.A.J. Reflectance technique for predicting soil organic matter. **1980**, *44*, 1282-1285.

41. Palta, J.P. Leaf chlorophyll content. *Remote sensing reviews* **1990**, *5*, 207-213.

42. Yu, D.; Kim, S.; Lee, H. Stomatal and non-stomatal limitations to photosynthesis in field-grown grapevine cultivars. *Biologia Plantarum* **2009**, *53*, 133-137.

43. Escalona, J.M.; Flexas, J.; Medrano, H. Stomatal and non-stomatal limitations of photosynthesis under water stress in field-grown grapevines. *Functional Plant Biology* **2000**, *27*, 87-87.

44. Jones, J.D.; Dangl, J.L.J.n. The plant immune system. **2006**, *444*, 323-329.

45. Steppuhn, A.; Baldwin, I.T. Induced defenses and the cost-benefit paradigm. In *Induced plant resistance to herbivory*; Springer: **2008**; pp. 61-83.

46. Nicaise, V.; Roux, M.; Zipfel, C.J.P.p. Recent advances in PAMP-triggered immunity against bacteria: pattern recognition receptors watch over and raise the alarm. **2009**, *150*, 1638-1647.

47. Zeyen, R.; Carver, T.; Lyngkjær, M.F. Epidermal cell papillae. In *The powdery mildews. A comprehensive treatise*; APS Press: **2002**; pp. 107-125.

48. von Röpenack, E.; Parr, A.; Schulze-Lefert, P.J.J.o.B.C. Structural analyses and dynamics of soluble and cell wall-bound phenolics in a broad spectrum resistance to the powdery mildew fungus in barley. **1998**, *273*, 9013-9022.

49. Müller, C.; Riederer, M.J.J.o.c.e. Plant surface properties in chemical ecology. **2005**, *31*, 2621-2651.

50. Greenberg, J.T.; Guo, A.; Klessig, D.F.; Ausubel, F.M.J.C. Programmed cell death in plants: a pathogen-triggered response activated coordinately with multiple defense functions. **1994**, *77*, 551-563.

51. Laloi, C.; Apel, K.; Danon, A.J.C.o.i.p.b. Reactive oxygen signalling: the latest news. **2004**, *7*, 323-328.

52. Jabs, T.J.B.p. Reactive oxygen intermediates as mediators of programmed cell death in plants and animals. **1999**, *57*, 231-245.

53. Alméras, E.; Stolz, S.; Vollenweider, S.; Reymond, P.; Mène-Saffrané, L.; Farmer, E.E.J.T.P.J. Reactive electrophile species activate defense gene expression in Arabidopsis. **2003**, *34*, 205-216.

54. Tanaka, R.; Hirashima, M.; Satoh, S.; Tanaka, A.J.P.; Physiology, C. The Arabidopsis-accelerated cell death gene ACD1 is involved in oxygenation of pheophorbide a: inhibition of the pheophorbide a oxygenase activity does not lead to the "stay-green" phenotype in Arabidopsis. **2003**, *44*, 1266-1274.

55. Grant, L.; Daughtry, C.; Vanderbilt, V.J.P.P. Polarized and specular reflectance variation with leaf surface features. **1993**, *88*, 1-9.

56. Vanderbilt, V.C.; Grant, L.J.I.T.o.G.; sensing, R. Plant canopy specular reflectance model. **1985**, 722-730.

57. Grant, L.; Daughtry, C.; Vanderbilt, V.J.R.s.o.e. Variations in the polarized leaf reflectance of Sorghum bicolor. **1987**, *21*, 333-339.

58. Bekefi, G.; Hirshfield, J.L.; Brown, S.C.J.T.P.o.F. Kirchhoff's Radiation Law for Plasmas with Non-Maxwellian Distributions. **1961**, *4*, 173-176.

59. Carter, G.A.; Rebbeck, J.; Percy, K.E.J.C.J.o.F.R. Leaf optical properties in Liriodendron tulipifera and Pinus strobus as influenced by increased atmospheric ozone and carbon dioxide. **1995**, *25*, 407-412.

60. Carter, G.A.; Knapp, A.K.J.A.j.o.b. Leaf optical properties in higher plants: linking spectral characteristics to stress and chlorophyll concentration. **2001**, *88*, 677-684.

61. Gilmore, A.M. How higher plants respond to excess light: Energy dissipation in photosystem II. In *Concepts in Photobiology*; Springer: **1999**; pp. 513-548.

62. Maxwell, K.; Johnson, G.N.J.J.o.e.b. Chlorophyll fluorescence—a practical guide. **2000**, *51*, 659-668.

63. Gamon, J.; Serrano, L.; Surfus, J.J.O. The photochemical reflectance index: an optical indicator of photosynthetic radiation use efficiency across species, functional types, and nutrient levels. **1997**, *112*, 492-501.

64. Butler, W.L.J.A.R.o.P.P. Energy distribution in the photochemical apparatus of photosynthesis. **1978**, *29*, 345-378.

65. Murchie, E.H.; Lawson, T.J.J.o.e.b. Chlorophyll fluorescence analysis: a guide to good practice and understanding some new applications. **2013**, *64*, 3983-3998.

66. Horton, P.; Johnson, M.P.; Perez-Bueno, M.L.; Kiss, A.Z.; Ruban, A.V.J.T.F.j. Photosynthetic acclimation: Does the dynamic structure and macro-organisation of

photosystem II in higher plant grana membranes regulate light harvesting states? **2008**, *275*, 1069-1079.

67. Kastberg, S.E. Understanding mathematical concepts: The case of the logarithmic function. University of Georgia, **2002**.

68. Horton, P.; Ruban, A.; Walters, R.J.A.r.o.p.b. Regulation of light harvesting in green plants. **1996**, *47*, 655-684.

69. Horton, P.; Hague, A.J.B.e.B.A.-B. Studies on the induction of chlorophyll fluorescence in isolated barley protoplasts. IV. Resolution of non-photochemical quenching. **1988**, *932*, 107-115.

70. Yahyaoui, W.; Harnois, J.; Carpentier, R.J.F.l. Demonstration of thermal dissipation of absorbed quanta during energy-dependent quenching of chlorophyll fluorescence in photosynthetic membranes. **1998**, *440*, 59-63.

71. Hall, A.; Lamb, D.; Holzapfel, B.; Louis, J. Optical remote sensing applications in viticulture-a review. *Australian journal of grape and wine research* **2002**, *8*, 36-47.

72. Naidu, R.A.; Perry, E.M.; Pierce, F.J.; Mekuria, T. The potential of spectral reflectance data for the detection of Grapevine leafroll-associated virus-3 in two red berried wine grape cultivars. *Computers and Electronics in Agriculture* **2009**, *66*, 38-45.

CHAPTER 7: GENERAL DISCUSSION AND FUTURE RESEARCH OPPORTUNITIES

7.1 General discussion and future research

The primary objective of this research was to examine the feasibility of using remote sensing data to improve efficiency of vineyard management with greater precision and maximizing economic and environmental benefits through zonal fruit harvesting and wine quality differences. To achieve the goal, remote sensing data analysis tools such as normalized difference vegetation index (NDVI) were applied for vineyard data collection and correlation analysis between significant vineyard management variables, physiological measurements, and different remote sensing data. These variables included leaf water status, soil moisture, canopy size, vine health, yield, and berry composition, which further impacts on wine quality. The remote sensing data included electromagnetic reflectance data and thermal emission data of a remotely piloted aircraft system (RPAS). The data-analysis techniques applied to those data to extract meaningful information include the normalized difference vegetation index (NDVI) and other spectral indices.

Through these studies, relevant vine and vineyard management data were used to determine the feasibility of using remote sensing for precision vineyard management and to support future research to develop site-specific crop management (SSCM) for the region. SSCM is designated to incorporate spatial variability into a farming decision-making system at the field or farm level. Its main goal is the better use of farming resources, which can increase production efficiency and quality while minimizing environmental impacts and risks.[1] SSCM mainly relies on variations in the field, such as spatial and temporal variation of crop quality and quantity.[2]

In chapters 3 and 4, conventional methods were employed to detect vineyard variability. For example, time-domain reflectometry (TDR) for measuring soil moisture, direct measurement

of leaf water potential using the pressure bomb, use of a porometer for measuring leaf stomatal conductance, ground scouting of vine size, hand harvest yield (kg), winter hardiness (LT50), and chemical analysis for grape quality were collected. Since these conventional methods have limitations, such as being time-consuming, are labour-intensive requiring elaborate procedures, and are restricted to small sample size, there remains a demand for indirect and non-conventional methods for rapid detection of vine status based upon remote sensing. Correlation analysis such as principal component analysis (PCA) and Pearson's correlation coefficient elucidated relationships between remote sensing data and those data collected through conventional methods. Furthermore, analysis of interpolated maps, coupled with Moran's I spatial analyses, was applied to determine the spatial distribution and patterns of relationships among the data. The combination of the statistical and spatial analyses allowed the remote sensing data collected to elucidate the variations for the viticulturally significant variables.

In chapter 5, the effects of zonal harvesting based upon remote sensing data on the variability of wine quality were investigated. Conventional methods of wine quality analysis such as basic chemical analysis, sensory sorting test, descriptive analysis, and aromatic compounds analysis were conducted to investigate the variation in wine quality between high and low NDVI interpolated maps. The results of this study show that remote sensing vigour zonation using NDVI can be effectively used to detect vineyard zones relating to variables affecting wine quality, as demonstrated in earlier studies.[3-7]

In chapter 6, the effects of biotic stress from virus infections on changes of electromagnetic (EM) reflectance spectrum of leaves were examined by hand-held spectrometer measurements. Many vineyards around the world suffer economic losses due to virus infections.[8] The conventional method for the grapevine virus detection is performed by the polymerase chain

reaction (PCR) test[9] with some challenges including high cost, time consuming, and rapid spread of the infections[10,11]. Therefore, the development of rapid and early virus detection methods would be beneficial to protect wine industries around the wine growing regions. The discovery of early-stage spectral signatures of the virus infected leaves is the key resolution to examine the feasibility of the remote sensing technologies for early virus detection. In this respect, the effect of visible symptoms of virus infection on the EM reflectance was also investigated with differentiating EM spectrum of virus asymptomatic leaves (early stage of virus infection) from these of healthy and virus symptomatic leaves.

Results of a correlation study between remote sensing NDVI and viticulturally important factors for the precision viticulture indicated that vine size and soil moisture had significant correlation to the remote sensing NDVI with temporal stability. This result is consistent with previous literature.[12-14] A plant's canopy reflects the effects of its local environment and stress.[15] By combining canopy measurements with yield measurements, yield-to-vine size ratios can be derived as supplemental indicators of product quality.[16] The vineyard balance can be achieved through pruning, leaf removal, and cluster thinning practices.[17] Therein, NDVI data can guide growers in monitoring vineyard balance and fruit quality and stratifying wine quality management by identifying and manipulating areas of different canopy growth.[18]

Another notable relationship was that NDVI and soil moisture (SM) had a strong inverse correlation at three out of six sites for three consecutive years. The sites with the strong correlation clearly presented considerable water retention, presumably due to soils with a clay profile and inadequate drain. Interestingly, however, in the vineyard with relatively well drained soil types, the NDVI was positively related to SM in 2015 and 2016. The results of previous studies also proved the negative correlation between NDVI and soil clay profile and soil water status resulting

from soil drainage problems and soil density.[19-21] To examine the feasibility of using remote sensing technologies for vineyard water management, it is necessary to survey a map of vineyard soil profiles and its soil drainage capacities since the absolute values of soil water status were not correlated to the vine health and stress level.

The indirect measurement of vine water status can be a useful option to develop a link between remote sensing data and vineyard water stress, however, a weaker correlation was observed between NDVI and leaf water potential (leaf ψ). Interestingly, leaf ψ had more variation and was more correlated to NDVI in the year with ample precipitation, which indicated sufficient water supply could lead to more variations in vegetative growth and influence the detectability of NDVI for vine stress. A previous study indicated that plant water stress improved water use efficiency without much loss of biomass production.[22] These results could guide further research to understand the optimum balance of water contents in soil and in grapevine, and its correlation matrix to the vegetative growth for quality grape and wine production. The specific investigation on the NDVI variation from different soil types or soil drainage will confirm the assumption of the impacts of variability in soil drainage on NDVI measurement. To unravel the matrix between plant water status and variation in vegetative growth, further research is needed into the measurement of NDVI variation in vines of different water status.

To examine the feasibility of using of remote sensing technologies for vineyard management is not an easy task because there is no clear general guideline for the level of vegetative growth, leaf ψ or soil moisture for optimum grape and wine production. It depends on the site, variety, and cultural practice of specific vineyard. To validate the effectiveness of remote sensing data and their suitability for zonal vineyard management, more research data is still needed. For example, in this research, only site 3 vineyard showed clear correlations of NDVI and all the

viticulturally important variables with temporal stability in all three years. Possible reasons for the abnormality of the high correlation rate in site 3 are the differences in row management, training system, and spray program. Between the rows in site 3 was purely soil cultivated while the other vineyards were covered by sod or cover crops. The training system in site 3 was a spur-pruned cordon system while the others were cane-pruned vertical shoot positioning system. The last distinct cultural practice in site 3 was the copper application for their pest management program through the growing season while no copper spray application observed in other vineyards sites. The copper spray created a blue colour background layer as the RPAS flight performed to get NDVI data. The effect of vineyard floor management, training systems, and colour of the background layer on NDVI detectability needs to be studied further.

Numerous researchers in viticulture have focused on the concept of "vine balance" and the balance between vegetative and reproductive growth as a general guideline to examine quality of grape and wine production.[23-26] However, the balance between crop level and crop quality relies on cultivar, soil types, climate, and cultural practice.[27-30] There are still many unknowns for application and evaluation of the vine balance in many areas including the Niagara Peninsula. In chapter 4, this study examined the vine balance using various spectral algorithms of reflectance data from the RPAS flight and from proximal sensing technologies and provided scientific and evidence-based support to benefit vineyard management, and productivity and quality of Cabernet franc grapes in Niagara vineyards. The results confirmed the presence of correlations between vineyard canopy reflectance data from the RPAS flight and from proximal sensing, and vineyard yield and compositions such as yield, berry weight, pH, berry phenols and anthocyanins level. Site yields and their detection by remote sensing NDVI were affected by annual climate. The dryer year (2016) showed more variation in yield level and more capability of detecting correlation

between the variables than these in regular growing seasons (2015 and 2017). The nature of yield variation in dry year could be explained by zonal difference of water use efficiency as described in chapter 3. In some vineyard sites, the water stress may induce the high water use efficiency without any loss of biomass production and reproductive process[22] while in the other sites, the positive conventional relationship between water availability and plant reproductive production was applied.

There was also an inverse correlation between NDVI and soil moisture on three of four sites with lower yield shift, indicating a substantial water standing and insufficient water drainage on these sites. Thus, water stress may be accompanied by soil drainage that affects the yield of a site and its detection by remote sensing NDVI. In previous studies, vegetative growth has been shown to affect berry composition and yield[31,32] and the amount of water consumed affects the amount of biomass produced by plants[33].

The impact of seasonal variations in vegetative growth on grape yield was also examined using proximal sensing (GreenSeeker®) at three important berry growth stages: berry set, lag phase, and veraison. The proximal sensing measurement at fruit set indicated more correlations to yield level than the measurements taken at lag phase and veraison, thus the vegetation at earlier growing season could have more impacts on reproductive process. PCA framework for all years would be performed to see how the scores move through PCA space and to identify clustering of points, which would be useful for effectively characterizing growing conditions within and among sites. Interestingly, a strong trend between remote sensing thermal emission data and pH was also seen throughout the sites in 2016 (dry year). In addition, the inverse trends observed between early developmental stages (fruit set and lag phase) of proximal NDVI measurements and pH. Therefore,

variation in remote sensing thermal emission data could be a key determinant of pH under water stress in early developmental stage.

Although NDVI is not the best indicator of variability in fruit composition, an inverse correlation between NDVI and phenols/anthocyanins was still observed in this study. Furthermore, the proximal NDVI measurements around veraison showed a better correlation with phenols and anthocyanins than these of earlier measurements. These results support previous studies that phenolic accumulation in berries are inversely correlated to vine canopies via fruit exposure to sunlight to the flavonoid biosynthesis[34-36] and the vegetation at the latter growing season could have more impacts on accumulation of phenols and anthocyanins level in berry[37].

Other remote sensing indices extracted from the RPAS's multi-spectral sensor were also examined to detect variabilities in yield components, berry composition, and early virus infections. It was proven that other indices, which were sensitive to measure leaf colour compounds, detected vineyard variations in grape quality and disease pressure more accurately than NDVI.[38] The results indicated that CI green and GNDVI, the ratio of green and NIR, showed the most capability of detecting variation in yield in most of sites with significant positive correlation. However, different pattern of correlation matrix observed in the correlation analysis for the berry composition. CI red edge and NDRE, the ratio of red edge and NIR, indicated negative or positive correlation with random patterns to most of the variables like Brix, pH, phenols, and anthocyanins. Two sites showed an identical negative correlation between variables while positive correlation observed in another site. The interpolated maps between NDVI and the measured variables in this study displayed similar spatial correlation pattern to its statistical one, which confirmed the compatibility of the spatial map analysis over other statistical tools for correlation basis analysis.

Remote sensing maps can be used to pinpoint target areas in vineyards for precision viticulture applications, such as selective harvesting, better fruit exposure, and drip irrigation target.[39]

This study examined the zonal effects of remote sensing parameter on variation in wine quality comparing wines from zone of low and high level of remote sensing NDVI. Although previous research demonstrated vineyard variation attributed to vegetative growth can influence fruit and wine chemistry and sensory attributes[6,40-43], researchers need to conduct more research to determine whether remote sensing data can effectively manage vineyards by zones and select crops for harvesting. This study demonstrates that NDVI-based remote sensing data has promise for guiding selective harvesting and subsequent production of distinct zonal wines. It was found that sensory sorting compared well with wine analysis results in differentiating wines from NDVI zones, which was consistent with previous studies that found tasting differences between wine types were more likely to be influenced by volatile aroma compounds rather than other chemical differences.[44,45]

Wine aromatic compounds analyzed by GC-MS were consistent with the wine sorting test results with different levels of various key odor active compounds in 2017. These results suggest that in cool climate grape growing areas like the Niagara Peninsula, cis-3-Hexenol ((Z)-3-hexenol) and 1-Hexanol could be critical odor active aroma compounds for indicating significant difference in wine quality from different NDVI levels. The high levels of cis-3-Hexenol ((Z)-3-hexenol) and through a series of enzymatic reactions, 1-hexanol can be synthesized from grape polyunsaturated fatty acids, which are commonly observed in plants grown under cool climate region due to a close relationship between concentration of unsaturated fatty acids and plant cold tolerance.[46-49]

There were also vintage variations for detectability of different flavour profiles between wines from high and low NDVI zones with high detection rate in 2017 vintage. The different

success in the sorting task and the wine aromatic compounds analysis between years could be further explained by changes in growing season climate. As precipitation and plant water availability levels are high in 2017, water stress in certain spots could limit vegetative growth and production quality, while the application of stress signals in a hot and dry year like 2016 may allow water to be used more efficiently at a whole vineyard level for uniform vegetative and reproductive growth.[22] Climate, sun exposure, and water availability play key roles in affecting the quality of grapes and wine aroma compounds over time.[43,50] The amount of water stress can greatly alter fruit quality, with mild water deficit vines producing berries with more sugar, anthocyanins, phenols and lower acid levels.[45,51,52] Global warming with rising temperature and causing more frequency of extreme climatic events has brought many concerns for agriculture-based industries. Drought and heat waves have severe consequences for many agricultural regions with more frequency of hot dry summers. The results from this study could help future research of the utilization of remote sensing technologies in investigating vine-water balance for fruit and wine quality, and in detecting heat and water stressed vineyard areas. Analysis of the vegetative and reproductive response in vineyard sites to extreme weather conditions will help determine the climatic effects of the future.

To better understand the distinguishing characteristics and the underlying chemistry of wines from different NDVI zones, sensory descriptive analysis (DA) and partial least squares regression (PLSR) were performed for 2016 vintage wines. The DA resulted in nearly identical wine groupings as the sorting test with low NDVI wines classified as vegetable, dried fruit, dark fruit, and spice with bitterness and astringency while high NDVI wines were classified as floral, red fruit, tropical fruit, and herbaceous with high acids, which is consistent with previous studies related to anthocyanin levels.[34-36] The PLSR results indicated that grape berry aroma compounds

or compounds produced by precursors such as C6 alcohol, aromatic alcohols, terpenes, and aromatic phenols could be important odor compounds distinct from different NDVI level. Trans-2-Hexenol ((E)-2-hexenol), isomer of cis-3-Hexenol ((Z)-3-hexenol), could be the other critical odor active aroma compound for indicating significant difference in wine quality from different NDVI levels since it may derive from grape polyunsaturated fatty acids through a cool climate specific cascade of enzymatic reactions (LOX). This study indicates some important messages to develop future research for utilization of remote sensing technologies to detect oenologically relevant vineyard zones for selective harvest, but it is necessary to develop more robust remote sensing indices that can be used for selective harvest and zonal winemaking in single vineyard block.

Lastly, the results of portable spectrometer reading for the effect of the visible symptoms of GLRaV-3 infection on the EM spectrums indicated that GLRaV-3 asymptomatic leaves had significantly higher light reflectance levels than these of healthy and symptomatic leaves throughout the visible (green and red), red edge, and NIR spectrums. The possible initiation of plant defense systems was induced by perception of pathogen attacks, even in the undamaged leaves soon after attack[53] and the hardening of the asymptomatic leaf surface walls at an early stage of the GLRaV-3 infection may interfere the penetration or absorption of the light radiation and these observed through the whole EM spectrums of the leaves[53-56]. However, the reduction of the increment rate of EM reflectance observed at the certain peak (700 nm) in the red edge range because of a decline in chlorophyll fluorescence emission and increase in heat production with nonphotochemical quenching (NPQ) action.[57-60]

Another distinct result was significantly lower light reflectance level of GLRaV-3 symptomatic leaves in green and red peaks. It could be explained that the degradation of

chlorophyll and other organ cells on the surface and interior of the leaves by hypersensitive response in the virus symptomatic leaves may interfere with the penetration or absorption of light radiation through the whole EM spectrum.[61-68] Interestingly, the relative inflection point (MaxΔRn) was consistent at 700 nm through the sites and treatments, which was consistent with the previous study indicating that the reflectance at 700 nm was primarily controlled by the chlorophyll content and was a measure of the red edge shift.[69] The strength of reflectance changes at the points was significantly lower in virus asymptomatic leaves than these in virus symptomatic and healthy leaves. The low reflectance relative increment rate could be caused by changes in chlorophyll fluorescence emission rates.[57-59] In the early or intermediate stages of stress, plant cells tend to produce more heat to release surplus energy, which lowers chlorophyll fluorescence emission level.[70] However, under severe stress conditions with activation of HR, photosystem II might also be severely damaged, leading to an increase in chlorophyll fluorescence with a decrease in NPQ activity and following spike of the increment rate of EM reflectance observed at the certain peak (700 nm) in red edge range.[71,72]

A multispectral RPAS data set was not able to predict GLRaV-3 infection based upon conventional spectral indices. A hyperspectral spectrometer, however, consistently identified significant differences between healthy and symptomatic leaves based on their reflectance spectra. Considering the potential for developing a narrow-band hyperspectral index for grapevine virus detection, this finding points to the need for further research. A detailed understanding of the mechanisms of plant early defense systems and their impact on the electromagnetic reflectance and fluorescence emission at the red edge peak, especially at 700 nm wavelength is required.

Although remote sensing data analysis tools were not associated with several other important variables for grape production, the research findings confirmed that remote sensing data

have a significant potential to differentiate specific zones of water stress, canopy size, yield, superior fruit compositions, and wine quality. Further investigation of elevation mapping derived from photogrammetry such as aspect, slope, irradiance would be beneficial to support results of this study. There were also some experimental challenges, such as visual assessment of virus symptoms, limited sample size, and time gaps between measurements, but this study confirmed that the mechanism of plant defense system against biotic stress could have impacts on the spectral behaviour of grapevine leaves and remote sensing technologies could be useful to detect the spectral behaviour changes from the stress. Even though there were some limitations including interruptions from other vegetation impacts between rows and vines, as a first step to develop an SSCM model for vineyard management, it also proposes future research opportunities to test and develop an efficient vineyard management decision-making model.

7.2 References

1. Plant, R.E. Site-specific management: the application of information technology to crop production. *Computers electronics in agriculture* **2001**, *10*, 9-29.

2. Bramley, R.; Lamb, D. Making sense of vineyard variability in Australia. In Proceedings of the Proc. Internat. Symp. on Precision Viticulture, Ninth Latin American Congr. on Viticulture and Oenology, **2003**; pp. 35-54.

3. Johnson, L.; Bosch, D.; Williams, D.; Lobitz, B. Remote sensing of vineyard management zones: Implications for wine quality. *Applied Engineering in Agriculture* **2001**, *17*, 557.

4. Priori, S.; Martini, E.; Biagi, M.; Andrenelli, M.; Magini, S.; Agnelli, A.; Natarelli, L.; Bucelli, P.; Comina, C.; Pellegrini, S. Improving wine quality through a harvest zoning based upon the combined use of proximal and remote sensing. In Proceedings of the Second Global Workshop on Proximal Soil Sensing, **2011**; pp. 152-155.

5. Bramley, R.G.; Hamilton, R. Terroir and precision viticulture: are they compatible? *Journal International des Sciences de la Vigne et du Vin* **2007**, *41*, 1.

6. Bramley, R.; Ouzman, J.; Boss, P.K. Variation in vine vigor, grape yield and vineyard soils and topography as indicators of variation in the chemical composition of grapes, wine and

wine sensory attributes. *Australian Journal of Grape and Wine Research* **2011**, *17*, 217-229.

7. Bramley, R.; Ouzman, J.; Thornton, C. Selective harvesting is a feasible and profitable strategy even when grape and wine production is geared towards large fermentation volumes. *Australian Journal of Grape and Wine Research* **2011**, *17*, 298-305.

8. Atallah, S.S.; Gómez, M.I.; Fuchs, M.F.; Martinson, T.E. Economic impact of grapevine leafroll disease on Vitis vinifera cv. Cabernet franc in Finger Lakes vineyards of New York. *American Journal of Enology and Viticulture* **2012**, *63*, 73-79.

9. Osman, F.; Leutenegger, C.; Golino, D.; Rowhani, A. Comparison of low-density arrays, RT-PCR and real-time TaqMan® RT-PCR in detection of grapevine viruses. *Journal of virological methods* **2008**, *149*, 292-299.

10. Maree, H.J.; Almeida, R.P.; Bester, R.; Chooi, K.M.; Cohen, D.; Dolja, V.V.; Fuchs, M.F.; Golino, D.A.; Jooste, A.E.; Martelli, G.P. Grapevine leafroll-associated virus 3. *Frontiers in microbiology* **2013**, *4*, 82.

11. Xiao, H.; Shabanian, M.; Moore, C.; Li, C.; Meng, B. Survey for major viruses in commercial Vitis vinifera wine grapes in Ontario. *Virology journal* **2018**, *15*, 127.

12. Johnson, L.F. Temporal stability of an NDVI-LAI relationship in a Napa Valley vineyard. *Australian Journal of Grape and Wine Research* **2003**, *9*, 96-101.

13. Debuisson, S.; Germain, C.; Garcia, O.; Panigai, L.; Moncomble, D.; Le Moigne, M.; Fadaili, E.; Evain, S.; Cerovic, Z. Using Multiplex® and Greenseeker™ to manage spatial variation of vine vigor in Champagne. In Proceedings of the 10th International Conference on Precision Agriculture. Denver, Colorado, **2010**.

14. Rey-Caramés, C.; Diago, M.; Martín, M.; Lobo, A.; Tardaguila, J. Using RPAS multi-spectral imagery to characterise vigor, leaf development, yield components and berry composition variability within a vineyard. *Remote Sensing* **2015**, *7*, 14458-14481.

15. Wiegand, C.; Richardson, A.J.A.J. Leaf Area, Light Interception, and Yield Estimates from Spectral Components Analysis 1. **1984**, *76*, 543-548.

16. Smart, R.; Robinson, M. *Sunlight into wine: a handbook for winegrape canopy management*; Winetitles: **1991**.

17. Hall, A.; Lamb, D.; Holzapfel, B.; Louis, J. Optical remote sensing applications in viticulture-a review. *Australian journal of grape and wine research* **2002**, *8*, 36-47.

18. Dobrowski, S.; Ustin, S.; Wolpert, J.J.A.J.o.G.; Research, W. Grapevine dormant pruning weight prediction using remotely sensed data. **2003**, *9*, 177-182.

19. Ledderhof, D.; Brown, R.; Reynolds, A.; Jollineau, M. Using remote sensing to understand Pinot noir vineyard variability in Ontario. *Canadian journal of plant science* **2016**, *96*, 89-108.

20. Myburgh, P.; Moolman, J. Ridging—a soil preparation practice to improve aeration of vineyard soils. *South African Journal of Plant and Soil* **1991**, *8*, 189-193.

21. Lambert, J.; Anderson, M.; Wolpert, J. Vineyard nutrient needs vary with rootstocks and soils. *California agriculture* **2008**, *62*, 202-207.

22. Jones, H.G. *Plants and microclimate: a quantitative approach to environmental plant physiology*; Cambridge university press: **2013**.

23. Shaulis, N.J.E.B.C.A.E.S. Cultural practices for New York vineyards. **1950**, *805*.

24. Kliewer, W.M.; Dokoozlian, N.K.J.A.J.o.E.; Viticulture. Leaf area/crop weight ratios of grapevines: influence on fruit composition and wine quality. **2005**, *56*, 170-181.

25. Filippetti, I.; Intrieri, C. Planting density and physiological balance: Comparing approaches to European viticulture in the 21st century. In Proceedings of the Proceedings of the ASEV 50th Anniversary Annual Meeting, Seattle, Washington, June 19-23, **2001**; pp. 296-308.

26. Howell, G.S.J.A.J.o.E.; Viticulture. Sustainable grape productivity and the growth-yield relationship: A review. **2001**, *52*, 165-174.

27. Ough, C.; Nagaoka, R.J.A.j.o.e.; viticulture. Effect of cluster thinning and vineyard yields on grape and wine composition and wine quality of Cabernet Sauvignon. **1984**, *35*, 30-34.

28. Palliotti, A.; Cartechini, A. Cluster thinning effects on yield and grape composition in different grapevine cultivars. In Proceedings of the XXV International Horticultural Congress, Part 2: Mineral Nutrition and Grape and Wine Quality 512, **1998**; pp. 111-120.

29. Poni, S.; Bernizzoni, F.; Briola, G.; Cenni, A. Effects of early leaf removal on cluster morphology, shoot efficiency and grape quality in two Vitis vinifera cultivars. In Proceedings of the VII International Symposium on Grapevine Physiology and Biotechnology 689, **2004**; pp. 217-226.

30. Reynolds, A.G.; Price, S.F.; Wardle, D.A.; Watson, B.T.J.A.J.o.E.; Viticulture. Fruit environment and crop level effects on Pinot noir. I. Vine performance and fruit composition in British Columbia. **1994**, *45*, 452-459.

31. Smart, R.E. Principles of grapevine canopy microclimate manipulation with implications for yield and quality. A review. *American Journal of Enology and Viticulture* **1985**, *36*, 230-239.

32. Terry, D.B.; Kurtural, S.K. Achieving vine balance of Syrah with mechanical canopy management and regulated deficit irrigation. *American journal of enology and viticulture* **2011**, *62*, 426-437.

33. Acevedo-Opazo, C.; Tisseyre, B.; Guillaume, S.; Ojeda, H. The potential of high spatial resolution information to define within-vineyard zones related to vine water status. *Precision Agriculture* **2008**, *9*, 285-302.

34. Drissi, R.; Goutouly, J.-P.; Forget, D.; Gaudillere, J.-P. Nondestructive measurement of grapevine leaf area by ground normalized difference vegetation index. *Agronomy Journal* **2009**, *101*, 226-231.

35. Lamb, D.W.; Weedon, M.; Bramley, R. Using remote sensing to predict grape phenolics and colour at harvest in a Cabernet Sauvignon vineyard: Timing observations against vine phenology and optimising image resolution. *Australian Journal of Grape and Wine Research* **2004**, *10*, 46-54.

36. Stamatiadis, S.; Taskos, D.; Tsadilas, C.; Christofides, C.; Tsadila, E.; Schepers, J.S. Relation of ground-sensor canopy reflectance to biomass production and grape color in two Merlot vineyards. *American Journal of Enology and viticulture* **2006**, *57*, 415-422.

37. Ojeda, H.; Andary, C.; Kraeva, E.; Carbonneau, A.; Deloire, A.J.A.j.o.E.; Viticulture. Influence of pre-and postveraison water deficit on synthesis and concentration of skin phenolic compounds during berry growth of Vitis vinifera cv. Shiraz. **2002**, *53*, 261-267.

38. Meggio, F.; Zarco-Tejada, P.J.; Núñez, L.C.; Sepulcre-Cantó, G.; González, M.; Martín, P. Grape quality assessment in vineyards affected by iron deficiency chlorosis using narrow-band physiological remote sensing indices. *Remote Sensing of Environment* **2010**, *114*, 1968-1986.

39. Arnó Satorra, J.; Martínez Casasnovas, J.A.; Ribes Dasi, M.; Rosell Polo, J.R. Precision viticulture. Research topics, challenges and opportunities in site-specific vineyard management. *Spanish Journal of Agricultural Research* **2009**, *7*, 779-790.

40. Cortell, J.M.; Halbleib, M.; Gallagher, A.V.; Righetti, T.L.; Kennedy, J.A. Influence of vine vigor on grape (Vitis vinifera L. cv. Pinot noir) anthocyanins. 2. Anthocyanins and pigmented polymers in wine. *Journal of agricultural and food chemistry* **2007**, *55*, 6585-6595.

41. Cortell, J.M.; Sivertsen, H.K.; Kennedy, J.A.; Heymann, H. Influence of vine vigor on Pinot noir fruit composition, wine chemical analysis, and wine sensory attributes. *American journal of enology and viticulture* **2008**, *59*, 1-10.

42. Reynolds, A.G.; Senchuk, I.V.; van der Reest, C.; De Savigny, C. Use of GPS and GIS for elucidation of the basis for terroir: Spatial variation in an Ontario Riesling vineyard. *American Journal of Enology and Viticulture* **2007**, *58*, 145-162.

43. Ristic, R.; Downey, M.O.; Iland, P.G.; Bindon, K.; Francis, I.L.; Herderich, M.; Robinson, S.P.J.A.J.o.G.; Research, W. Exclusion of sunlight from Shiraz grapes alters wine colour, tannin and sensory properties. **2007**, *13*, 53-65.

44. CHAPMAN, D.M.; ROBY, G.; EBELER, S.E.; GUINARD, J.X.; MATTHEWS, M.A. Sensory attributes of Cabernet Sauvignon wines made from vines with different water status. *Australian Journal of Grape and Wine Research* **2005**, *11*, 339-347.

45. Koundouras, S.; Marinos, V.; Gkoulioti, A.; Kotseridis, Y.; van Leeuwen, C. Influence of vineyard location and vine water status on fruit maturation of nonirrigated cv. Agiorgitiko (Vitis vinifera L.). Effects on wine phenolic and aroma components. *Journal of Agricultural and Food Chemistry* **2006**, *54*, 5077-5086.

46. Kalua, C.; Boss, P.K.J.A.J.o.G.; Research, W. Comparison of major volatile compounds from Riesling and Cabernet Sauvignon grapes (Vitis vinifera L.) from fruitset to harvest. **2010**, *16*, 337-348.

47. García, E.; Chacón, J.; Martínez, J.; Izquierdo, P.J.F.s.; international, t. Changes in volatile compounds during ripening in grapes of Airén, Macabeo and Chardonnay white varieties grown in La Mancha region (Spain). **2003**, *9*, 33-41.

48. Watkins, P.; Wijesundera, C.J.T. Application of zNose™ for the analysis of selected grape aroma compounds. **2006**, *70*, 595-601.

49. Vilanova, M.; Genisheva, Z.; Bescansa, L.; Masa, A.; Oliveira, J.M.J.P. Changes in free and bound fractions of aroma compounds of four Vitis vinifera cultivars at the last ripening stages. **2012**, *74*, 196-205.

50. De Orduna, R.M.J.F.R.I. Climate change associated effects on grape and wine quality and production. **2010**, *43*, 1844-1855.

51. Shellie, K.C. Vine and berry response of Merlot (Vitis vinifera L.) to differential water stress. *American Journal of Enology and Viticulture* **2006**, *57*, 514-518.

52. Roby, G.; Harbertson, J.F.; Adams, D.A.; Matthews, M.A. Berry size and vine water deficits as factors in winegrape composition: anthocyanins and tannins. *Australian Journal of Grape and Wine Research* **2004**, *10*, 100-107.

53. Steppuhn, A.; Baldwin, I.T. Induced defenses and the cost-benefit paradigm. In *Induced plant resistance to herbivory*; Springer: **2008**; pp. 61-83.

54. Nicaise, V.; Roux, M.; Zipfel, C.J.P.p. Recent advances in PAMP-triggered immunity against bacteria: pattern recognition receptors watch over and raise the alarm. **2009**, *150*, 1638-1647.

55. Zeyen, R.; Carver, T.; Lyngkjær, M.F. Epidermal cell papillae. In *The powdery mildews. A comprehensive treatise*; APS Press: **2002**; pp. 107-125.

56. Müller, C.; Riederer, M.J.J.o.c.e. Plant surface properties in chemical ecology. **2005**, *31*, 2621-2651.

57. Gilmore, A.M. How higher plants respond to excess light: Energy dissipation in photosystem II. In *Concepts in Photobiology*; Springer: **1999**; pp. 513-548.

58. Maxwell, K.; Johnson, G.N.J.J.o.e.b. Chlorophyll fluorescence—a practical guide. **2000**, *51*, 659-668.

59. Gamon, J.; Serrano, L.; Surfus, J.J.O. The photochemical reflectance index: an optical indicator of photosynthetic radiation use efficiency across species, functional types, and nutrient levels. **1997**, *112*, 492-501.

60. Butler, W.L.J.A.R.o.P.P. Energy distribution in the photochemical apparatus of photosynthesis. **1978**, *29*, 345-378.

61. Carter, G.A.; Rebbeck, J.; Percy, K.E.J.C.J.o.F.R. Leaf optical properties in Liriodendron tulipifera and Pinus strobus as influenced by increased atmospheric ozone and carbon dioxide. **1995**, *25*, 407-412.

62. Carter, G.A.; Knapp, A.K.J.A.j.o.b. Leaf optical properties in higher plants: linking spectral characteristics to stress and chlorophyll concentration. **2001**, *88*, 677-684.

63. Bekefi, G.; Hirshfield, J.L.; Brown, S.C.J.T.P.o.F. Kirchhoff's Radiation Law for Plasmas with Non-Maxwellian Distributions. **1961**, *4*, 173-176.

64. Grant, L.; Daughtry, C.; Vanderbilt, V.J.R.s.o.e. Variations in the polarized leaf reflectance of Sorghum bicolor. **1987**, *21*, 333-339.

65. Vanderbilt, V.C.; Grant, L.J.I.T.o.G.; Sensing, R. Plant canopy specular reflectance model. **1985**, 722-730.

66. Grant, L.; Daughtry, C.; Vanderbilt, V.J.P.P. Polarized and specular reflectance variation with leaf surface features. **1993**, *88*, 1-9.

67. Laloi, C.; Apel, K.; Danon, A.J.C.o.i.p.b. Reactive oxygen signalling: the latest news. **2004**, *7*, 323-328.

68. Jabs, T.J.B.p. Reactive oxygen intermediates as mediators of programmed cell death in plants and animals. **1999**, *57*, 231-245.

69. Gitelson, A.A.; Merzlyak, M.N.; Lichtenthaler, H.K.J.J.o.p.p. Detection of red edge position and chlorophyll content by reflectance measurements near 700 nm. **1996**, *148*, 501-508.

70. Yahyaoui, W.; Harnois, J.; Carpentier, R.J.F.l. Demonstration of thermal dissipation of absorbed quanta during energy-dependent quenching of chlorophyll fluorescence in photosynthetic membranes. **1998**, *440*, 59-63.

71. Murchie, E.H.; Lawson, T.J.J.o.e.b. Chlorophyll fluorescence analysis: a guide to good practice and understanding some new applications. **2013**, *64*, 3983-3998.

72. Horton, P.; Johnson, M.P.; Perez-Bueno, M.L.; Kiss, A.Z.; Ruban, A.V.J.T.F.j. Photosynthetic acclimation: Does the dynamic structure and macro-organisation of photosystem II in higher plant grana membranes regulate light harvesting states? **2008**, *275*, 1069-1079.

APPENDICES

Tables

Table A1. Quality report of RPAS remote sensing data processing by Air-Tech Solutions, Inverary, ON (please double click the image).

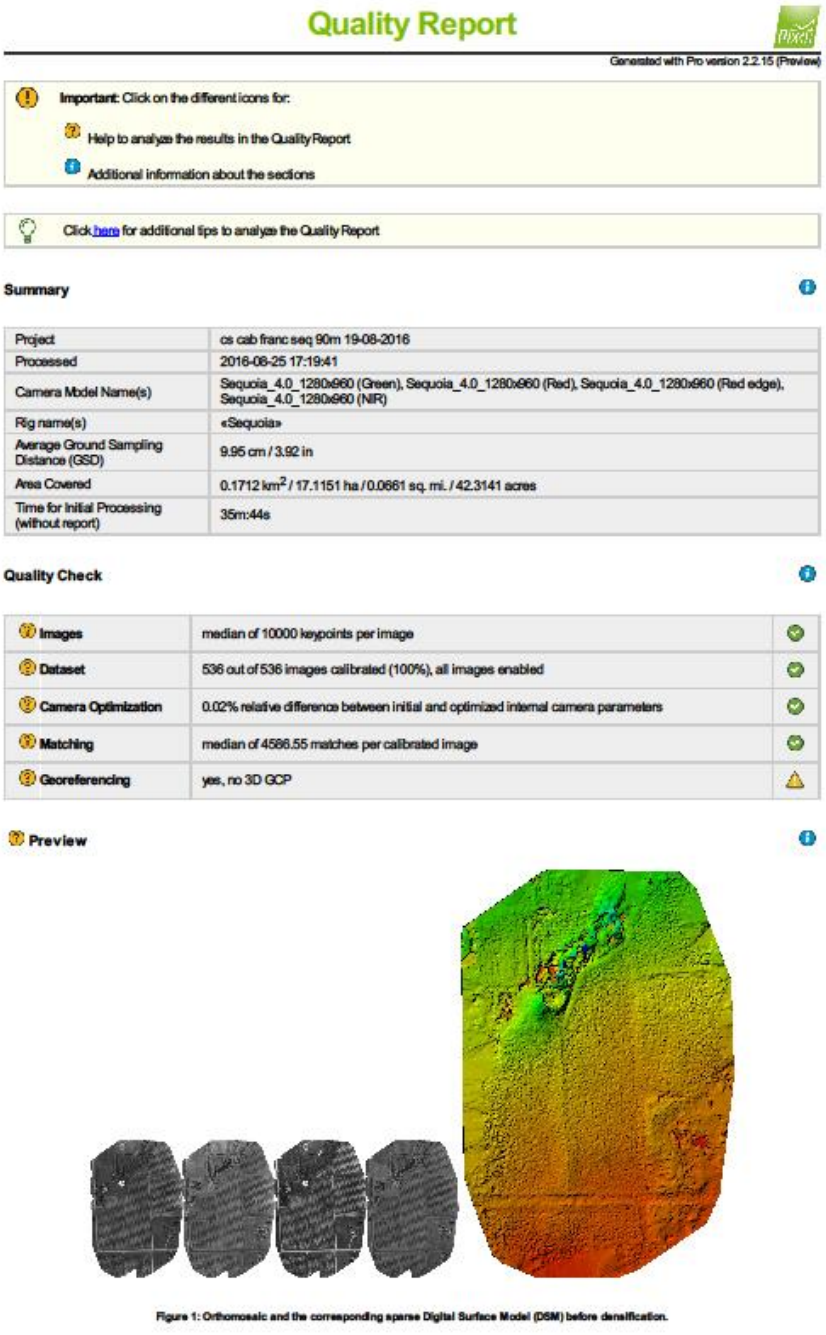

Quality Report

Generated with Pro version 2.2.15 (Preview)

Important: Click on the different icons for:

Help to analyze the results in the Quality Report

Additional information about the sections

Click here for additional tips to analyze the Quality Report

Summary

Project	cs cab franc seq 90m 19-08-2016
Processed	2016-08-25 17:19:41
Camera Model Name(s)	Sequoia_4.0_1280x960 (Green), Sequoia_4.0_1280x960 (Red), Sequoia_4.0_1280x960 (Red edge), Sequoia_4.0_1280x960 (NIR)
Rig name(s)	«Sequoia»
Average Ground Sampling Distance (GSD)	9.95 cm / 3.92 in
Area Covered	0.1712 km^2 / 17.1151 ha / 0.0661 sq. mi. / 42.3141 acres
Time for Initial Processing (without report)	35m:44s

Quality Check

Images	median of 10000 keypoints per image	✓
Dataset	536 out of 536 images calibrated (100%), all images enabled	✓
Camera Optimization	0.02% relative difference between initial and optimized internal camera parameters	✓
Matching	median of 4586.55 matches per calibrated image	✓
Georeferencing	yes, no 3D GCP	⚠

Preview

Figure 1: Orthomosaic and the corresponding sparse Digital Surface Model (DSM) before densification.

Table A2. End-point PCR results in GRBV presence for three virus infected sites: – and +: negative and positive respectively in the PCR.

Site	Row	Panel	GRBV	Site	Row	Panel	GRBV	Site	Row	Panel	GRBV
Site 1	3	4	–	Site 2	4	12	+	Site 3	2	9	+
	3	12	+		4	37	–		2	21	–
	3	20	+		7	37	+		4	21	–
	3	28	–		7	22	–		4	9	–
	3	36	–		7	7	+		6	9	–
	8	36	–		10	12	+		6	21	–
	8	28	–		10	37	+		8	21	–
	8	20	–		13	37	–		8	9	–
	8	12	+		13	22	+		10	9	+
	8	4	–		13	7	–		10	21	–
	13	4	+		16	12	+		12	21	–
	13	12	–		16	37	+		12	9	+
	13	20	–		19	37	+		14	9	–
	13	28	–		19	22	–		14	21	–
	13	36	–		19	7	+		16	21	–
	18	36	+		22	12	+		16	9	+
	18	28	+		22	37	–		18	9	+
	18	20	+		25	37	–		18	21	–
	18	12	+		25	22	+		20	21	–
	18	4	+		25	7	+		20	9	–

Table A3. Pearson's correlation results between GRBV presence and remote sensing indices in the two virus infected vineyards. Those variables with significant (95% confidence) were listed in bold, with blank cells representing no correlation: blue boxes= positive relationship, red boxes= negative relationship. Abbreviations: NIR= Near infrared, NDVI= Normalized difference vegetation Index, NDRE= Red edge normalized vegetation index, GNDVI= NDVI green, GRVI= Green-red vegetation index, MTCI= MERIS terrestrial chlorophyll index, RTVI core= Core red edge triangular vegetation index.

	Correlation matrix			p-values		
Variables	Site1	Site2	Site3	Site1	Site2	Site3
Green	-0.111	0.126	0.339	0.641	0.597	0.143
Red	0.102	0.202	-0.025	0.668	0.394	0.915
RedEdge	-0.298	0.326	0.407	0.201	0.161	0.075
NIR	-0.236	0.337	**0.446**	0.317	0.146	**0.049**
NDVI	-0.164	-0.080	0.168	0.489	0.736	0.480
NDRE	0.284	-0.060	-0.259	0.225	0.801	0.270
MTCI	0.170	-0.075	0.080	0.473	0.752	0.737
RTVI core	0.255	0.184	0.122	0.279	0.437	0.610
GNDVI	-0.033	0.024	-0.260	0.889	0.919	0.267
GRVI	-0.268	-0.354	0.434	0.254	0.125	0.056

Figures

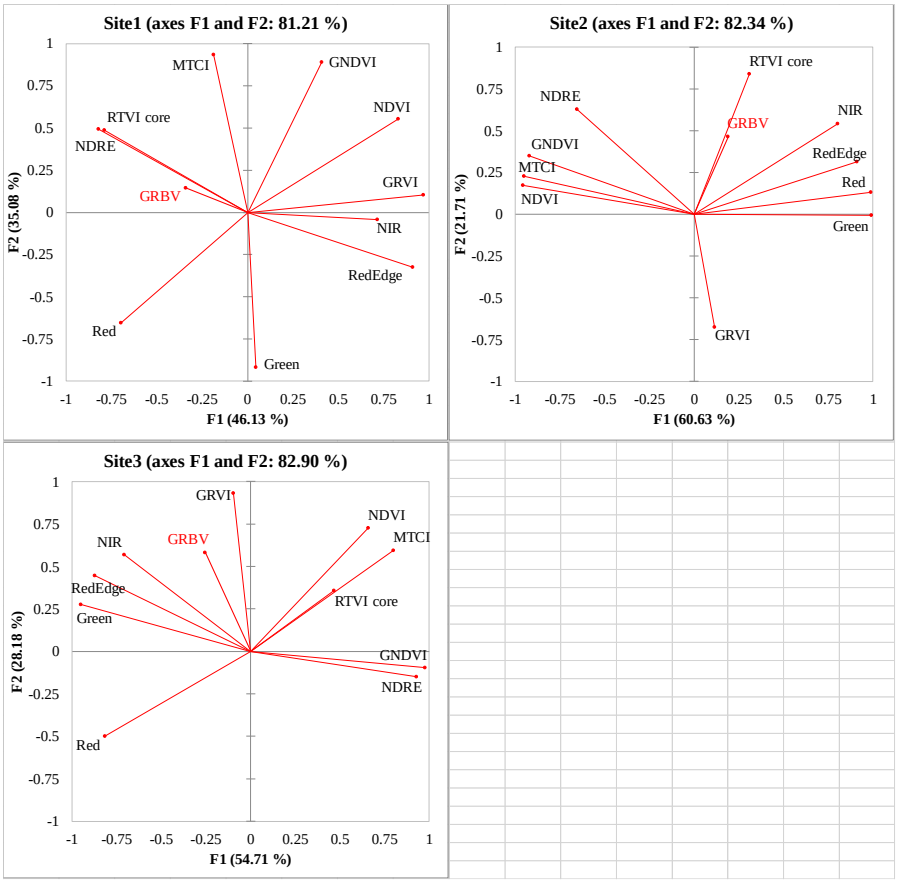

Figure A1. PCA results for GRBV presence vs. remote sensing indices including green, red, red edge, NIR, NDVI, NDRE, GNDVI, GRVI, MTCI, and RTVI core. Abbreviations: NIR= Near infrared, NDVI= Normalized difference vegetation Index, NDRE= Red edge normalized vegetation index, GNDVI= NDVI green, GRVI= Green-red vegetation index, MTCI= MERIS terrestrial chlorophyll index, RTVI core= Core red edge triangular vegetation index.